TAMPEREEN TEKNILLINEN YLIOPISTO
TAMPERE UNIVERSITY OF TECHNOLOGY

Marco D'Ignazio

Undrained shear strength of Finnish clays for stability analyses of embankments

Julkaisu 1412 • Publication 1412

Tampere 2016

Tampereen teknillinen yliopisto. Julkaisu 1412
Tampere University of Technology. Publication 1412

Marco D'Ignazio

Undrained shear strength of Finnish clays for stability analyses of embankments

Thesis for the degree of Doctor of Science in Technology to be presented with due permission for public examination and criticism in Rakennustalo Building, Auditorium RG202, at Tampere University of Technology, on the 21st of September 2016, at 12 noon.

Tampereen teknillinen yliopisto - Tampere University of Technology
Tampere 2016

Supervisor and Custos
Professor Tim Länsivaara, Tampere University of Technology

Preliminary Assessors
Professor Gustav Grimstad, Norwegian University of Science and Technology (NTNU)
Dr. Suzanne Lacasse, Norwegian Geotechnical Institute (NGI)

Opponents
Prof. Emer. Michele Jamiolkowski, Politecnico di Torino
Dr. Suzanne Lacasse, Norwegian Geotechnical Institute (NGI)

ISBN 978-952-15-3804-9 (printed)
ISBN 978-952-15-3806-3 (PDF)
ISSN 1459-2045

I. ABSTRACT

The thesis deals with the undrained shear strength (s_u) of Finnish clays. The research study focuses on the evaluation and modelling of undrained shear strength for total stress stability analyses of embankments and it studies some special features of sensitive clays.

Firstly, a multivariate database of Finnish clay data points is compiled in order to derive correlations for undrained shear strength specific to Finnish clays. For each data point, information on s_u from field vane, consolidation stresses and other physical properties is available. The dependency of s_u on overconsolidation ratio (OCR) and index parameters is studied. The new correlations are derived through regression analyses. Results show that the dependency of s_u on index parameters is more marked when the uncorrected field vane measurements are considered. On the other hand, when measured s_u is corrected for strain rate and converted into mobilized s_u, such dependency becomes negligible. The new correlations are validated through comparison with existing correlations from the literature. Bias and uncertainties of the new transformation models are evaluated through an independent database consisting of clay data points from Sweden and Norway. The main result is that the new correlations are characterized by lower uncertainty than the other commonly used correlation models.

In order to study some of the special characteristics of soft sensitive clays, the Perniö failure test is analyzed through the finite element method (FEM) using the advanced NGI-ADPSoft model, which includes anisotropy and strain-softening behavior of sensitive clays. A series of laboratory and in-situ tests are used to determine the anisotropic shear strength of Perniö clay and Perniö dry crust. Stability analyses are performed using the software PLAXIS 2D and the influence of stress path dependency and post-peak strength reduction on the failure load is evaluated. Calculated displacements are compared to field measurements from the experiment. A good agreement is observed between field observations and calculation results. The study indicates that both s_u anisotropy and strain-softening have a notable impact on the undrained behavior of the Perniö embankment. Furthermore, it was shown how the modelling of post-peak properties influences the computed failure mechanism.

The issue of undrained shear strength increase in clayey layers under old embankments due to consolidation is studied through CPTU and field vane test results from Murro test embankment. Previous test results suggested a decrease of shear strength under the embankment after a few years of consolidation. The new test results show that the strength has increased and the soil has reached its normally consolidated state. Undrained shear strength and preconsolidation pressure are assessed using existing as well as calibrated transformation models. Data from the Murro test site shows that s_u has increased by over 50% in the uppermost part of the deposit.

Engineering aspects related to the topics object of study are discussed and some complex issues are addressed from a practical point of view. Firstly, some indications on the use of the new correlations for s_u of Finnish clays are provided. Secondly, suggestions about how to derive soil parameters for FE total stress soil models are given. Finally, a simplified methodology is proposed to model strength increase in total stress analyses.

II. ACKNOWLEDGMENTS

In everyone's life, there is a limited number of situations where the world is sending you a message, which normally contains an opportunity. If you grab it, you get lucky. Finland has been my luck, as it opened the door to the world. After spending one semester in 2011 as an exchange student at Tampere University of Technology, I thought that my mission here was not accomplished yet. I felt like Finland could have given a lot to me and, at the same time, I could have given a lot of myself to such a unique country. After five years, this special adventure comes to an end. My luggage is now full of experiences, knowledge and new people that I came across.

If I am who I am now, huge merit goes to Prof. Tim Länsivaara, from Tampere University of Technology. Hence, my first and biggest thanks goes to him, who first believed that I was the right person to carry out such a demanding project. He brought me into his Geotechnical group in 2012, when I was only a young graduate, and he always made me feel his trust during all the time we worked together. Tim has definitely become one of the most important persons in my life, and I truly believe that all this was only the beginning of our cooperation. I will be lifelong grateful to him.

I would like to thank my pre-examiners, Dr. Suzanne Lacasse from the Norwegian Geotechnical Institute (NGI), Oslo, and Prof. Gustav Grimstad from the Norwegian University of Science and Technology (NTNU), Trondheim, for their valuable comments on my thesis. I express my gratitude to Prof. Emer. Michele Jamiolkowski from Politecnico di Torino, a luminary of Geotechnical Engineering, for acting as my main opponent, together with Dr. Suzanne Lacasse. I feel honored that such important and respected professionals could evaluate my research work.

I have to warmly thank my expert colleagues, Dr. Ville Lehtonen and Dr. Juho Mansikkamäki, for all the time they have dedicated to me and for their precious guidance. They have always been ready any time I felt lost in the tunnel of research, and they have never refused to give me a hand. They have followed me during all my studies, and significantly contributed to my personal as well as professional growth. Besides two workmates, I found two good friends.

I wish to express my thanks to FTA's R&D project manager Erkki Mäkelä, and to M. Sc. Jaakko Heikkilä from Arcus Oy, since without them my project would not have existed. My gratitude goes also to the TUT President's Doctoral Program from where I received most of my personal funding. I also want to thank all the people from the Department of Civil Engineering, and in particular the secretary Eija Haapaniemi, for her everlasting positive attitude.

I wish to thank Dr. Hans Petter Jostad from the Norwegian Geotechnical Institute (NGI), for his guidance during and after my stay at NGI in 2013. I am glad to have the opportunity to move to Norway and keep working with him at NGI. Another special thanks goes to Prof. Kok-Kwang Phoon and Prof. Siew Ann Tan from the National University of Singapore, for hosting me in Singapore in 2014 as a visiting student. Their contribution to the success of my work is simply priceless.

Far from home, in Finland I felt like home, thanks to the "family" that I found here in Tampere. First of all, Bruno, an amazing and trustworthy friend more than just a

colleague. I am gonna miss the vitality of Milo, the stories and the “wait a minute” of “Waqa waqa” Waqar, the king of gags Davide, the out of one’s mind expressions in Italian by Ugo, the wisdom and irony of Lucio, Kashi’s life theories, the British posture and the harmony of Matteo, the “no jela posso fà” of Leo at 11am, the unpredictability of Ale the Export Manager, the live music performances with “The Red Sofa”, the long chats and cappuccinos with Roberto, the firm “Sergio & Palmone” and “Saravopekka”, and all the awesome people that I met during the last five years. Unfortunately, I cannot list all of them as I would need an entire chapter. I will always keep you guys in my heart.

I would also like to thank all my fantastic friends from my hometown, Lanciano, and from Italy, for always keeping me into their minds. Distance does not make true friendship fade away. Fabio, Tiziano, Stefano the Doctor, Pumba, Bisby, Ludo, Luca and all the Grillstock crew. And also Manuele, my wonderful “compare”, Stefano and Niccolò, magnificent and inseparable friends.

Most important, I would like to dedicate this thesis to my father Ezio, my mother Maria Grazia, my brother Andrea, my unforgettable grandparents and all my family. I am grateful to them if I have learned what sense of duty is and to appreciate and love my life.

Last but not least, I must thank Finland. It is thanks to such an amazing place if I met what most precious I have in my life. Thank you Nelli, for supporting me during all the tough and happy moments.

Georg W. F. Hegel said: “Nothing great in the world has been ever accomplished without passion”. Let passion drive you, #FinoAllaFine.

Kiitos.

Tampere
September 2016

Marco D'Ignazio

III. TABLE OF CONTENTS

IV. NOTATION

Latin letters

a	Attraction
a^*	Area correction factor for cone resistance
a_1	Rounding ratio
b	Bias factor
c'	Effective cohesion
c_1	Shape parameter for strain-softening curve (NGI-ADPSoft model)
c_2	Shape parameter for strain-softening curve (NGI-ADPSoft model)
d	Sample diameter
e	Void ratio
k_x	Soil permeability in the horizontal direction
k_y	Soil permeability in the vertical direction
l_{int}	Internal length parameter (NGI-ADPSoft model)
m	SHANSEP exponent
m	Stress exponent (Hardening Soil model)
p'	Mean effective stress $p' = (\sigma'_1+\sigma'_2+\sigma'_3)/3$. For triaxial stress state $\sigma'_2=\sigma'_3$
p_p	Isotropic preconsolidation stress (Soft Soil model)
p^{ref}	Reference stress (often 100 kPa) in the Hardening Soil model
q	Deviatoric stress $q = (\sigma_1-\sigma_3)/2$
q	Applied load
q_c	Measured cone resistance
q_f	Maximum deviatoric stress (Hardening Soil model)
q_t	Corrected cone resistance
q_{soft}	Computed FE failure load in the Perniö failure test using NGI-ADPSoft model
q_{test}	Observed failure load in the Perniö failure test
s_u	Undrained shear strength
s_u^{PS}	Undrained shear strength from plane strain test
s_u^{TXC}	Undrained shear strength from triaxial compression

s_u^{FV}	Undrained shear strength from field vane
$s_{u(mob)}$	Mobilized undrained shear strength $s_{u(mob)} = s_u^{FV} \cdot \mu$
s_u^{re}	Remolded undrained shear strength
s_u^{A}	Undrained shear strength for active loading
$s_u^{A}{}_{ref}$	Reference undrained shear strength for active loading (NGI-ADP and NGI-ADPSoft model)
$s_u^{A}{}_{inc}$	s_u^A increase with depth (NGI-ADP and NGI-ADPSoft model)
s_u^{DSS}	Undrained shear strength for direct simple shear loading
s_u^{P}	Undrained shear strength for passive loading
s_{ur}^{A}	Residual undrained shear strength for active loading
s_{ur}^{DSS}	Residual undrained shear strength for direct simple shear loading
s_{ur}^{P}	Residual undrained shear strength for passive loading
s_u^{DSS}/s_u^{A}	Normalized direct simple shear strength
s_u^{P}/s_u^{A}	Normalized passive strength
s_{ur}^{A}/s_u^{A}	Normalized residual active strength
s_{ur}^{DSS}/s_u^{A}	Normalized residual direct simple shear strength
s_{ur}^{P}/s_u^{A}	Normalized residual passive strength
s_u^{avg}	Average undrained shear strength $s_u^{avg} = (s_u^A + s_u^{DSS} + s_u^P)/3$
s_{up}	Peak undrained shear strength
$s_{u\ 15\%}$	Undrained shear strength at 15% of axial strain
s_{uv}	Undrained shear stress mobilized on the vertical plane of the vane
s_{uh}	Undrained shear stress mobilized on the horizontal plane of the vane
s_{uv}	Undrained shear stress from dry crust samples cut vertically
s_{uh}	Undrained shear stress from dry crust samples cut horizontally
p_n	Shear stress distribution factor for horizontal shear planes
t_{sb}	Shear band thickness
u	Pore pressure
u_x	Displacement in horizontal direction
u_0	Hydrostatic pore pressure
u_2	Pore pressure acting behind the cone
$\boldsymbol{x}_i$	Integration point coordinate
x_{ref}	Reference x-coordinate for $s_u^{A}{}_{ref}$ (NGIADPSoft model)
y_{ref}	Reference depth for $s_u^{A}{}_{ref}$ (NGIADPSoft model)

$\Delta y_{ref}/\Delta x$	Reference depth gradient (NGI-ADPSoft model)
w	Water content
$w(\boldsymbol{x})$	Gauss distribution function for non-local strain
z^*	Depth where $\Delta s_u = 0$
A	Plastic resistance number
B	Ratio between creep index and compression index
C_c	Compression index
C_s	Swelling index
C_α	Creep index
E	Elastic loading/unloading stiffness
E_{50}	Secant modulus at 50% strength in the Hardening Soil model
E_{oed}	Oedometer modulus
E_{ur}	Young's modulus for unloading reloading
F	Yield function
F	Multivariable function
F_{soft}	Peak s_u reduction factor for perfectly plastic analysis
G_0	Initial shear modulus (also G_{max})
K_0	Lateral earth pressure coefficient
K_0^{nc}	K_0 of normally consolidated soil
N_{kt}	Cone factor for undrained shear strength from q_t
$N_{\Delta u}$	Cone factor for undrained shear strength from u_2
$N_{kt}(\sigma'_p)$	Cone factor for preconsolidation pressure from q_t
P_a	Atmospheric pressure (101.3 kPa)
R_f	Failure ratio (Hardening Soil model)
S	SHANSEP strength ratio for normally consolidated clay
S_r	Degree of saturation
S_t	Sensitivity ($S_t = s_u/s_u^{re}$)
T	Tangent elasto-plastic modulus
Y_i	Secondary input parameter
V	Integral of $w(\boldsymbol{x})$
V_s	Shear wave velocity (m/s)

Greek symbols

α	Factor which defines the ratio of undrained shear strength and consolidation stress
α	Non-local strain parameter (NGI-ADPSoft model)
δ	Coefficient of variation of ε
Δ	Increment
ε	Axial strain
ε	Variability term with mean = 1 and COV = δ
$\boldsymbol{\varepsilon}^p$	Plastic strain
$\boldsymbol{\varepsilon}^p$*	Non-local strain
ϕ'	Effective friction angle
γ_{tot}	Total unit weight
γ'	Submerged unit weight
γ	Shear strain (%)
γ_s	Deviatoric shear strain
$\gamma_p{}^C$	Shear strain at peak in triaxial compression
$\gamma_p{}^{DSS}$	Shear strain at peak in direct simple shear
$\gamma_p{}^E$	Shear strain at peak in triaxial extension
$\gamma_r{}^C$	Shear strain at residual state in triaxial compression
$\gamma_r{}^{DSS}$	Shear strain at residual state in direct simple shear
$\gamma_r{}^E$	Shear strain at residual state in triaxial extension
γ_p	Plastic shear strain
$\gamma_p{}^p$	Plastic peak shear strain
$\gamma_r{}^p$	Plastic residual shear strain
κ_*	Modified swelling index (Soft Soil model)
κ_1	Hardening control parameter (NGI-ADP and NGI-ADPSoft model)
κ_2	Softening control parameter (NGI-ADPSoft model)
λ	Plastic multiplier
λ*	Modified compression index (Soft Soil model)
μ	Correction factor for field vane strength based on plasticity
μ_r	Correction factor for rate effect in the dry crust

μ_d	Correction factor for disturbance due to vane insertion in the dry crust
$\underline{\sigma}$	Stress increment vector
σ	Standard deviation
σ'_v	Vertical effective stress
σ'_p	Vertical preconsolidation pressure
σ'_{pCRS}	Vertical preconsolidation pressure from CRS oedometer test
σ'_{pIL}	Vertical preconsolidation pressure from IL oedometer test
σ_c	Cell pressure
σ_v	Vertical total stress
σ_{v0}	Initial vertical total stress
σ'_{v0}	Initial vertical effective stress
τ	Shear stress
τ_0/s_u^A	Initial mobilization $\tau_0 = (\sigma_{10}-\sigma_{30})/2$ (NGI-ADP and NGI-ADPSoft model)
ν'	Effective Poisson's ratio
ν_{und}	Undrained Poisson's ratio
ξ	Reduction factor for DSS strength increment
ψ	Dilatancy angle

Acronyms

ADP	Acronym for undrained analysis based on active (A), direct simple shear (D) and passive (P) types of loading
CIUC	Isotropically consolidated undrained triaxial compression test
CK_0UC	K_0-consolidated undrained triaxial compression test
CK_0UE	K_0-consolidated undrained triaxial extension test
COV	Coefficient of variation
CPTU	Piezocone test
CRS	Constant rate of strain oedometer test
CSL	Critical state line
DSS	Direct simple shear
FEM	Finite Element Method

FOS	Factor of safety
FTA	Finnish Transport Agency
FV	Field vane test
IL	Incrementally loaded oedometer test
LEM	Limit Equilibrium Method
LI	Liquidity index
LL	Liquid limit
MIT	Massachusetts Institute of Technology
NGI	Norwegian Geotechnical Institute
OCR	Overconsolidation ratio
OCR_{CRS}	Overconsolidation ratio from CRS oedometer test
OCR_{IL}	Overconsolidation ratio from IL oedometer test
PI	Plasticity index
PL	Plastic limit
POP	Pre-overburden pressure
SHANSEP	Stress History and normalized Soil Engineering Properties
TXC	Triaxial compression
TXE	Triaxial extension
TUT	Tampere University of Technology

Common subscripts

$_0$	Initial state
$_1$	Major principal stress or strain
$_3$	Minor principal stress or strain
$_p$	Preconsolidation state
$_r$	Residual state

Common superscripts

^{A}	Active
^{DSS}	Direct Simple Shear

P	Passive
C	Compression (triaxial)
E	Extension (triaxial)
PS	Plane strain

1. Introduction

1.1 Background and scope of the research work

A notable part of the Finnish railway network is built on soft soils, especially in coastal areas. Geotechnical design in these areas is still nowadays quite challenging, mainly because of the high compressibility and the low shear strength (as low as less than 10 kPa near the ground surface) of the subsoil.

The continuously evolving society requires increase in efficiency and capacity of the railway transportation, meaning that the traffic loads (i.e. axle loads of freight trains) should be increased. As a consequence, this would have a negative impact on the stability of geotechnical structures (e.g. railway embankments) because of the increased allowable load intensity. Therefore, stability conditions of railway tracks should be systematically assessed and monitored in order to fulfil the safety requirements before increasing the axle loads.

In soft soil areas such aspects become of great importance for both new and existing embankments. Stability on the weak natural subsoil may not be guaranteed for the new design loads and, hence, countermeasures may be necessary (e.g. soil improvement) to meet the required safety level.

For embankments built on soft clay foundations, the most critical situation occurs when the load is applied quickly enough to generate excess pore pressure during loading. Pore pressures do not have sufficient time to dissipate because of the low permeability of the soil. As a consequence, the available shear strength in the soil is lower than if the pore pressures were dissipated during the loading process. Such a behavior is commonly referred to as “undrained” or “short-term”, as opposed to the “drained” or “long-term” behavior.

The available soil resistance under undrained conditions is called “undrained shear strength” (s_u). Undrained shear strength is the most important parameter in undrained stability calculations of embankments, and, therefore, it should be carefully and reliably assessed.

Undrained shear strength can be determined in several ways, from both in-situ and laboratory tests. In several countries, including Finland and Sweden, s_u is normally assessed from the field vane test. The main reason is that field vane test is a cost-effective test that is performed directly on site within a relatively short time frame. The most commonly used vane apparatus is the Nilcon vane tester, equipped with a slip coupling located above the vane to measure rod friction during testing. However, a recent study by Ukonjärvi (2016) revealed that the Nilcon vane may provide unrealistically low undrained shear strength values because of the too large rod friction measured, as the slip coupling does not always work as planned. This underestimation may lead to too conservative design solutions.

Unreliable determination of soil parameters will directly affect the results of stability calculations, regardless whether the analyses are carried out using the “$\phi = 0$” approach in Limit Equilibrium Method (LEM) or the Finite Element Method (FEM).

In this perspective, the Finnish Transport Agency commissioned and funded the RASTAPA research project (2009-2015). The project was carried out by the Tampere University of Technology, with the main purpose of enhancing the "state-of-practice" of stability calculation methods in soft clays and to develop new tools of practical usefulness for everyday design tasks.

Two doctoral theses have been already published in relation to the RASTAPA project. Mansikkamäki (2015) studied the applicability of several finite element models for undrained effective stress stability analysis in soft Finnish clays. Lehtonen (2015) focused on modelling undrained shear strength and excess pore pressure in Limit Equilibrium Method based on effective strength parameters.

The main purpose of this thesis is to improve the knowledge and modelling of undrained shear strength of Finnish clays for total stress stability analyses. The work is directly linked to the RASTAPA project, and is complementary to the work done by Lehtonen (2015) and Mansikkamäki (2015).

This thesis aims to improve the "state-of-practice" of undrained shear strength evaluation and modelling for total stress stability calculations of embankments on Finnish clays. Correlations for s_u specific to Finnish clays are presented for the first time. Aspects such as strength anisotropy and strain-softening behavior of sensitive clays, shear strength of surficial weathered clays and undrained shear strength increase under old embankments are studied and critically discussed. The advantage over traditional methods would be smaller uncertainty in the calculated safety level.

1.2 Issues related to undrained shear strength for total stress stability analyses

A typical soil profile that is applicable for stability problems in Finnish railway environment includes the embankment, possibly fill layers on the subgrade, a stiff layer of weathered clay, and soft soil layers (clay and/or silt) underlain by stiffer coarse layers and/or bedrock.

With regard to embankments stability, the most problematic layers are generally the soft layers, where the majority of deformations tend to localize. In Finland, and in general in Scandinavia, soft clays or silts are mostly normally consolidated or slightly over consolidated. The overconsolidation is, in most of the cases, due to aging (e.g. Bjerrum 1973).

Finnish clays are further characterized by medium to high plasticity and they often belong to the family of "sensitive" clays. Sensitive clays are classified based on their sensitivity (S_t), defined as $S_t = s_u/s_u^{re}$ where s_u is the undrained shear strength and s_u^{re} is the remolded undrained shear strength, defined from a standard test such as field vane in the field or fall cone in the laboratory. According to SFS-EN ISO 14688-2 (2004), sensitivity is low when $S_t < 8$, medium when $S_t = 8 - 30$ or high when $S_t > 30$. Clays with $S_t > 50$ are referred to as "quick" clays. The undrained shear strength can be even lower than 10 kPa near the ground surface. For very sensitive clays or quick clays, the remolded undrained shear strength (s_u^{re}) can be lower than 0.5 kPa (e.g. Locat and Demers 1988; Karlsrud and Hernandez-Martinez 2013).

According to the Finnish guidelines for stability analyses (Ratahallintokeskus 2005), the undrained safety level of a railway embankment is determined referring to a situation where a train is standing still on the tracks. The traffic load is essentially short-term and the subsoil response must be considered as undrained even for fully consolidated soil layers located underneath old embankments. Hence, undrained shear strength is the key parameter.

As earlier mentioned, in Finnish design practice undrained shear strength is normally determined from field vane tests, with all the uncertainties related to test execution and testing apparatus. The undrained shear strength s_u from field vane is hence corrected according to e.g. Bjerrum (1972) and given as an input parameter in a "$\phi = 0$" analysis in Limit Equilibrium Method (LEM). A factor of safety (FOS) is, hence, evaluated.

Nevertheless, lots of uncertainties underlie the measurements that are later converted into design values, especially when using the Nilcon vane (Ukonjärvi 2016). Indeed, because of the high rod friction measured, s_u may be severely underestimated. There are cases where s_u seems to remain almost constant or even decrease with depth at great depths, which is simply unrealistic (Mansikkamäki 2015). As a consequence, the FOS obtained from total stress stability calculations, where s_u is given as an input parameter, will result unrealistically low.

Undrained shear strength is a rather complex parameter. For a given soil element, there is no unique value of s_u. Besides all the uncertainties coming from testing, s_u is further affected by some physical factors. Among them, the dependencies of undrained shear

strength on preconsolidation pressure, shearing rate and direction of loading are probably the most significant. Therefore, parameter selection for stability calculation becomes generally very challenging, especially when soil investigation is limited or affected by poor quality of the recovered test specimens.

The undrained shear strength predicted by field vane can be used as input parameter in both LEM and FEM analyses. Unlike LEM, finite element method requires the additional input of stiffness parameters. Therefore, some existing correlations for soil stiffness must be used (e.g. Duncan and Buchignani 1976) if laboratory test results are not available.

The undrained behavior of sensitive clays is further characterized by special features such as s_u anisotropy and strain-softening behavior in the post-peak regime. In Finland, these aspects are normally neglected in design, as extensive testing would be required for a thorough understanding of the phenomena, even though they may significantly affect the stability.

Moreover, strength of dry crust layers, which commonly overlay soft clay layers, is normally characterized by high uncertainty because of the non-homogenous structure of the weathered clay. The undrained shear strength s_u in such layers is often approximate from the field vane test through empirical rules (e.g. Leroueil et al. 1990) and often assumed as a constant.

For railway embankments built on normally or slightly overconsolidated clays, as in Finnish coastal areas, the consolidation process induced by the embankment load is likely to cause an increase in preconsolidation pressure and, consequently, in undrained shear strength in the clay layers. Such a favourable result may turn useful when the impact of the increased traffic loads on the railway truck has to be evaluated. By thoughtfully accounting for this phenomenon, more economical solutions can be adopted in case stability needs to be improved. For some cases, stability countermeasures may not be necessary if the strength increase guaranteed the required safety level.

1.3 Aim and premise of the work

The primary objective of this thesis is to enhance the knowledge and modelling of undrained shear strength of Finnish clays for stability analyses of embankments. Specifically, the following aspects have been addressed in this work:

i) Derivation of transformation models for undrained shear strength (s_u) specific to Finnish clays.

A multivariate database of field vane data points from 24 test sites from Finland is used for the purpose of deriving new transformation models specific to Finnish clays, to convert basic clay properties into undrained shear strength. The new correlation equations are validated through an independent database of field vane data points from Sweden and Norway. The aim is to quantify the uncertainty of the existing transformation models for s_u and develop new transformation models for Finnish clays characterized by lower uncertainty than the commonly used correlations for s_u.

ii) Investigate the importance of strength anisotropy and strain-softening in stability calculations.

The practical implications of taking into account some special features of sensitive clays, including anisotropy of undrained shear strength and post-peak strain-softening, are evaluated through a finite element (FE) study of the Perniö failure test (Lehtonen et al. 2015). Strength and stiffness parameters of Perniö clay are thoroughly defined from laboratory as well as field tests, and exploited for advanced modelling using the user-defined total stress NGI-ADPSoft soil model (Grimstad et al. 2010), implemented in PLAXIS 2D. The aim is to study the importance of modelling s_u anisotropy and strain-softening in stability analyses on Finnish sensitive clays.

iii) Improve the modelling of undrained shear strength of dry crust layers.

Dry crust layers have formed because of weathering and cementation processes and they normally consist of stiff organic bonded clay. A correct assessment of the soil properties of these layers is quite challenging because of their non-uniform structure. Some authors (e.g. La Rochelle 1974) reported how field vane test tends to overestimate the available shear strength in the clay crust and, therefore, alternative testing is needed for a reliable estimate of s_u. In this study, the aim is to assess the reliability of conventional laboratory tests for determining the mechanical properties of Perniö dry crust. The FE analysis of Perniö failure test will act as a validation tool.

iv) Evaluate the undrained shear strength increase under old embankments due to consolidation.

For embankments that have been consolidating for several years, the available undrained strength in the clayey subsoil has increased and a positive effect is expected on the factor of safety. Taking this aspect into account would possibly guarantee sufficient safety level

against the increasing traffic loads, thus leading to a more cost-effective design. In order to study this phenomenon in Finnish clays, measurements from the Murro test embankment are exploited to assess the increase in undrained shear strength under the embankment after several years of consolidation. The aim is to derive a simple methodology to model the phenomenon of s_u increase in practice.

2. Factors affecting the undrained shear strength of clays

2.1 Undrained shear strength as a function of preconsolidation pressure

The undrained shear strength is commonly approximated as a function of the preconsolidation pressure (σ'_p) which is obtained from the oedometer stress-strain curve. A positive trend between undrained shear strength (s_u) and preconsolidation pressure (σ'_p) has been reported by several authors. For instance, Mesri (1975) suggested, based on the data of Bjerrum (1972), that the in-situ mobilized undrained shear strength [$s_{u(mob)}$] along a failure surface is a linear function of the preconsolidation pressure [eq. (2.1)].

$$s_{u(mob)} = \alpha \cdot \sigma'_p \tag{2.1}$$

Mayne and Mitchell (1988) confirmed that there is a direct proportionality between undrained shear strength from field vane and preconsolidation pressure from oedometer tests (Fig. 2.1), thus validating the concepts expressed by Mesri (1975).

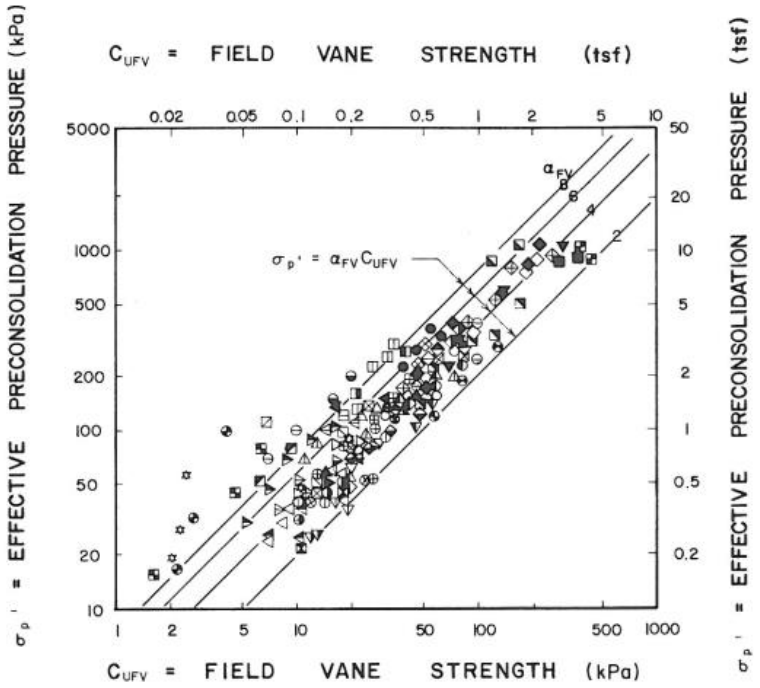

Fig. 2.1: Observed relationship between apparent preconsolidation pressure from laboratory oedometer and field vane (Mayne and Mitchell 1988).

Ladd and Foott (1974) proposed a framework to describe the variation of s_u with OCR [eq. (2.2)]:

$$\frac{s_u}{\sigma'_v} = S \cdot OCR^m = \left(\frac{s_u}{\sigma'_v}\right)_{NC} \cdot \left(\frac{\sigma'_p}{\sigma'_v}\right)^m \tag{2.2}$$

where S and m are coefficients dependent on the material and the test type. S is the normalized undrained shear strength for normally consolidated state, while m governs the shape of the $s_u = f(\text{OCR})$ function.

Eq. (2.3) can be reorganized to give the s_u/σ'_p ratio as a function of OCR [eq. (2.3)]:

$$\frac{s_u}{\sigma'_p} = S \cdot OCR^{(m-1)} \tag{2.3}$$

This framework is commonly known as SHANSEP (Stress History and Normalized Soil Engineering Properties) (Ladd and Foott 1974). The SHANSEP model was later adopted and validated by several authors (for example, Jamiokowski et al. 1985; Larsson et al. 2007; Karlsrud and Hernandez-Martinez 2013).

The exponent m was observed to vary between 0.75 and 0.95 (Jamiolkowski et al. 1985), thus indicating that the relationship s_u-σ'_p is generally non-linear. Note that $m = 1$ would reduce eq. (2.2) to eq. (2.1) with $S = \alpha$.

Ching and Phoon (2012) and Ching and Phoon (2014*c*), based on a global database consisting of 6310 clay data points collected from several studies, concluded that m appears to be significantly lower than 1 on average, regardless of the test type performed. In particular, Ching and Phoon (2014*c*) reported that m values for CIUC, CK_0UC, CK_0UE, and DSS are significantly less than 1, in agreement with the findings of Kulhawy and Mayne (1990), and that the hypothesis $m = 1$ can be rejected with 95% confidence.

Based on critical state soil mechanics, the assumption $m = 1$ seems in principle erroneous. For instance, the modified Cam Clay model (Schofield and Wroth 1968) predicts $m = 1 - C_s/C_c$, where C_c and C_s are the compression and swelling indices, respectively, of a clay. This implies that m is always lower than 1 for normally consolidated to lightly overconsolidated clays, which are known to be properly modelled by modified Cam Clay. (Ching and Phoon 2014*c*)

Karlsrud and Hernandez-Martinez (2013) observed, for Norwegian clays, $S = 0.08$~0.35 and $m = 0.844$~0.95, depending on the test type, water content/plasticity and sample quality.

A detailed review of existing correlations for undrained shear strength and a closer look at S and m parameters is given in section 2.5.

Finally, an increase in preconsolidation pressure due to consolidation under an external load (e.g. embankment load) will lead to an increase in undrained shear strength, as suggested by eq. (2.1) and eq. (2.2). This aspect is though fully surveyed in Chapter 4.

2.2 Undrained shear strength as a function of strain rate

Undrained shear strength is not a unique parameter. The rate of strain used in a test will affect s_u because of the viscoplastic properties of clays. In general, soft clay behavior is largely influenced by creep, as reported by several authors (e.g. Arulandan et al. 1971; Holzer et al. 1973; Augustesen et al. 2004).

Constant rate of strain (CRS) oedometer test results have shown how the preconsolidation pressure tends to increase with increasing strain rate. (Vaid et al. 1979; Graham et al. 1983; Leroueil et al. 1985; Länsivaara 1995, 1999).

The effect of strain rate on the preconsolidation pressure of Finnish clays is described by Länsivaara (1995, 1999, 2012) and shown by eq. (2.4):

$$\frac{\sigma'_{p2}}{\sigma'_{p1}} = \left(\frac{\dot{\varepsilon}_2}{\dot{\varepsilon}_1}\right)^B \qquad (2.4)$$

Where σ'_{p2} and σ'_{p1} are the preconsolidation pressure values from CRS oedometer tests executed at strain rates $\dot{\varepsilon}_2$ and $\dot{\varepsilon}_1$, respectively. The variation of preconsolidation pressure with rate of strain was found to be a function of the ratio between the creep index and the compression index of the soil ($B=C_\alpha/C_c$). For Finnish clays, Länsivaara (1995; 1999; 2012) suggested B = 0.068-0.079 (trend line in Fig. 2.2). For instance, for B = 0.068-0.079 and $\dot{\varepsilon}_2/\dot{\varepsilon}_1$ = 10, the preconsolidation pressure is increased by 17-20%.

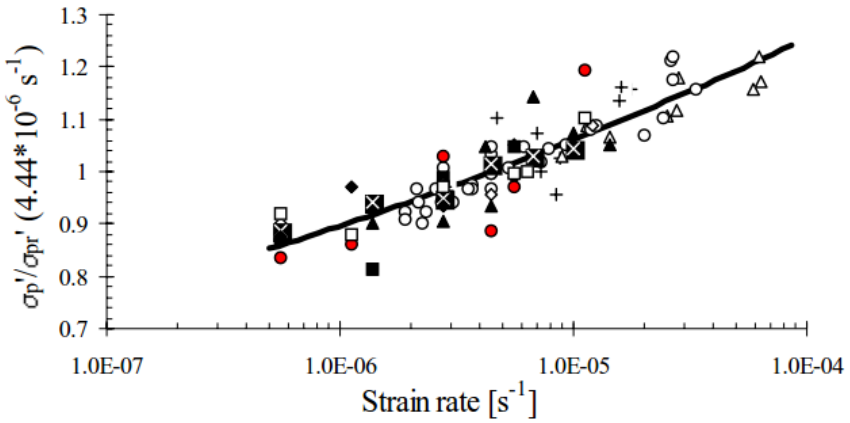

Fig. 2.2: Normalized preconsolidation pressure-strain rate relationship for Finnish clays, 11 sites (Länsivaara 1995).

It is common practice in Finland, as in other countries such as Norway or Sweden, to determine the preconsolidation pressure from CRS oedometer tests. As suggested by Leroueil et al. (1985), Leroueil (1988) and Leroueil (1996), stress-strain curves from CRS oedometer tests differs quite significantly from those provided by conventional 24 h incrementally loaded (IL) oedometer tests. σ'_p will result larger in CRS than in the 24h IL test because of strain rate effects (Leroueil 1996). In addition, Leroueil (1996) indicated that the preconsolidation pressure from CRS oedometer test (σ'_{pCRS}) is typically 25% larger than σ'_p deduced from IL test (σ'_{pIL}). For one site in Finland, Kolisoja et al. (1989) reported $\sigma'_{pCRS}/\sigma'_{pIL}$ equal to 1.16. Hoikkala (1991) observed $\sigma'_{pCRS}/\sigma'_{pIL}$ equal to 1.3 for three different Finnish sites. Länsivaara (1999), based on the data collected by Leroueil

(1996) on clays from several countries, suggested $\sigma'_{pCRS}/\sigma'_{pIL}$ = 1.27. Karlsrud and Hernandez-Martinez (2013) reported, for Norwegian clays, $\sigma'_{pCRS}/\sigma'_{pIL}$ equal to 1.10-1.18.

Kulhawy and Mayne (1990) observed that also undrained shear strength changes as a function of strain rate during loading. In general, for a log cycle increase in strain rate, s_u increases by 10%. By considering a testing rate of 1%/h as a standard reference rate, the variation of s_u with rate of strain can be expressed as:

$$\frac{s_u}{s_{u(1\%/h)}} = 1.0 + 0.1\left[\log_{10}(rate/1\%)\right] \qquad (2.5)$$

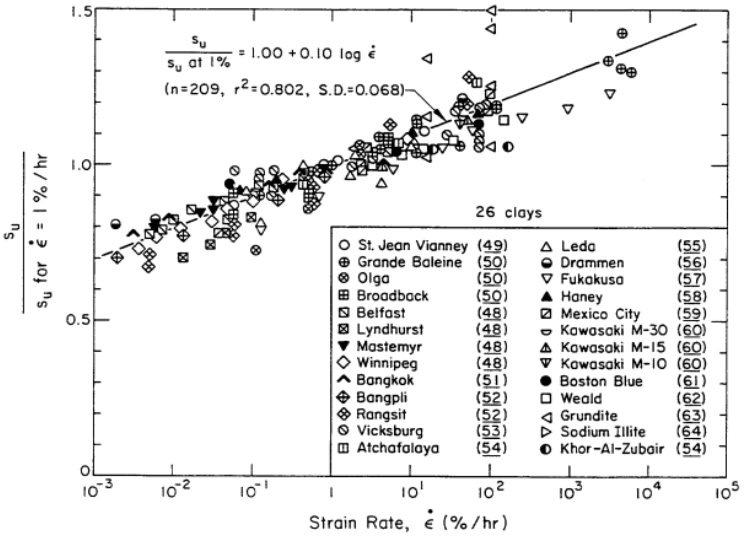

Figure 4-46. Strain Rate Influence on s_u

Fig. 2.3: Strain rate influence on s_u (Kulhawy and Mayne 1990).

More in general, when soft clays are subjected to "fast" undrained loading, the stress-strain response will be stiffer than in a "slow" type of loading (Berre and Bjerrum 1973, Lefebvre and Leboeuf 1987, Graham et al. 1983, Leroueil et al. 1985).

Fig. 2.4 shows the impact of strain-rate on clay specimens sheared at different testing speeds in undrained triaxial compression. Both peak and post-peak response are influenced by the rate of strain used the test. On the other hand, peak strains at failure do not seem to be influenced by the different loading rate. Moreover, as illustrated by Fig. 2.4*b*, smaller build-up of excess pore pressure will result in higher shear stresses generated.

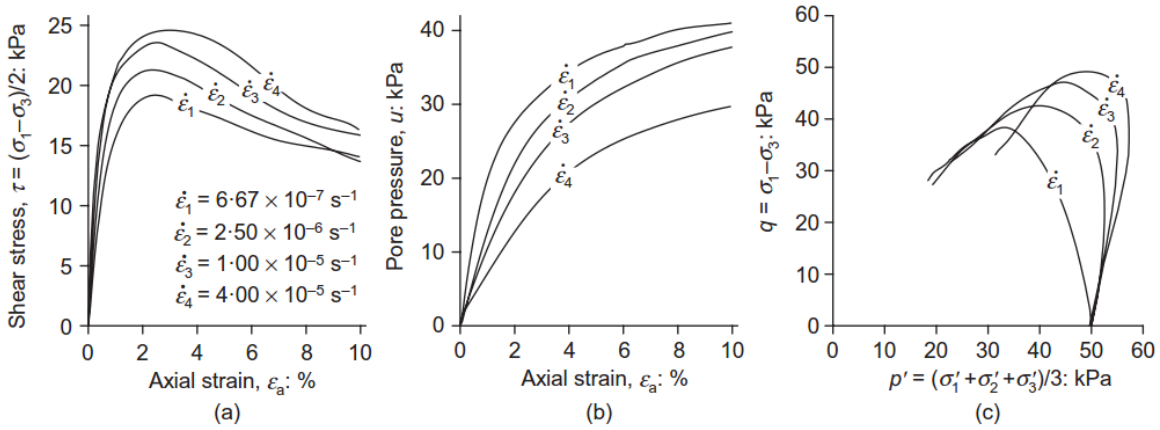

Fig. 2.4: Triaxial test results illustrating the effect of shear rate on *a*) shear stress, *b*) excess pore pressure, *c*) effective stress paths (Lehtonen et al. 2015)

Studies carried out by Arulandan et al. (1971) and Holzer et al. (1973) have shown that failure can occur in soft clays under an applied constant load even several days after the load has been applied. Such a phenomenon is commonly referred to as "undrained creep". The viscous properties of clays and the rate/time dependent behavior of shear-induced pore pressure let the clay sustain the load for certain period of time before failure occurs.

Arulandan et al. (1971), based on undrained creep triaxial tests, observed that there is a threshold level of deviator stress beyond which undrained creep will lead first to an increase in rate of strain and pore pressure and then rupture. Time to failure was found to be inversely proportional to the deviator stress level reached.

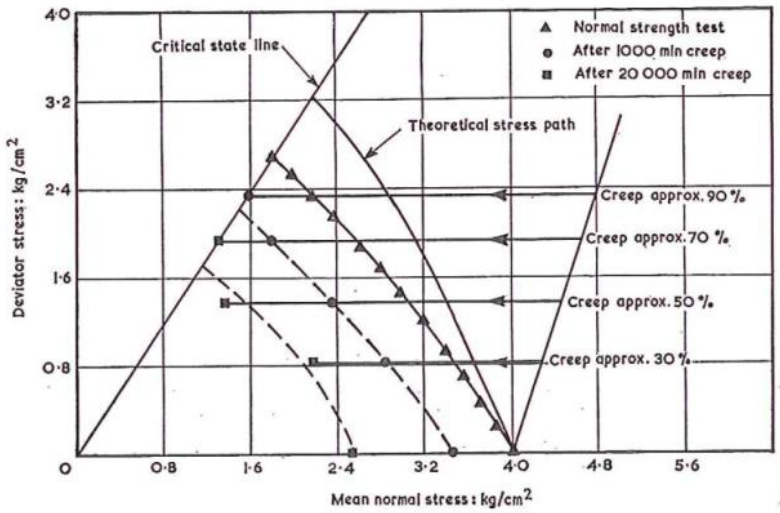

Fig. 2.5: Undrained creep at various deviator stress levels (in percentage of a reference compression test) (Arulandan et al. 1971).

2.3 Creep and aging effects

Creep can be defined as the ongoing deformation under a constant applied load, caused by the viscous properties of the soil skeleton.

For geotechnical structures built on soft clay deposits, creep behavior may significantly affect both design and performance of the structure during its lifetime.

According to Bjerrum (1973), a clay which has come to equilibrium under its own weight without experiencing any significant secondary consolidation can be classified as "young" normally consolidated clay. "Young" clays are just capable of carrying their self-weight. Any additional load will cause relatively large settlements.

On the other hand, when a "young" clay is subjected to secondary or delayed consolidation under its own weight for hundreds or thousands of years, it will be subjected to further settlement (Bjerrum 1973; Hanzawa 1995). As a consequence, the structural arrangement of particles will result in a more stable configuration, meaning greater apparent preconsolidation pressure and, hence, greater strength and reduced compressibility. Under some favorable chemical conditions, cementation of the soil skeleton may also occur, caused by chemical reactions, providing the clay with additional strength (Suzuki and Yashuara, 2007).

Fig. 2.6 shows field vane test results for a "young" and an "aged" clay. A clear difference in the measurements can be observed. The aged clay possesses higher strength resulting from the increased apparent preconsolidation pressure caused by a "structuration" process.

In terms of undrained stress-strain response, such aged or structured clays normally exhibit high distinct peak shear strengths. Beyond peak state, the shear strength reduces dramatically as a result of bonds breakage and loss of structure, with consequent generation of excess pore pressure.

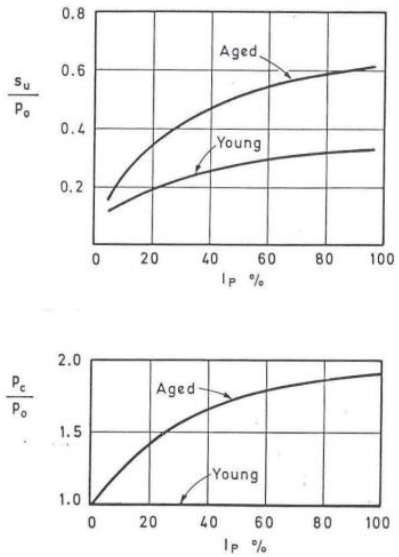

Fig. 2.6: Typical values of normalized field vane strength ($s_u/p_0=s_u^{FV}/\sigma'_v$) and p_c/p_0 (or σ'_p/σ'_v=OCR) observed in late glacial and post glacial clays (after Bjerrum 1973).

2.4 Anisotropy of undrained shear strength

A major aspect characterizing soft sensitive clays is the dependency of undrained shear strength on the stress path followed during undrained shearing, namely the anisotropy. Anisotropy is often neglected in design, even though it might both positively or negatively affect the performance of a geotechnical structure.

Stress-strain-strength anisotropy can originate from stress-induced anisotropy as well as inherent anisotropy, induced by the depositional characteristics of the subsoil (Bjerrum 1973; Hicher et al. 2000; Karstunen et al. 2005). Shape and orientation of the clay particles are likely to cause structural anisotropy. Particles orientation is likely to be induced by some electrochemical properties. In addition, more macroscopic structure can be found in varved layers of variable particle size. (Jamiolkowski et al. 1985)

In slope stability and bearing capacity problems of shallow and deep foundations, strength anisotropy plays a key role, as the undrained shear strength is known to vary along the slip surface based on orientation and magnitude of the major principal stresses (Bjerrum 1973).

In Finnish engineering design practice, stability analyses of e.g. embankments are normally conducted as total stress analysis using an average isotropic undrained shear strength determined by field vane test. However, the undrained shear strength is highly anisotropic and this should be accounted for, as often done in Norway and Sweden.

Bjerrum (1973) proposed a simple approach to model the varying anisotropic undrained shear strength along a slip surface. The method consisted of measuring undrained shear strength from test types which are relevant to different locations of the potential failure surface. This approach is called "*ADP*", where "*A*" stands for active, "*D*" for direct shear and "*P*" for passive (Fig. 2.7).

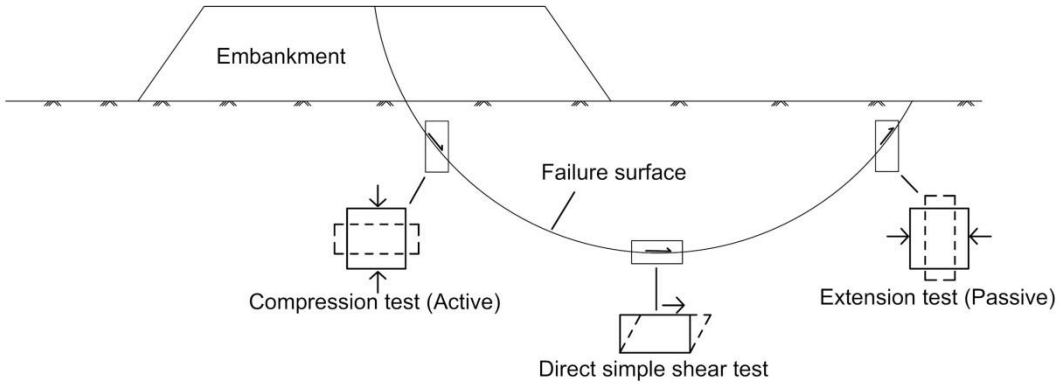

Fig. 2.7: Anisotropic strength along a slip surface (after Bjerrum 1973).

Anisotropy can be reliably measured in the laboratory through triaxial (or plane strain) compression and extension tests together with direct simple shear tests, provided that the soil specimens are anisotropically consolidated, before shearing, at stress level representative of the in-situ conditions (Bjerrum and Landva 1966; Berre 1969; Bjerrum 1973).

Experimental observations indicated that the stress-strain response of clay specimen sheared in compression (active, triaxial or plane strain) or in extension (passive, triaxial or plane strain), may be quite different. Dissimilarities do not only involve the measured shear stresses (strength anisotropy), but also the shear strains required to mobilize peak strengths according to the direction of the major principal stress.

In general, for normally consolidated to slightly overconsolidated soft clays, the shear strain level needed to mobilize the compression, or active, strength (inclination of major principal stress is 0° from the vertical), is lower than the shear strain that would mobilize the extension, or passive, strength (inclination of major principal stress is 90° from the vertical). This is true even for isotropically consolidated samples, indicating that fabric anisotropy has a major role (Jamiolkowski et al. 1985). In addition, the strength for direct simple shear (DSS) conditions is normally mobilized to a strain level between compression and extension, as suggested by the experimental results by e.g. Karlsrud and Hernandez-Martinez (2013) shown in Fig. 2.8.

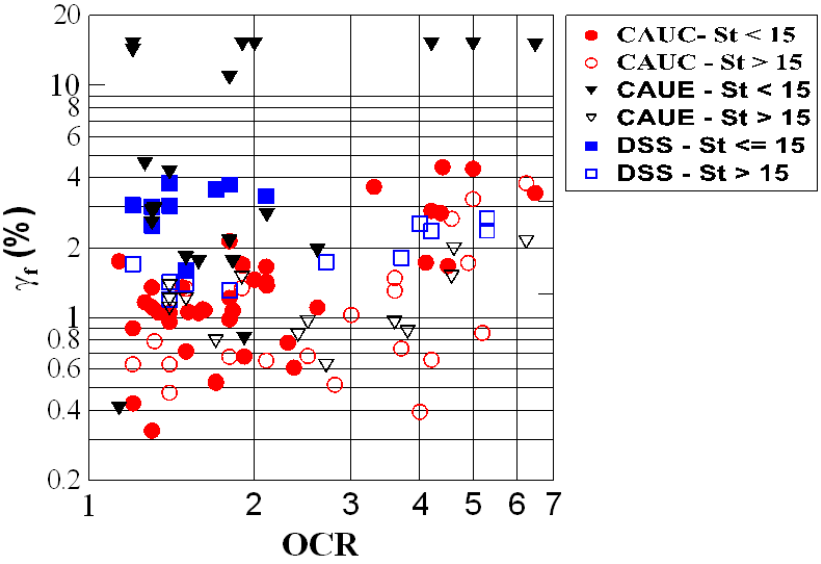

Fig. 2.8: Shear strains at failure versus OCR (Karlsrud and Hernandez-Martinez 2013).

According to Bjerrum (1973), Ladd et al. (1977), Larsson (1980) and Jamiolkowski et al. (1985), the anisotropy is lowest when the clay is highly plastic, while anisotropy increases with decreasing plasticity. The main implication is that there is a positive trend between the anisotropy ratio s_u^P/s_u^A and the liquid limit or plasticity index of the soil. s_u^P and s_u^A are the peak undrained shear strengths from triaxial or plane strain extension and compression tests, respectively. The observed trend was further verified for the anisotropy ratio in direct simple shear (s_u^{DSS}/s_u^A) by the same authors (Fig. 2.9).

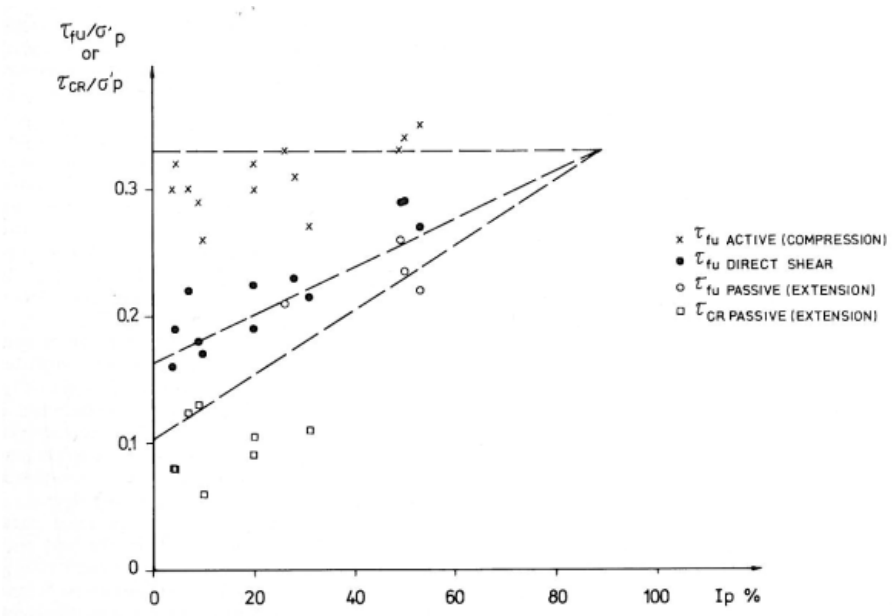

Fig. 2.9: Normalized undrained shear strength from some Scandinavian inorganic clays (Larsson 1980).

However, Mayne (1983) and Won (2013) pointed out that such a trend might lack of consistency as it is based on limited test results and might have been influenced by the definition of failure in extension tests (Won 2013). Dependency of anisotropy on plasticity index should be though verified by careful examination of site characteristics, clay structure, mineralogy, soil history and spatial variability (Won 2013).

Failure in triaxial extension tests can be defined in two ways, according to Tanaka et al. (2001):

- Definition A: strength at the same strain level (typically less than 2%) as the peak strength from a compression test
- Definition B: peak strength (necking failure) or strength at 15% of axial strain if the peak is not observed.

Based on the adopted definition, undrained shear strength from triaxial extension tests can notably change, as briefly illustrated in Fig. 2.10. The difference in anisotropy ratio between two definitions can be considerably high, as shown in Fig. 2.11.

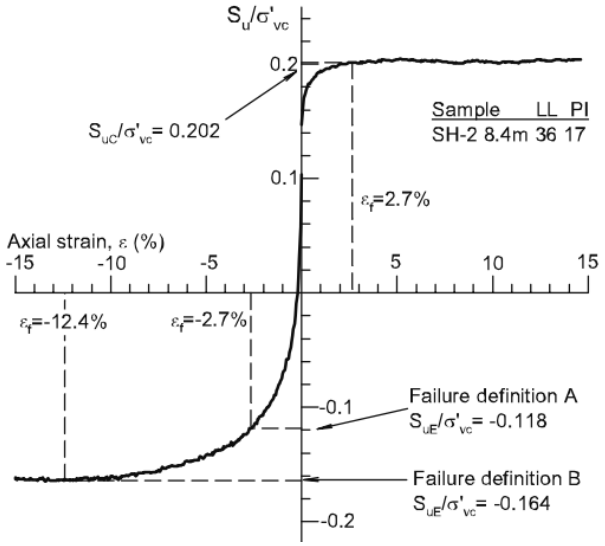

Fig. 2.10: An example of the definitions of failure for CK_0UE test (Won 2013).

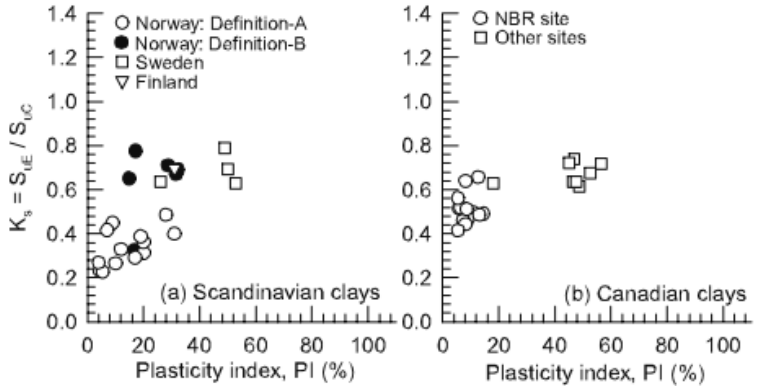

Fig. 2.11: Anisotropic strength ratio versus plasticity index for *a*) Scandinavian clays and *b*) Canadian clays (adapted after Won 2013).

Thakur et al. (2014*b*) collected data on anisotropic undrained shear strength of Norwegian clays measured from triaxial compression, direct simple shear and triaxial extension tests. The anisotropic strength ratio for both extension and DSS conditions was found to be linearly depending on the plasticity index (Fig. 2.12).

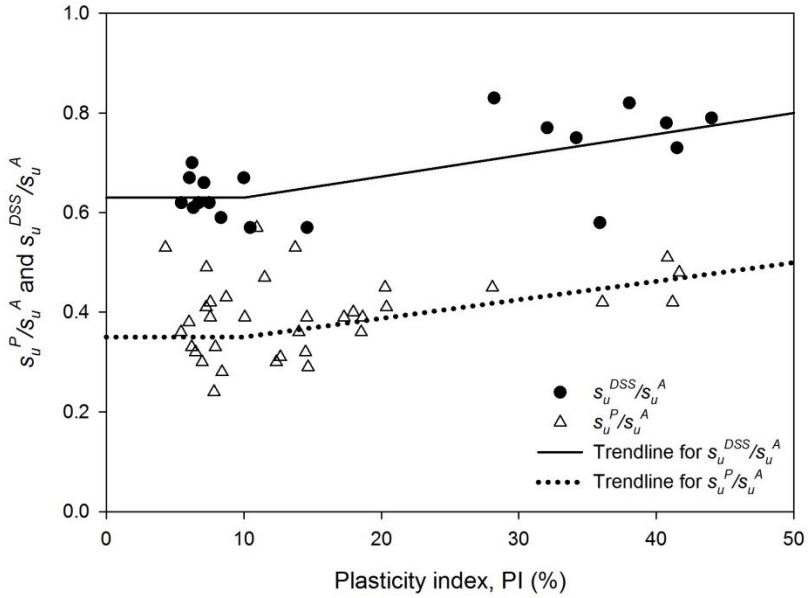

Fig. 2.12: Anisotropy ratio vs plasticity index for Norwegian clays (after Thakur et al. 2014*b*)

In Table 2.1 s_u^{DSS}/s_u^A and s_u^P/s_u^A values for several clays from different studies are summarized. Table 2.1 suggests a fairly high variability of the anisotropic strength ratio. s_u^P/s_u^A values range from 0.30 to 0.81, while s_u^{DSS}/s_u^A values vary between 0.53 and 0.89.

Nevertheless, anisotropy can be further defined from the effective stress point of view. Anisotropy is more generally referred to as a function of the shape and the inclination of the initial yield surface. For a given isotropic yield surface, as assumed by the Modified Cam Clay model (Schofield and Wroth 1968), the shear strength will have the same magnitude for both compression and extension types of loading. However, this does not occur when the yield surface presents an initial inclination, meaning that an initial anisotropy exists in the soil. Länsivaara (1995, 1999), suggested that a yield surface can be simply estimated if critical state friction angle and preconsolidation pressure are known. The yield surface can be assumed to be elliptical in shape; the preconsolidation

pressure will determine its size and its rotation can be fitted by assuming that an associated flow rule is valid for the yield surface at the intersection point with the K_0^{nc}-line. The value for K_0^{nc} can be determined e.g. by the well-known Jaky's equation $1 - \sin\phi'$ (Jaky 1944).

Fig. 2.13 shows two idealized undrained effective stress paths from triaxial compression and triaxial extension in the *q-p'* space. $s_u^A > s_u^P$ because of the shape and inclination of the initial yield surface.

Table 2.1. Anisotropy ratio of soft clays.

Author	s_u^{DSS}/s_u^A	s_u^P/s_u^A
Jamiolkowski et al. (1985)	0.53-0.79	0.51-0.61
Ladd (1991)	0.72-0.89	0.5-0.81
Karlsrud et al. (2005) (Norwegian clays)	0.6-0.8	0.3-0.55
Lunne and Andresen (2007)	0.78-0.82	0.59-0.65
Karlsrud and Hernandez-Martinez (2013), Norwegian low sensitive clays (S_t < 15)	0.57-0.82	0.3-0.52
Karlsrud and Hernandez-Martinez (2013), Norwegian sensitive clays (S_t > 15)	0.56-0.66	0.22-0.32
Thakur et al. (2014*b*) Norwegian clays (PI<10%)	0.63	0.35
Thakur et al. (2014*b*) Norwegian clays (PI>10%)	0.63-0.80	0.35-0.50

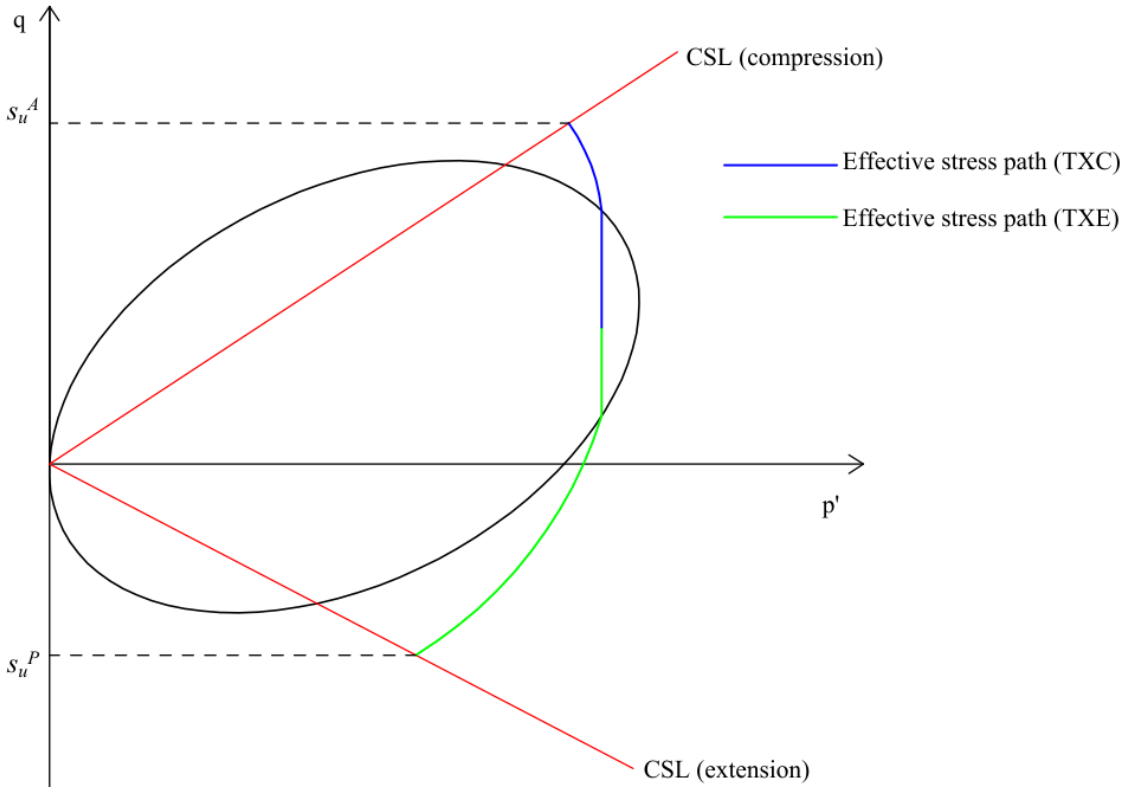

Fig. 2.13: Schematization of undrained compression/extension stress paths for slightly overconsolidated anisotropic clays.

2.5 Transformation models for undrained shear strength

The dependency of undrained shear strength (s_u) on the preconsolidation pressure (σ'_p) and plasticity has been studied by several authors, because of its practical usefulness.

Chandler (1988), based on the earlier work by Skempton (1954), suggested that there is a linear correlation between s_u determined from field vane shear test (s_u^{FV}) normalized against the preconsolidation pressure and the plasticity index (PI). The validity of the correlation [eq. (2.6)] is extended to both normally consolidated (NC) and overconsolidated (OC) clays. However, critical judgement must be applied when dealing with fissured, organic, sensitive, or other special clays.

$$\frac{s_u^{FV}}{\sigma'_p} \approx 0.11 + 0.0037 \cdot PI \tag{2.6}$$

Hansbo (1957) observed, for Scandinavian clays, s_u^{FV}/σ'_p to be linearly dependent on the liquid limit (LL) of the clay [eq. (2.7)]. Larsson (1980), collected field vane strength data points in Scandinavian clays and proposed a correlation equation similar to eq. (2.6), as described by eq. (2.8):

$$\frac{s_u^{FV}}{\sigma'_p} \approx 0.45 \cdot LL \tag{2.7}$$

$$\frac{s_u^{FV}}{\sigma'_p} \approx 0.08 + 0.0055 \cdot PI \tag{2.8}$$

According to Bjerrum (1972), undrained shear strength from field vane should be corrected in order to account for rate effects and converted to s_u mobilized [$s_{u(mob)}$]. Standard field vane test is normally performed at high speed of rotation. Therefore, the strain rates induced in the soil are much higher than in conventional laboratory tests (e.g. triaxial tests, direct simple shear tests). As a consequence, the measured peak shear strength is overestimated and, therefore, a correction is needed [eq. (2.9)]:

$$s_{u(mob)} = s_u^{FV} \cdot \mu \tag{2.9}$$

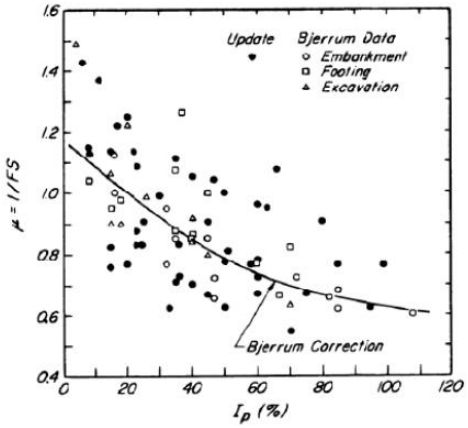

Fig. 2.14: Bjerrum's correction factor for field vane strength (Terzaghi et al. 1996).

The parameter μ is a correction factor that accounts for rate effects, anisotropy and it is commonly known to be dependent on the plasticity.

In the Finnish guidelines for embankment stability (Ratahallintokeskus 2005), μ is defined as a function of the liquid limit [eq. (2.10)]:

$$\mu = \frac{1.5}{1 + LL/100} \tag{2.10}$$

Mesri (1975) suggested a unique relationship for $s_{u(mob)}$ of clays and silts [eq. (2.11)], corresponding approximately to direct simple shear (DSS) condition, independent of plasticity:

$$s_{u(mob)} = 0.22 \cdot \sigma'_p \tag{2.11}$$

However, Larsson (1980) pointed out how eq. (2.11) overpredicts $s_{u(mob)}$ in very low-plastic clays, while it underestimates $s_{u(mob)}$ in high-plastic clays. For NC to low OC clays with low to moderate plasticity index (PI), Jamiolkowski et al. (1985) suggested [eq. (2.12)]:

$$\frac{s_{u(mob)}}{\sigma'_v} = (0.23 \pm 0.04) \cdot OCR^{0.8} \tag{2.12}$$

The transformation model suggested by Jamiolkowski et al. (1985) is based on the SHANSEP framework [eq. (2.2)] proposed by Ladd and Foott (1974). Note that m = 1 would reduce eq. (2.2) to eq. (2.1) with S = 0.22.

Larsson et al. (2007) studied eq. (2.2) for inorganic Scandinavian soft clays. Triaxial compression (TXC), direct simple shear (DSS) and triaxial extension (TXE) tests were collected and exploited to study the anisotropy of undrained shear strength, according to the *ADP* framework (Bjerrum 1973). The parameter m was found to be roughly constant and equal to 0.8. Experimental observations indicated that S is nearly material independent for TXC [eq. (2.13)], while it is strongly material dependent for DSS [eq. (2.14)] and TXE [eq. (2.15)], increasing with increasing liquid limit (LL).

$$\frac{s_u^{\,A}}{\sigma'_v} = 0.33 \cdot OCR^{0.8} \tag{2.13}$$

$$\frac{s_u^{\,DSS}}{\sigma'_v} = (0.125 + 0.205 \cdot LL/1.17) \cdot OCR^{0.8} \tag{2.14}$$

$$\frac{s_u^{\,P}}{\sigma'_v} = (0.055 + 0.275 \cdot LL/1.17) \cdot OCR^{0.8} \tag{2.15}$$

Based on eq. (2.13), (2.14) and (2.15), the anisotropic undrained shear strength of a clay deposit can be estimated for ADP analysis of geotechnical structures (e.g. stability,

bearing capacity). For instance, Fig. 2.15*a* illustrates the variation of the anisotropic s_u for a given LL = 60%. Strength from triaxial compression is generally higher than for DSS conditions, in turn higher than in triaxial extension.

Fig. 2.15*b* show the undrained shear strength of a homogeneous, saturated clay deposit with γ'=5 kN/m^3, OCR=1.3 and LL=60%.

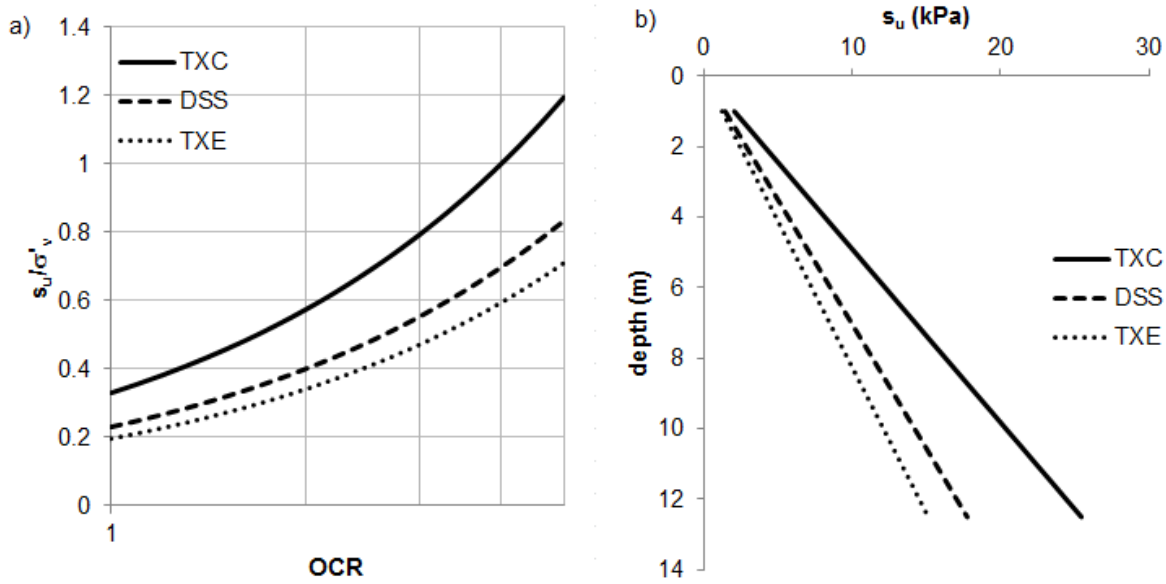

Fig. 2.15: *a*) normalized s_u vs. OCR for LL=60% and *b*) anisotropic s_u for a homogeneous and saturated clay deposit (LL=60%, OCR=1.3, γ'=5 kN/m^3) according to Larsson et al. (2007).

Karlsrud and Hernandez-Martinez (2013) studied the relationship s_u/σ'_v - OCR for clays from data collected from 22 sites in Norway and 1 in UK. Laboratory tests (TXC, DSS, TXE) were carried out on high-quality block samples taken using the Sherbrooke sampler (Lefebvre and Poulin 1979). Experimental results suggested that the undrained shear strength well correlates to the natural water (*w*) content, in combination with OCR [eq. (2.16), (2.17) and (2.18), for TXC, DSS and TXE, respectively].

More specifically, peak undrained strengths were observed to increase with increasing water content. Possible reasons to explain the observed phenomena might be e.g. the open structure typical of Norwegian clays (Rosenqvist 1953; 1966), which allows the soil to retain a quantity of pore water even higher than the liquid limit, or the increasing rate effects with plasticity (Bjerrum 1972).

$$\frac{s_u^{\ A}}{\sigma'_v} = (0.27 + 0.10 \cdot w) \cdot OCR^{(0.58+0.33 \cdot w)} \tag{2.16}$$

$$\frac{s_u^{\ DSS}}{\sigma'_v} = (0.14 + 0.18 \cdot w) \cdot OCR^{(0.35+0.77 \cdot w)} \tag{2.17}$$

$$\frac{s_u^{\ P}}{\sigma'_v} = (0.26 \cdot w) \cdot OCR^{(0.86+0.30 \cdot w)} \tag{2.18}$$

Mesri (1989) suggested that $s_{u(mob)}$ can be derived from laboratory test results (triaxial and direct simple shear tests), provided that the estimated slip surface consists of equal segments of compression, direct simple shear and extension modes of shear [eq. (2.19)].

$$s_{u(mob)} = \frac{1}{3}\left[\frac{s_u{}^{A}}{\sigma'_p} + \frac{s_u{}^{DSS}}{\sigma'_p} + \frac{s_u{}^{P}}{\sigma'_p}\right]\sigma'_p \ \mu_t \tag{2.19}$$

where μ_t is a time-to-failure correction factor, to be applied to TXC, DSS and TXE strengths before using them to assess $s_{u(mob)}$ for field instability situations.

Ching and Phoon (2012) derived a global correlation equation for the mobilized undrained shear strength [$s_{u(mob)}$] as a function of OCR and sensitivity (S_t). The model was constructed based on a large database of structured clays (CLAY/5/345), consisting of 345 clay data points from several countries [eq. (2.20)].

$$\frac{s_{u(mob)}}{\sigma'_v} = 0.229 \cdot OCR^{0.823} \cdot S_t{}^{0.121} \tag{2.20}$$

For some special clays (e.g. surficial weathered clays), preconsolidation pressure is rather difficult to determine. Hence, undrained shear strength cannot be directly estimated from e.g. eq. (2.1). For such clays, commonly referred to as bonded clays, it is also quite difficult to derive correlations for s_u because of their non-homogeneous structure. A separate survey on the formation and mechanical behavior of such clays is presented in Chapter 3.

2.6 Strain-softening and strain localization

Sensitive clays are characterized by an "open" soil structure with presence of bonds. Such an open structure let the soil retain an amount of water which can be even higher than the liquid limit. The soil can maintain its maximum strength until it is loaded undrained beyond it. After that, the structure tends to collapse and the resistance is dramatically reduced (Rosenqvist 1953; 1966). Such a phenomenon is called strain-softening: *"When subjected to a shear or a consolidation test, the clay shows a brittle behavior characterized by the fact that at a very small strain a critical stress level is reached, beyond which the magnitude and rate of deformations are large."* (Bjerrum 1973).

Strain-softening behavior of soft sensitive clays can be clearly observed in Fig. 2.16. Undrained triaxial compression tests (CIUC) at different depths on specimens of quick clay from Tiller, Norway, provide evidence of how the post-peak response is governed by drop of shear strength and consequent excess pore pressure increase. In the *q-p'* space, where $q = \sigma_1 - \sigma_3$ and $p' = 1/3 \cdot (\sigma'_1 + 2\sigma'_3)$, the stress path plunges downwards after reaching the maximum deviator stress, with a gradient controlled by the friction angle at critical state.

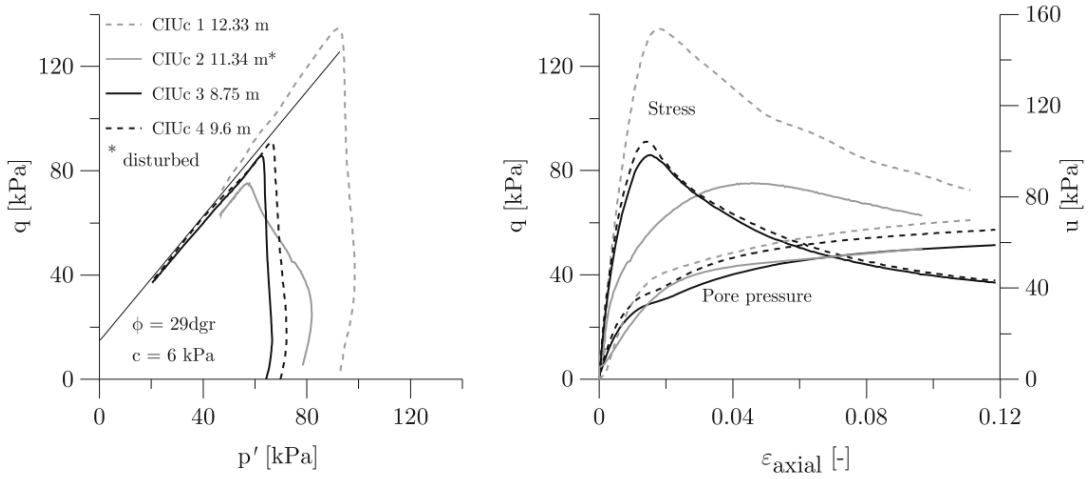

Fig. 2.16: CIUC triaxial tests on a sensitive clay from Tiller, Norway (Gylland et al. 2014).

Sensitive clays can be defined as instable materials. Local failure and strain localization will occur after the maximum shear stress is reached, with resulting development of a shear band in the initially homogeneous soil. According to Desrues and Viggiani (2004), the effect of reduction in shear stresses caused by post-peak softening will be larger when the shear strains are localized and all the further deformation will tend to accumulate in the shear band.

Strain-softening of soft clays and strain localization have been thoroughly studied, at laboratory scale, by several authors over the last decades.

Bjerrum (1961) initially suggested that the strength decrease after peak was directly related to excess pore pressure development during shearing, with resulting drop of effective stress in the soil.

Skempton (1964) indicated that reductions in the friction angle and in the cohesion may trigger the post-peak strength reduction in overconsolidated clays.

Burland (1990), Burland et al. (1997) and Vermeer et al. (2004) showed how cohesion softening is generally more dramatic than friction softening.

Janbu (1985) suggested the uniqueness of the effective strength parameters (c', ϕ') for soft sensitive clays. c' and ϕ' were found to be independent of type of loading (drained or undrained) and stress state (peak or post-peak).

Some authors (e.g. Bernander 2000; Thakur et al. 2005; Jostad et al. 2006; Thakur 2007, 2011; Gylland 2012; Gylland et al. 2014) confirmed the initial hypothesis provided by Bjerrum (1961), namely that for sensitive clays the post-peak strength reduction is mainly due to shear induced pore pressure.

Thakur et al. (2014*a*) concluded that strain-softening in soft sensitive clays is likely to be provoked by shear-induced pore pressure, at laboratory strain level of 10-20% (Fig. 2.17). It was also recommended that the concept of friction and cohesion softening could be more suitable for overconsolidated clays and perhaps soft sensitive clays at very large strains.

Strain-softening was found to be also affected by time dependent phenomena: Bernander and Svensk (1982) and Bernander (1985) reported that the rate of softening increases with increasing strain rate, possibly as a result of some local drainage effects.

Jostad et al. (2006) demonstrated that for sensitive clays, when applying high displacement rates the shear band thickness is governed by time dependent effects caused by local drainage of pore water as well as visco-plastic shear strains. Moreover, it was found that visco-plastic effects may also prevent the shear band to develop before full mobilization of the peak friction.

Gylland et al. (2014) conducted a thorough experimental study on strain localization in Norwegian sensitive clays, using a modified triaxial device. The main conclusion from this study was that the global post-peak behavior of sensitive clays is notably dependent on the strain rate applied and that shear band thickness is highly rate dependent, decreasing with increasing strain rate. Observed shear bands from triaxial specimens were characterized by a thickness (t_{sb}) in the range 1-3 mm. Such observations are probably not only linked to generation and dissipation of excess pore water pressure in the proximity of the shear band, but also to changes occurring in soil microstructure due to breakage of bonds and inter-particle sliding in the zone of shearing.

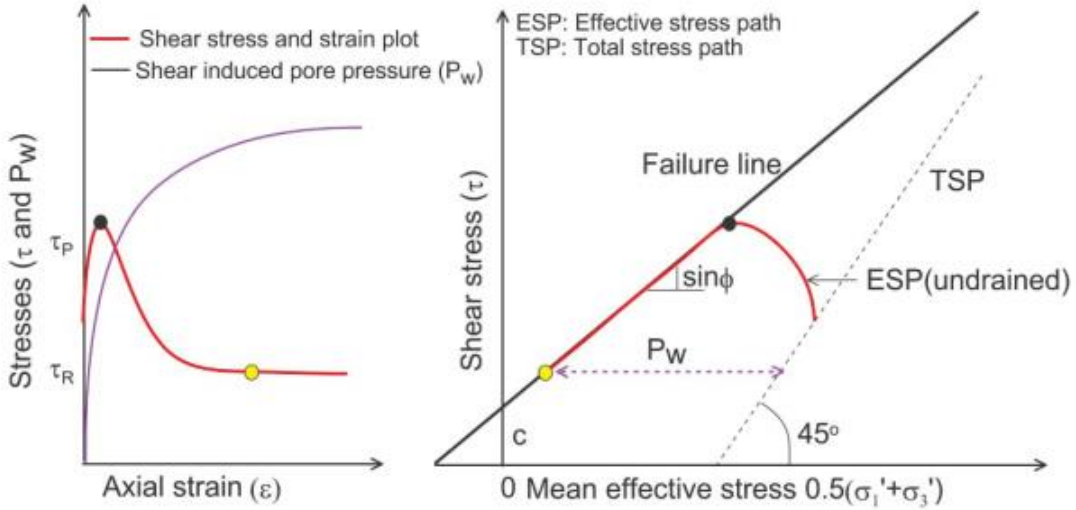

Fig. 2.17: Idealization of undrained strain-softening in soft sensitive clays seen at the laboratory strain level up to 20% (Thakur et al. 2014*a*). Note that the term "TSP" should be "Inclination of TSP", as the total stress path is not shown in the figure.

2.6.1 **Progressive failure mechanism**

The basic assumption in slope stability analyses performed using Limit Equilibrium Method (LEM) is that a given undrained shear strength, independent of strain level and direction of loading, is mobilized along a potential failure surface. However, according to several authors (e.g. Terzaghi and Peck 1948; Skempton 1964; Bishop 1967, 197; Bjerrum 1967), this is an erroneous assumption for soft sensitive clays.

Indeed, the mobilized shear strength may vary from peak to residual (large-strain) shear strength, and the strength distribution along the failure surface is governed by the strain-softening behavior. This phenomenon is commonly known as "progressive failure".

A straightforward but exhaustive description of the progressive failure mechanism is given by Skempton (1964): when in a clay mass the peak shear strength is passed at some particular point, the strength at that point will start dropping and further stress will be transmitted at some other point in the soil mass, causing the peak to be overcome at that point too. As a direct effect, a true chain reaction is established until a failure surface will develop further in the soil due to structural instability induced by the strain-softening behavior. Eventually, when failure occurs, the shear strength will turn into residual strength along the whole slip surface. Failure may though occur even before the strength at large strain is attained throughout the clay (Skempton 1964). However, once failure has started, the average undrained shear strength along the failure surface will decrease towards a residual value.

Fig. 2.18 describes the mechanism of downward progressive failure for a strain-softening material, induced by a triggering load. Local stress-strain diagrams are used to illustrate different loading stages and the shear stress distribution along a potential slip surface together with a global load displacement diagram.

When loading is applied up to a level within the global pre-peak hardening regime, the soil response is still governed by the elastic stiffness and, therefore, no failure occurs. Local strain-softening occurs when the load is further increased and peak strength is first passed at some point along the slip surface. Any further attempt of increasing the applied load will move the stress level towards a post-peak softening regime, where the available shear strength will tend to residual values, thus causing failure in the soil mass.

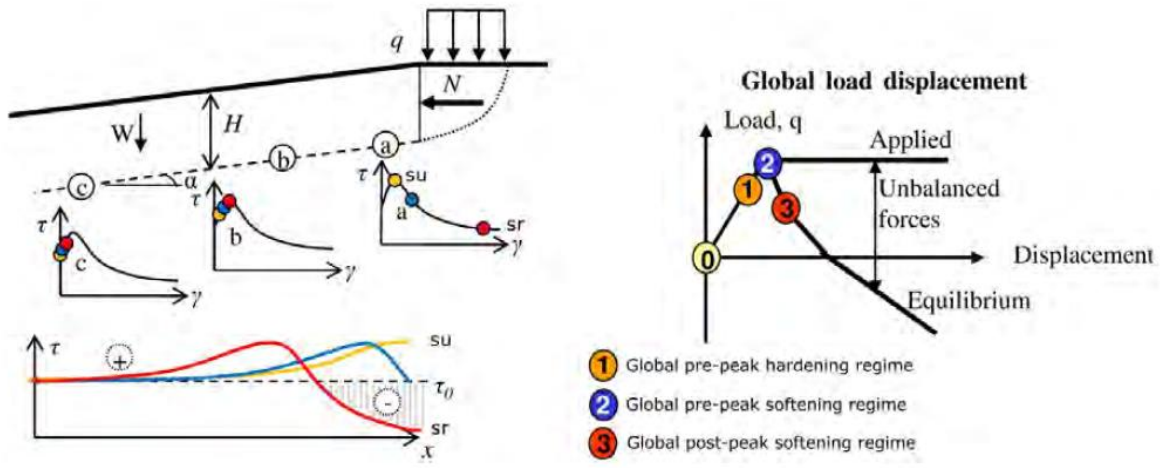

Figure 2.18. Schematization of downward progressive failure mechanism (Gylland et al. 2011).

Accounting for and modelling progressive failure in geotechnical design is always challenging. Some authors (e.g. Lefebvre and La Rochelle 1974) suggested using directly the residual strength values, while others (e.g. Dascal et al. 1972, Jostad et al. 2014) proposed to simply reduce the peak strengths by a correction factor.

From a practical point of view, Jostad et al. (2014) studied the impact of strain-softening and progressive failure in design of fills on gently inclined slopes on soft sensitive clays using the finite element analyses. The main outcome was that the peak undrained shear strength can be reduced by a scaling factor (F_{soft}) and used as input parameter for limit equilibrium analyses with the hypothesis of perfect plasticity. An average F_{soft} = 1.09 was estimated, suggesting that a reduction of the peak strength of about 9% would provide the same bearing capacity achieved when softening is taken into account in the calculation.

3. Mechanical behavior of dry crust layers

3.1 Formation and characterization of dry crust layers

Weathered clay crust (or dry crust) layers are the products of phenomena such as oxidation, desiccation, freezing-thawing and fluctuation of the ground water table. Dry crust layers are normally stiffer than the subsoil, partially saturated (at least in their top part) and characterized by the presence of fissures. Moreover, water content is generally low, while the shear strength is higher than the underlying subsoil.

A dry crust layer is normally located on top of a soft soil deposit. The thickness of a dry crust in Finnish clay deposits can vary between 1 and 4 m and, hence, it can significantly affect the stability of shallow geotechnical structures (i.e. embankments).

Ringesten (1988) made a comprehensive study of the characteristics of weathered clay crusts from different sites in Sweden. Results have shown that:

a. Weathered crust layers are characterized by very high strength, even 10 to 50 times higher than the underlying subsoil. Furthermore, the strength seems to be affected by seasonal changes in the water content.

b. The dry crust is made of strain hardening material. Therefore, no preconsolidation pressure could be observed.

c. Sensitivity (S_t) can vary between 1 (insensitive clay) and 4 (very low sensitive clay).

d. A confined compression modulus of 3-4 MPa was measured for low loads and equal in the horizontal and vertical directions.

e. The bulk density (γ_{tot}) was observed to increase as a result of the crust formation, from 15-16 kN/m^3 to about 19 kN/m^3.

f. The properties show irregular distribution with depth.

g. No correlations could be found between the characteristics of dry crust layers and heavily overconsolidated clays.

h. A larger amount of coarse material was found in the upper part of the dry crust than in the lower part, which seems to be more homogeneous. The frequently observed loose structure of the upper bonded clay is the result of desiccation from evaporation and freezing, which forms larger particles or aggregates with higher porosity.

i. The permeability was observed to vary seasonally with the moisture content and strongly influenced by the fissure system. The desiccated, unloaded, bonded clay is characterized by a very high permeability, especially in the direction where fissures are oriented. Changes in natural water content cause the dry crust material to swell and fissures to close, thus decreasing the permeability to values

comparable to those of the soft clay of the same origin. The fissures can also close because of loading.

j. The time-dependent effects seemed to be much greater than in overconsolidated clays. The influence of macrofabric, including fissures system and cavities, was studied through comparison between a large-scale oedometer test with a diameter of 700 mm and a standard oedometer test. It was concluded that the higher strains measured in the large-scale test were caused by creep in the macrofabric and not by movements in the microfabric.

The onset of a dry crust formation coincides with the clay liquid phase cut-off, or with the lowering of pore pressure, for example by drainage caused by vegetation, evaporation, drainage system etc. Gas is released into small bubbles. Then, the clay is contracted by the menisci in the gas-liquid interfaces, consolidating as the menisci draw the structure together. The clay micro-structure is subjected to cementation by chemical-physical bonds and stiffness will increase as the cementation process progresses. Calcium carbonate is probably the main cementing agent. The weathered clay is, therefore, a strain hardening material, with a structure which differs from that of an overconsolidated clay.
Scanning electron microscopy, together with chemical analysis, showed a rather open structure with particle arrangement with no preferred orientation. Clay minerals aggregated to units often had a laminated appearance. Bonded clay particles had a pronounced bladed form. The bonds need time to develop and result in very stable products that can last many thousands of years. (Ringesten 1988)

3.2 Undrained shear strength of dry crust layers

When evaluating the stability of an embankment, it is of high importance to assess the potential available strength in the dry crust. Part of the slip surface generally intersects this layer, especially in the active side of shearing. Nevertheless, taking undisturbed samples of dry crust is rather challenging because of the non-homogeneous as well as fissured structure.

Research studies have been conducted by some authors on the determination of the undrained shear strength s_u of weathered clay crusts, using both in-situ and laboratory tests. Practical difficulties were encountered when trying to obtain undisturbed samples. Therefore, in-situ tests seemed more suitable than laboratory tests for assessing the mechanical properties. Furthermore, clay crust is generally non-saturated and, consequently, testing using conventional test procedures is not straightforward.

However, field vane test was found to overestimate s_u in such fissured stiff clays (La Rochelle 1974; Lefebvre et al. 1987; Khan 1993).

Leroueil et al. (1990) suggested, for practical use in stability analysis of embankments, a criterion to assess the shear strength of the dry crust from field vane test results as shown in Fig. 3.1. The assumption made is that the design strength is one third of the measured field vane strength. This approach is also used in Finnish design practice and included in the guidelines of the Finnish Transport Agency (Ratahallintokeskus 2005) for geotechnical design of embankments.

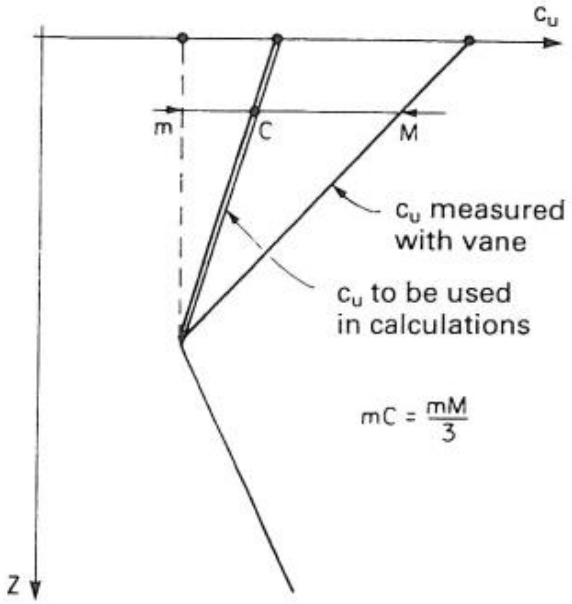

Fig. 3.1: Method of correction of measured shear strength in the weathered crust (Leroueil et al. 1990).

Lo et al. (1970) conducted an experimental study on fissured soils using laboratory field vane equipment. Results from this study indicate that the strength of fissured clays measured from field vane would correspond to the intact strength measured on small laboratory samples. One possible explanation could be that cracks do not affect the performance of a field vane test, as the test itself causes an initial disturbance to the soil due to the insertion of the vane.

La Rochelle (1974) evaluated the impact of the dry crust on the stability of instrumented embankments on sensitive clays. The main conclusion was that by assuming the mobilization of the full vane strength measured in the dry crust, the factor of safety is overestimated. On the other hand, assuming a strength value equal to the minimum strength measured on top of the underlying soft layer, would lead to a quite conservative and unrealistic safety level.

Lefebvre et al. (1987) compared different test results on a superficial clay crust located in the region of Quebec (Canada). The shear strength measured from in-situ shear box, plate loading tests and triaxial tests, resulted lower than the strength measured from field vane. The dilatant behavior was considered the main cause for the high strength measured by the field vane and that the shear strength of a dry crust under an embankment load would be a function of that load. For this reason, it was suggested to use the field vane only for measuring the thickness of the dry crust.

Khan (1993) measured the shear strength of a weathered clay crust located in the Ottawa region (Canada) from different test types, i.e. field vane, piezocone and triaxial tests. In agreement with previous studies, field vane was observed to overestimate the strength of the clay crust (Fig. 3.2).

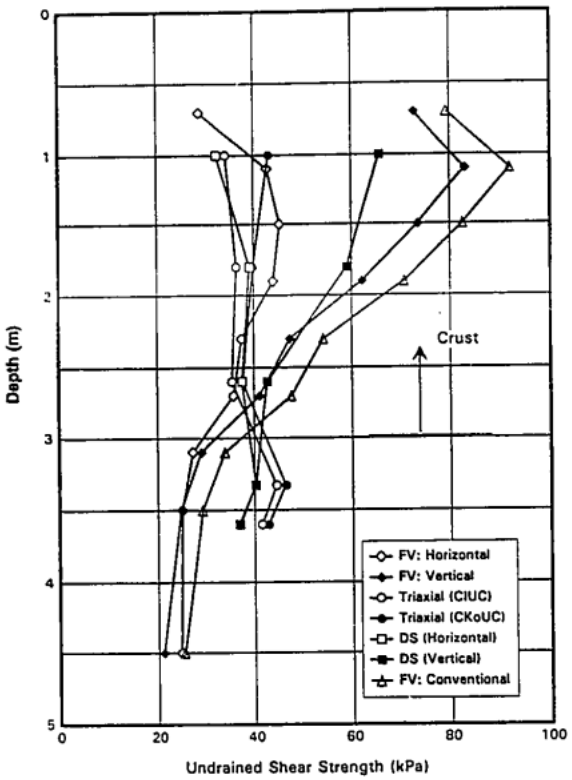

Fig. 3.2: Undrained shear strengths in Canadian weathered clay crust from field vane, triaxial compression and direct shear test (Khan 1993).

Based on the outcomes of this study, a model to derive shear strength from measured vane torque moment was proposed [eq. (3.1) and eq. (3.2)]. The model accounts for shear stress distribution around the field vane, effects of fissuring, influence of horizontal effective stress on failure planes and rate effects.

$$s_{uv} = \frac{M}{\pi D^3}\left(\frac{p_n}{p_n + K_s}\right)\mu_r \mu_D \tag{3.1}$$

$$s_{uh} = \frac{M}{\pi D^3}\left(\frac{p_n \cdot K_s}{p_n + K_s}\right)\mu_r \mu_D \tag{3.2}$$

where s_{uv} and s_{uh} are the undrained shear stresses mobilized on the vertical and horizontal plane, respectively. M is the measured torque moment, D the diameter of the vane, p_n the shear stress distribution factor for horizontal shear planes, $K_s = s_{uh}/s_{uv}$ is the anisotropy ratio, μ_r and μ_d correction factors for rate effect and disturbance due to vane insertion, respectively.

4. Undrained shear strength increase under embankments

4.1 General principles and empirical models

The performance of embankments built on soft clays can be significantly affected by the consolidation phenomena occurring in the subsoil. Normally, the short-term stability is evaluated prior to construction of the embankment by mean of a total stress analysis, where the undrained shear strength is determined from field vane measurements and reduced according to e.g. Bjerrum (1972).

However, consolidation occurs in time in the subsoil because of the stress increase caused by external loads (e.g. embankment construction). Excess pore pressure will first develop because of the low permeability of the clay, and later dissipate with accompanying volume change (settlement). As a consequence, the available strength will increase as a result of the higher effective stresses induced in the soil.

Soil layers which have been consolidating under old embankments for several years, show greater undrained shear strength than the undisturbed soil prior to construction, as reported by some authors (Tavenas et al. 1978; Slunga 1983; Larsson and Matsson 2003). By accounting for such strength increase, the factor of safety will result higher than at the initial stage (e.g. Tavenas et al. 1978; Slunga 1983).

The reason why the shear strength increase should be carefully evaluated is that the greater available strength can be exploited, for example, if the embankment needs to be raised or widened or if the traffic load/speed is to be increased.

Moreover, a correct assessment of the undrained shear strength increase due to consolidation is very useful in stage-construction of embankments. A stage-construction consists of applying a load in steps in order to provide the soil with sufficient time to consolidate and, therefore, allow the strength to increase before the following loading step. The main practical usefulness of stage-construction method is that embankments can be raised without any supporting structures or soil improvement which could be needed for a single stage construction.

For geotechnical structures built on clay deposits where the ground water table is located in the proximity of the ground surface, buoyancy effects will have an impact on the final stress distribution and, hence, should not be neglected. The reason is that the soil located above the groundwater level will become submerged because of settlement and the unit weight will decrease, with consequent decrease of effective stress.

The fundamental aspect to account for when assessing the strength increase due to consolidation is the direct relation between the preconsolidation pressure and undrained shear strength discussed in section 2.1. Such a relation is valid independent of how the preconsolidation pressure has been reached, either mechanically due to load induced effective stress increase, or due to secondary consolidation (or aging).

As discussed in section 2.3, soft clay deposits may show OCR higher than 1 because of aging effect without necessarily having previously experienced a higher overburden

stress. As shown in Fig. 4.1, where the line A-B represents the process of aging, the clay gains additional strength and becomes over consolidated with $s_u = s_{uf}$, effective vertical stress equal to σ'_{v0} and preconsolidation pressure equal to σ'_p. For a given stress increase ($\Delta\sigma_v$), s_u will increase along C-D, provided that the final effective vertical stress is higher than σ'_p. In contrast, below σ'_p, s_u will be equal to s_{uf}.

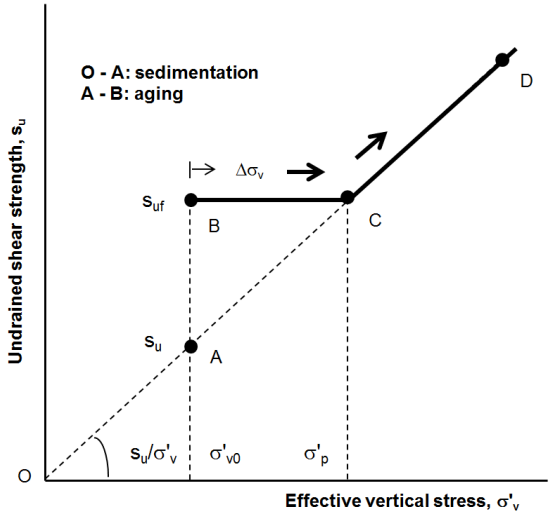

Fig. 4.1: Relationship between s_u, σ'_v and σ'_p (after Suzuki and Yashuara, 2007).

However, as suggested by Larsson and Matsson (2003), in overconsolidated soil, an increase in effective stress due to consolidation can lead to a change (although relatively small) in undrained shear strength, even in case the preconsolidation pressure is not exceeded. This can be well understood from eq. (2.2) by Ladd and Foott (1974).

In order to evaluate the undrained shear strength increase, Slunga (1983) suggested:

$$\Delta s_u = (0.20 - 0.25) \cdot \Delta\sigma'_p \qquad (4.1)$$

where $\Delta\sigma'_p$ is the increase in consolidation stress and equal to the difference between the maximum effective vertical stress induced by the embankment load (σ'_{vmax}) and the initial preconsolidation pressure (σ'_p) [$\Delta\sigma'_p = (\sigma'_{vmax} - \sigma'_p)$]. For normally consolidated clays $\sigma'_p = \sigma'_{v0}$.

For a case where there is some undissipated excess pore pressure in the soil, eq. (4.1) becomes:

$$\Delta s_u = (0.20 - 0.25) \cdot (\sigma'_{v\max} - \sigma'_p - u) \qquad (4.2)$$

where $u = 0.25 \cdot \Delta\sigma'_p$.

Larsson and Matsson (2003), based on experimental observations from test embankments in Sweden, proposed that the shear strength increase can be estimated from the shear wave velocities measured below the embankment and at the embankment sides. It was also pointed out that the relation between undrained shear strength and shear wave velocity is sensitive to liquid limit and soil density, and their variation should be accounted for [eq. (2.25)].

$$s_u \approx \frac{V_s^{\,2} \cdot \rho \cdot LL}{504} \tag{4.3}$$

Practical difficulties in using eq. (4.3), led to a more straightforward approach, as suggested by eq. (4.4):

$$s_{u2} \approx s_{u1}\left(\frac{V_{s2}}{V_{s1}}\right)^2 \tag{4.4}$$

Where s_{u2} is the undrained shear strength below the loaded area, s_{u1} the undrained shear strength in the natural ground, V_{s2} and V_{s1} the shear wave velocities below the loaded area and in the natural ground, respectively.

4.2 Evaluation of shear strength increase from test embankments

4.2.1 Finland

Slunga (1983) investigated the strength increase under an old 2 m high embankment located on the railway line between Kerava and Porvoo in Southern Finland. The soil conditions at the testing site consisted of a 1.5-2 m thick dry crust on top of a 7 m thick deposit of slightly overconsolidated (OCR=1.5-1.6) soft sensitive clay. Field vane, triaxial compression and undrained direct shear tests were performed at three different locations: under the embankment, 6 m and 19 m off the centre-line of the embankment. Field vane tests were conducted using different vane geometries and also with an inclination of 45° from the ground.

All the test results showed a marked strength increase in the top 5 m below the embankment, with a magnitude up to 50% of the initial strength (Fig. 4.2). Field vane results showed that the strength of the clay is highly anisotropic and that the undrained shear strength measured on the horizontal surface (s_{uh}) of the vane is greater than that measured on the vertical surface (s_{uv}). Furthermore, the ratio s_{uh}/s_{uv} was found to be higher under the embankment because of the embankment weight.

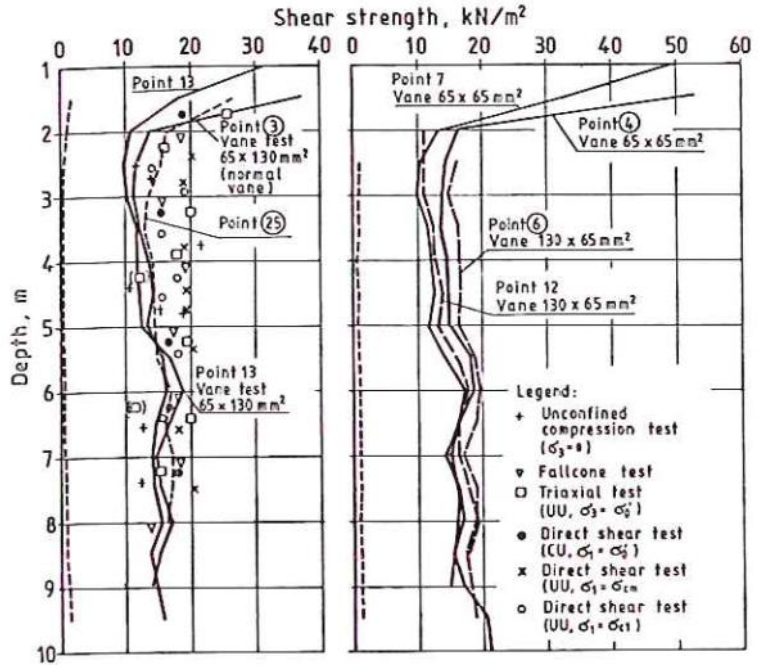

Fig. 4.2: Results of vane tests and laboratory tests on samples from under the embankment (points 3, 4, 6 and 25) and at the toe of it (points 7, 12 and 13). (Slunga 1983)

The calculated safety factors under a train load of 100 kN/m demonstrated that by neglecting the strength increase, the resisting forces in the soil are similar or even lower than the mobilizing forces caused by the embankment and the applied load. In addition, it was suggested that the actual factor of safety is also dependent on the way of using the shear strength in the dry crust and of using the short term train load as external force in a stability analysis.

4.2.2 **Sweden**

Larsson and Matsson (2003) have investigated long-term settlement and shear strength increase under three instrumented test embankments built on Swedish soft compressible clays: the square test fill at Lilla Mellösa and the circular and road-like test embankments at Skå-Edeby. The embankment height was 2.5 m at Lilla Mellösä and 1.5 m at Skå-Edeby for both the circular and the road-like embankment. The shear strength increase was investigated from seismic cross-hole tomography, field vane, piezocone (CPTU) and direct simple shear tests.

The reason for choosing the cross-hole tomography as investigation method is suggested by the well documented relation between undrained shear strength and shear wave velocity (e.g. Larsson and Mulabdic 1991). Shear wave velocity under the embankment can be measured from one side to the other by the cross-hole method, with no need to access to the embankment itself. Such a method may turn useful when shear strength assessment is required and, for instance, the traffic on a road or railway cannot be interrupted.

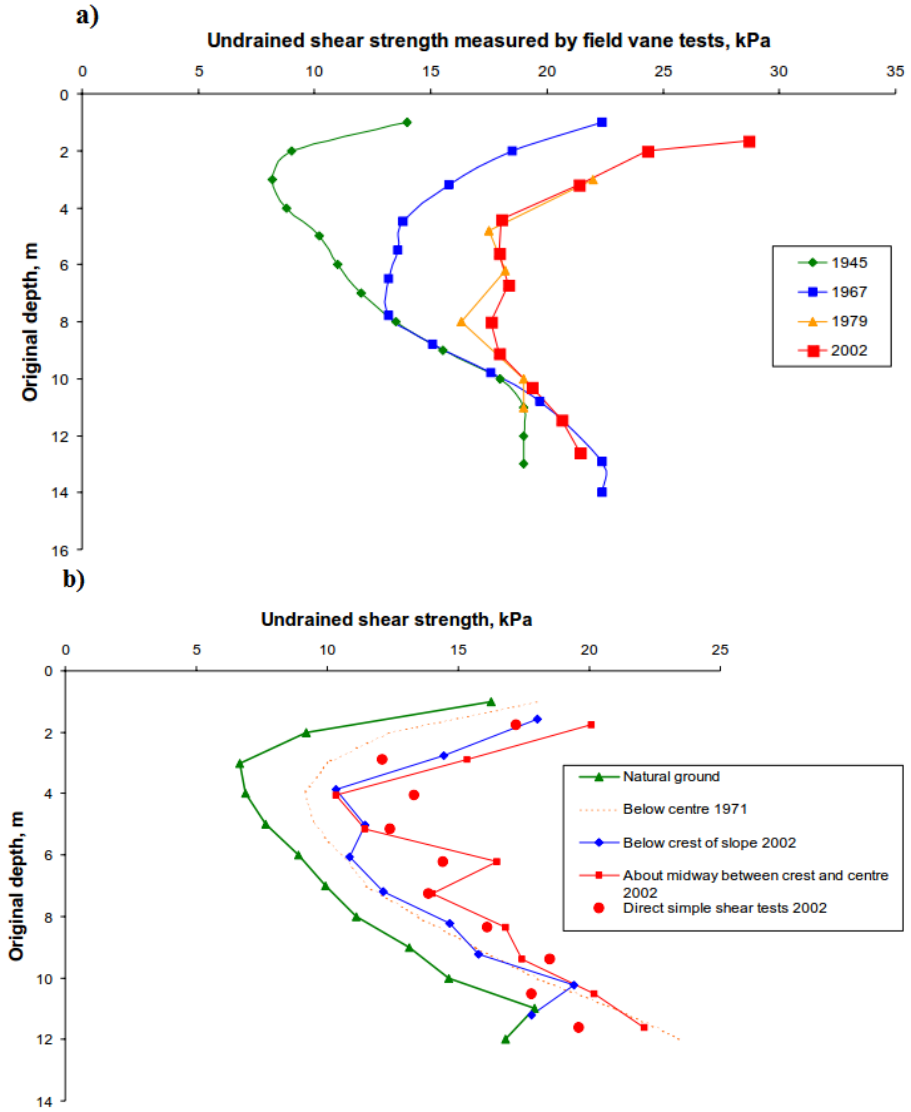

Fig. 4.3: Measured undrained shear strength below *a*) the test fill at Lilla Mellösa and *b*) below the circular test fill at Skå-Edeby at various times (after Larsson and Matsson 2003).

Test results at Lilla Mellösa (Fig. 4.3*a*) suggested that the shear strength during the first period increased only in the top 8 m, while the maximum strength has been possibly reached 34 years after construction, in 1979. More recent measurements did not show any further remarkable gain in strength. Laboratory tests showed increased preconsolidation pressure and a significant decrease in water content and permeability below the embankment, while the liquid limit seemed not to show any changes.

Based on the test results at Skå-Edeby (Fig. 4.3*b*), a considerable shear strength increase has occurred between the different testing events. The shear strength below the crest is somewhat similar but lower than below the center of the fill. Consistency between field vane and direct simple shear tests was observed, as DSS showed similar strength values than field vane. An increase of preconsolidation pressure, together with a reduction in permeability below the embankments was also observed. Furthermore, the shear strength evaluated from CPT test resulted higher than from the other test results, probably because of the varved nature of the soil and the accompanying difficulties in selecting correct values of liquid limit to be used to estimate a cone factor.

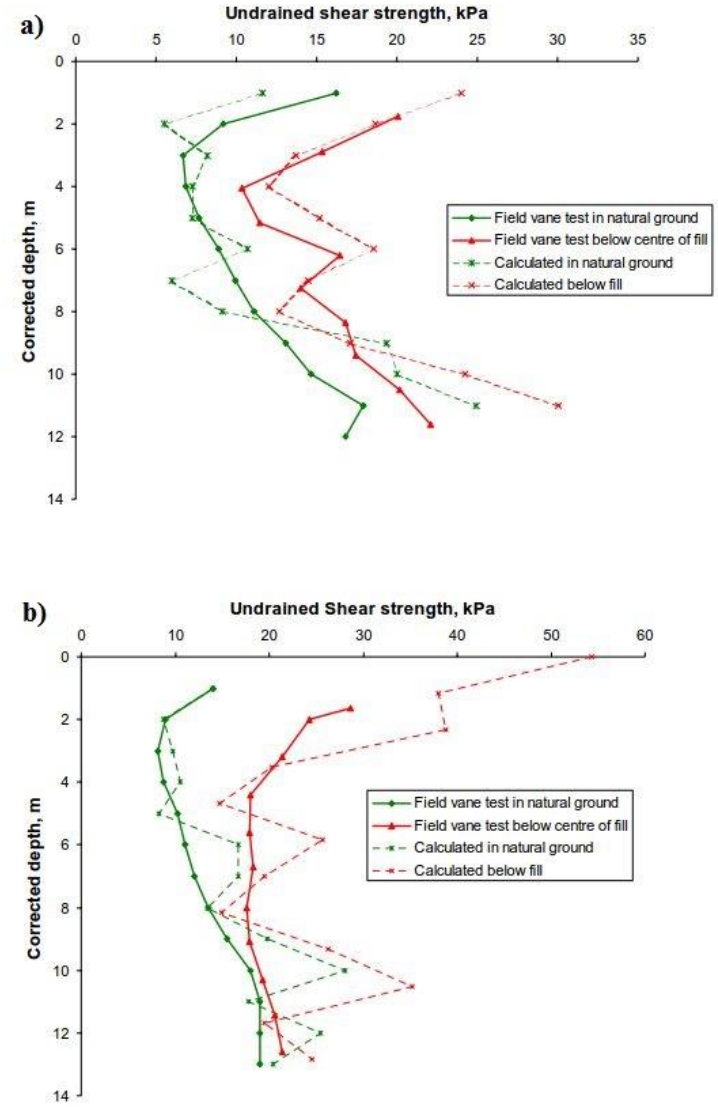

Fig. 4.4: Evaluated undrained shear strength using eq. (4.3). The levels below the loaded areas are corrected for the estimated settlements. *a*) At the circular fill at Skå-Edeby *b*) At the square fill at Lilla Mellösa. (after Larsson and Matsson 2003).

A considerable shear strength increase was also observed from the measured shear wave velocities under the embankments. Comparison between field vane test results and eq. (4.3) and eq. (4.4) has shown that s_u calculated from eq. (4.3) provides a too coarse estimation of the strength values, while eq. (4.4) results in better strength predictions.

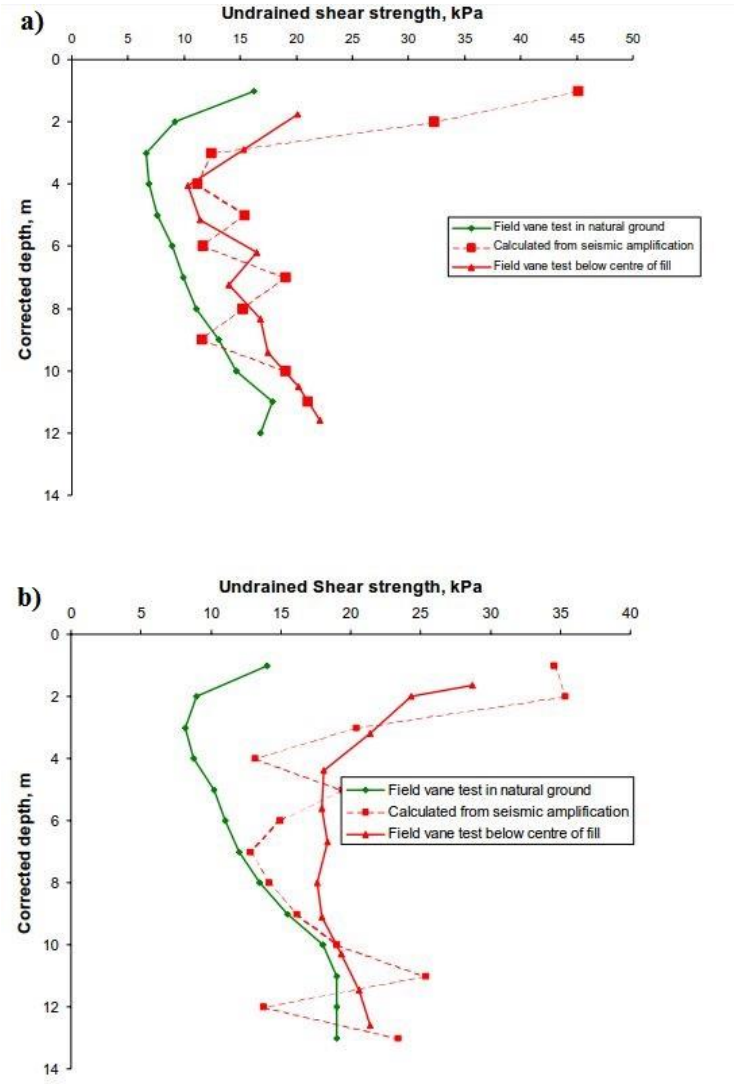

Fig. 4.5: Evaluated undrained shear strength using eq. (4.4). The levels below the loaded areas are corrected for the estimated settlements. *a*) At the circular fill at Skå-Edeby *b*) At the square fill at Lilla Mellösa (after Larsson and Matsson 2003).

4.2.3 **Canada**

Tavenas et al. (1978) reported experimental observations collected from stage-construction of seven high embankments built on soft clays on the north shore of the St. Lawrence Valley in Canada. The embankments were 8.5-9.0 m high.

In all the studied cases, the consolidation process has produced a reduction in the s_u/σ'_v ratio at all possible locations under the seven embankments (Fig. 4.6). Vane shear and oedometer tests were used to evaluate the initial s_u/σ'_p ratio, while the simultaneous observations of s_u from vane and pore pressure were exploited to assess s_u/σ'_v during construction. It was concluded that when the clay consolidates to an effective stress level beyond the preconsolidation pressure, both an increase in the field vane strength and a reduction in the s_u/σ'_v ratio are observed. Furthermore, the s_u/σ'_v ratio appears to decrease more significantly in highly plastic clays from a high initial s_u/σ'_p; while it is only lightly reduced in low plastic clays. Overall, the final s_u/σ'_v did not show a marked dependency on plasticity.

The reduction of s_u/σ'_v seems to occur rapidly as soon as σ'_p is exceeded and, hence, the normally consolidated state reached. This was also confirmed by the pore pressure readings. However, no significant changes were observed during further consolidation. This might be explained by the fact that the transition to normally consolidated state causes a change in the clay structure, with consequent modification of the yield surface of the clay.

Observations further suggested that reductions in s_u/σ'_v are not necessarily accompanied by a strength increase, as observed in some cases where the field vane strength after consolidation did not show any notable difference from the initially measured strength. Nevertheless, momentary s_u reduction may occur when s_u/σ'_v decreases in the early phases of consolidation.

A summary of the experimentally observed changes in the strength ratio under old embankments from different locations is reported in Table 4.1.

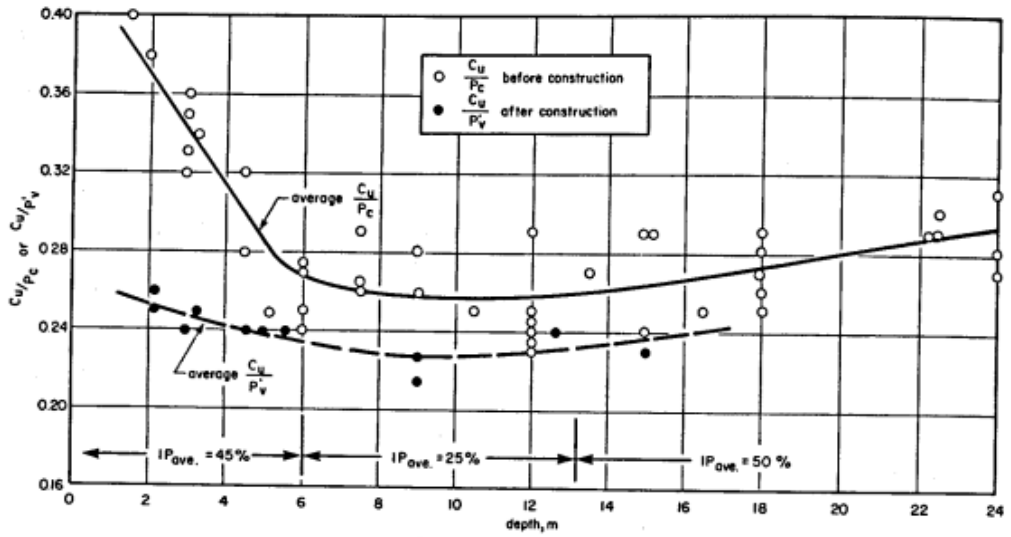

Fig. 4.6: Variation of the s_u/σ'_v ratio under the embankments (Tavenas et al. 1978)

Table 4.1. Variation of s_u/σ'_v from the initial s_u/σ'_p under embankments from different locations.

Reference	Location	Initial s_u/σ'_p	s_u/σ'_v	Time elapsed between construction and measurements	Notes
Eden and Poorooshasb (1968*a*,*b*)	Ottawa, Canada	0.23-0.33	0.16-0.20	3.5 years	no significant changes in field vane strength
Holtz and Broms (1972)	Skå-Edeby, Sweden	0.22-0.28	0.21-0.25	14 years	s_u increase observed
Tavenas et al. (1974)	Saint-Alban test B section, Canada	0.26	0.21	2.5 years	s_u increase observed
Tavenas et al. (1978)	Eastern township highway, Montreal, Canada	0.32	0.24	12 years	no significant changes in field vane strength
Tavenas et al. (1978)	Rang Saint-Georges, Canada	0.26-0.35	0.22	3 years	s_u increase observed
Tavenas et al. (1978)	Rang du Fleuve, Canada	0.33-0.34	0.24	2.5 years	s_u increase observed

5. Correlations for undrained shear strength of Finnish soft clays

5.1 Introduction

Correlations for undrained shear strength of Swedish and Norwegian clays are available in the literature (e.g. Larsson and Mulabdic 1991; Larsson et al. 2007; Karlsrud and Hernandez-Martinez 2013). Some of them are presented in section 2.5. However, a similar model calibrated from an adequately large soil database of Finnish soft clays is still missing. For this reason, correlation models for Swedish clays or the simple relation proposed by Mesri (1975) of eq. (2.11) are normally used in Finnish design practice when proper testing is limited or not available.

In this chapter, correlations for undrained shear strength specific to Finnish clays are derived and presented for the first time. The main idea is to provide engineers with a simple and usable framework of equations to assess s_u for stability calculations. The proposed correlations are meant to provide a reliable estimate of s_u for preliminary total stress stability analyses and/or as a reference to compare or validate test results. As sufficient data from undrained triaxial compression/extension tests on Finnish clays is not available, s_u anisotropy is not studied. The new correlations are derived from field vane measurements. Therefore, the results presented later in this chapter refer to s_u which roughly corresponds to DSS loading conditions.

Two large databases consisting of multivariate clay data points are compiled. The first database consists of 216 field vane data points from 24 test sites in Finland. Undrained shear strength from field vane (s_u^{FV}), vertical effective stress (σ'_v), vertical preconsolidation pressure (σ'_p), natural water content (w), liquid limit (LL), plastic limit (PL) and sensitivity ($S_t = s_u/s_u^{re}$) are simultaneously known for each data point. As a consequence, information on plasticity index (PI=LL–PL) and liquidity index [LI = (w–PL)/(LL-PL)] is also available. The second independent multivariate database is extrapolated from the global database CLAY/10/7490 compiled by Ching and Phoon (2014*a*). This database has the scope to act as a comparison and validation tool. It consists of 168 field vane data points from Sweden (12 sites) and Norway (7 sites).

Only a limited number of multivariate soil databases is available in the literature. A summary is given in Table 5.1. Ching and Phoon (2014*a*) suggested labeling a multivariate database as: (soil type)/(number of parameters of interest)/(number of data points). Based on this nomenclature, the two databases compiled in this study are *i*) F-CLAY/7/216 for Finnish clays (where "F" stands for Finland) and *ii*) S-CLAY/7/168 for Scandinavian clays (where "S" stands for Scandinavia). The 7 parameters in these databases consisted of undrained shear strength (s_u^{FV}), effective vertical stress (σ'_v), vertical preconsolidation pressure (σ'_p), index parameters (w, LL, PL) and sensitivity (S_t).

Table 5.1. Summary of multivariate clay databases [D'Ignazio et al. 2016].

Database	Reference	Parameters of interest	# data points	# sites/ studies	Range of properties		
					OCR	PI	S_t
CLAY/5/345	Ching and Phoon (2012)	LI, s_u, s_u^{re}, σ'_p, σ'_v	345	37 sites	1~4		Sensitive to quick clays
CLAY/7/6310	Ching and Phoon (2013)	CIUC, CK_0UC, CK_0UE, DSS, FV, UU, UC	6310	164 studies	1~10	Low to very high plasticity	Insensitive to quick clays
CLAY/6/535	Ching et al. (2014)	s_u/σ'_v, OCR, $(q_t-\sigma_v)/\sigma'_v$, $(q_t-u_2)/\sigma'_v$, $(u_2-u_0)/\sigma'_v$, B_q	535	40 sites	1~6	Low to very high plasticity	Insensitive to quick clays
CLAY/10/7490	Ching and Phoon (2014*a*)	LL, PI, LI, σ'_v/P_a, σ'_p/P_a, s_u/σ'_v, S_t, $(q_t-\sigma_v)/\sigma'_v$, $(q_t-u_2)/\sigma'_v$, B_q	7490	251 studies	1~10	Low to very high plasticity	Insensitive to quick clays

Note: LL = liquid limit; PI = plasticity index; LI = liquidity index; σ'_v = vertical effective stress; σ'_p = preconsolidation stress; s_u = undrained shear strength; s_u^{re} = remolded s_u; CIUC = s_u from isotropically consolidated undrained compression test; CK_0UC = s_u from K_0-consolidated undrained compression test; CK_0UE = s_u from K_0-consolidated undrained extension test; DSS = s_u from direct simple shear test; FV = s_u from field vane; UU = s_u from unconsolidated undrained compression test; UC = s_u from unconfined compression test; S_t = sensitivity; OCR = overconsolidation ratio, $(q_t-\sigma_v)/\sigma'_v$ = normalized cone tip resistance; $(q_t-u_2)/\sigma'_v$ = effective cone tip resistance; u_0 = hydrostatic pore pressure; $(u_2-u_0)/\sigma'_v$ = normalized excess pore pressure; B_q = pore pressure ratio = $(u_2-u_0)/(q_t-\sigma_v)$; and P_a = atmospheric pressure = 101.3 kPa.

The main purpose of this work is to study the dependency of undrained shear strength of Finnish inorganic clays on overconsolidation ratio (OCR), natural water content (w), liquid limit (LL), plasticity index (PI), liquidity index (LI) and sensitivity (S_t) using the data contained in F-CLAY/7/216.

Firstly, the compilation of F-CLAY/7/218 and S-CLAY/7/168 databases is presented. Secondly, two dimensionless databases based on 10 dimensionless parameters are derived from the 7 basic parameters: water content (w), liquid limit (LL), plasticity index (PI), liquidity index (LI), overconsolidation ratio (OCR), normalized mobilized undrained shear strength against vertical effective stress [$s_{u(mob)}/\sigma'_v$], preconsolidation pressure [$s_{u(mob)}/\sigma'_p$], normalized undrained shear strength from field vane against vertical effective stress (s_u^{FV}/σ'_v), preconsolidation pressure (s_u^{FV}/σ'_p), and sensitivity (S_t). These dimensionless databases are labelled as F-CLAY/10/216 and S-CLAY/10/168, and compared to existing transformation models in the literature.

To develop more refined correlations for Finnish clays, outliers are removed from F-CLAY/10/216 based on criteria which account for soil nature, mechanical characteristics and statistical considerations. Then, the resulting F-CLAY/10/173 database is used to derive the new transformation models for undrained shear strength.

Consistency of the new models is firstly evaluated by comparison with existing correlations for Scandinavian clays and, lastly, by calculating the biases and uncertainties associated with S-CLAY/10/168.

5.2 Analysis of multivariate clay databases

5.2.1 F-CLAY/7/216 and S-CLAY/7/168

The compiled database of Finnish clays consists of 216 field vane data points from soft clay sites in Finland. Each data "point" contains multivariate information, i.e. information from different tests conducted in close proximity. Information on 7 different basic parameters measured at comparable depths and sampling locations is available: undrained shear strength (s_u^{FV}), effective vertical stress (σ'_v), vertical preconsolidation pressure (σ'_p), index parameters (w, LL, PL) and sensitivity (S_t). This database is labeled as F-CLAY/7/216 ("F" for Finland) following the nomenclature proposed by Ching and Phoon (2014a).

Clay data points are collected from Gardemeister (1973), Lehtonen et al. (2015), together with data from recent soil investigations performed by Tampere University of Technology, Finland (Selänpää 2015). Gardemeister (1973) collected a large number of field vane and oedometer tests carried out at different locations in Finland. However, some of the test sites were characterized by highly organic and/or silty soils and, therefore, were not considered.

The basic statistics of the 7 clay parameters in F-CLAY/7/216 are summarized in Table 5.2. The parameters σ'_v and σ'_p are normalized to the atmospheric pressure, P_a (P_a = 101.3 kPa). The statistics presented are the mean value, coefficient of variation (COV), minimum value (Min) and maximum value (Max). The numbers of available data points (n) are reported in the second column.

Table 5.2: Basic statistics of the 7 basic parameters in F-CLAY/7/216 [D'Ignazio et al. 2016].

Variable	n	Mean	COV	Min	Max
s_u^{FV} **(kPa)**	216	21.443	0.501	5	75
σ'_v/P_a	216	0.464	0.485	0.074	1.609
σ'_p/P_a	216	0.948	0.515	0.251	2.884
LL	216	66.284	0.298	22.0	125.0
PL	216	27.740	0.204	10.0	50.0
w	216	76.340	0.268	25.0	150.0
S_t	216	17.447	0.789	2.0	64.0

Clay properties cover a wide range of plasticity index (PI) values (2~95) and natural water content (w) values (25~150). Sensitivity (S_t) values range from 2 (insensitive clays) to 64 (quick clays).

A second independent database of Swedish and Norwegian clays consisting of 168 field vane data points is extracted from the global CLAY/10/7490 database (Ching and Phoon 2014*a*). This database is labelled as S-CLAY/7/168 ("S" for Scandinavia) and it contains multivariate information on the same 7 basic aforementioned parameters. S-CLAY/7/168 is compiled to be used as an independent set of data for comparison with F-CLAY/7/216 in subsequent analyses.

Full information on all the 7 parameters is available for only 59 data points. Information on 6 parameters with the exception of S_t is though known for the remaining 109 data points. The main practical consequence here is that the influence of S_t on s_u is more difficult to discern in the case of S-CLAY/7/168. Basic statistics of the 7 clay parameters in S-CLAY/7/168 are reported in Table 5.3.

The full multivariate F-CLAY/7/216 and S-CLAY/7/168 databases are shown in detail in Appendix A.

Table 5.3: Basic statistics of the 7 basic parameters in S-CLAY/7/168 [D'Ignazio et al. 2016].

Variable	*n*	Mean	COV	Min	Max
s_u^{FV} **(kPa)**	168	16.346	0.505	5.62	48.75
σ'_v/P_a	168	0.503	0.632	0.068	2.101
σ'_p/P_a	168	0.786	0.726	0.150	3.116
LL	168	71.055	0.396	22.77	201.81
PL	168	29.448	0.344	2.73	73.92
w	168	76.631	0.347	17.27	180.11
S_t	59	12.068	0.779	3.0	42.5

A broad physical overview of the databases is provided in Fig. 5.1, which shows how the data points are positioned in the plasticity chart. Fig. 5.2 indicates that there is a positive trend between water content (w) and liquid limit (LL). Moreover, the water content seems generally higher than the liquid limit.

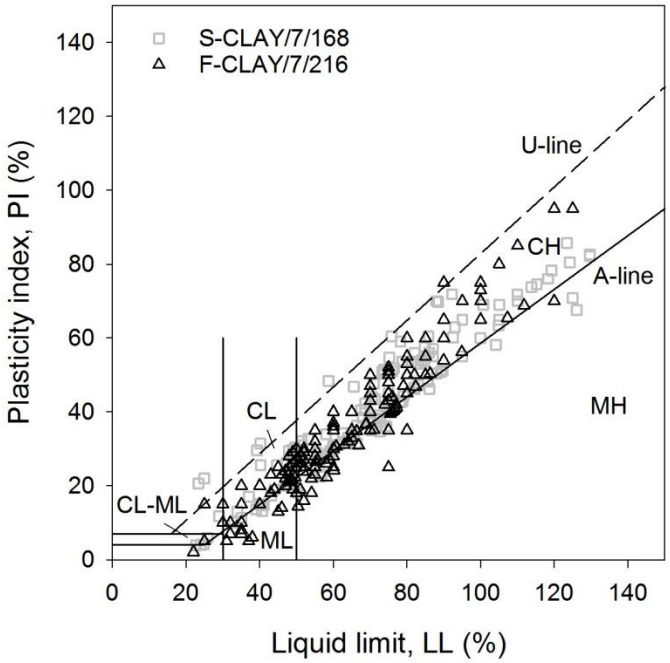

Fig. 5.1: Plasticity chart [D'Ignazio et al. *2016*].

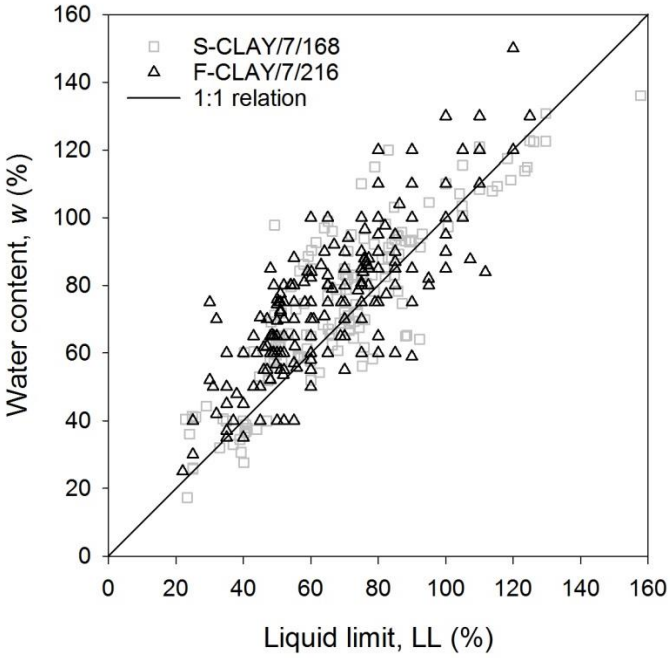

Fig. 5.2: Water content vs liquid limit for F-CLAY/7/216 and S-CLAY/7/168 [D'Ignazio et al. *2016*].

5.2.2 **Dimensionless databases: F-CLAY/10/216 and S-CLAY/10/168**

Ten (10) dimensionless soil parameters of primary interest are derived from the 7 basic clay parameters appearing in F-CLAY/7/216 and S-CLAY/7/168. The measured s_u^{FV} values are converted into $s_{u(mob)}$ through the correction factor of eq. (2.10). According to e.g. Bjerrum (1972; 1973) and Mesri and Huvaj (2007), $s_{u(mob)}$ represents the in-situ strength mobilized in embankment and slope failures.

Parameters can be categorized into two groups:

1. Index properties, including natural water content (w), liquid limit (LL), plasticity index (PI) and liquidity index (LI).
2. Stresses and strengths, including overconsolidation ratio (OCR = σ'_p/σ'_v), normalized mobilized undrained shear strength against vertical effective stress [$s_{u(mob)}/\sigma'_v$] and preconsolidation pressure [$s_{u(mob)}/\sigma'_p$], normalized undrained shear strength from field vane against vertical effective stress (s_u^{FV}/σ'_v), preconsolidation pressure (s_u^{FV}/σ'_p), and sensitivity ($S_t = s_u/s_u^{re}$, where s_u^{re} is the remolded undrained shear strength).

Fig. 5.3*a* shows the variation of the normalized undrained shear strength $s_{u(mob)}/\sigma'_v$ with overconsolidation ratio (OCR) for F-CLAY/10/216 and S-CLAY/10/168. A slightly higher mean trend of $s_{u(mob)}/\sigma'_v$ vs. OCR can be observed for Finnish clays. Such a difference could depend on the method used to determine the preconsolidation pressure (σ'_p). Indeed, as discussed in section 2.2, preconsolidation pressure values obtained from an oedometer test are strongly dependent on the strain rate used in the test. As suggested by Länsivaara (1999), $\sigma'_{pCRS}/\sigma'_{pIL} = 1.27$.

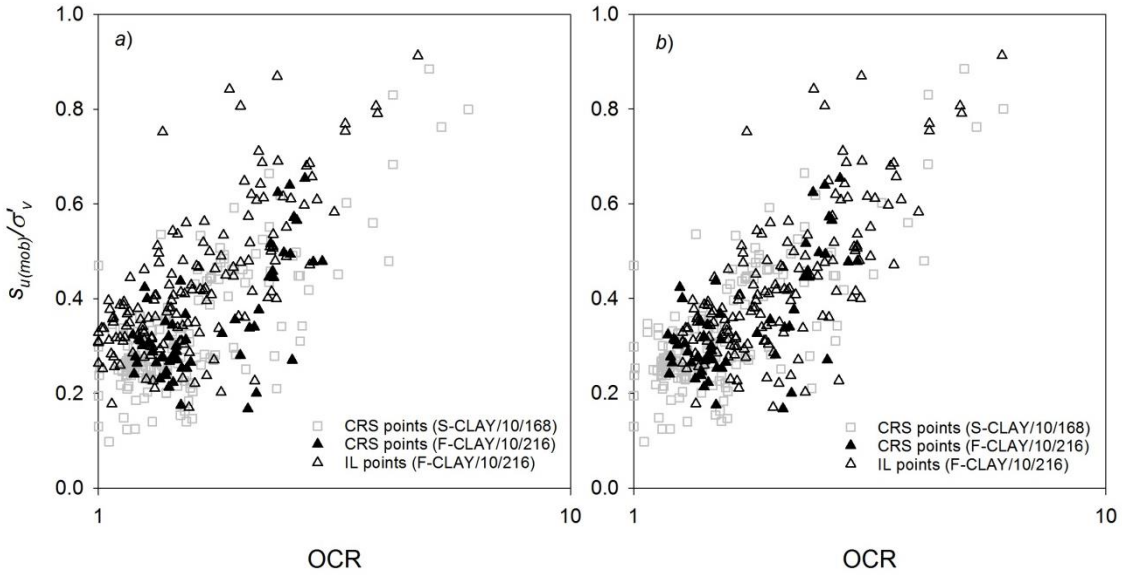

Fig. 5.3: $s_{u(mob)}/\sigma'_v$ against OCR for *a*) raw data points and *b*) data points corrected to σ'_p from CRS oedometer test using $\sigma'_{pCRS}/\sigma'_{pIL} = 1.27$ [D'Ignazio et al. 2016].

Upon examination of the original references [listed in Table A1 of Ching and Phoon (2014*a*)] which contain the clay data of S-CLAY/7/168, it seems that σ'_p points were measured from CRS oedometer test results. However, F-CLAY/7/218 contains only 56 σ'_{pCRS} points, while the remaining 162 points were measured from 24h IL tests (σ'_{pIL})

(Fig. 5.3*a*). Therefore, in order to make data suitable for direct comparison, a first-order correction based on the proposal by Länsivaara (1999) is applied to the σ'_{pIL} data points from Finland (Fig. 5.3*b*).

By applying $\sigma'_{pCRS}/\sigma'_{pIL} = 1.27$ to the 162 σ'_{pIL} values in F-CLAY/10/216, the undrained shear strength data points from Finland seem to follow a trend which is more similar to the trend of the data points in S-CLAY/10/168 (Fig. 5.3*b*). Additionally, as the CRS data points from Finland seem to adapt reasonably well to the trend of CRS data points in S-CLAY/10/168, it is plausible that the difference between the two databases in the $s_{u(mob)}/\sigma'_v$ versus OCR plot is primarily caused by the difference between the CRS and IL test, rather than a difference in the nature of the clay.

The basic statistics of the 10 dimensionless parameters are summarized in Table 5.4 and Table 5.5 for the dimensionless databases, which are labeled as F-CLAY/10/216 and S-CLAY/10/168, respectively.

Tab. 5.4: Basic statistics of 10 dimensionless soil parameters in F-CLAY/10/216, derived from the 7 basic parameters in F-CLAY/7/216 [D'Ignazio et al. 2016].

Variable	*n*	Mean	COV	Min	Max
$s_{u(mob)}/\sigma'_v$	216	0.458	0.715	0.167	2.754
$s_{u(mob)}/\sigma'_p$	216	0.209	0.281	0.081	0.469
s_u^{FV}/σ'_v	216	0.513	0.712	0.176	2.938
s_u^{FV}/σ'_p	216	0.234	0.293	0.083	0.594
OCR	216	2.170	0.467	1.18	7.50
LL	216	66.284	0.298	22.0	125.0
PI	216	38.545	0.482	2.0	95.0
w	216	76.340	0.268	25.0	150.0
LI	216	1.443	0.459	0.425	4.800
S_t	216	17.447	0.789	2.0	64.0

Tab. 5.5: Basic statistics of 10 dimensionless soil parameters in S-CLAY/10/168, derived from the 7 basic parameters in S-CLAY/7/168 [D'Ignazio et al. 2016].

Variable	*n*	Mean	COV	Min	Max
$s_{u(mob)}/\sigma'_v$	168	0.329	0.417	0.098	0.885
$s_{u(mob)}/\sigma'_p$	168	0.210	0.269	0.088	0.470
s_u^{FV}/σ'_v	168	0.386	0.469	0.098	0.974
s_u^{FV}/σ'_p	168	0.244	0.311	0.088	0.490
OCR	168	1.664	0.476	1.00	6.07
LL	168	71.06	0.396	22.77	201.81
PI	168	41.61	0.496	3.91	127.89
w	168	76.63	0.347	17.27	180.11
LI	168	1.267	0.507	0.60	5.50
S_t	59	12.068	0.779	3.00	42.50

5.2.3 **Comparison with existing transformation models**

Data points contained in F-CLAY/10/216 and S-CLAY/10/168 are compared with existing and widely used correlations in order to validate them for Finnish and Scandinavian clays. Most of the available transformation models are generally illustrative of certain types of clays and geographical locations. The basis for these models is normally empirical. Very often, information on the basic statistics is not available for such models (such as those in Table 5.4 and Table 5.5). Therefore, engineering judgment should be exercised while comparing global models to site-specific models, as differences are to be expected (Ching and Phoon 2014*a*, 2014*b*).

The 11 transformation models analyzed are labeled using the following template: (primary input parameter)-(target parameter)-(secondary input parameter). They are categorized into four types (see Table 5.6 and Table 5.7):

1. Type A. Models for S_t, including two LI-(s_u^{re}/P_a) models and two LI-(S_t) models.
2. Type B. Models for preconsolidation stress, including one LI-(σ'_p/P_a)-S_t model. Basic statistics of σ'_p/P_a are reported in Table 5.2 and 5.3 and not included in the dimensionless databases, as s_u^{FV} and $s_{u(mob)}$ are the parameters of primary interest for this study.
3. Type C. Models for shear strength, including one PI-[$s_{u(mob)}/\sigma'_p$] model, one OCR-[$s_{u(mob)}/\sigma'_v$] model, and one OCR-[$s_{u(mob)}/\sigma'_v$]-S_t model.
4. Type D. Models for shear strength, including two PI-(s_u^{FV}/σ'_p) and one LL-(s_u^{FV}/σ'_p). These three models are compared to raw field vane strength data points, as they were originally derived from uncorrected measurements.

Figs. 5.4-5.11 show the comparison between data points from F-CLAY/10/216 and S-CLAY/10/168 and the existing correlations. For the models with S_t as secondary input parameter, points are divided into two groups according to sensitivity (S_t) values, following the definition of "low to medium sensitive" (S_t < 15) and "highly sensitive" (S_t > 15) clays suggested by Karlsrud and Hernandez-Martinez (2013) for Norwegian clays.

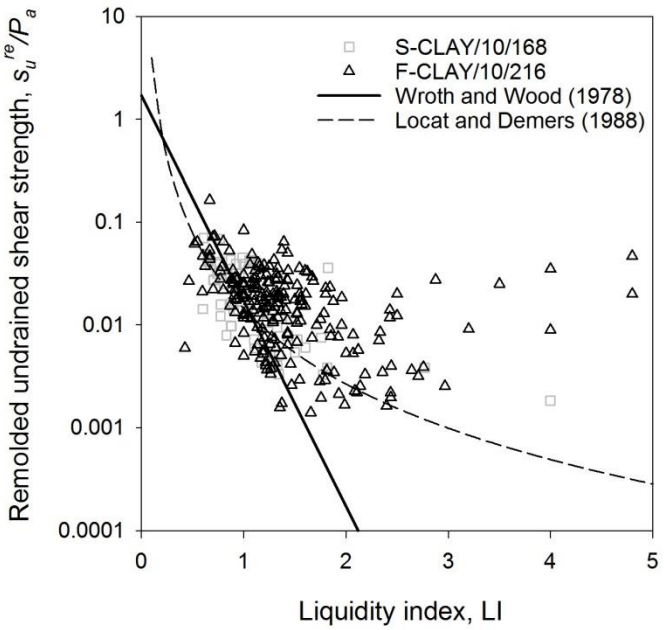

Fig. 5.4: LI-(s_u^{re}/P_a) models [D'Ignazio et al. 2016].

For liquidity index (LI) greater than 1, the LI-(s_u^{re}/P_a) model by Wroth and Wood (1978) deviates significantly from the data points. However, the transformation model by Locat and Demers (1988) seems more adaptable to the trend observed for LI < 2 (Fig. 5.4). However, consistency is not found for LI > 2, as some of the data points deviate dramatically from the mean trend.

Fig. 5.5 suggests that the trend of the data points for LI lower than 2 can be reasonably catched by the LI-(S_t) model by Bjerrum (1954), despite the high scatter. The global model by Ching and Phoon (2012), on the other hand, appears to be more descriptive of the upper bound of the database rather than the mean trend.

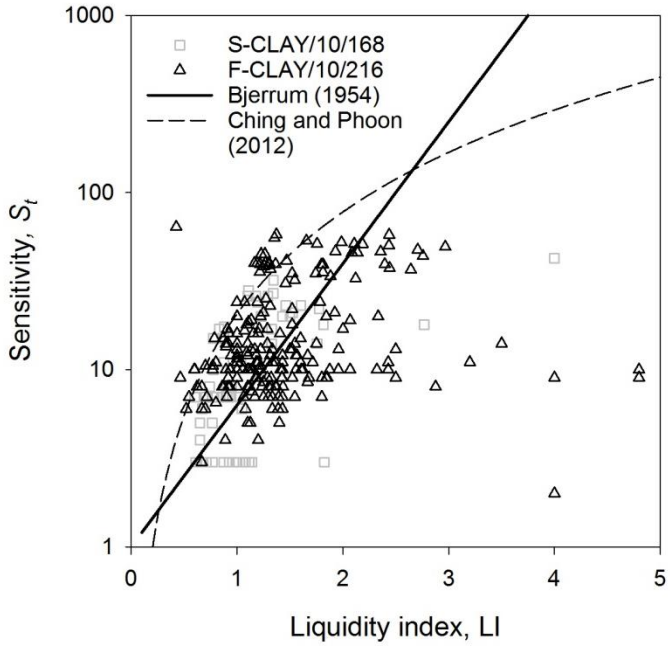

Fig. 5.5: LI-S_t models [D'Ignazio et al. 2016].

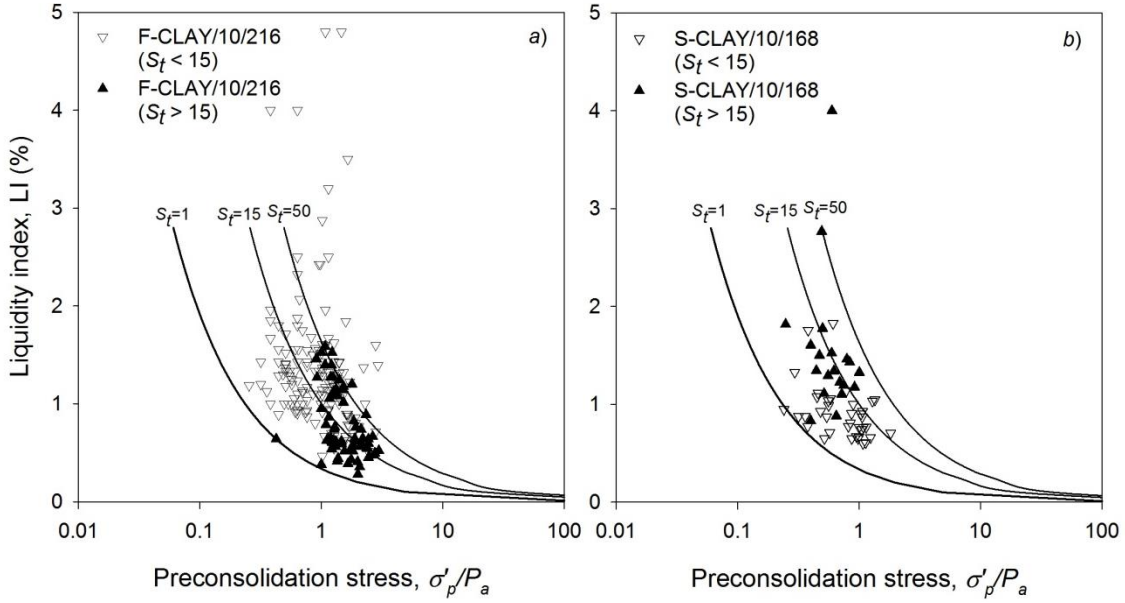

Fig. 5.6: LI-(σ'_p/P_a)-S_t model by Ching and Phoon (2012) for *a*) F-CLAY/10/216 and *b*) S-CLAY/10/168 [D'Ignazio et al. 2016].

Agreement cannot be observed between the LI-(σ'_p/P_a)-S_t model by Ching and Phoon (2012) and the data points in F-CLAY/10/216 for S_t < 15 (Fig. 5.6*a*). The model appears to give a better description of the highly sensitive clays (S_t > 15) in F-CLAY/10/216, as most of the points are confined between the LI-(σ'_p/P_a)-S_t lines for S_t = 15 and S_t = 50 (Fig. 5.6*a*). Conversely, the low to medium sensitive clay points (S_t < 15) in S-CLAY/10/168 are comprised between the LI-(σ'_p/P_a)-S_t boundary lines for S_t = 1 and S_t = 15 (Fig. 5.6*b*). However, for S_t > 15 the models do not provide a good fit to the data.

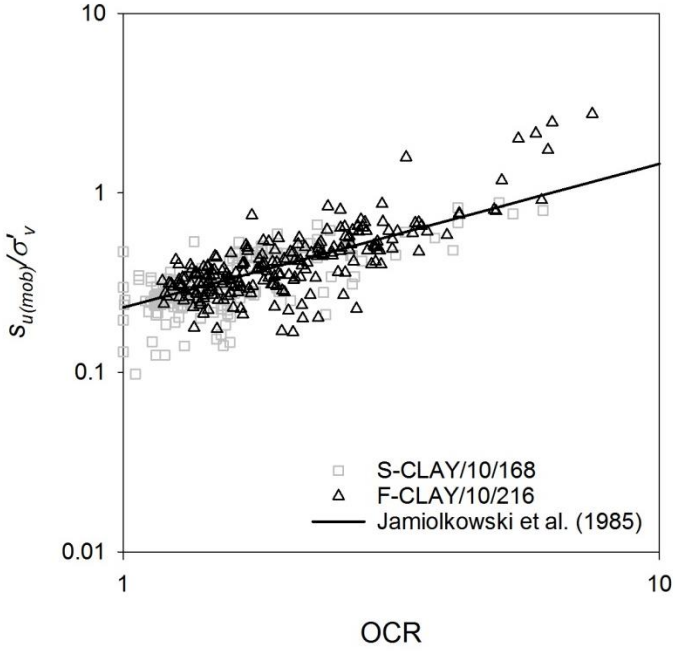

Fig. 5.7: OCR-[$s_{u(mob)}/\sigma'_v$] model proposed by Jamiolkowski et al. (1985) [D'Ignazio et al. 2016].

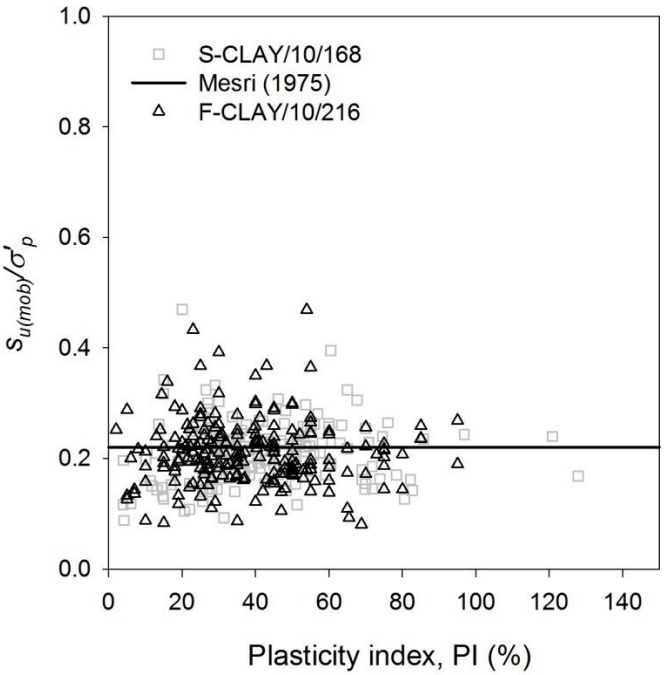

Fig. 5.8: PI-[$s_{u(mob)}/\sigma'_p$] model proposed by Mesri (1975, 1989) [D'Ignazio et al. 2016].

As suggested by Fig. 5.7, the OCR-[$s_{u(mob)}/\sigma'_v$] transformation model by Jamiolkowski et al. (1985) [eq. (2.12)] provides a reasonable description of the mean trend of the data. For OCR < 8, there seems to be a strong relation between undrained shear strength and overconsolidation ratio (OCR). A deviation from the trend line occurs for OCR values greater than 5. However, data points with OCR > 5 are located near the ground surface, where the soil might be fissured or characterized by high organic content. Therefore, limited interest is posed on those points, as this study focuses on intact inorganic clays.

The PI-[$s_{u(mob)}/\sigma'_p$] model by Mesri (1975, 1989) [eq. (2.11)] suggests $s_{u(mob)}$ to be independent of the plasticity index (PI). As shown in Fig. 5.8, $s_{u(mob)}/\sigma'_p$ does not seem to vary with PI, thus validating Mesri's hypothesis.

Data points in Fig. 5.9 seem to disagree with the OCR-[$s_{u(mob)}/\sigma'_v$]-S_t model by Ching and Phoon (2012) [eq. (2.20)], which suggests undrained shear strength to be also dependent on sensitivity (S_t), besides OCR.

The LL-(s_u^{FV}/σ'_p) model by Hansbo (1987) [eq. (2.7)] does not seem to adapt to the trend of the data points in Fig. 5.10. The PI-(s_u^{FV}/σ'_p) models of Fig. 5.11 appears to be more suitable for both F-CLAY/10/216 and S-CLAY/10/168, despite the high scatter observed along the trend lines given by Larsson (1980) [eq. (2.8)] and Chandler (1988, after Skempton 1957) [eq. (2.6)].

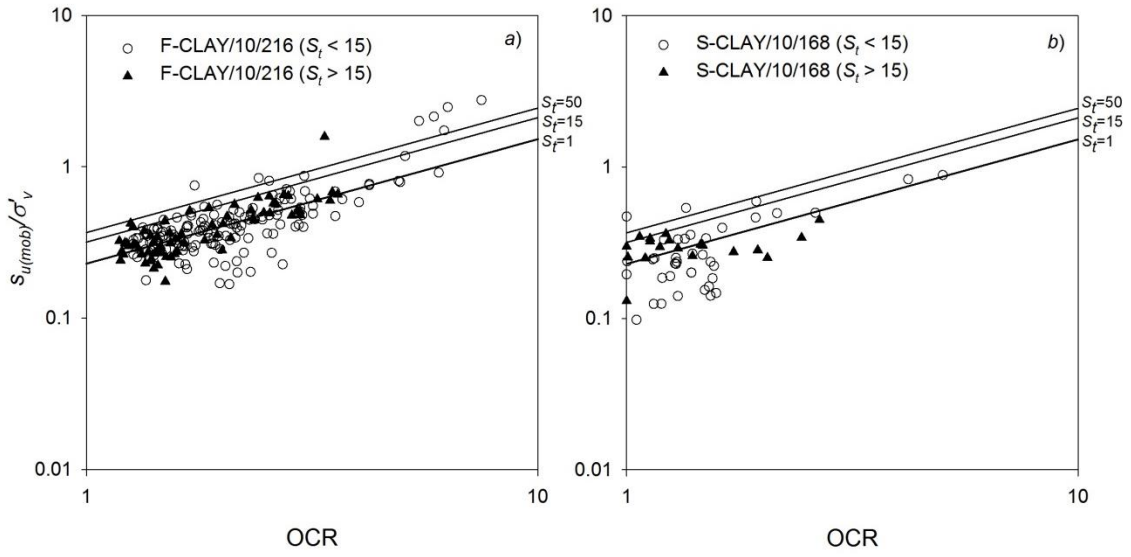

Fig. 5.9: OCR-[$s_{u(mob)}/\sigma'_v$]-S_t model by Ching and Phoon (2012) for *a*) F-CLAY/10/216 and *b*) S-CLAY/10/168 [D'Ignazio et al. 2016].

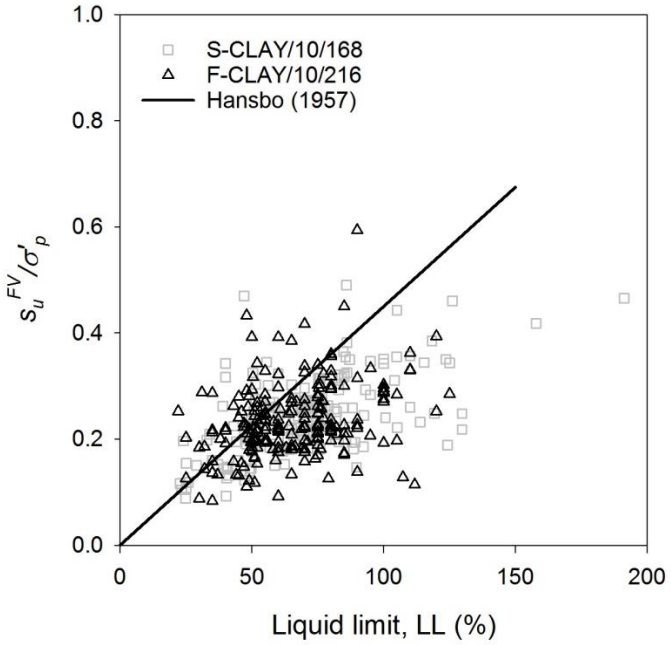

Fig. 5.10: LL-(s_u^{FV}/σ'_p) model proposed by Hansbo (1957) [D'Ignazio et al. 2016].

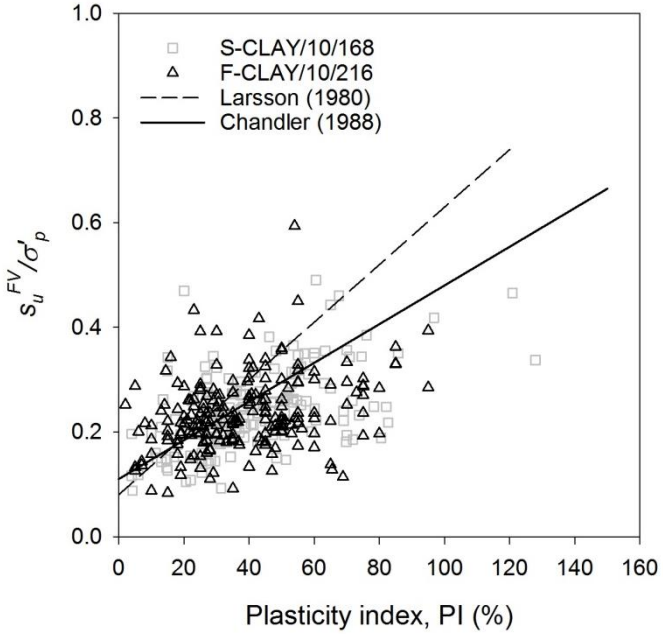

Fig. 5.11: PI-(s_u^{FV}/σ'_p) models proposed by Larsson (1980) and Chandler (1988) [D'Ignazio et al. 2016].

5.2.4 **Bias and uncertainties of the existing transformation models**

Bias factor (denoted by b), and coefficient of variation (COV, denoted by δ) are calculated and examined for the transformation models described in section 5.2.3, with respect to F-CLAY/10/216 and S-CLAY/10/168 databases.

The parameters b and δ represent the sample mean and the COV, respectively, of the ratio:

(actual target value)/(predicted target value)

This means that if b = 1, the model provides an unbiased prediction. For example, the actual target value of the OCR-[$s_{u(mob)}/\sigma'_v$] transformation model of eq. (2.12) is $s_{u(mob)}/\sigma'_v$ and the predicted target value is $0.23OCR^{0.8}$. When $s_{u(mob)}/\sigma'_v$ and OCR are simultaneously known:

$$\textit{(actual target value)/(predicted target value)} = (s_{u(mob)}/\sigma'_v)/(0.23OCR^{0.8})$$

According to Ching and Phoon (2014*a*):

$$\varepsilon = \textit{(actual target value)/(b x predicted target value) = (actual target value)/(unbiased prediction)}$$

where ε is the so called "variability term" with mean = 1 and COV = δ. If δ = 0, no data scatter exists for the transformation model, meaning that the prediction is deterministic.

Bias factors and COVs for all the analyzed correlation equations are summarized in Table 5.6 for F-CLAY/10/216 and in Table 5.7 for S-CLAY/10/168. Bias factor, COV of ε, number of data points used for each calibration are denoted, respectively, by b, δ, n.

The LI-(s_u^{re}/P_a) model by Locat and Demers (1988) underpredicts the actual values by a factor of 4.05 for F-CLAY/10/216 (Table 5.6) and 1.60 for S-CLAY/10/168 (Table 5.7).

Bjerrum's (1954) transformation model provides conservative prediction for both Finnish and Scandinavian clays. Nevertheless, these predictions are vitiated by considerable uncertainty, as the COV of ε varies between 61 and 302% for type A models.

A similar conclusion can be drawn for the LI-(σ'_p/P_a)-S_t model by Ching and Phoon (2012). The marked deviation from the mean trend lines (about 50-60%) of both F-CLAY/10/216 and S-CLAY/10/168, along with δ greater than 1 for Finnish clays, and equal to 0.61 for Scandinavian clays, would result in highly uncertain predicted target values. Therefore, models of Type A and B are "biased" with respect to both F-CLAY/10/216 and S-CLAY/10/168.

On the other hand, different observations are made for the transformation models of type C and D (undrained shear strength models). Bias factors (b) close to 1 and coefficients of variation (δ) lower than 0.30 are calculated for models of type C [$s_{u(mob)}/\sigma'_v$ is the target parameter]. The only exception is represented by the OCR-[$s_{u(mob)}/\sigma'_v$]-S_t model [eq. (2.20)], characterized by a bias factor of 0.71-0.77 and a COV of 0.32-0.36. These results

would indicate that the mobilized undrained shear strength of inorganic Scandinavian clays can be modelled through well-known transformation equations with relatively low uncertainty. For instance, equation 2.11 can be adjusted for Finnish sensitive clays by taking into account the calibrated bias factor (b) from F-CLAY/10/216 database as $s_{u(mob)}/\sigma'_p = b[0.22] = 0.95[0.22] = 0.209$, with COV ($\delta$) = 0.28, which would indicate relatively low variability.

A bias factor b varying between 0.82 and 0.97, accompanied by δ values ranging from 0.31 to 0.43, is calculated for type D models (s_u^{FV}/σ'_p is the target parameter). This would suggest that predicted values from these models are characterized by reasonably low variability. In particular, the PI-(s_u^{FV}/σ'_p) model proposed by Chandler (1988) [eq. (2.6)] is nearly "unbiased" with respect to both databases, as b varies between 0.96-0.97 and δ between 0.31 and 0.35.

Table 5.6. Transformation models in literature and their calibration results for F-CLAY/10/216 [after D'Ignazio et al. 2016].

					Calibration results	
Type	Relationship	Literature	n	Transformation model	Bias factor, b	COV of $\varepsilon = \delta$
A	LI-(s_u^{re}/P_a)	Wroth and Wood (1978)	216	$s_u^{re}/P_a = 1.7\exp(-4.6LI)$	-	-
		Locat and Demers (1988)	216	$s_u^{re}/P_a = 0.0144LI^{-2.44}$	4.05	3.02
	LI-(S_t)	Bjerrum (1954)	216	$S_t = 10^{0.8LI}$	1.56	1.40
		Ching and Phoon (2012)	216	$S_t = 20.726LI^{1.910}$	0.57	1.94
B	LI-(σ'_p/P_a)-S_t (for S_t<15)	Ching and Phoon (2012)	216	$\sigma'_p/P_a = 0.235LI^{-1.319}S_t^{0.536}$	2.02	0.94
	LI-(σ'_p/P_a)-S_t (for S_t>15)	Ching and Phoon (2012)	216	$\sigma'_p/P_a = 0.235LI^{-1.319}S_t^{0.536}$	0.95	0.47
C	PI-[$s_{u(mob)}/\sigma'_p$]	Mesri (1975; 1989)	216	$s_{u(mob)}/\sigma'_p = 0.22$	0.95	0.28
	OCR-[$s_{u(mob)}/\sigma'_v$]	Jamiolkowski et al. (1985)	216	$s_{u(mob)}/\sigma'_v = 0.23OCR^{0.8}$	1.06	0.30
	OCR-[$s_{u(mob)}/\sigma'_v$]-S_t	Ching and Phoon (2012)	216	$s_{u(mob)}/\sigma'_v = 0.229OCR^{0.823}S_t^{0.121}$	0.77	0.32
D	LL-(s_u^{FV}/σ'_p)	Hansbo (1957)	216	$s_u^{FV}/\sigma'_p = 0.45LL$	0.84	0.38
	PI-(s_u^{FV}/σ'_p)	Larsson (1980)	216	$s_u^{FV}/\sigma'_p = 0.08+0.0055PI$	0.89	0.43
		Chandler (1988)	216	$s_u^{FV}/\sigma'_p = 0.11+0.0037PI$	0.97	0.35

Table 5.7. Transformation models in literature and their calibration results for S-CLAY/10/168 [after D'Ignazio et al. 2016].

					Calibration results	
Type	Relationship	Literature	*n*	Transformation model	Bias factor, *b*	COV of $\varepsilon = \delta$
A	LI-(s_u^{re}/P_a)	Wroth and Wood (1978)	59	$s_u^{re}/P_a = 1.7\ \exp(-4.6LI)$	-	-
		Locat and Demers (1988)	59	$s_u^{re}/P_a = 0.0144LI^{-2.44}$	1.60	0.96
	LI-(S_t)	Bjerrum (1954)	59	$S_t = 10^{0.8LI}$	1.48	0.65
		Ching and Phoon (2012)	59	$S_t = 20.726LI^{1.910}$	0.49	0.61
B	LI-(σ'_p/P_a)-S_t (for S_t<15)	Ching and Phoon (2012)	59	$\sigma'_p/P_a = 0.235LI^{-1.319}S_t^{0.536}$	1.23	0.51
	LI-(σ'_p/P_a)-S_t (for S_t>15)	Ching and Phoon (2012)	59	$\sigma'_p/P_a = 0.235LI^{-1.319}S_t^{0.536}$	0.84	0.54
C	PI-[$s_{u(mob)}/\sigma'_p$]	Mesri (1975; 1989)	168	$s_{u(mob)}/\sigma'_p = 0.22$	0.96	0.27
	OCR-[$s_{u(mob)}/\sigma'_v$]	Jamiolkowski et al. (1985)	168	$s_{u(mob)}/\sigma'_v = 0.23OCR^{0.8}$	0.97	0.25
	OCR-($s_{u(mob)}/\sigma'_v$)-S_t	Ching and Phoon (2012)	168	$s_{u(mob)}/\sigma'_v = 0.229OCR^{0.823}S_t^{0.121}$	0.71	0.36
D	LL-(s_u^{FV}/σ'_p)	Hansbo (1957)	168	$s_u^{FV}/\sigma'_p = 0.45LL$	0.82	0.34
	PI-(s_u^{FV}/σ'_p)	Larsson (1980)	168	$s_u^{FV}/\sigma'_p = 0.08+0.0055PI$	0.85	0.37
		Chandler (1988)	168	$s_u^{FV}/\sigma'_p = 0.11+0.0037PI$	0.96	0.31

5.3 s_u/σ'_v transformation models for F-CLAY/10/173 database

5.3.1 Removal of outliers in F-CLAY/10/216

The purpose of this study is to derive new correlations to enhance the knowledge on how undrained shear strength is related to index parameters and consolidation stresses. In order to obtain more refined and reliable results, data points in F-CLAY/10/216 are examined in detail and outliers are removed to improve the quality of the database. Three criteria based on physical nature of the soil, mechanical characteristics and statistical considerations are used to assess the quality of the collected information. The adopted criteria are defined as follows:

i) Points located near the ground surface are removed, as they are likely to belong to dry crust layers. Surficial weathered layers are normally partially saturated and present cracks and fissures. The field vane strength measured from these layers is generally higher than the actual available strength, as discussed in section 3.2. Dry crust layers overlying Finnish clay deposits are on average 1-2 m thick. Therefore, points located up to 1.50 m from the ground surface are discarded.

ii) Points where $s_{u(mob)}/\sigma'_p$ is lower than the initial stress mobilization in the soil for normally consolidated state, i.e. $\tau_0/\sigma'_p = 0.5\cdot(1-K_0) = 0.15$ are removed. K_0 is the earth pressure coefficient at rest calculated from Jaky's (1944) well-known equation ($K_0 = 1 - \sin\phi'$). $\tau_0 = 0.15$ implies $\phi' = 18°$, which may represent, according to the author's experience, a low boundary value for friction angle of Finnish soft clays.

iii) Statistical outliers are removed through the 2σ criteria [95% confidence interval of $s_{u(mob)}/\sigma'_v$]. σ is the standard deviation of the variable $s_{u(mob)}/\sigma'_v$. Data points where, for a given *i-th* element of the sample the criteria $|[s_{u(mob)}/\sigma'_v]_i - \text{mean}[s_{u(mob)}/\sigma'_v]| > 2\sigma$ is satisfied, are removed. Outliers are commonly removed from a data set through the 3σ criteria, which represent the 99% confidence interval of the data. A more selective criterion than the 3σ was preferred in this study, in alternative to a debatable "visual" removal criteria, because of the inherent soil variability of clay deposits. Undrained shear strength profiles from field vane test are likely to show marked fluctuations from the mean trend. Such variability may hinge upon the inherent variability of soil layers, in terms of e.g. grain size distribution or index properties. Furthermore, sample disturbance may affect the preconsolidation pressure (σ'_p) values and, hence, the ratio $s_{u(mob)}/\sigma'_p$.

The removed data points are 43 out of 216, corresponding to 20% of the population. In detail, 10, 24, and 9 points are discarded based on criteria i), ii) and iii), respectively. Therefore, the new correlations will be based on 173 clay data points where undrained shear strength from field vane (s_u^{FV}), vertical effective stress (σ'_v), vertical preconsolidation pressure (σ'_p), natural water content (w), liquid limit (LL), plastic limit (PL) and sensitivity (S_t) are known.

The refined dimensionless database is hereinafter referred to as F-CLAY/10/173. Updated basic statistics of F-CLAY/10/173 database are presented in Table 5.8. The effects of the outliers removal procedure are clearly visible from Table 5.9, as a reduction of the COV can be observed for all the dimensionless variables. Index parameters and sensitivity are

not remarkably influenced by the procedure. However, OCR range changes considerably from 1.2~7.50 to 1.2~3.70. OCR values lower than 4 are though expected to be found in clay deposits in Finland. For this reason, strength of Finnish clays presenting OCR values higher than 4 will not be surveyed in this study.

Tab. 5.8: Basic statistics of the data points after removal of outliers (database F-CLAY/10/173) [D'Ignazio et al. 2016].

Variable	*n*	Mean	COV	Min	Max
$s_{u(mob)}/\sigma'_v$	173	0.399	0.284	0.213	0.690
$s_{u(mob)}/\sigma'_p$	173	0.213	0.183	0.148	0.338
s_u^{FV}/σ'_v	173	0.447	0.306	0.226	0.920
s_u^{FV}/σ'_p	173	0.239	0.203	0.148	0.394
OCR	173	1.91	0.31	1.18	3.69
LL	173	66.4	0.29	22	125.0
PI	173	38	0.47	2	95.0
w	173	78.3	0.25	25.00	150.0
LI	173	1.48	0.43	0.46	4.80
S_t	173	18.80	0.76	2.00	58.0

Tab. 5.9: Change in the basic statistics of the data points before and after removal of outliers (database F-CLAY/10/216 vs. F-CLAY/10/173).

	n		Mean		COV		Min		Max	
Variable	*Before*	*After*	*Before*	*After*	*Before*	*After*	*Before*	*After*	*Before*	*After*
$s_{u(mob)}/\sigma'_v$	216	173	0.458	0.399	0.715	0.284	0.167	0.213	2.754	0.690
$s_{u(mob)}/\sigma'_p$	216	173	0.209	0.213	0.281	0.183	0.081	0.148	0.469	0.338
s_u^{FV}/σ'_v	216	173	0.513	0.447	0.712	0.306	0.176	0.226	2.938	0.920
s_u^{FV}/σ'_p	216	173	0.234	0.239	0.293	0.203	0.083	0.148	0.594	0.394
OCR	216	173	2.170	1.91	0.467	0.31	1.18	1.18	7.50	3.69
LL	216	173	66.284	66.4	0.298	0.29	22.0	22	125.0	125.0
PI	216	173	38.545	38	0.482	0.47	2.0	2	95.0	95.0
w	216	173	76.340	78.3	0.268	0.25	25.0	25.00	150.0	150.0
LI	216	173	1.443	1.48	0.459	0.43	0.425	0.46	4.800	4.80
S_t	216	173	17.447	18.80	0.789	0.76	2.0	2.00	64.0	58.0

5.3.2 **Derivation of the new transformation models**

The new transformation models for undrained shear strength of Finnish clays are derived based on the SHANSEP framework of eq. (2.2).

Linear regression analyses are carried out using the "fminsearch" algorithm implemented into the mathematical software Matlab 2012. "fminsearch" function, according to MATLAB user's manual (1995), gives the minimum of an unconstrained multivariable function through a derivative free method (unconstrained linear optimization). The multivariable function $F = f(s_{u,i}/\sigma'_v, \text{OCR}, Y_j)$ is defined as follows:

$$F = \frac{s_{u,i}}{\sigma'_v} = S \cdot OCR^m \cdot Y_j^\gamma \tag{5.1}$$

where $s_{u,i} = \{s_{u,1} = s_{u(mob)}, s_{u,2} = s_u^{FV}\}$, $Y_j = \{Y_1 = \text{PI}, Y_2 = \text{LL}, Y_3 = w, Y_4 = \text{LI}, Y_5 = S_t\}$. The scalar coefficients S, m and γ and the coefficient of determination (r^2) for the new OCR-($s_{u,i}/\sigma'_v$)-Y_j transformation models are provided in Table 5.10. The coefficient of determination (r^2) of the correlations varies in the interval 0.62-0.70. When using a different multivariable function, for instance assuming S and m as linear functions of Y_j (see e.g. Karlsrud and Hernandez-Martinez 2013), the r^2 values do not significantly differ from those presented in Table 5.10.

The outcomes of the regression analyses (Table 5.10) indicate that for the OCR-(s_u^{FV}/σ'_v)-Y_j transformation model, s_u^{FV}/σ'_v increases with increasing PI, LL, w while it decreases with increasing LI. s_u^{FV}/σ'_v seems independent of S_t. In contrast, the dependency on index parameters is less visible for the OCR-[$s_{u(mob)}/\sigma'_v$]-Y_j model, as $s_{u(mob)}/\sigma'_v$ seems to only lightly correlate with secondary input parameters. Such a conclusion could be drawn by simply looking at the scalar coefficient γ for the OCR-[$s_{u(mob)}/\sigma'_v$]-Y_j models in Table 5.10. For γ values greater than 0, s_u increases with increasing Y_j; on the contrary, for negative values of γ, s_u reduces with increasing Y_j.

Table 5.10. Linear regression coefficients for multivariable function F [D'Ignazio et al. 2016].

Transformation model	Secondary input parameter (Y_j)	S	m	γ	r^2
OCR - [$s_{u(mob)}/\sigma'_v$] – Y_j	Y_1 (PI)	0.242	0.763	-0.013	*0.67*
	Y_2 (LL)	0.245	0.760	-0.005	*0.67*
	Y_3 (w)	0.246	0.760	0.027	*0.67*
	Y_4 (LI)	0.241	0.770	0.045	*0.67*
	Y_5 (S_t)	0.242	0.762	0.006	*0.67*
OCR - (s_u^{FV}/σ'_v) – Y_j	Y_1 (PI)	0.328	0.756	0.165	*0.68*
	Y_2 (LL)	0.319	0.757	0.333	*0.70*
	Y_3 (w)	0.296	0.788	0.337	*0.69*
	Y_4 (LI)	0.281	0.770	-0.088	*0.63*
	Y_5 (S_t)	0.280	0.786	-0.013	*0.62*

Although γ values seem to indicate that the $s_{u(mob)}/\sigma'_v$ - OCR trend is influenced by Y_j parameters, it should be emphasized how the term Y_j^{γ} of eq. (5.1) is nearly equal to unity, as γ tends to zero for the OCR-[$s_{u(mob)}/\sigma'_v$]-Y_j transformation model. The main outcome is that $s_{u(mob)}/\sigma'_v$ is only slightly dependent or nearly independent of the secondary input variable Y_j, and, at the same time, it is markedly dependent on OCR. This result agrees with the findings of Jamiolkowski et al. (1985). However, as discussed in Chapter 2, Mesri (1975, 1989) suggested m = 1, while, as shown in Table 5.9, for Finnish clays m results lower than 1.

Finally, by assuming γ = 0 and averaging the S and m values of the five OCR-[$s_{u(mob)}/\sigma'_v$]-Y_j correlation equations of Table 5.9, for Finnish soft clays [eq. (5.2)]:

$$\frac{s_{u(mob)}}{\sigma'_v} \approx 0.244 \cdot OCR^{0.763} \qquad (5.2)$$

which nearly corresponds to the unbiased transformation model of eq. (2.12) by Jamiolkowski et al. (1985). The calibrated bias factor (b) from F-CLAY/10/216 database for the OCR-[$s_{u(mob)}/\sigma'_v$] model by Jamiolkowski et al. (1985) is equal to 1.06, as reported in Table 5.6. This implies $s_{u(mob)}/\sigma'_v = b(0.23)\mathrm{OCR}^{0.8} = 0.244\mathrm{OCR}^{0.8}$ with a coefficient of variation equal to 0.30.

5.3.3 **Validation of the new transformation models**

Results presented in Table 5.10 denote that the OCR-(s_u^{FV}/σ'_v)-Y_j transformation model is strongly dependent on index parameters. As already shown in section 2.5, similar observations were also made by Larsson et al. (2007) and by Karlsrud and Hernandez-Martinez (2013) for clay specimens tested under triaxial compression, triaxial extension and direct simple shear conditions. It was shown how the anisotropic undrained shear strength of Scandinavian and Norwegian clays increases with increasing liquid limit and natural water content, respectively. Such results may be justified by the high strain rates typically used in laboratory tests, where failure occurs within a few hours, if compared to strain rates in the field, where failure may be reached after several days.

However, while undrained TXC, TXE, DSS tests are normally performed at a rate of strain of 1%/h, field vane test induces in the clay strain rates typically 50-60 times larger (i.e. 60%/h, Ching et al. 2013).

As suggested by e.g. Jamiolkowski et al. (1985) and Chandler (1988), field vane and DSS strength are somewhat comparable. s_u^{DSS} is used in Sweden as reference test for calibration of e.g. CPT and field vane test (e.g. Larsson and Mulabdic 1991; Westerberg et al. 2015). However, a direct comparison between s_u^{DSS} and s_u^{FV} may lack of consistency, as a correction should be applied to s_u^{FV} to account for the strain-rate difference between laboratory test and field (Bjerrum 1972). Therefore, equations (2.14) and (2.17) for DSS strength will be only used for qualitative comparison with the correlations derived in section 5.3.2.

The OCR-(s_u^{FV}/σ'_v)-Y_j transformation model is compared to eq. (2.14) and eq. (2.17) in Fig. 5.12 and Fig. 5.13, respectively. Fig. 5.12 seems to indicate that the normalized field vane strength is generally higher than the DSS strength. Exception in made for clays with LL > 100%. This is possibly a consequence of the limited amount of data points with LL > 100% available in F-CLAY/10/173.

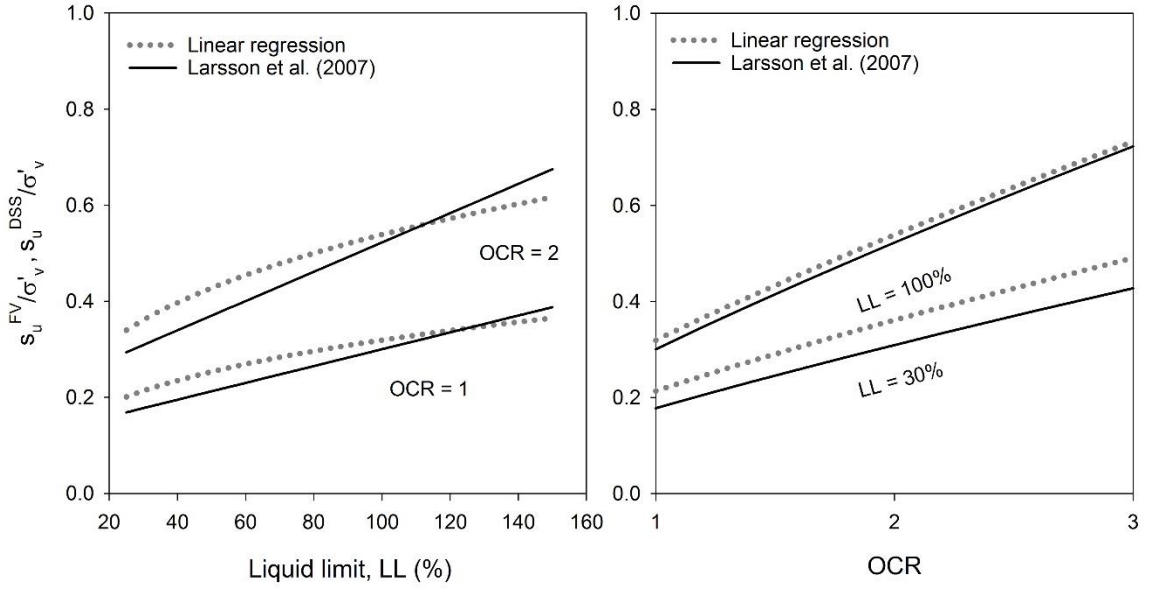

Fig. 5.12: comparison between OCR-(s_u^{FV}/σ'_v)-LL for Finnish clays and OCR-(s_u^{DSS}/σ'_v)-LL model by Larsson et al. (2007) for Swedish clays [D'Ignazio et al. 2016].

More uncertainties appear for the models where the natural water content (w) is the secondary input parameter. Eq. (2.17) for s_u^{DSS} seems to notably deviate from the mean trend of F-CLAY/10/173 data points (Fig. 5.13). Eq. (2.17) intersects the OCR-(s_u^{FV}/σ'_v)-w line, thus suggesting that for a certain number of combinations of OCR and w, s_u^{DSS} of Norwegian clays would be higher than s_u^{FV} of Finnish clays. One possible explanation for such unexpected finding could be that eq. (2.17) is based only on a limited number of DSS tests, as reported by Karlsrud and Hernandez-Martinez (2013). Another possible reason could be the difference in the water content intervals of the data points. Indeed, the water content of the specimens tested by Karlsrud and Hernandez-Martinez (2013) was about 25~80%, while the new OCR-(s_u^{FV}/σ'_v)-w model is calibrated from an ampler range of w (w = 25-150%). Hence, eq. (2.17) must be carefully used as, based on this study, consistency is found only for values of natural water content lower than 60%.

Fig. 5.14 shows the variation of the OCR-(s_u^{FV}/σ'_v)-LL model for various LL ranges. For Finnish sensitive clays, trend lines (solid lines) for given LL values move gently upwards for increasing liquid limit (LL). The illustrated trend lines seem to find consistency with the points from the S-CLAY/10/168 database, grouped based on the LL ranges chosen.

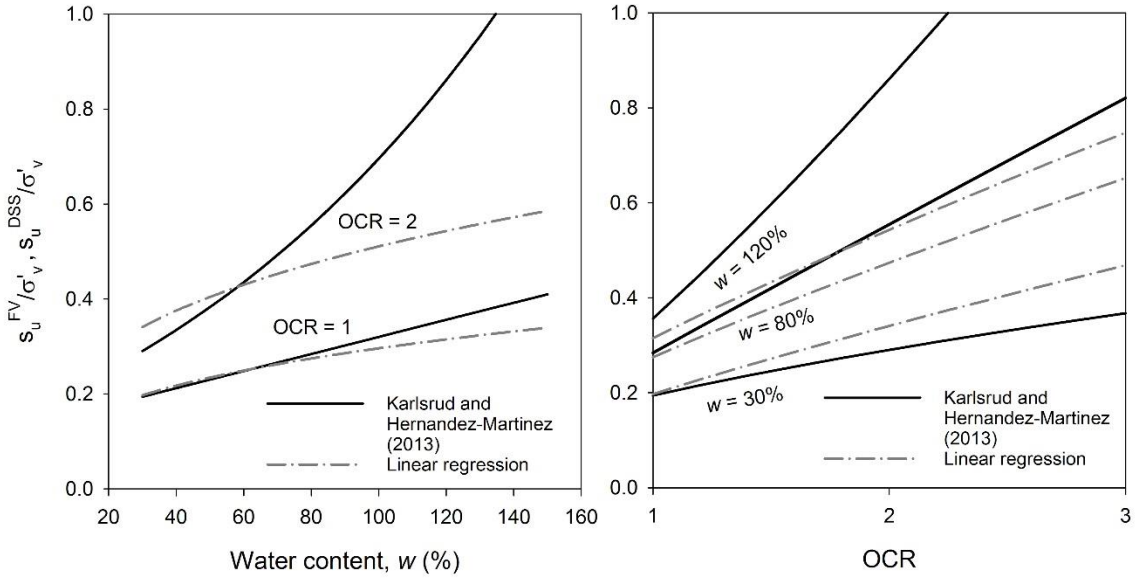

Fig. 5.13: comparison between OCR-(s_u^{FV}/σ'_v)-w for Finnish clays and OCR-[s_u^{DSS}/σ'_v]-w model by Karlsrud and Hernandez-Martinez (2013) for Norwegian clays [D'Ignazio et al. 2016].

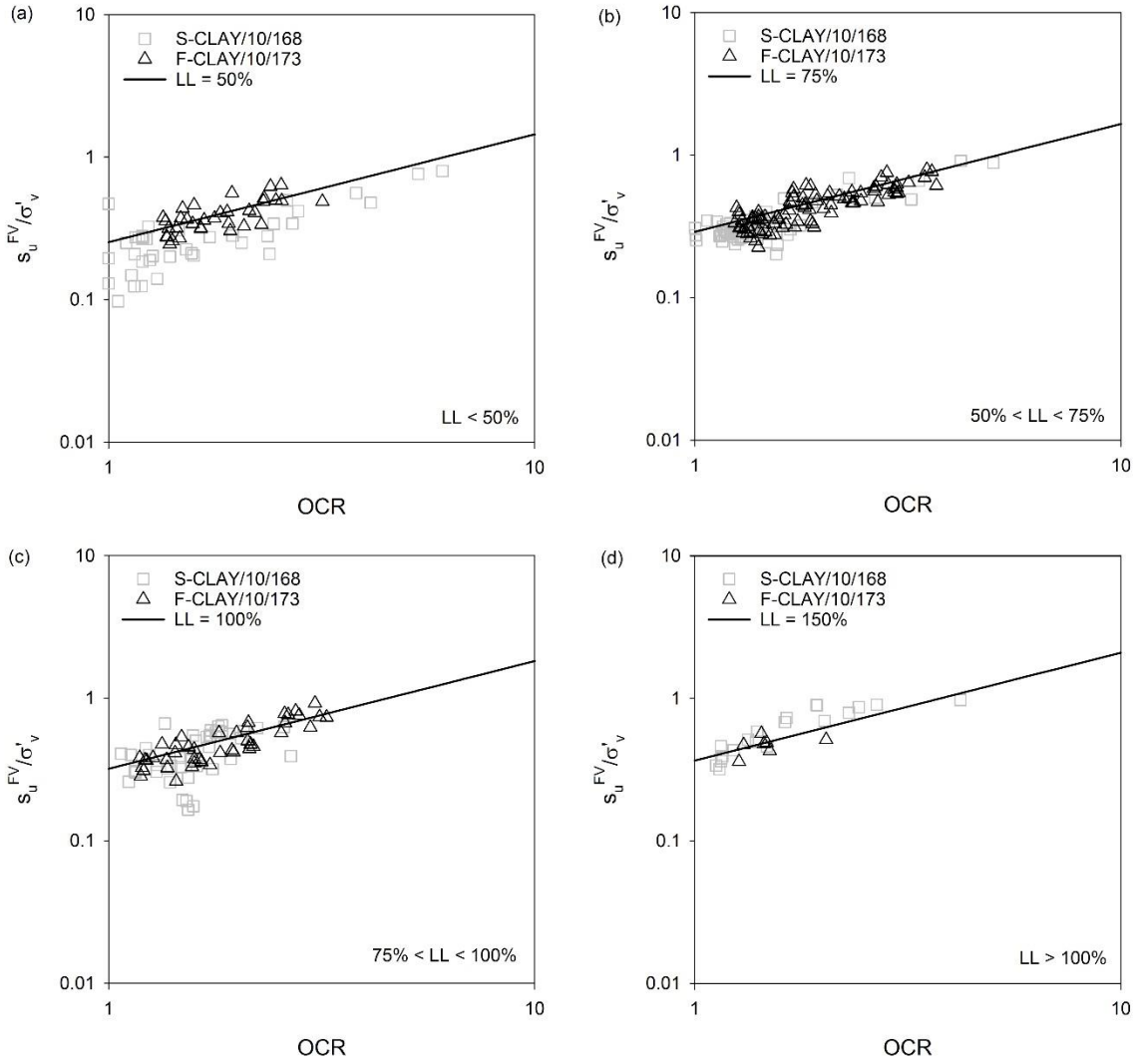

Fig. 5.14: Comparison between measured (calibration and validation) data and OCR-(s_u^{FV}/σ'_v)-LL model for Finnish clays for various LL ranges [D'Ignazio et al. 2016].

5.3.4 **Bias and uncertainties of the new transformation models**

Bias factor (b) and coefficient of variation of ε (δ) are evaluated for the transformation models of section 5.3.2 through the independent S-CLAY/10/168 database of clays from Sweden and Norway. b and δ of the new correlation equations are listed in Table 5.11.

Calculated b values fall into the range 0.94-0.97 for the new models when PI, LL, w and LI are considered, along with COV values lower than 0.3. The only exception is made for the OCR-(s_u^{FV}/σ'_v)-LI model which has δ = 0.33. This implies that the new correlations are almost "unbiased" with respect to S-CLAY/10/168 database.

The OCR-(s_u^{FV}/σ'_v)-S_t and OCR-[$s_{u(mob)}/\sigma'_v$]-S_t models show the lowest bias factors and the highest coefficients of variation. One possible explanation could be that b and δ of the models with S_t as secondary input parameter are estimated from a lower number of data points (n = 59) than the other models (n = 168).

In addition, the new correlations seem less "biased" than the existing type C and type D models presented in section 5.2.3. In particular, s_u^{FV} from the new equations is less "biased" (b~1) than s_u^{FV} from type D models of Table 5.6, as δ values of Table 5.10 are generally lower than 0.3, while δ from Table 5.6 varies between 0.35 and 0.43. Moreover, predictions of the new $s_{u(mob)}$ models from Table 5.11 are characterized by the lowest uncertainty, as the coefficient of variation (δ) can be as low as 0.25.

Table 5.11. Transformation models for Finnish clays and their calibration results for S-CLAY/10/168 [D'Ignazio et al. 2016].

			Calibration results	
Relationship	n	Transformation model	Bias factor, b	COV of $\varepsilon = \delta$
OCR-[$s_{u(mob)}/\sigma'_v$]-PI	168	$s_{u(mob)}/\sigma'_v = 0.242\text{OCR}^{0.763}\text{PI}^{-0.013}$	0.94	0.26
OCR-[$s_{u(mob)}/\sigma'_v$]-LL	168	$s_{u(mob)}/\sigma'_v = 0.245\text{OCR}^{0.760}\text{LL}^{-0.005}$	0.94	0.25
OCR-[$s_{u(mob)}/\sigma'_v$]-w	168	$s_{u(mob)}/\sigma'_v = 0.246\text{OCR}^{0.760}w^{0.027}$	0.94	0.25
OCR-[$s_{u(mob)}/\sigma'_v$]-LI	168	$s_{u(mob)}/\sigma'_v = 0.241\text{OCR}^{0.770}\text{LI}^{0.045}$	0.95	0.26
OCR-[$s_{u(mob)}/\sigma'_v$]-S_t	59	$s_{u(mob)}/\sigma'_v = 0.242\text{OCR}^{0.762}S_t^{0.006}$	0.90	0.34
OCR-(s_u^{FV}/σ'_v)-PI	168	$s_u^{FV}/\sigma'_v = 0.328\text{OCR}^{0.756}\text{PI}^{0.165}$	0.95	0.29
OCR-(s_u^{FV}/σ'_v)-LL	168	$s_u^{FV}/\sigma'_v = 0.319\text{OCR}^{0.757}\text{LL}^{0.333}$	0.94	0.26
OCR-(s_u^{FV}/σ'_v)-w	168	$s_u^{FV}/\sigma'_v = 0.296\text{OCR}^{0.788}w^{0.337}$	0.97	0.27
OCR-(s_u^{FV}/σ'_v)-LI	168	$s_u^{FV}/\sigma'_v = 0.281\text{OCR}^{0.770}\text{LI}^{-0.088}$	0.95	0.33
OCR-(s_u^{FV}/σ'_v)-S_t	59	$s_u^{FV}/\sigma'_v = 0.280\text{OCR}^{0.786}S_t^{-0.013}$	0.91	0.44

5.4 Discussion

The determination of vertical preconsolidation pressure (σ'_p) is of great importance for assessing the undrained shear strength of clays. As reported in Table 5.10, the undrained shear strength of Finnish clays is markedly dependent on the overconsolidation ratio (OCR) and, hence, on σ'_p.

The importance of the test procedure used for evaluating σ'_p is discussed in section 2.2. Based on the work by Leroueil (1996) and Länsivaara (1999), σ'_p values for Finnish clays determined from IL oedometer test (σ'_{pIL}) were increased by a factor of 1.27 to compensate the discrepancy with CRS oedometer test, which are normally used in Scandinavia. The effect of the ratio $\sigma'_{pCRS}/\sigma'_{pIL}$ on the mobilized s_u has been evaluated. When using $\sigma'_{pCRS}/\sigma'_{pIL}$ = 1.20, the coefficients *S* and *m* of eq. (2.2) become 0.253 and 0.764, respectively, thus indicating a slightly higher $s_{u(mob)}$ than from eq. (5.2). On the contrary, a moderately lower undrained shear strength is obtained for $\sigma'_{pCRS}/\sigma'_{pIL}$ = 1.35. *S* and *m* become then 0.237 and 0.747, respectively.

In addition, when using a correction factor (μ) for s_u^{FV} which differs from the one presented in eq. (2.10), the linear regression coefficients seem to lightly diverge from those presented in Table 5.9, although the r^2 values remain substantially the same. The multiplier μ used to transform s_u^{FV} into $s_{u(mob)}$ was reported by several authors as dependent on plasticity. In particular, Helenelund (1977) and Larsson et al. (2007) reported μ as a function of liquid limit, while Bjerrum (1972) suggested μ as a function of plasticity index. Table 5.12 summarizes the SHANSEP coefficients *S* and *m* assuming different transformation models for μ, derived for the OCR-[$s_{u(mob)}/\sigma'_v$] model.

Table 5.12. SHANSEP coefficients for OCR-[$s_{u(mob)}/\sigma'_v$] transformation model based on different correction factors for field vane strength in the literature.

Reference in the literature	*S*	*m*
Bjerrum (1972)	0.238	0.745
Helenelund (1977)	0.242	0.747
Larsson and Åhnberg (2005)	0.23	0.745
Finnish Guidelines [eq. (2.10)]	0.244	0.763

The usefulness of eq. (5.2) is highly practical, as it can be exploited when information on preconsolidation pressure, unit weight and groundwater table are known, to estimate the undrained shear strength variation with depth of a clay layer. Furthermore, when the corrected undrained shear strength from field vane [$s_{u(mob)}$] is known, eq. (5.2) can serve as a tool for assessing the in-situ OCR at each s_u measurement points and, therefore, provide information on the OCR variation with depth. The OCR, representative of CRS test results, can be expressed as:

$$OCR_{CRS} \approx 6.35 \cdot \left[\frac{s_{u(mob)}}{\sigma'_v} \right]^{1.31} \qquad (5.3)$$

5.5 Conclusions

A calibration database of multivariate clay data points from Finland is compiled in this study for the first time. The main purpose was to provide correlations for undrained shear strength (s_u) of Finnish clays and survey the dependency of s_u on the overconsolidation ratio (OCR), natural water content (w), liquid limit (LL), plasticity index (PI), liquidity index (LI) and sensitivity (S_t).

According to the results of this study, uncorrected undrained shear strength from field vane (s_u^{FV}), OCR and index parameters (PI, LL, w and LI) are interdependent, except for sensitivity (S_t), which seems to have a minor influence on s_u^{FV}.

On the contrary, the mobilized undrained shear strength of Finnish soft clays [$s_{u(mob)}$] seems mainly function of OCR and not significantly affected by third-order information.

Consistency of the new transformation models was firstly checked through comparison with existing transformation models for undrained shear strength of Swedish and Norwegian clays and, secondly, through evaluation of bias factor and coefficient of variation with respect to another independent validation database.

From the validation process, it seemed that the trend suggested by the new equations is comparable to the relation suggested by Larsson et al. (2007) for DSS strength of Scandinavian clays. However, more discrepancies were encountered when comparing the new models to the DSS strength equation for Norwegian clays proposed by Karlsrud and Hernandez-Martinez (2013).

Furthermore, bias factors and coefficients of variation associated with the validation database were checked. Consistency was found from the validation process, as predicted target values resulted almost unbiased.

Finally, the new equations specific to Finnish clays have bias factors (b) closer to 1 than the existing correlations, showing coefficients of variations as low as 0.25.

6. Perniö failure experiment: total stress analysis considering anisotropy

6.1 Introduction

The Perniö failure test is back-analyzed in order to study the anisotropic undrained behavior of a Finnish soft sensitive clay. Perniö test site is located in Salo, on the West coastal area of Finland, near the city of Turku. A total stress soil model, implemented into the finite element software PLAXIS 2D, is exploited for this purpose. The soil model used can take into account strength anisotropy and strain-softening behavior of sensitive clays. Therefore, progressive failure mechanisms can be modelled.

Soil anisotropy is very often neglected in practical geotechnical applications in Finland. For this reason, this study focuses on the main consequences of modelling undrained shear strength anisotropy in Finnish clays, as undrained shear strength is normally derived from field vane measurements and assumed as isotropic.

6.2 Perniö failure test

6.2.1 Test description

In October 2009, the Finnish Transport Agency (Liikennevirasto), in collaboration with Tampere University of Technology (TUT), conducted a full-scale embankment failure experiment in Perniö, Western Finland. The main purpose of the test was to collect field information of a failure caused by a rapidly applied load on a railway embankment founded on soft clay. At the same time, the test was a good chance to evaluate the performance of various instruments for real-time monitoring of embankment stability.

A condition where the load is rapidly applied is, for instance, a train coming to a standstill on a railway embankment. Such an issue is of high concern of the Finnish Transport Agency, as large part of the Finnish railway network is located on soft clay areas and since the undrained response of soft clays is known to be dependent on intensity and duration of loading. Time dependency of yield-induced pore pressure is known to influence the undrained response of clays and it may affect the undrained capacity. When a stopped train load is sustained for a certain period of time, undrained deformations induced by the viscous properties of the clay can occur. Failure due to undrained creep may also occur after several days. Another issue of high concern of the Finnish Transport Agency is that factors of safety (*FOSs*) calculated using traditional methods resulted too low at several locations across the railway network. Therefore, the Perniö failure test will serve as *i*) source of field data on the time-dependent characteristics of clays and *ii*) benchmark test for calibration of stability calculation methods in soft clays.

Fig. 6.1: Test site and containers before loading (Lehtonen et al. 2015).

For a realistic simulation of the conditions of a train coming to a standstill, a new highly instrumented embankment made of crushed ballast was built and equipped with concrete sleepers and rails, in order to match a typical Finnish train axle configuration. Four (4) modified shipping containers were placed on top of the railway embankment to model one car, as shown in Fig. 6.1, and filled with sand through a conveyor belt. A continuous filling process was designed to guarantee a homogeneous load distribution in all the containers.

The general stratigraphy of the test area is presented in the cross section of Fig. 6.2. The instrumented 60 m long, 0.55 m thick and 3.2 m wide (top) railway embankment was placed on top of an old 1.5 m thick fill layer made of sand and gravel. The fill was built on top of a 0.8-0.9 m thick dry clay crust layer, followed by a 3.5 to 4.5 m thick layer of soft sensitive clay. A varved silty clay layer composed of thin clay, silt, and sandy silt layers underlies the upper soft clay and extends for approximately 1.5 m over a fairly stiff sand layer 2 to 8 m thick. At the time of the experiment, the groundwater table was found at a depth of about 1.3 m from the ground surface. In order to reduce stability and control direction and extent of failure, a 2 m deep ditch was excavated approximately 13.5 m from the centreline of the embankment.

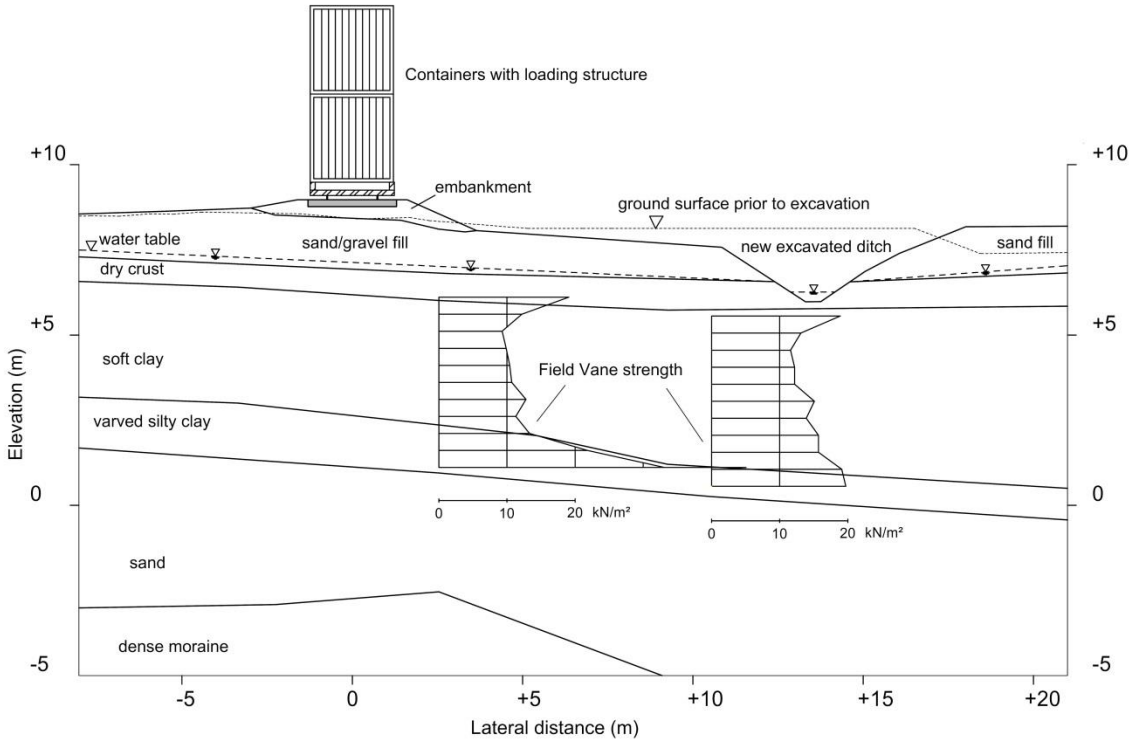

Fig. 6.2: Stratigraphy of the test site from A-A cross section [D'Ignazio et al. *In press*].

The extensive instrumentation placed in the test area consisted of: *i*) 37 strain-gauge based pore pressure transducers positioned in four groups: under the embankment centerline, under the embankment toe, halfway between the embankment and the ditch and next to the ditch; *ii*) 27 surveying prisms on the soil surface and the loading containers; *iii*) 9 automatic two axis inclinometers, installed in three cross sections; *iv*) 3 settlement tubes with a total of 53 pressure transducers; *v*) 5 total stress earth pressure transducers under the embankment; *vi*) 76 slip surface measurement tubes with surveying points on the surface; *vii*) 32 strain gauges on the frameworks for weighing the containers. The instrumentation layout is shown in Fig. 6.3 and described in detail by Lehtonen et al. (2015).

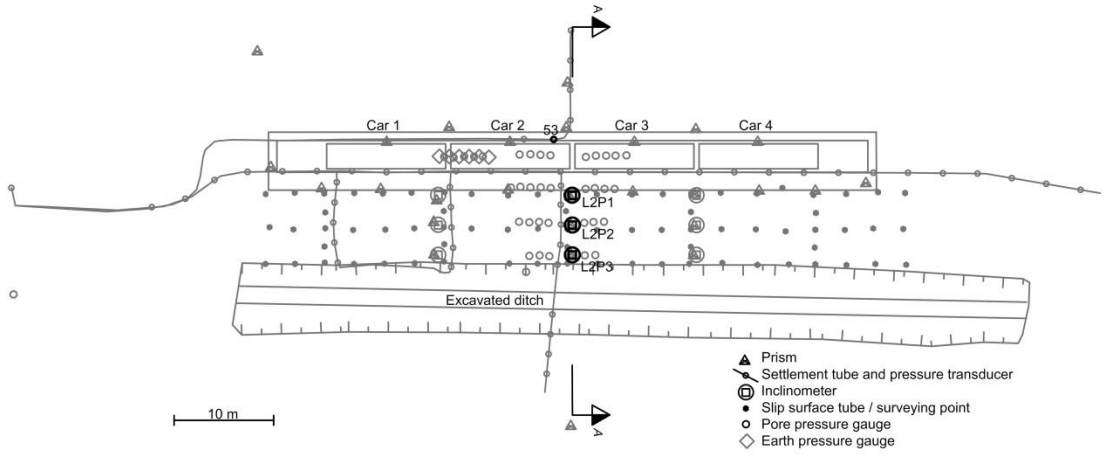

Fig. 6.3: Instrumentation layout [D'Ignazio et al. *In press*, after Lehtonen et al. 2015].

Since the embankment behavior was expected to be mainly governed by the sensitive clay, most of the instrumentation was placed in this layer. Therefore, the majority of the gathered data are related to the soft Perniö clay.

The duration of the load-to-failure process was about 30 hours. During the first day of loading, the applied load reached 24 kPa. The loading process was stopped during the night. During the following day, the load was applied in 5 kPa steps until a distributed vertical force of 217 kN/m was measured for cars 2 and 3 (Fig. 6.4). A bearing pressure of about 87 kPa was measured at the end of loading over a 2.5 m wide loading area. However, the embankment reached failure only two hours after the last loading step. Rate of pore pressure and displacements were observed to increase both during loading and during the time elapsed between the end of loading and failure.

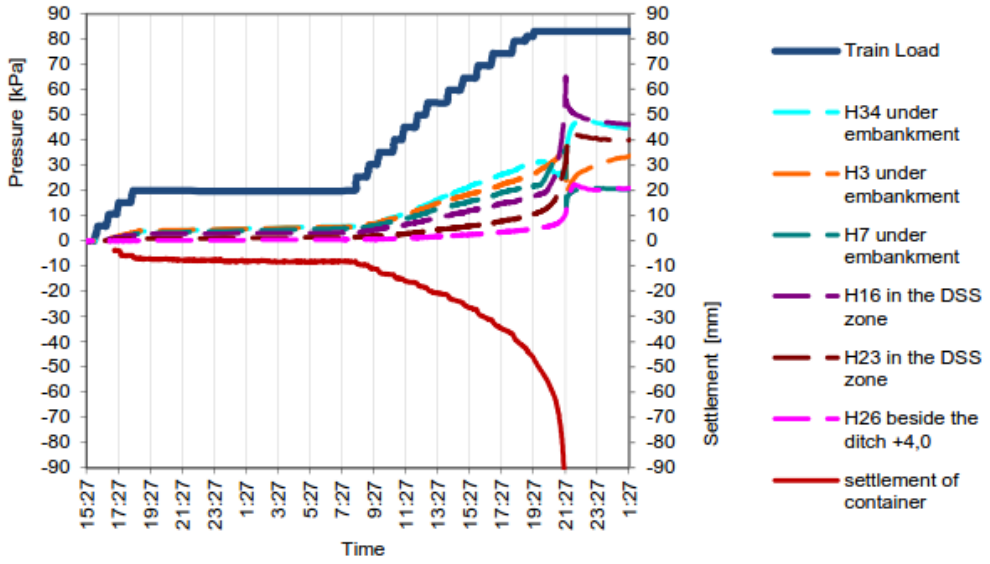

Fig. 6.4: Train load, excess pore pressure and settlement during loading (Mansikkamäki 2015).

6.2.2 **Characteristics of Perniö clay**

Fig. 6.5 and Table 6.1 show the general characteristics of Perniö clay. According to SFS-EN ISO 14688-2 (2005) standard, Perniö clay can be classified as highly sensitive (S_t = 30-51). Undrained shear strength values lower than 0.5 kPa were observed from Fall Cone tests for remolded state.

The measured clay content varies from 48 to 81%. Natural water content (w) values range from 48% to 109%, while liquid limit (LL) measured from Fall Cone test varies from 38 to 82%. Plastic limit (PL) was only measured on samples collected slightly outside of the test area. The few available test results suggest PL in the range 29-36%. Therefore, the plasticity index (PI=LL-PL) of Perniö clay falls into the interval 36-49%, as suggested by Lehtonen et al. (2015).

Tab. 6.1. Characteristics of Perniö clay (D'Ignazio et al. *In press*).

Parameter	**Unit**	**Value**
Unit weight (γ)	kN/m^3	15.4
Water content (w)	%	48-109
Liquid limit (LL)	%	38-82
s_u (field vane, s_u^{FV})	kPa	9-12 on top of the layer, increasing 1.15 kPa/m
Remolded s_u (s_u^{re})	kPa	< 0.5
Sensitivity (S_t)	-	30-51
Over consolidation ratio (OCR)	-	< 1.5 (soft sensitive clay); > 2 (stiff clay)
Clay content	%	48-81

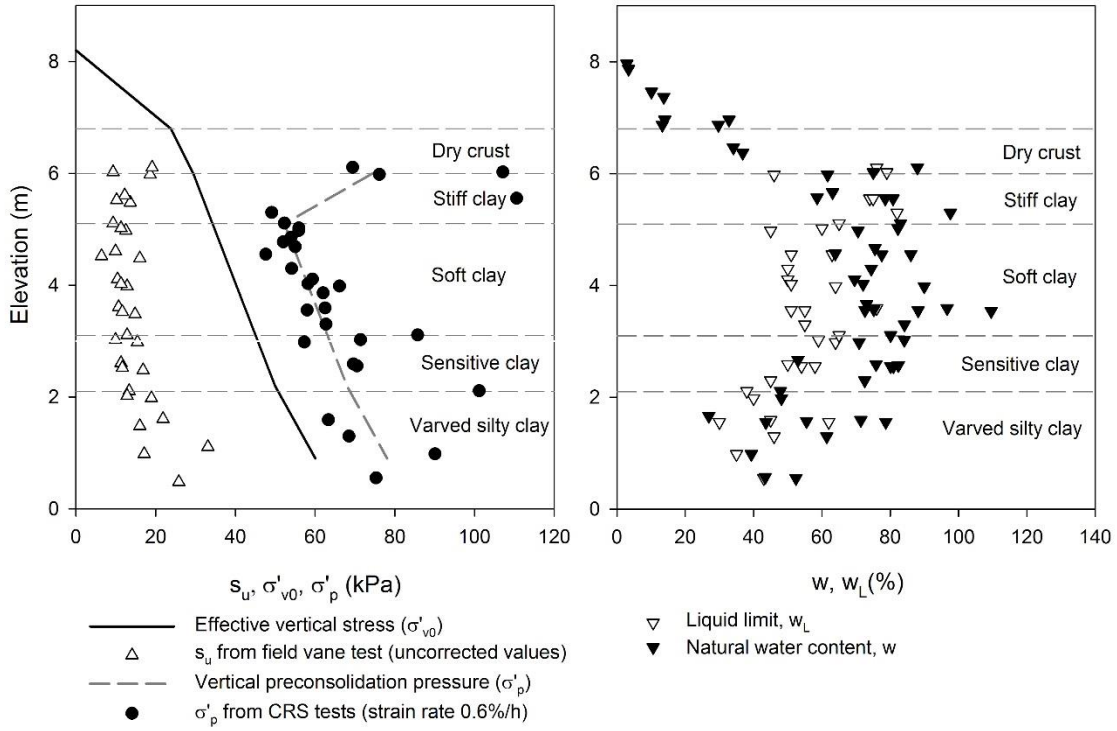

Fig. 6.5: General characteristics of Perniö clay, from samples taken over the test area [D'Ignazio et al. *In press*].

CRS oedometer test results indicate that the soft clay in Perniö is slightly overconsolidated, with OCR values generally lower than 1.5. However, in the top portion of the clay foundation situated right below the dry crust (hereinafter called "stiff clay"), OCR values higher than 2-3 are measured.

CRS test results from Perniö and derivation of preconsolidation pressure are extensively presented in Mansikkamäki (2015). It was pointed out how according to the Lunne et al. (1997*a*) criteria, all samples taken with the 50 mm piston sampler are of "Good to Fair" or "Poor" quality. However, even though the sample quality was not excellent, it seemed to be quite uniform for all the tested specimens.

Field vane test was performed at the test site to assess the undrained shear strength of Perniö clay. The minimum undrained shear strength of 9 to 12 kPa was measured in the upper part of the soft clay, increasing with depth of about 1.15 kPa/m. Hence, based on the classification suggested by Leroueil et al. (1990), Perniö clay can be classified as a "very soft" clay (s_u = 10-20 kPa).

High scatter in the preconsolidation pressure values is visible at elevation of about 3 m. On the other hand, in the top part of the soft clay (Fig. 6.5), measured points seem fairly well grouped. This might indicate that a more sensitive sublayer is present, from where it could be more difficult to obtain good samples.

6.2.3 **Failure mechanism and observations**

According to Lehtonen et al. (2015) the shape of the failure mechanism can be well approximated from the pre-failure pore pressure readings coupled with inclinometer readings. However, a clear and distinct slip surface was difficult to detect.

The development of the shear zone seems to start behind the railway sleepers, proceeding further down in the soft clay layer under the embankment toe, before smoothly bending up and finally reaching the bottom of the ditch. Based on this interpretation, shearing seems to occur differently over three distinct areas along the shear band (Fig. 6.6): an active zone under the load application area, a direct shear zone beneath the embankment toe and a passive zone of shearing which moves upwards and outwards towards the ditch.

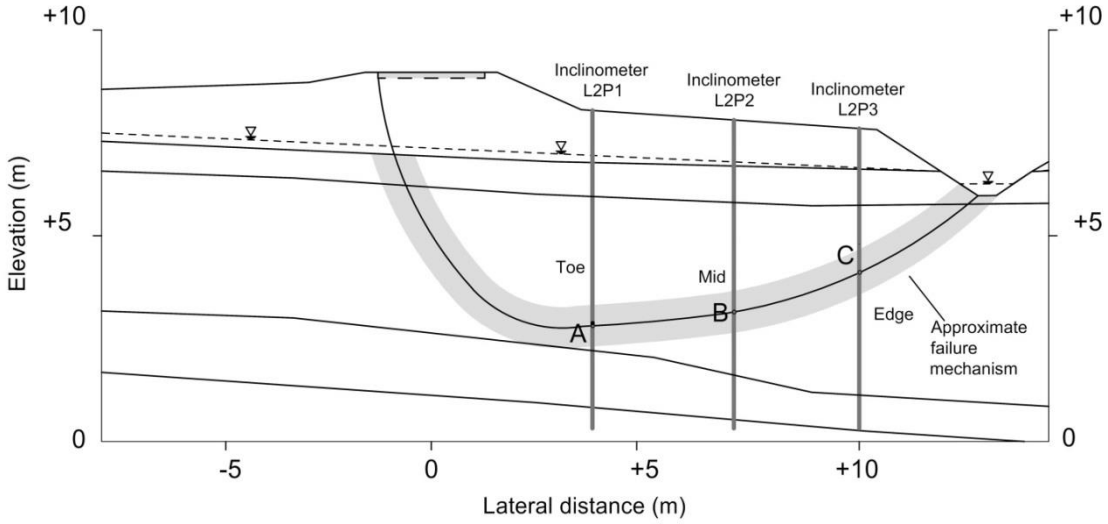

Fig. 6.6: Interpreted failure mechanism [D'Ignazio et al. *In press*, after Lehtonen et al. 2015].

Failure occurred in the Perniö test because of undrained viscous phenomena under a constant applied load, as suggested by Lehtonen et al. (2015). Failure was probably initiated locally under the embankment, before spreading further progressively over time under undrained conditions.

Inclinometers L2P1, L2P2 and L2P3 recorded the highest horizontal movements in the soft clay. Displacements in the soil increased further during the two hours where the load was maintained constant.

Experimental studies carried out by Arulandan et al. (1971) and Holzer et al. (1973) have shown that a there is a threshold level of deviator stress beyond which undrained creep will cause an increase in strain rate and pore pressure until failure. In addition, time to failure was found to be inversely proportional to the deviator stress level reached.

In general, the response of clay specimens subjected to "fast" undrained shearing is stiffer than for a "slow" type of loading (Berre and Bjerrum 1973; Lefebvre and Leboeuf 1987; Graham et al. 1983*a*: Leroueil et al. 1985). This concept is schematized in Fig. 6.7. The effective stress path A-B may represent an ideal "standard" or "slow" undrained test, while the stress path A-C-E would ideally describe a "fast" undrained test. A situation

which has possibly occurred during the Perniö test is described by the stress path A-C-D: the clay was quickly loaded up to a deviator stress level beyond a theoretical threshold value, which was not sufficient to cause failure straight away. The embankment collapsed only after some time because of undrained creep, under a constant load. If the loading process had continued further, the embankment would have probably failed at a higher load than the measured 87 kPa (point E). Therefore, the stress path A-C-D may be consistent with field situations where a heavy train is suddenly stopped and left for a certain period of time, until failure.

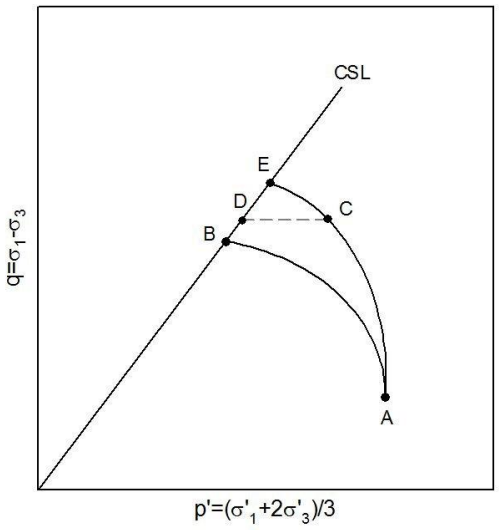

Fig. 6.7: Idealized stress paths for Perniö clay [D'Ignazio et al. *In press*].

The evolution of shear strains with time is presented in Fig. 6.8. Measured horizontal movements from inclinometers L2P1, L2P2 and L2P3, placed at the mid-section of the test, were used to estimate the magnitude of pre-failure shear strains, according to eq. (6.1):

$$\gamma = \frac{\Delta u_x}{\Delta z} \tag{6.1}$$

where γ is the shear strain, Δu_x is the incremental horizontal displacement between two consecutive measurement points located along the inclinometer and Δz is the distance between the two points.

The evolution of shear strain with time at points A, B, C, situated along the interpreted shear band (as shown in Fig. 6.6) based on the position of inclinometers L2P1, L2P2, L2P3, respectively, is shown in Fig. 6.8. Very small deformations could be observed during the first day of loading, when the applied load reached 24 kPa. When the loading process was resumed after the night, both strain and rate of strain showed an increase until the loading ended. A further increase of strain and strain rate could be observed during the two hours before failure, when the applied load was kept constant and equal to 87 kPa.

Readings from inclinometer L2P1 suggest that the shear strain gradient changed about 3-4 hours before failure, simultaneously with yielding of the soft clay. A similar yield point was identified by Lehtonen et al. (2015) from pore pressure readings. The elaborated data

presented in Fig. 6.8 seemed to further indicate that during the test the strain rate increased by over a tenfold, thus justifying the high measured failure load.

At a given time, the differences in terms of mobilized shear strains at different locations along the shear band would suggest a downward progressive type of shear mechanism which caused failure, triggered by the external load (Fig. 6.8). At the start of yielding, recorded shear strains may indicate that the soil at points A, B, C is still in the pre-peak hardening regime. Peak strength might have been passed at some location, i.e. under the embankment where displacements were however not measured. After that point, the further increased load may have caused the soil under the embankment to move towards the post-peak softening regime. Failure did not occur immediately because of the viscous properties of the clay.

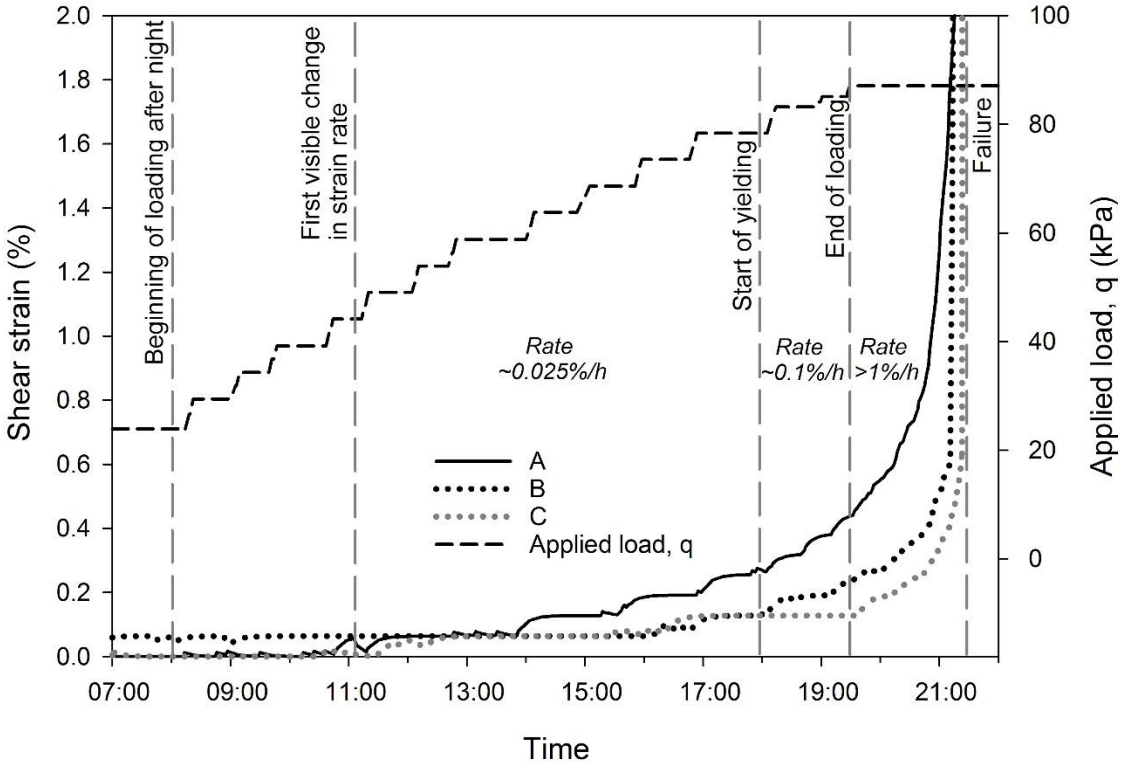

Fig. 6.8: Shear strain versus time and applied load from inclinometers L2P1, L2P2, L2P3 [D'Ignazio et al. *In press*].

6.3 Anisotropic total stress models for clays

6.3.1 NGI-ADP soil model

The NGI-ADP soil model (Grimstad et al. 2012) is an elasto-plastic model based on the anisotropic undrained shear strength concept. The anisotropic behavior follows the ADP framework suggested by Bjerrum (1973), where the undrained shear strength profiles for active (A), direct simple shear (D) and passive (P) loadings are given directly as input parameters. Input peak undrained shear strengths (s_u^A, s_u^{DSS}, s_u^P) and corresponding shear strains (γ^C, γ^{DSS}, γ^E) in the three directions of shearing represented by active plane strain or triaxial compression (TXC), direct simple shear (DSS) and passive plane strain or triaxial extension (TXE), describe the non-linear hardening anisotropic behavior (Fig. 6.9). By interpolation between the three input curves, the model is able to predict the anisotropic behavior of saturated clays for a general 3D stress state.

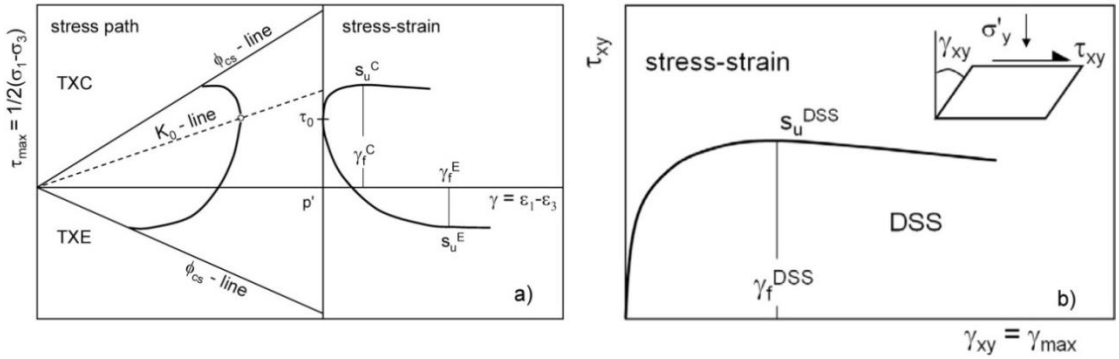

Fig. 6.9: Typical stress paths and stress–strain curves for *a*) triaxial compression (TXC) and extension (TXE) tests (Grimstad et al. 2012) and *b*) direct simple shear (DSS) tests (Andresen et al. 2011) with definition of stress/strain quantities [D'Ignazio et al. *In press*].

Since triaxial testing is more commonly used than plane strain, test results from triaxial tests are often used directly to model plane strain problems, although they give slightly conservative results for plane strain conditions (e.g. Ladd et al. 1977). For simplicity, the plane strain "A=active" strength is assumed equal to the triaxial compression strength, and correspondingly, the plane strain "P=passive" strength is taken equal to the triaxial extension strength.

The undrained tests used to derive the input parameters should be consolidated anisotropically to the in-situ stress (CK_0UC and CK_0UE tests). For this reason, the curves presented in Fig. 6.10 start from an initially mobilized shear stress τ_0. The inclination of the curves at small strain comes from the initial shear modulus G_0.

The undrained shear strength in the model is assumed to vary linearly with depth within a soil layer. A constant $s_u^A{}_{ref}$ at a reference depth y_{ref}, along with strength increase magnitude $s_u^A{}_{inc}$, defines the input TXC undrained shear strength profile in the soil layer. Above y_{ref}, s_u is constant and equal to $s_u^A{}_{ref}$. For some special user defined version of the model, the reference depth y_{ref} for inclined clay layers can be defined by a reference x-coordinate x_{ref} and a gradient $\Delta y_{ref}/\Delta x$.

DSS and TXE strengths are defined as fractions of the TXC strength (s_u^A) through the input of the anisotropy ratio for DSS (s_u^{DSS}/s_u^A) and extension (s_u^P/s_u^A), respectively.

Finally, the model formulation does not include rate effects, cyclic behavior, softening and shear-induced pore pressure.

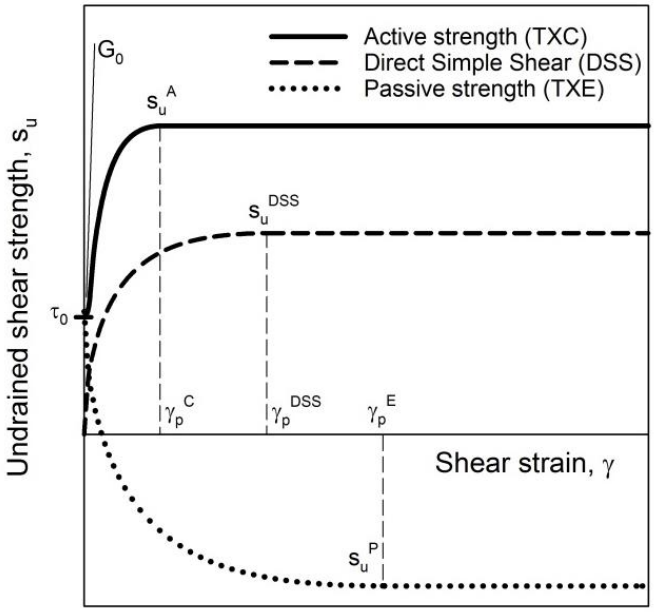

Fig. 6.10: Input parameters for NGI-ADP model.

6.3.2 **NGI-ADPSoft soil model and FE modelling of strain-softening**

A special version of the NGI-ADP model, the NGI-ADPSoft model (Grimstad et al. 2010), can take into account the anisotropic post-peak strain-softening behavior normally observed during undrained tests on soft sensitive clays. The softening curves are described by direct input of the residual undrained shear strengths (s_{ur}^{A}, s_{ur}^{DSS}, s_{ur}^{P}) and corresponding shear strains (γ_r^{C}, γ_r^{DSS}, γ_r^{E}) in the same three directions of shearing (Fig. 6.11).

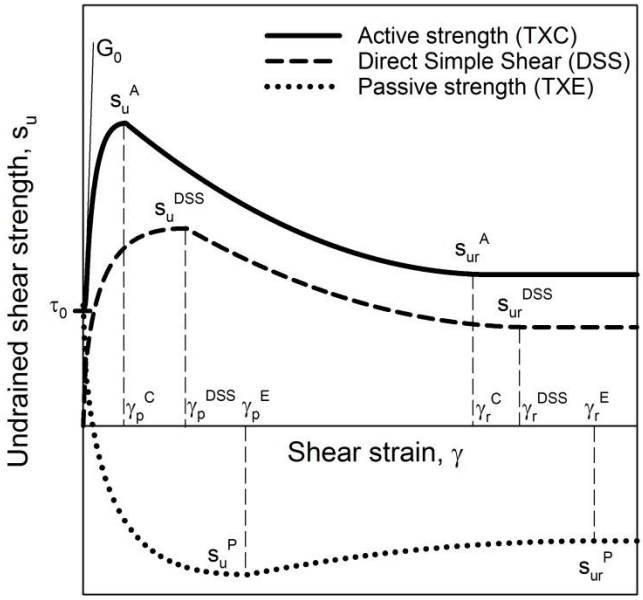

Fig. 6.11: Input parameters for NGI-ADPSoft model [D'Ignazio et al. *In press*].

From a purely mechanical standpoint of view, strain-softening turns out in development of plastic strains for a decreasing yield stress or a contracting yield surface. A hardening rule for softening materials may be defined based on a consistency condition as follows (see e.g. Nordal 2012):

$$\left\{\frac{\partial F}{\partial \underline{\sigma}}\right\}^{T} d\underline{\sigma} - A d\lambda = 0 \tag{6.2}$$

where $d\underline{\sigma}$ represents the stress increment vector, $\{\partial F/\partial \underline{\sigma}\}^{T}$ the yield surface gradient, λ the plastic multiplier and A the plastic resistance number.

The softening curve has a negative tangent elasto-plastic modulus T, as shown in Fig. 6.12. T is defined as in eq. (6.3):

$$\frac{1}{T} = \frac{1}{E} + \frac{1}{A} \tag{6.3}$$

where E is the elastic loading/unloading stiffness.

In the post-peak softening regime, both first and second term in eq. (6.2) are negative. This implies positive values of $d\lambda$, being A also negative [from eq. (6.3)]. From the physical point of view, $d\lambda > 0$ indicates increasing plastic strain during softening.

An implication of strain-softening behavior is that while for a given strain increment the continuing stress-strain curve at peak stress is unique, for a given stress increment the response will lose its uniqueness. Indeed, because of reduced shear stress, both plastic softening and elastic unloading are theoretically possible (Fig. 6.12). This bifurcation problem can be adequately solved by numerical methods e.g. Finite Element Method, in order to guarantee equilibrium of stresses, material behaviour and compatibility of strains during loading (Jostad et al. 2006).

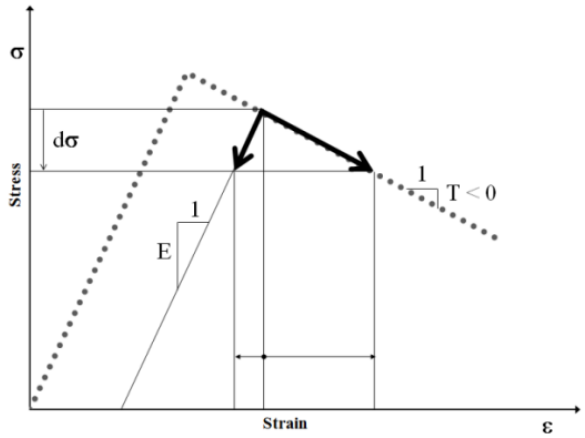

Figure 6.12: Schematization of the post-peak bifurcation problem (D'Ignazio and Länsivaara 2015, after Nordal 2012).

For strain-softening materials, the FEM presents issues related to FE discretization (mesh). As observations suggested that shear strain and, consequently, magnitude of undrained strain-softening increase with reducing shear band thickness (see section 2.6), a regularization technique is required in order to overcome the dependency of both thickness and orientation of the shear band on the adopted mesh.

In this way, the element size will not be performing as an internal length parameter and the thickness of the shear band will not end up at its minimum size (Bazant 1976; Pietruszczak and Mròz 1981). A detailed review of the most common regularization techniques is, for instance, given by De Borst et al. (1993).

In addition, both peak capacity and global post-peak response are affected when mesh refinement is done without a proper regularization technique (Gylland 2012).

One simple way of introducing an internal length scale and avoid the problem of mesh dependency is to use the "over non-local" strain approach (Brinkgreve 1994), which is based on the non-local strain approach proposed by Eringen (1981). The "over non-local" strain approach is included in the formulation of NGI-ADPSoft model.

The non-local strain is calculated as an integrated weighted average shear strain within a specified zone (defined by input of an internal length parameter, l_{int}) around the actual Gauss point [see eq. (6.4)]. In order to avoid the shear band thickness (t_{sb}) to be affected

by orientation and size of the elements, the internal length should be selected sufficiently larger than the element size.

$$\Delta\underline{\varepsilon}^{p*}(\underline{x}_i) = \Delta\underline{\varepsilon}^{p}(\underline{x}_i) - \alpha\Delta\underline{\varepsilon}^{p}(\underline{x}_i) + \frac{\alpha}{V}\int\left(w(\underline{x})\cdot\Delta\underline{\varepsilon}^{p}(\underline{x})\right)dV \qquad (6.4)$$

where $\Delta\boldsymbol{\varepsilon}^{p*}$ is the non-local strain increment, $\Delta\boldsymbol{\varepsilon}^{p}$ the plastic strain increment, $w(\boldsymbol{x})$ is the Gauss distribution function (or weighting function), V is the integral of $w(\boldsymbol{x})$ over the volume and $\boldsymbol{x_i}$ the integration point coordinates.

The thickness of the shear band, calculated according to eq. (6.5) suggested by Brinkgreve (1994), is simultaneously controlled by the internal length (l_{int}) together with a regularization parameter α.

$$t_{sb} = \pi\cdot l_{\mathrm{int}}\cdot\left[\ln\left(\frac{\alpha}{\alpha-1}\right)\right]^{\frac{1}{2}} \qquad (6.5)$$

Vermeer and Brinkgreve (1994) and Jostad and Grimstad (2011), recommended $\alpha = 2$ for the numerical integration of the local strain. The effective shear band thickness t_{sb} is then 2.62 times l_{int}.

The main advantage of using the over non-local regularization technique is represented by the straightforward implementation into a non-linear finite element program. The main reason is that the governing finite element equations do not need any reformulation, which is normally required for the other types of regularization techniques (De Borst et al. 1993). The regularization based on the non-local strain approach can be entirely solved at the material point level, with only additional information on the strains in the neighboring elements. Therefore, the strain regularization can be included and solved by a user-defined material model implemented in a commercial finite element program (e.g. Grimstad et al. 2010).

6.3.3 **Formulation of NGI-ADP and NGI-ADPSoft soil models**

The formulation of NGI-ADP and NGI-ADPSoft soil models for a general 3D stress space is based on an anisotropic approximated Tresca yield criterion (Grimstad et al. 2012). The yield function *F* for NGI-ADP and NGI-ADPSoft models is defined by eq. (6.6) and eq. (6.7), respectively.

$$F = \sqrt{H(\omega)\cdot \hat{J}_2} - \kappa_1 \cdot \frac{s_u{}^A + s_u{}^P}{2} = 0 \tag{6.6}$$

$$F = \sqrt{H(\omega)\cdot \hat{J}_2} - \kappa_1 \cdot (1-\kappa_2)\cdot \frac{s_u{}^A + s_u{}^P}{2} - \kappa_2 \cdot \frac{s_{ur}{}^A + s_{ur}{}^P}{2} = 0 \tag{6.7}$$

Where $\hat{J}_2$ is the modified second deviatoric invariant. The function $H(\omega)$ approximates the Tresca criterion. The hardening parameters κ_1 and κ_2 are computed from eq. (6.8) and eq. (6.9). The yield criterion for NGI-ADP model is obtained for $\kappa_2 = 0$ in eq. (6.7).

$$\kappa_1 = 2 \cdot \frac{\sqrt{\gamma^p / \gamma_p{}^p}}{1+\gamma^p / \gamma_p{}^p}, \text{ for } \gamma^p < \gamma_p{}^p \tag{6.8}$$

$$\kappa_2 = \left(\frac{\gamma^p - \gamma_p{}^p}{\gamma_r{}^p - \gamma_p{}^p}\right)^{c_1} \cdot \left(2 - \frac{\gamma^p - \gamma_p{}^p}{\gamma_r{}^p - \gamma_p{}^p}\right)^{c_2}, \text{ for } \gamma_p{}^p < \gamma^p < \gamma_r{}^p \tag{6.9}$$

γ_p, $\gamma_p{}^p$ and $\gamma_r{}^p$ are the plastic shear strain, plastic "peak" shear strain and plastic "residual" shear strain, respectively. The softening parameter κ_2, in this version of the model (NGI 2011), is ruled by two shape parameters c_1 and c_2. For $c_1 = 1$ and $c_2 = 0$, a linear softening curve will describe the transition from peak to residual state (Fig. 6.13).

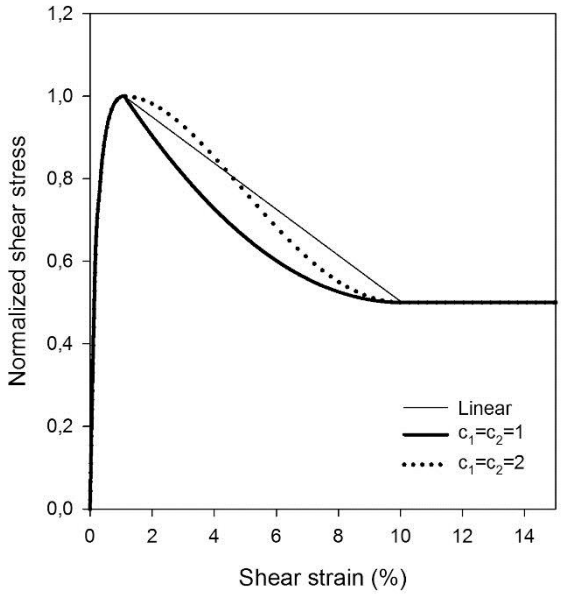

Fig. 6.13: Impact of shape parameters c_1 and c_2 on the post-peak behavior predicted by NGI-ADPSoft soil model [D'Ignazio et al. *In press*].

The function $H(\omega)$ is defined as:

$$H(\omega) = \cos^2\left[\frac{1}{6}\arccos(1 - 2 \cdot a_1 \cdot \omega)\right] \tag{6.10}$$

where

$$\omega = \frac{27}{4}\frac{\hat{J}_3^{\,2}}{\hat{J}_2^{\,3}} \tag{6.11}$$

Where $\hat{J}_3$ is the third deviatoric invariant and a_1 the rounding ratio, defined as the ratio between s_u^{TXC} and s_u^{PS}. a_1 = 0.97-0.99 is always chosen as default value.

The parameters γ_p^p and γ_r^p have similar stress path dependency of undrained shear strength. The interpolation function for γ_p^p and γ_r^p is described in detail in Grimstad et al. (2012), Grimstad et al. (2010) and in NGI (2011).

Fig. 6.14 shows the NGI-ADP yield criterion for plane strain conditions. Contours of plastic shear strain and the elliptical failure curve (κ_1 = 1) in the plane strain deviatoric stress plot are shown.

In Fig. 6.15, the failure criterion of the NGI-ADP model in the π plane (for Cartesian stresses) with default rounding ratio is shown. The criterion is continuous, differentiable and described by a single function (Grimstad et al. 2012).

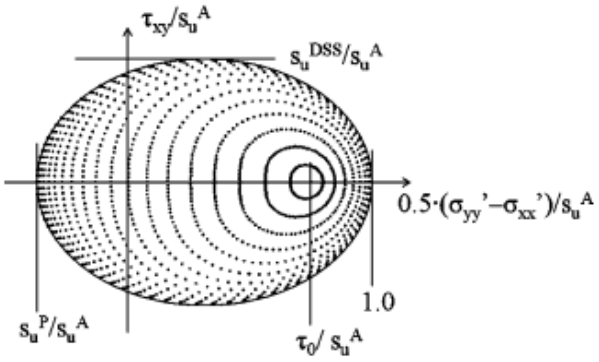

Fig. 6.14: "Typical" deviatoric plane strain plot of equal shear strain contours for the NGI-ADP model (Grimstad et al. 2012).

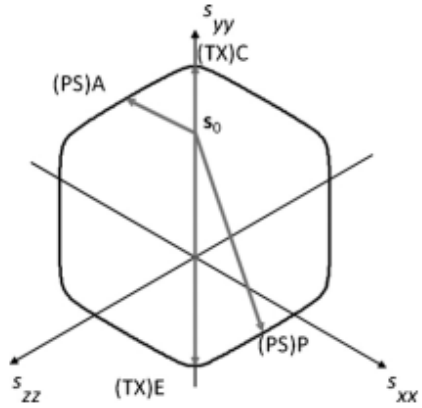

Fig. 6.15: Failure criterion used in the NGI-ADP model in the π-plane (Grimstad et al. 2012).

6.4 Model parameters for FEM analysis

6.4.1 Soft clay

The soft Perniö clay is modelled using the NGI-ADPSoft model. Soil parameters are determined from anisotropically consolidated triaxial compression (CK_0UC) and extension (CK_0UE) tests, along with in-situ tests.

Specimens for triaxial tests are obtained from large diameter (d = 86 mm) piston samples collected in 2013. Samples were taken from a location about 50 m off the test area. The general stratigraphy is similar to the test area, except for the sand fill that is not present. On the other hand, the dry crust is thicker than in the test area. Field vane test results from 2009 are also exploited for a more detailed characterization of the in-situ strength at the test location.

However, direct simple shear (DSS) tests are not in use in Finland. Jamiolkowski et al. (1985) and Chandler (1988) suggest that DSS strength is somewhat comparable to the shear strength measured from field vane. Hence, field vane data from 2009 are used to verify the DSS strength of Perniö clay predicted by some existing correlations.

Preconsolidation pressure (σ'_p) values are evaluated from CRS (constant rate of strain) oedometer tests. CRS tests in Finland are normally conducted at a constant speed of 0.0015 mm/min (0.6%/h). No correction for strain rate is applied to σ'_p in this study. Based on CRS test results, the preconsolidation pressure in the soft clay (Fig. 6.5) first decreases with depth for about 1 m below the dry crust and then increases with depth with an average POP (pre-overburden pressure) equal to 18 kPa. POP is defined, for a given depth, as the difference between the vertical preconsolidation pressure and the in-situ effective vertical stress (POP = σ'_p-σ'_{v0}). As a consequence of the strong dependency of s_u on σ'_p, the interpreted σ'_p profile would indicate that the undrained shear strength must also first decrease up to z = 5 m and then increase with depth. As the thickness of the sand fill layer was constant throughout the whole area before the ditch was excavated, it was assumed that POP did not vary towards the ditch.

A detailed description of the triaxial tests conducted in 2013 on Perniö clay is contained in Lehtonen (2015). The main purposes of the test campaign were the assessment of strength anisotropy of Perniö clay and the determination of undrained shear strength at different OCR values. Preconsolidation pressure was determined from new CRS oedometer test results.

Two parallel 35.8 mm diameter specimens were trimmed from the samples in order to conduct one compression and one extension test from the same depth. Specimens for triaxial compression and extension tests were approximately consolidated to the in-situ stress state before shearing. Stress path controlled undrained shearing was carried out at a standard axial strain rate of 1%/h.

The measured peak undrained shear strengths from triaxial test results are compared to existing correlations for anisotropic undrained shear strength of Scandinavian clays (Larsson et al. 2007) and Norwegian clays (Karlsrud and Hernandez-Martinez 2013) (Fig.

6.16). The studied correlations are all based on the SHANSEP framework of eq. (2.2) and presented in section 2.5.

According to Karlsrud and Hernandez-Martinez (2013), the SHANSEP parameters *S* and *m* correlate with the natural water content of the clay [eq. (2.16), (2.17), (2.18)]. Larsson et al. (2007) suggested *S* and *m* as a function of the liquid limit (LL) of the soil [eq. (2.13), (2.14), (2.15)]. The average liquid limit of Perniö clay is 57 (Lehtonen et al. 2015).

Test results indicate that the normalized peak strength for triaxial compression (s_u^A/σ'_v) can be fairly well described by eq. (2.16) using w = 90%, for OCR < 2. Eq. (2.13) correlates also relatively well with measurements, even though it underestimates some of the TXC results. Eq. (2.15) for LL = 57% seems to adapt reasonably well to the measured normalized strength for triaxial extension (s_u^P/σ'_v). In contrast, Eq. (2.18) for w = 90% overpredicts the test results.

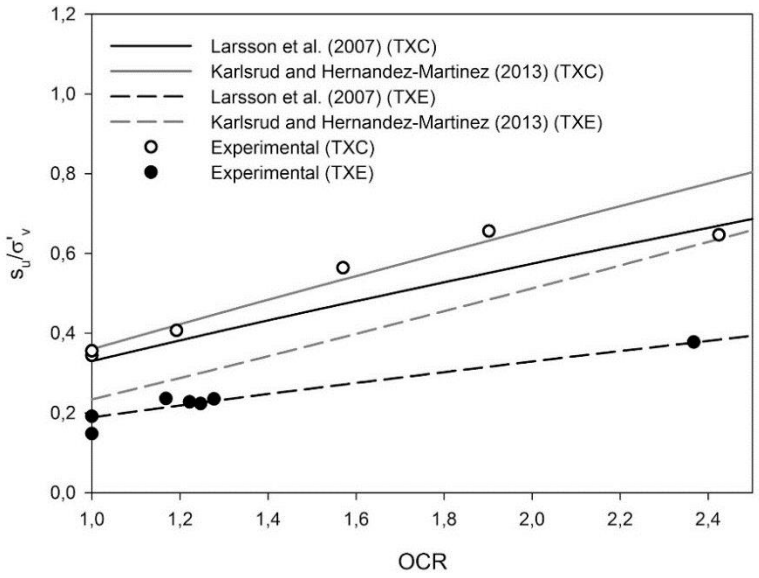

Fig. 6.16: Peak values of s_u/σ'_v plotted against the overconsolidation ratio (OCR) and comparison with existing correlations in the literature [D'Ignazio et al. *In press*].

The strength for direct simple shear (DSS) conditions is derived by direct comparison of the field vane measurements with existing transformation models [eq. (2.12), (2.14), (2.17), (2.20), (5.2)]. As discussed in section 2.5, field vane test is performed rather quickly. Therefore, the induced rate of strain is quite high if compared to conventional DSS tests. Strength anisotropy must be also taken into account because of the geometry of the vane. For this reason, measured strength values are corrected for plasticity according to eq. (2.10) in order to convert measured values into strength values [$s_{u(mob)}$] representative of DSS conditions. An average correction factor equal to 0.95 was calculated.

In Fig. 6.17 the normalized corrected field vane strength of Perniö clay is plotted against OCR. Eq. (2.20) by Ching and Phoon (2012) and eq. (2.17) by Karlsrud and Hernandez-Martinez (2013) do not seem to fit the measured data. On the other hand, despite the observable high scatter, eq. (2.12) by Jamiolkowski et al. (1985), eq. (2.14) by Larsson et al. (2007) and eq. (5.2) seem to fit the mean trend of the data points for OCR values lower than 2.5.

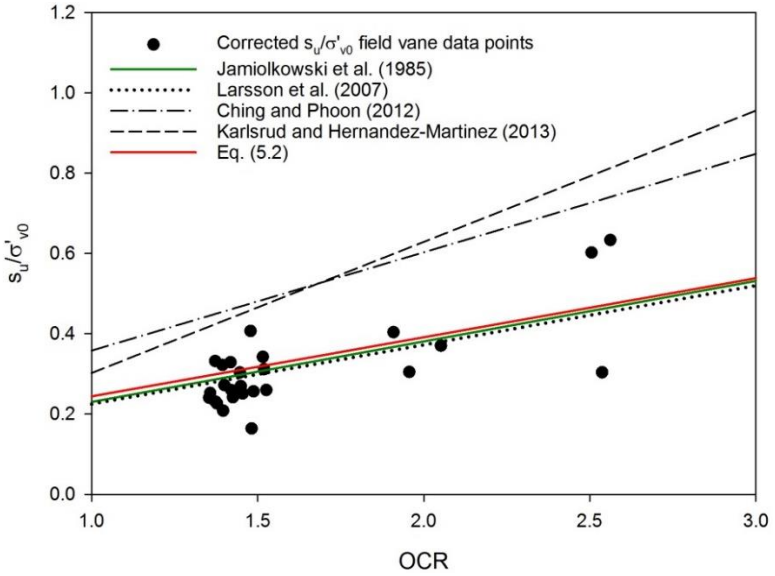

Fig. 6.17: Normalized field vane strength of Perniö clay versus DSS strength correlations [after D'Ignazio et al. *In press*].

Finally, from the triaxial test results a peak anisotropy ratio (s_u^P/s_u^A) equal to 0.5 is estimated. An anisotropy ratio for DSS (s_u^{DSS}/s_u^A) equal to 0.65 is also evaluated. The observed values of s_u^P/s_u^A and s_u^{DSS}/s_u^A are consistent with the findings of Jamiolkowski et al. (1985), Karlsrud et al. (2005), Karlsrud and Hernandez-Martinez (2013). According to Ladd et al. (1977), for PI = 36-49%, $s_u^P/s_u^A \approx 0.60$ and $s_u^{DSS}/s_u^A \approx 0.80$. Thakur et al. (2014*b*) suggest, for the same PI range, s_u^P/s_u^A = 0.45-0.50 and s_u^{DSS}/s_u^A = 0.74-0.80 for Norwegian clays. While the measured s_u^P/s_u^A is consistent with the predicted values by Thakur et al. (2014*b*), the s_u^{DSS}/s_u^A ratio estimated using eq. (2.12), eq. (2.14) and eq. (5.2) seems too low. Nevertheless, uncertainties underlie also the s_u^P/s_u^A ratio, as it was derived based on a limited number of tests (see Fig. 6.16). The influence of s_u^P/s_u^A and s_u^{DSS}/s_u^A on the FE results is however discussed later in section 6.5.6.

The anisotropic undrained shear strength profile at the test site is shown in Fig. 6.18.

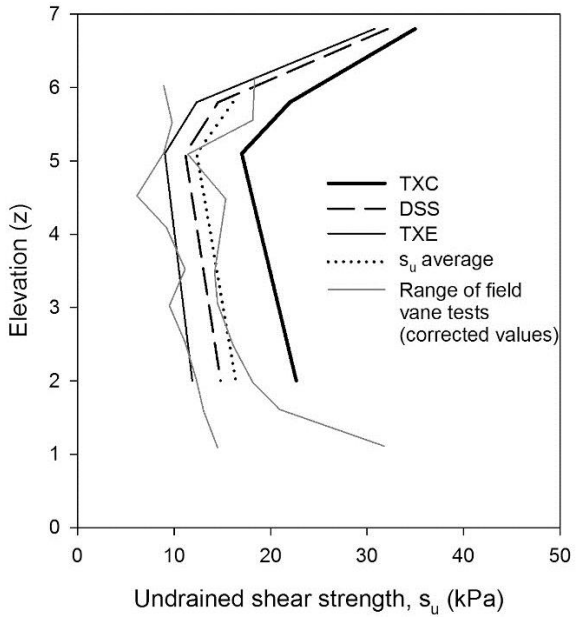

Fig. 6.18: Anisotropic undrained shear strength profile for Perniö site [D'Ignazio et al. *In press*].

The stress-strain behavior of Perniö clay is modelled from the CK_0UC and CK_0UE tests which seemed to be of the highest quality. As shown in Fig. 6.19, the NGI-ADPSoft model can be properly fitted to test results.

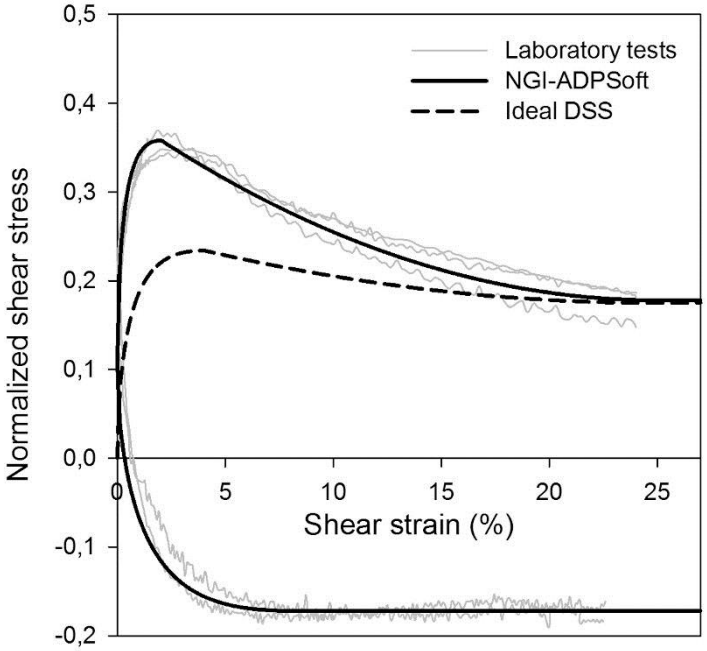

Fig.6.19: NGI-ADPSoft model curve fitting to CAUC and CAUE tests on Perniö clay [D'Ignazio et al. *In press*].

Strain-softening clearly occurs in compression after a peak shear strain of about 2% (brittle behavior), while for extension no distinct peak could be observed before 8-10% strain level. The residual input strength level is taken at 25% shear strain, corresponding to the end of the test. At this strain level, the shear strength is about 50% of the peak compression strength.

The more sensitive layer is modelled under a very simplistic assumption, namely that the shear strength at 25% strain is lower than in the soft clay (about 40% of the peak versus 50%), as shown in Fig. 6.20.

Peak strain for DSS shearing is reasonably assumed to lie between the peak strain for compression and extension, and taken equal to 4%, based on the experimental observations by Karlsrud and Hernandez-Martinez (2013) on Norwegian clays.

The author's experience suggests that for Finnish sensitive clays the 86 mm piston sampler used tends to assure a better sample quality than the 50 mm piston sampler. A similar conclusion was drawn by Mataić (2016) for Perniö clay. However, some disturbance may have occurred in the tested specimens as a result of sampling, transportation, storage and trimming operations.

The stress-strain response of soft clays can be notably affected by sample disturbance, as reported by Lunne et al. (1997*a*) and Lunne et al. (2006). It was found that sample disturbance can cause a reduction in peak strengths, an increase in shear strains at failure and higher shear strength at large strain. Lunne et al. (2006) further demonstrated how

s_u^P/s_u^A and s_u^{DSS}/s_u^A are affected by sample quality, by comparing test results from piston (54, 76 and 95 mm diameter) and block (250 mm diameter) samples.

Input parameters for NGI-ADPSoft model are summarized in Tab. 6.2. Reasonable choices are made with regard to soil parameters for the varved silty clay. The clay layers below the embankment are modelled so that y_{ref} varies according to a gradient ($\Delta y_{ref}/\Delta x$), in order to keep $s_u = s_u^A{}_{ref}$ at any point on top each layer. The initial K_0 value is calculated according to Kulhawy and Mayne (1990).

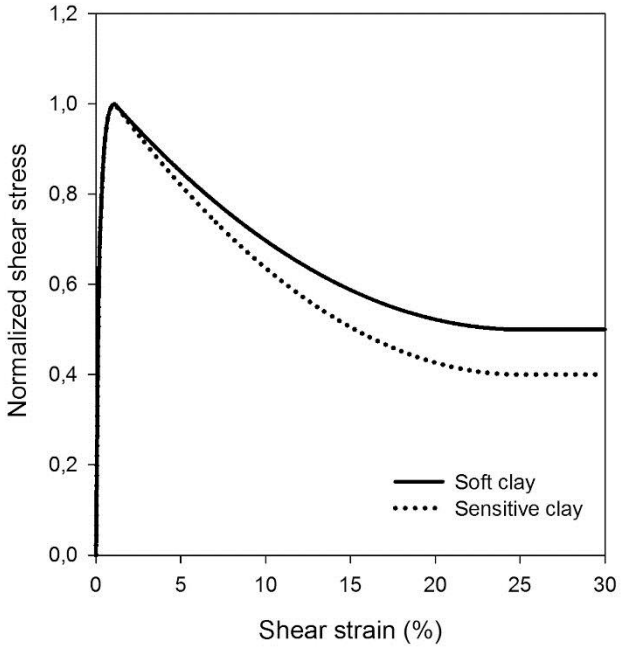

Fig. 6.20: Modelling of sensitive layer [D'Ignazio et al. *In press*].

Tab. 6.2: Input parameters for NGI-ADPSoft model (after D'Ignazio et al. *In press*).

Parameter	**Unit**	**Description**	**Stiff clay**	**Soft clay**	**Sensitive clay**	**Silty clay**
Material type	-	Material type	Drained	Drained	Drained	Drained
γ_{tot}	-	Total unit weight	15	15	15	17.8
G_0/s_u^A		Initial stiffness	700	700	700	700
$s_u^A{}_{ref}$	kPa	Reference active shear strength	22	17	19.4	22.5
$s_u^A{}_{inc}$	kPa/m	s_u^A increase with depth	-7.1	1.8	1.8	3
y_{ref}	m	Reference depth	6.3†/5.8‡	5.6†/5.1‡	3.8	-8
x_{ref}	m	Reference x-coordinate	-8†/4.7‡	-8†/4.7‡	4.7	3
$\Delta y_{ref}/\Delta x$	-	Reference depth gradient	-0.042†/0‡	-0.042†/0‡	0	-0.08
γ_p^C	%	Shear strain at peak in TXC	2	2	2	3
γ_p^{DSS}	%	Shear strain at peak in DSS	4	4	4	3
γ_p^E	%	Shear strain at peak in TXE	8	8	8	3
γ_r^C	%	Shear strain at residual state in TXC	25	25	25	25
γ_r^{DSS}	%	Shear strain at residual state in DSS	25	25	25	25
γ_r^E	%	Shear strain at residual state in TXE	25	25	25	25
τ_0/s_u^A	-	Initial mobilization	0.11	0.3	0.3	0.4
s_u^P/s_u^A	-	Normalized passive strength	0.5	0.5	0.5	0.5
s_u^{DSS}/s_u^A	-	Normalized DSS strength	0.65	0.65	0.65	0.65
s_{ur}^A/s_u^A	-	Normalized residual active strength	0.5	0.5	0.4	0.5
s_{ur}^{DSS}/s_u^A	-	Normalized residual DSS strength	0.5	0.5	0.4	0.5
s_{ur}^P/s_u^A	-	Normalized residual passive strength	0.5	0.5	0.4	0.5
ν'	-	Poisson's ratio	0.495	0.495	0.495	0.495
K_0	-	Lateral stress coefficient	0.77	0.65	0.65	0.65
c_1	-	Shape parameter	1	1	1	1
c_2	-	Shape parameter	1	1	1	1
α	-	Non-local strain parameter	2	2	2	2
l_{int}	m	Internal length	0.4	0.4	0.4	0.4

† For inclined layers below the embankment.
‡ For horizontal layers below the ditch.

6.4.2 **Coarse layers**

Coarse layers are modelled as hardening materials using the Hardening Soil model (Schanz et al. 1999) implemented in PLAXIS and described in detail in the software user's manual (Plaxis 2012).

The behavior of the sand fill and the lower stiff sandy layer, together with the shallow embankment made of crushed ballast, is described by a non-linear drained stress-strain behavior, where the stiffness is dependent on the stress level.

The Hardening Soil model is based on the idea of curve-fitting a hyperbolic function to describe the deviatoric stress-vertical strain relationship in a drained triaxial test. The hyperbola tends asymptotically to the upper limiting deviator stress at failure q_a (Fig. 6.21). Hence, the failure criterion should be defined so that the maximum deviator stress is lower than q_a to obtain reasonable strain level at failure. In the model formulation, q_f is limited by the Mohr-Coulomb failure criteria and it is by default assumed equal to $0.90q_a$.

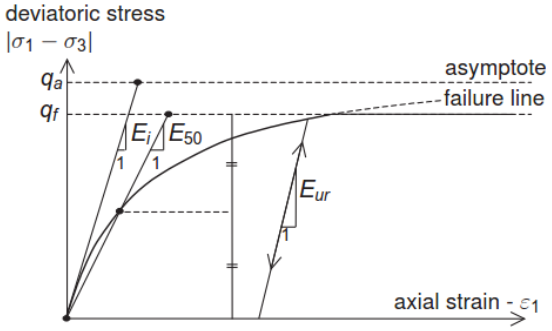

Fig. 6.21: Hyperbolic stress-strain relation in primary loading for a standard drained triaxial test (Plaxis 2012).

$$q_f = \left(c \cdot \cot\phi' - \sigma'_3\right) \cdot \frac{2 \cdot \sin\phi'}{1 - \sin\phi'} \tag{6.8}$$

where $q_f = R_f \cdot q_a$ and $\sigma'_3 = \sigma_3 - u$. R_f default value is 0.90.

In this study, coarse layers are modelled as drained materials. Shear strength is defined from effective strength parameters c' and ϕ'.

However, undisturbed samples are generally difficult to collect in sand layers. Therefore, deriving strength and stiffness parameters may result quite challenging. For this reason, parameters for Hardening Soil model are derived according to the Finnish Road Design Manual (Tiehallinto 2011). For a reference pressure (p^{ref}) of 100 kPa, the oedometer stiffness E_{oed}^{ref} is chosen equal to the secant stiffness for drained triaxial loading E_{50}^{ref}, while the unloading/reloading stiffness E_{ur}^{ref} is taken equal to 3 times E_{50}^{ref}, as suggested by the user's manual of Plaxis (Plaxis 2012).

Values of friction angles and dilatancy angles used were derived and discussed by Mansikkamäki (2015). Input parameters for the Hardening Soil model are reported in Table 6.3.

Tab. 6.3: Input parameters for Hardening Soil model (coarse layers) (D'Ignazio et al. *In press*).

Parameter	**Unit**	**Description**	**Embankment**	**Sand fill**	**Lower sand**
Material type		Material type used in the calculation	Drained	Drained	Drained
γ_{tot}	kN/m^3	Total unit weight	21	19	19
E_{50}^{ref}	MPa	Secant stiffness for CD triaxial	100	30	30
E_{oed}^{ref}	MPa	Tangent oedometer stiffness	100	30	30
E_{ur}^{ref}	MPa	Unloading/Reloading stiffness	250	90	90
m	-	Power for stress dependent stiffness	0.5	0.5	0.5
c'	kPa	Effective cohesion	1	1	1
p^{ref}	kPa	Reference stress for stiffness	100	100	100
POP	kPa	Pre-overburden pressure	0	20	0
ϕ'	^{o}	Friction angle	38	36	36
ψ	^{o}	Dilatancy angle	8	6	6
ν'	-	Effective Poisson's ratio	0.3	0.3	0.3

6.4.3 **Dry crust**

Field vane test results from 2009 show uncorrected undrained shear strength values well over 50 kPa in the dry crust (Lehtonen 2011). However, field vane test is known to overestimate the available strength in clay crust layers, as discussed in Chapter 3. La Rochelle et al. (1974) suggest that this is mostly due to the presence of fissure patterns, which are likely to be the reason why the strength measured on a small scale (field vane) is larger than on a large scale (e.g. a failure surface). Therefore, undrained shear strength of Perniö dry crust was studied through isotropically consolidated triaxial compression tests (CIUC), which are known to provide a sufficiently reliable estimate of s_u in such layers (Khan 1993).

Samples of dry crust were taken from a secondary site (about 50 m off the test location) where the dry crust is overlaid by an organic superficial layer, while in the test area an old sand fill was located on top of the clay crust. Samples were collected down to 1.80 m from the ground surface using cubic steel block samplers with 150 mm size. The bottom of the dry crust reaches roughly the depth of 1.50 m.

The sampled material was extruded from the block sampler through a cylindrical plastic sampler greased internally with oil. In this way, lateral friction during insertion and extrusion was reduced. Finally, the cut specimens were tested in triaxial compression and in CRS oedometer. CIUC tests were also performed on samples cut in horizontal direction in order to assess strength anisotropy. The diameter of the triaxial specimens was 50 mm, with height/diameter ratio of 2.

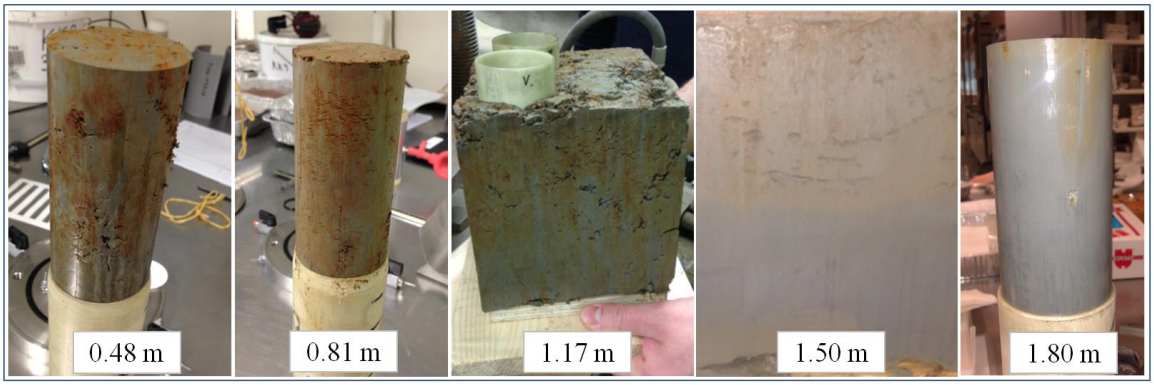

Fig. 6.22: Samples of Perniö dry crust from different depths.

From a visual inspection of the samples, the structure of the dry crust appears to be non-homogeneous (Fig. 6.22). The top part (up to 1.0-1.20 m depth) is characterized by the presence of fissures, mostly oriented horizontally, and by a dark brown colour, probably as a result of some oxidization processes. Cracks become less visible and almost absent for the samples taken below 1.20 m depth, where the structure of the material seems more homogeneous and characterized by the greyish colour typical of Perniö clay. Sparse organic material was found in some of the extruded specimens (e.g. small roots), which made testing difficult and constituted the reason why several specimens could not be tested, as results might have been notably affected.

General characteristics of Perniö dry crust are shown in Fig. 6.23-6.24. Natural water content (w) increases with depth from 40% at 0.50 m to almost 90% at 1.80 m in the soft

clay. Plasticity index (PI) varies between 24% and 47%, without showing any distinct trend with depth. However, the highest PI value (47%) was observed at 1.80 m in the soft clay. The unit weight above 1 m depth is about 16.5 kN/m^3, while it reduces to roughly 15 kN/m^3 in the lower part of the layer. Sensitivity values show high scatter and no specific trend could be observed. S_t values seem to vary on a wide range (S_t=1.5~64). Organic content ranges from 2.1 to 3.3%, with peak at 1.20 m depth. The average clay content (size < 0.002 μm) measured was 55%. The void ratio increases with depth towards the more homogeneous layers, up to values higher than 2.

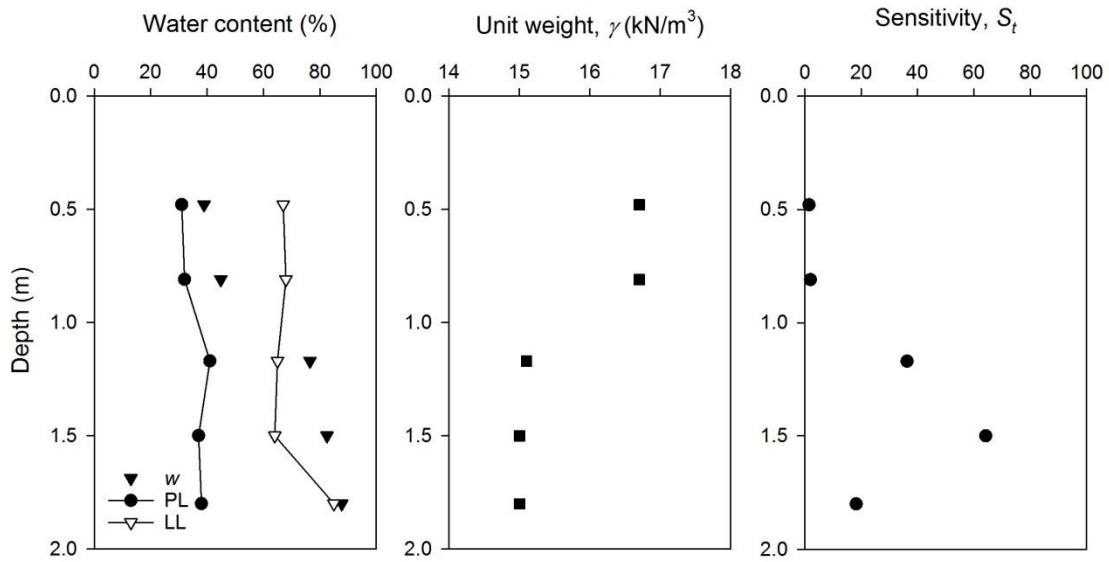

Fig. 6.23: Water content, unit weight and sensitivity of Perniö dry crust.

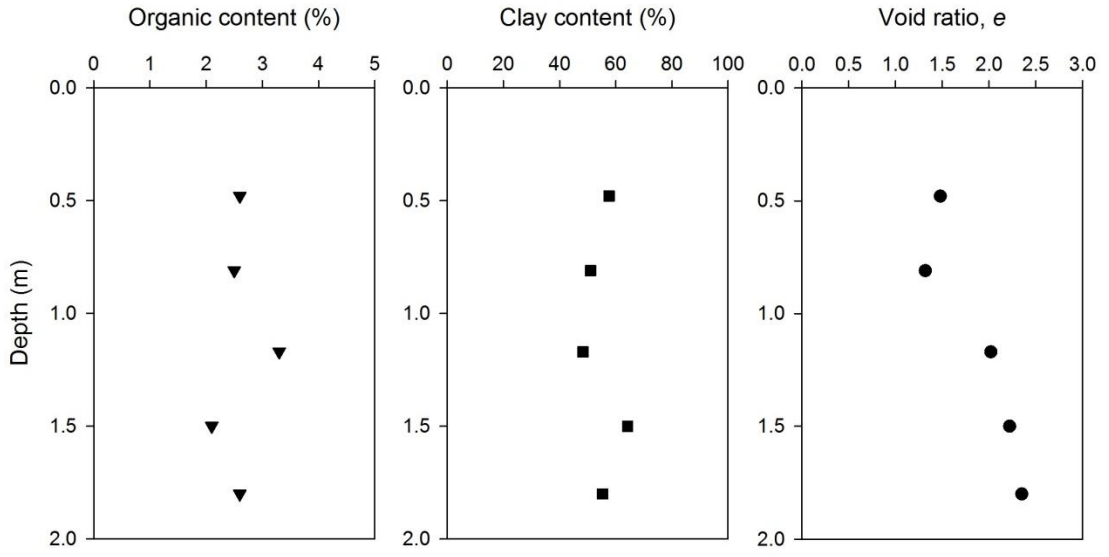

Fig. 6.24: Humus content, clay content and void ratio of Perniö dry crust.

CRS oedometer tests were performed at different depths. No preconsolidation pressure could be detected in the top 1.50 m (see e.g. Fig. 6.25). This is consistent with the conclusions drawn by Ringensten (1988), as reported in Chapter 3, who analysed dry crust layers from different locations in Sweden. However, such a result could be expected as the presence of fissures and organic material would lead to several difficulties in getting undisturbed samples for CRS tests, where specimens are only 15 mm thick. Only

below 1.50 m preconsolidation pressure was visible, suggesting OCR values between 2 and 3 in the clay located right below the dry crust.

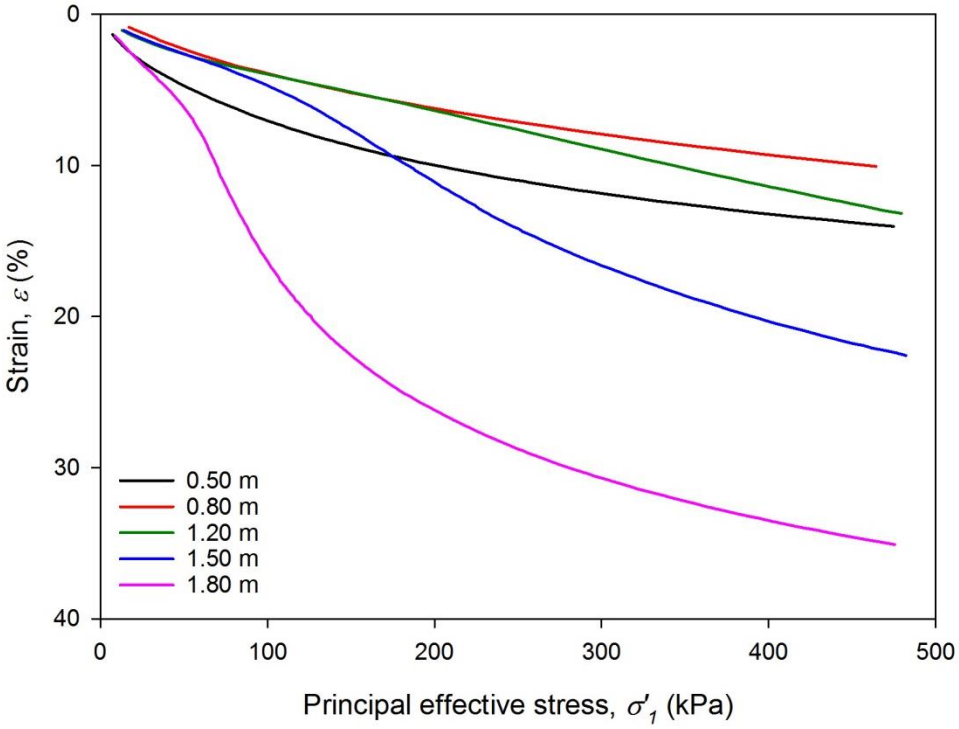

Fig. 6.25: CRS oedometer stress-strain curves from Perniö dry crust block samples (strain rate 0.06%/h).

An issue in triaxial testing of dry crust samples is the estimate of the consolidation pressure (cell pressure) to be used. Therefore, an assumption on the lateral stress coefficient needs to be made. Khan (1993) suggested K_0 values higher than 1 in the proximity of the ground surface, decreasing with depth up to K_0 values close to the K_0 of the underlying clay. Based on this, a K_0 value close to unity was chosen for all the CIUC tests. Tests were carried out at a standard strain rate of 1% axial strain per hour.

Results from CIUC tests on horizontally and vertically cut specimens are presented in Fig. 6.26, Fig. 6.27 and summarized in Table 6.4. Peak (or maximum) strength (s_{up}) and strength values at large strain ($s_{u15\%}$, at 15% axial strain) are also presented.

The maximum measured triaxial compression strength for samples cut in vertical direction is on average 35 kPa at 0.80 m depth, decreasing towards the soft clay layer. The observed CIUC strength values were lower than those suggested by the field vane (s_u > 50 kPa). The average measured ratio between s_u from horizontal samples (s_{uh}) and s_u from vertical samples (s_{uv}) is 0.88 (Fig. 6.26), which gives some information on the structural anisotropy of the dry crust. Even though stress-induced anisotropy was not studied, as a correct estimate of s_u^P/s_u^A would require triaxial compression and extension tests from samples cut in the same direction, s_{uh}/s_{uv} is assumed to be equal to s_u^P/s_u^A in this study.

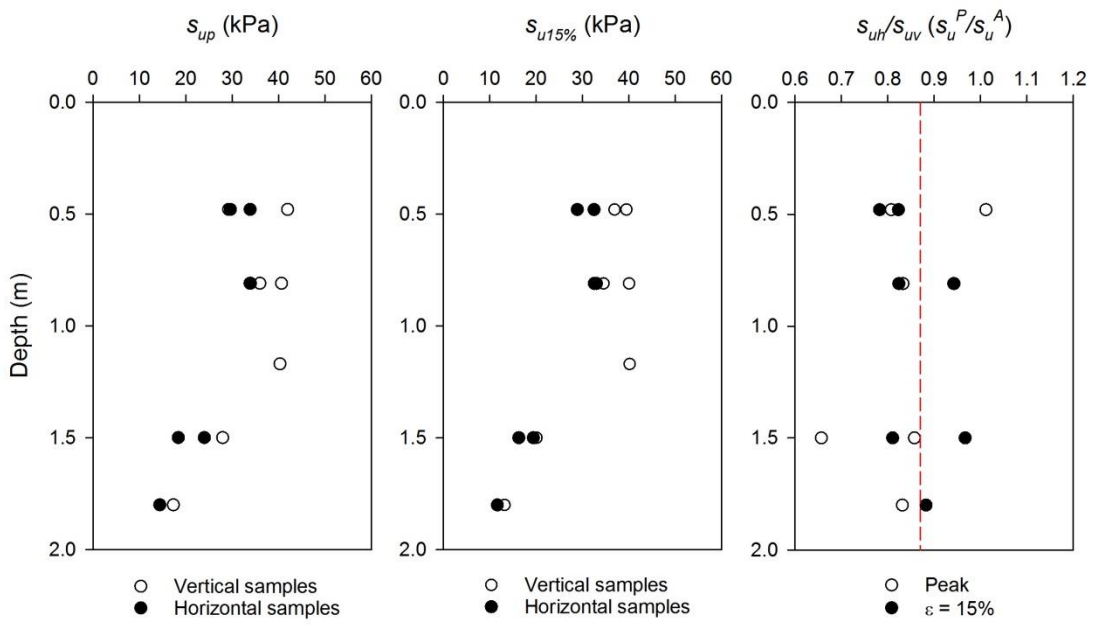

Fig. 6.26: Anisotropy ratio and undrained shear strength of Perniö dry crust.

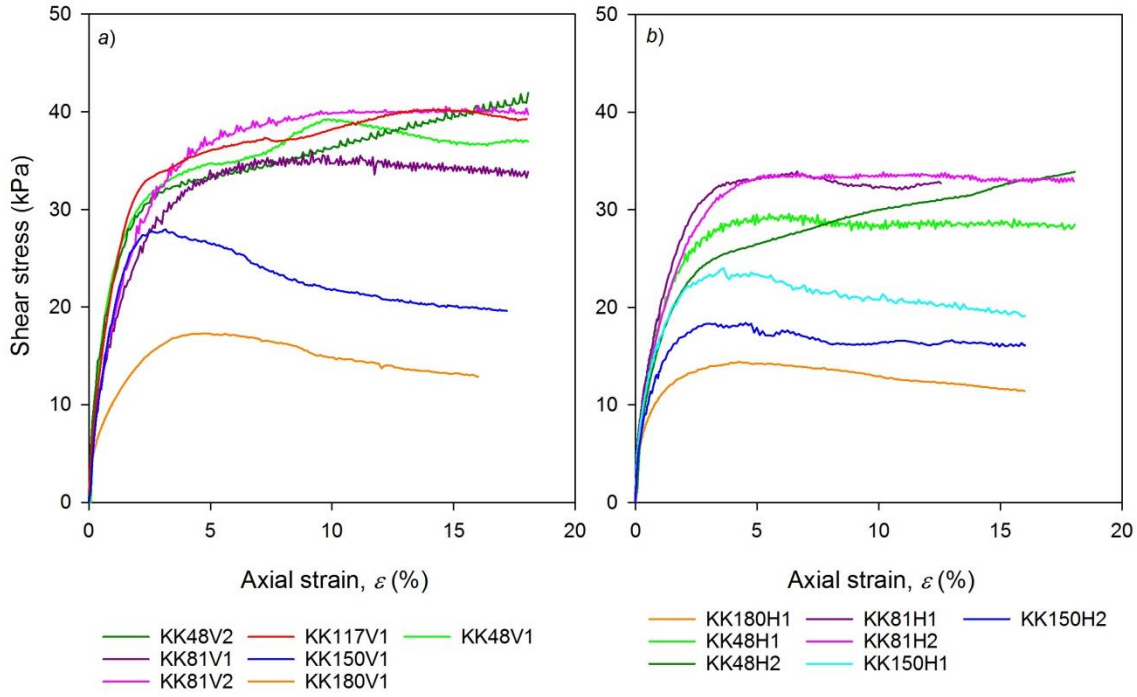

Fig. 6.27: CIUC test results on block samples of Perniö dry crust cut *a*) vertically and *b*) horizontally.

Table 6.4. Summary of CIUC test results on block samples of Perniö dry crust.

			In-situ stress state (approx.)	Cell pressure	Test results	
Test ID	Type	Depth (m)	σ'_{v0} (kPa)	σ_c (kPa)	s_{up} (kPa)	$s_{u15\%}$ (kPa)
KK48V1	CIUC	0.48	7.9	16	29.24	36.90
KK48V2	CIUC	0.48	7.9	9	41.94	39.45
KK81V1	CIUC	0.81	13.4	15	35.97	34.52
KK81V2	CIUC	0.81	13.4	14	40.62	40.03
KK117V1	CIUC	1.17	17.6	17	40.29	40.14
KK150V1	CIUC	1.50	19.8	19	27.97	20.06
KK180V1	CIUC	1.80	21.7	18	17.31	13.19
KK48H1	CIUC	0.48	7.9	16	29.59	28.88
KK48H2	CIUC	0.48	7.9	10	33.88	32.48
KK81H1	CIUC	0.81	13.4	12	33.92	32.53*
KK81H2	CIUC	0.81	13.4	14	33.84	32.99
KK150H1	CIUC	1.50	19.8	17	23.99	19.40
KK150H2	CIUC	1.50	19.8	17	18.38	16.26
KK180H1	CIUC	1.80	21.7	17	14.40	11.64

*The test was stopped before ε = 15%. $s_{u15\%}$ corresponds to the last measurement.

The stress-strain behavior observed from samples taken at different depths is not uniform. The uppermost part of the dry crust shows a marked dilatant behavior after reaching the yield stress. Below 0.48 m and up to 1.20-1.50 m, the strain hardening behavior seems to dominate the undrained response of the soil, as suggested by Ringesten (1988). On the other hand, below 1.50 m depth the soil is characterized by lower strength values, with some strain-softening which occurs in the post-peak regime.

The top 80 cm of the weathered crust is not fully saturated, with degree of saturation (S_r) of 85-95% (seasonal fluctuations of the groundwater table and periodic rainfalls may have some influence). However, in this study the clay crust is modelled as a total stress material. Therefore, partially saturated conditions will not constitute an issue, as suction is implicitly included in the undrained shear strength.

At the test location, the upper 0.50-0.80 m of the soil was probably removed prior to construction of the old sand fill. Therefore, only samples taken below 0.5 m are used to derive the soil parameters for FE analyses. It was further assumed that no strength increase has occurred in the dry crust caused by the sand fill construction. Furthermore, the dilatant behavior observed from tests from the uppermost part of the layer is neglected, as the upper part of the dry crust was removed.

Two different finite element soil models are used to describe the hardening stress-strain behavior of Perniö dry crust: the isotropic Hardening Soil model and the anisotropic NGI-ADP model. Soil parameters for the two models were derived from curve fitting of CIUC triaxial test results, using the Soil Testing tool in PLAXIS.

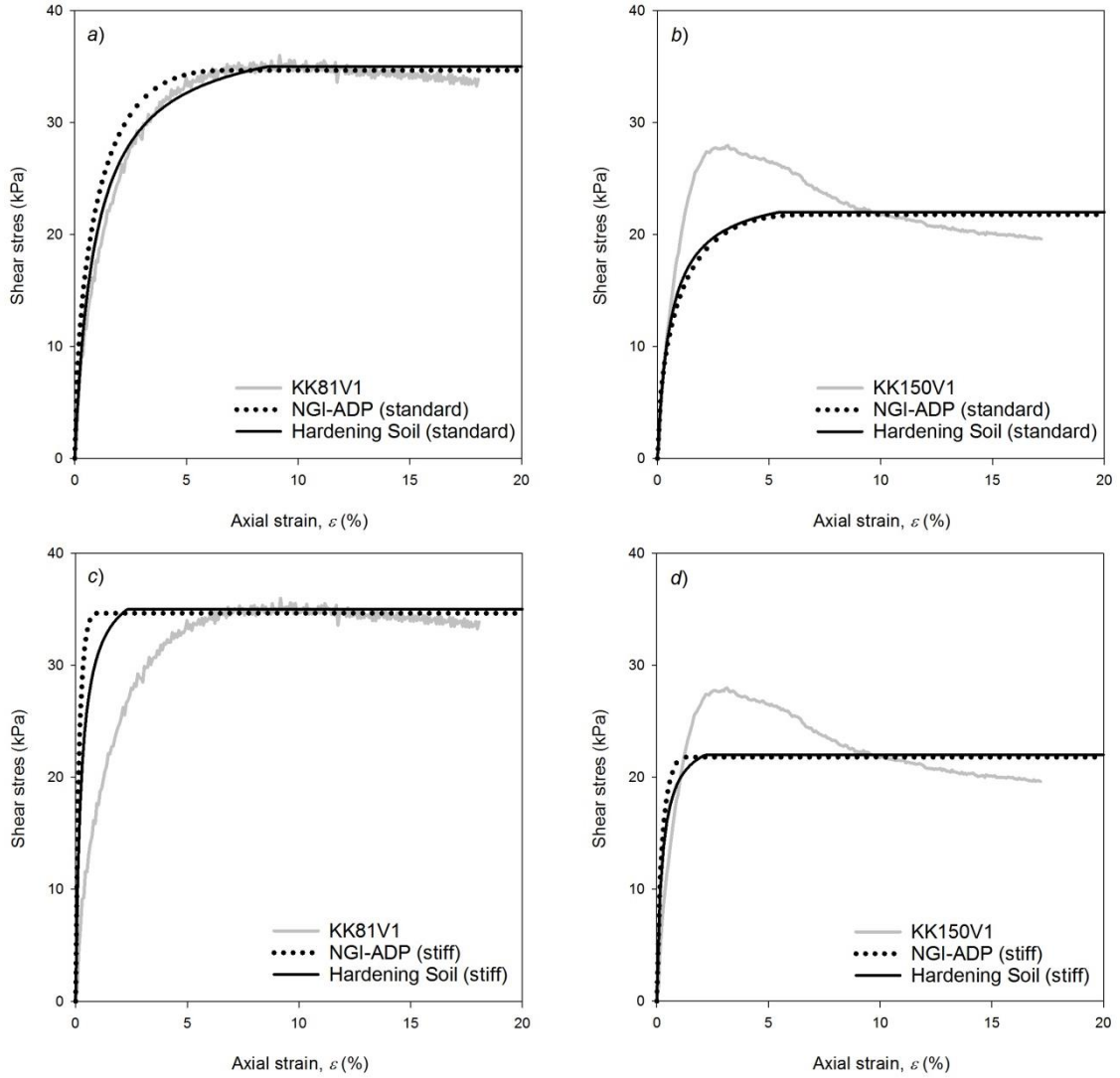

Fig. 6.28: Curve fitting of FE soil models using *a*) standard parameters for KK81V1 test, *b*) standard parameters for KK150V1 test, *c*) stiff parameters for KK81V1 test and *d*) stiff parameters for KK150V1 test.

Fig. 6.28 shows the stress-strain behavior predicted by the two soil models. Both Hardening Soil and NGI-ADP models provide a good fit to the laboratory data for specimens taken above 1 m (Fig. 6.28*a*) because of their capability of capturing the non-linearity of stiffness. On the other hand, by using the simple Mohr-Coulomb model, the predicted stiffness would be linear and hence not representative of the laboratory test results. In addition, as a constant strength criterion is used, the two models predict the triaxial failure load equally. Strain-softening is not taken into account, as it seems less dramatic than in the soft clay. Therefore, from tests exhibiting strain-softening behavior, s_u at large strain is taken as input parameter (Fig. 6.28*b*). Input parameters for Hardening Soil and NGI-ADP soil models are summarized in Table 6.5 and Table 6.6, respectively.

It must be however pointed out that when using the "standard" fitting parameters, stiffness in the lower part of the dry crust (Fig. 6.28*b*) seems highly underestimated. Therefore, a second set of parameters (hereinafter referred to as "stiff") was derived to better describe stiffness at small strain. When using the "stiff" fitted parameters of Table 6.5 and Table 6.6, the modelled stress-strain behavior of specimens taken below 1.20 m

seems more representative of the CIUC test results (Fig. 6.28*c-d*). However, stiffness of the upper part of the dry crust appears to be overestimated.

It could though be expected that sample disturbance may have caused the measured stiffness to be lower than in-situ, especially in the top 1.0-1.20 m of the dry crust, as discontinuities as well as organic material were found even in the best samples. Therefore, the "stiff" set of parameters seems more suitable for the calculation, being more representative of the tests which were expected to be of the highest quality.

In section 6.4.1, the peak compression shear strain determined for the soft clay is 2%. A logical assumption is made under the hypothesis that peak stresses in the dry crust are mobilized at the same strain level as in the soft clay. The effect of stiffness parameters on measured displacements is discussed in section 6.5.6.

Tab. 6.5: Input parameters for NGI-ADP model (dry crust).

Parameter	**Unit**	**Description**	**Standard**	**Stiff**
Material type	-	Material type	Undrained (C)	Undrained (C)
γ_{tot}	-	Total unit weight	16.5	16.5
G_0/s_u^A		Initial stiffness	700	700
$s_u^A{}_{ref}$	kPa	Reference active shear strength	35	35
$s_u^A{}_{inc}$	kPa/m	S_u increase with depth	-13	-13
y_{ref}	m	Reference depth	0	0
x_{ref}	m	Reference x-coordinate	-7	-7
γ_p^C	%	Shear strain at peak in CAUC	10	2
γ_p^{DSS}	%	Shear strain at peak in DSS	10	2
γ_p^E	%	Shear strain at peak in CAUE	10	2
τ_0/s_u^A	-	Initial mobilization	0	0
s_u^P/s_u^A	-	Normalized passive strength	0.88	0.88
s_u^{DSS}/s_u^A	-	Normalized DSS strength	0.92	0.92
ν_{und}	-	Poisson's ratio	0.495	0.495
K_0	-	Lateral stress coefficient	1	1

Tab. 6.6: Input parameters for Hardening Soil model (dry crust).

Parameter	**Unit**	**Description**	**Standard**	**Stiff**
Material type		Material type	Undrained (B)	Undrained (B)
γ_{tot}	kN/m^3	Total unit weight	16.5	16.5
E_{50}^{ref}	MPa	Secant stiffness for CD triaxial	4	10
E_{oed}^{ref}	MPa	Tangent oedometer stiffness	4	10
E_{ur}^{ref}	MPa	Unloading/Reloading stiffness	12	30
m	-	Power for stress dependent stiffness	1	1
$s_{u\,max}$	kPa	Undrained shear strength	35	35
s_u *increase*	kPa/m	Undrained shear strength increase	-13	-13
p^{ref}	kPa	Reference stress for stiffness	100	100
ν'	-	Poisson's ratio	0.3	0.3

6.5 Finite element analysis

6.5.1 Methodology

The cross section used for the FE analyses is the mid (A-A) cross section of the embankment (Fig. 6.2). Section A-A was not only the most instrumented, but probably also the most representative of plane-strain conditions.

The finite element mesh used for the calculations consisted of 3432 15-noded triangular elements. The average size of the element is 0.32 m (Fig. 6.29). When generating the mesh, the global coarseness was set to "very fine". Further cluster refinement was applied to the soft clay layers.

The conditions applied to the boundaries of the plane-strain model consisted of *i*) a fully fixed bottom boundary, where movements were prevented both in the horizontal and the vertical direction *ii*) partially fixed vertical sides, where movements in the horizontal direction were not allowed (roller conditions).

The on-site construction sequence is fully reproduced in the calculations, assuming fully undrained conditions in the clay layers. The initial stresses in the soil are generated assuming a purely "K_0" consolidation for horizontal layers, even though layers seem gently inclined. However, calculation results are not influenced by the stress generation procedure.

In a second stage, the excavation of the lateral ditch is modelled and the construction of the embankment simulated, before modelling the whole load-to-failure process.

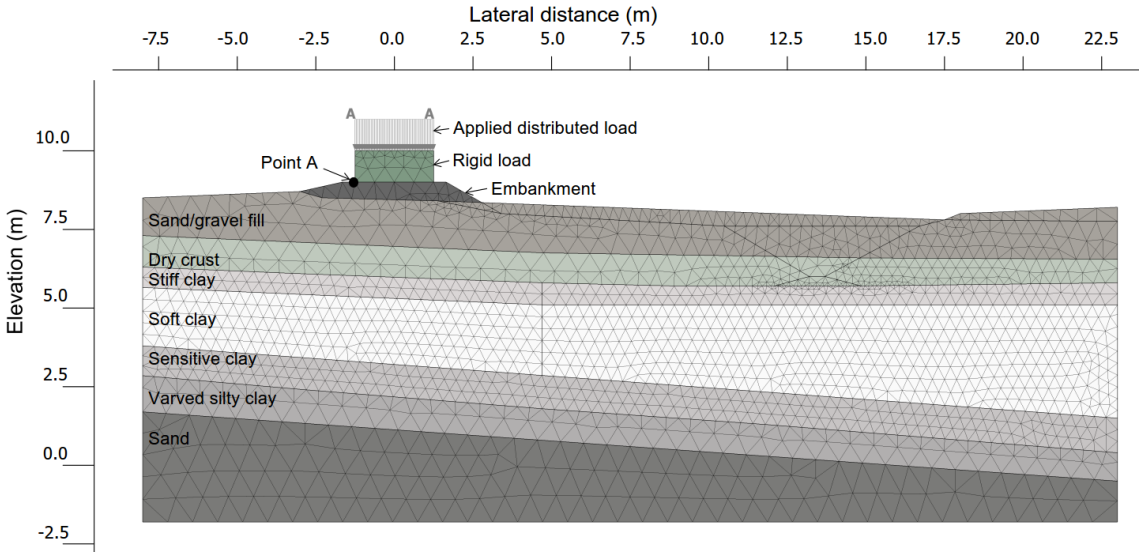

Fig. 6.29: Finite Element mesh [D'Ignazio et al. *In press*].

The load applied on top of the embankment is simulated through a 1 m high rigid block, modelled as linear elastic material. For deformation analyses, the unit weight of the rigid block is changed according to the load step phase. For failure and post-failure analyses, the incremental multiplier procedure is adopted: a distributed load is placed on top of the

rigid block with given unit weight of 1 kN/m^3, and incremented by load steps of 1 kPa each. The calculation is stopped when a vertical displacement of the embankment equal to about 1 m is reached at point A (located as in Fig. 6.29). A vertical displacement of 1 m roughly corresponds to the settlement measured before the containers fell on their side after failure. The choice of using a rigid load would possibly provide a better description of the loading over rails and the effect of the concrete sleepers.

The load-settlement behavior is modelled through three separate phases. In a first phase, a load of 24 kPa is applied over a period of 0.11 days, corresponding to approximately 2.6 hours, and kept constant during a second phase for 0.56 days (roughly 13.4 hours). The latter simulates the interruption of the loading process during the night. In the third and last phase, a load corresponding to the peak failure load calculated from the incremental multipliers procedure is applied over a period of 0.55 days.

The influence on the failure mechanism of the previously identified more "sensitive" clay layer (section 6.4.1) is studied through two separate analyses. In a first analysis, the same post-peak behavior of the soft clay is assumed (50% of the peak strength at large strain). In a second analysis, the strength at large strain is reduced by 20% (40% of the peak strength), as shown in Fig. 6.20. Finally, the dry crust is modelled using the anisotropic NGI-ADP model with the "stiff" set of parameters of Table 6.5.

6.5.2 **Failure load**

A peak failure load (q_{soft}) equal to 80.8 kPa was computed from the incremental multipliers analysis. Mansikkamäki (2015) indicates that the duration of the loading process had a high impact on the bearing capacity achieved in the Perniö test, as a consequence of the rate dependency of undrained shear strength. Mansikkamäki (2015) estimated, supported by advanced FE analyses using time-dependent soil models, that if the embankment had been loaded slowly enough, the failure load would have been lower than the 87 kPa (q_{test}) measured.

3D analyses of Perniö failure test carried out by Mansikkamäki and Länsivaara (2012) and Mansikkamäki (2015) have shown that the 3D failure load is 5-12 % higher than in plane strain. Hence, the calculated value of q_{soft} = 80.8 kPa can be considered a good estimate since rate as well as 3D effects were not taken into account in the calculations. Furthermore, such a result shows consistency with field observations despite uncertainties in the input parameters, i.e. the spatial distribution of the actual shear strengths.

A purely anisotropic elasto-plastic analysis is carried out to evaluate the effect of strain-softening on the failure load. Strengths at large strain are set equal to peaks in the three directions of loading ($s_u^{A,DSS,P} = s_{ur}^{A,DSS,P}$). The outcome is a peak load 6.2% higher than when including strain-softening behavior.

Furthermore, the influence of anisotropy on the peak capacity is studied by using an average isotropic undrained shear strength equal to $s_u^{avg} = (s_u^{A}+s_u^{DSS}+s_u^{P})/3$ as input parameter. In this case, the failure load results 8.9% higher (88 kPa versus 80.8 kPa).

For the hypothesis of $s_u^{avg} = s_u^{DSS}$ the computed load at failure does not show a marked difference from the anisotropic analysis with softening (0.4% lower maximum load). However, by taking the measured field vane strength (s_u^{FV}, corrected values) as average undrained shear strength, the capacity is reduced by 8.5%.

Calculated failure loads from all the analyses performed are summarized in Table 6.7.

Tab. 6.7: s_u vs. calculated failure load in the Perniö failure test.

Input undrained shear strength (s_u)	**Anisotropy**	**Softening**	**Failure load (kPa)**
Anisotropic (ADP)	Yes	Yes	80.8
Anisotropic (ADP)	Yes	No	85.8
$s_u^{avg} = (s_u^{A}+s_u^{DSS}+s_u^{P})/3$	No	No	88
s_u^{DSS}	No	No	80.5
s_u^{FV} (field vane average, corrected values)	No	No	73.9

Failure capacity of the Perniö embankment seems also to be affected by the strength of the dry crust layer. When using s_u measured from field vane (i.e. average s_u = 40 kPa), the failure load becomes 94 kPa. Furthermore, neither stiffness parameters nor soil model used to describe the dry crust behavior (see Table 6.5-6.6) had any remarkable impact on the load at failure.

6.5.3 **Failure mechanism**

The embankment failure mechanism is modelled by conducting two parallel analyses. The purpose is to evaluate the influence of the sensitive clay layer on the shear band development. Firstly, the soft clay layer is modelled as a single layer, and secondly divided into two layers with slightly different behavior at large strain, as described in Section 6.4.1.

Calculation results indicate that shear bands from the analyses seem to share the same starting and ending points. However, the main differences can be observed under the embankment, in the active side of shearing.

Calculated shear bands at failure (1 m vertical displacement of the embankment) from incremental deviatoric strain ($\Delta\gamma_s$) from the analyses and approximated observed failure mechanism are illustrated in Fig. 6.30.

By assuming that post-peak behavior is the same for both soft and sensitive clay layers, the interpreted shear zone from the test seems to go lightly deeper than the mechanism predicted by the FE analysis. When differences in strain-softening behavior are included, the failure mechanism is dragged down to a greater depth, in agreement with field observations. Nevertheless, the approximate failure zone appears to steeply reach the top of the stiff silty clay layer, while in the model it bends up more smoothly towards the ditch.

The maximum depth of the computed shear band is reached at a point which has approximately 5 m horizontal distance from the centreline of the embankment. Field observation suggested though that the maximum depth was reached at a point only 3.0 to 3.5 m from the centreline (Fig. 6.6 and Fig. 6.30).

Finally, the peak failure load does not seem to be dependent on the different computed failure mechanisms.

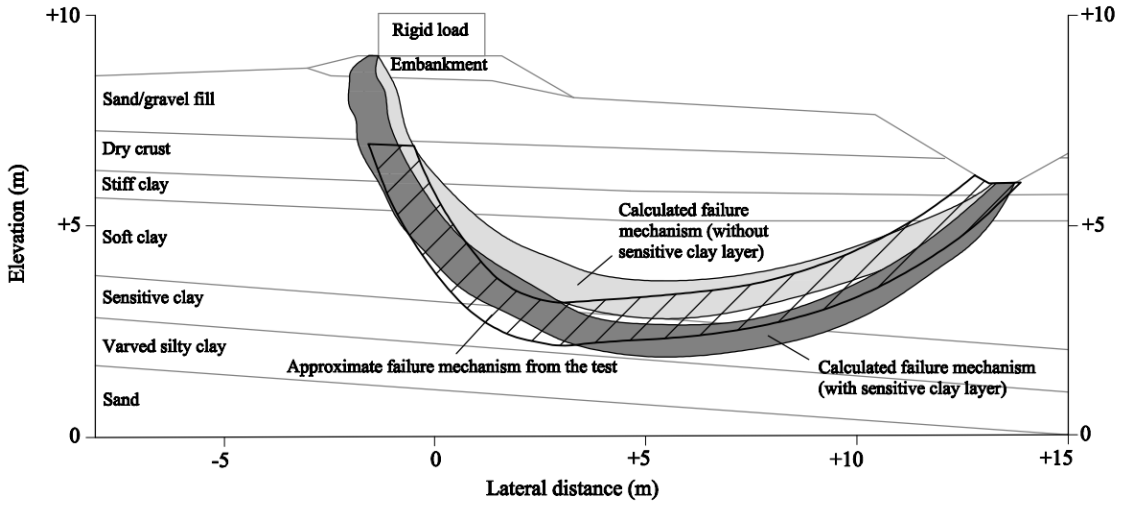

Fig. 6.30: Comparison between the observed failure mechanism and the calculated shear bands from the FE analyses [D'Ignazio et al. *In press*].

6.5.4 **Displacements**

The load-settlement curve for point A is presented in Fig. 6.31, based on the scenario described by the soil parameters of Table 6.2. The calculated vertical displacement from the FE analysis is compared to the measured settlement from settlement transducer 53 (located as shown in Fig. 6.3). After reaching a vertical displacement of about 0.11 m measured from the top of the embankment, failure occurred after a few seconds and stopped when the containers tipped over. The sensitive clay layer is included in this calculation.

Even though viscous phenomena are not taken into account, settlement can be predicted with relatively low error (Fig. 6.31). Calculated displacement seem though slightly overpredicted after the onset of first yielding (about 3.5 hours before failure). On the other hand, settlement right before failure is predicted with high accuracy.

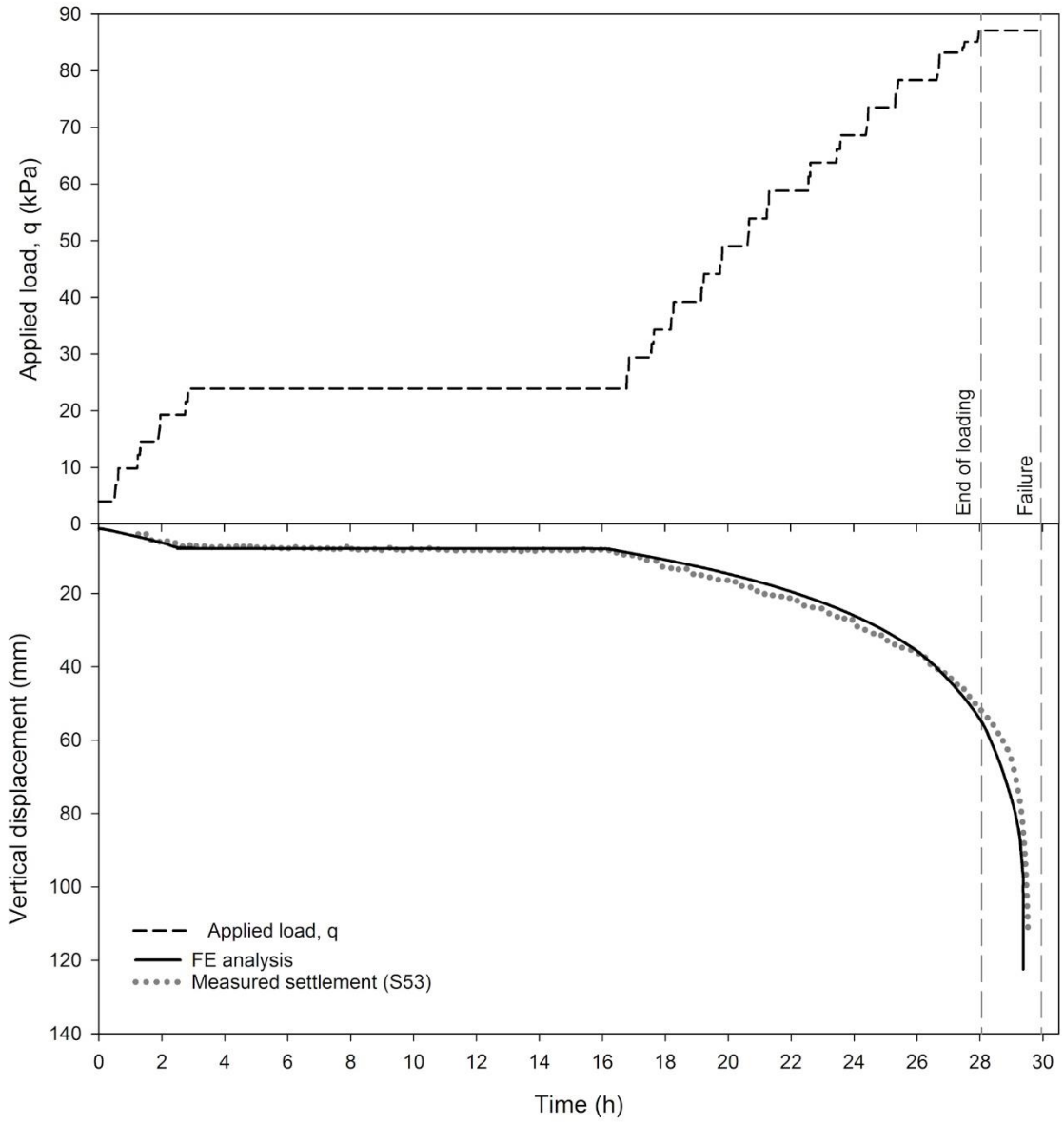

Fig. 6.31: Load-Time-Settlement [D'Ignazio et al. *In press*].

Horizontal displacements during loading were recorded by 9 individual inclinometers located in the foundation soils, and placed in three sections at the toe of the embankment, at the mid and edge of the ditch. Three tubes were placed in each section. The inclinometer tubes are listed from the embankment towards the ditch progressively with numbers from 1 to 3.

Fig. 6.32 shows calculated and measured pre-failure horizontal displacements, u_x, against the *z* coordinate at the toe of the embankment, at the Mid and Edge of the excavated ditch from inclinometers L2P1, L2P2 and L2P3, respectively. Observed displacements were caused by applied loads of 68.5, 78.5 and 87 kPa (last loading step at 19:30). Given loads equal to 68.5 kPa and 78.5 kPa correspond to 78% and 90% of q_{test} = 87 kPa. As $q_{soft} < q_{test}$, field data are compared to horizontal movements caused by loads corresponding to 78%, 90%, 99% and 100% of q_{soft}.

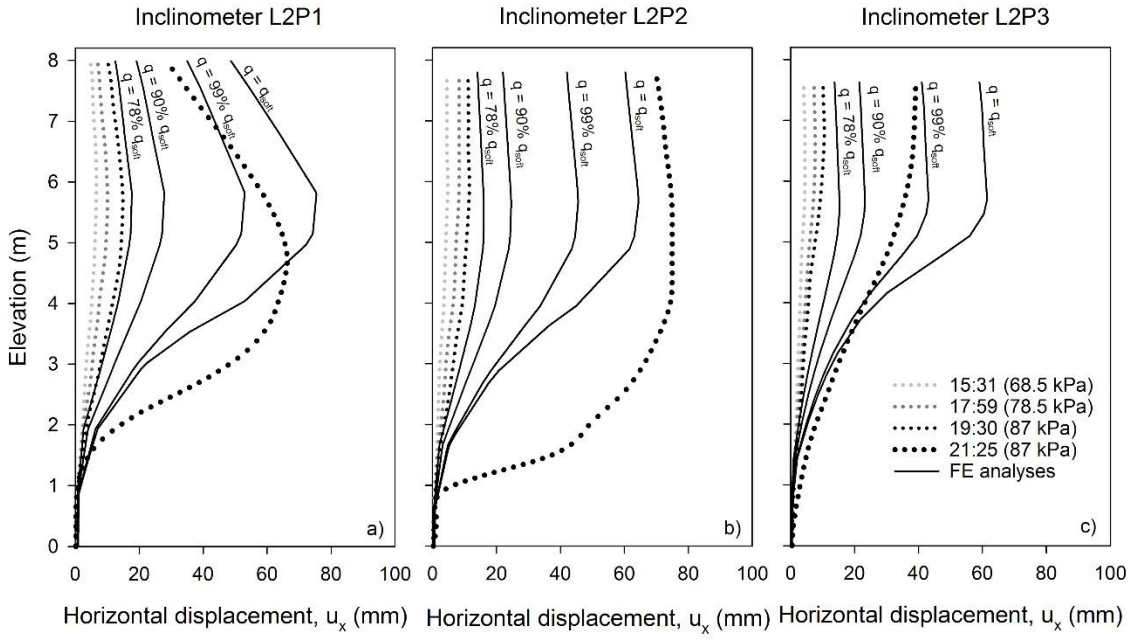

Fig. 6.32: Measured and calculated horizontal displacements for section A-A [D'Ignazio et al. *In press*].

Measured displacements seem generally smaller than the NGI-ADPSoft model predictions, except for measurements at larger strain from inclinometer L2P1 and L2P2, where the maximum horizontal displacement (u_x^{max}) is modelled with relatively low error.

However, an accurate modelling of the variation of horizontal strains with depth right before failure was rather difficult to achieve, especially in the lower layers at elevation of 2-3 m. This may suggest that the computed shear band at peak occurred at a higher elevation than in the real experiment (as if the sensitive layer was not modelled, see Fig. 6.30). In contrast, lateral displacement profiles at small strains could be reproduced reasonably well, even though the calculated values resulted higher than in the test.

6.5.5 **Evolution of progressive failure**

Contours of hardening parameters κ_1 and κ_2 are shown in Fig. 6.33 and Fig. 6.34, respectively, corresponding to different embankment settlements. The post-peak softening control parameter κ_2 is equal to 1 when the residual strength is fully mobilized, and varies between zero and 1 between peak and residual state. The pre-peak hardening control parameter κ_1 is equal to 1 when the peak strength is reached, and varying between zero and 1 in the pre-peak hardening regime.

For a perfectly plastic material, failure occurs when all the material points along a critical slip surface have reached the maximum shear stress. Conversely, with NGI-ADPSoft model the unstable global condition (failure) is already reached when the shear stress at some location along the shear band has passed the peak shear strength ($\kappa_2 > 0$). Under these conditions, the mobilized shear strength in the surrounding soil is still lower than the peak strength (Fig. 6.34). By further increasing strains, the resistance in the post-peak (softening) zone will reduce more rapidly than the increase in the pre-peak (hardening) zone. Therefore, the global resistance will be reduced.

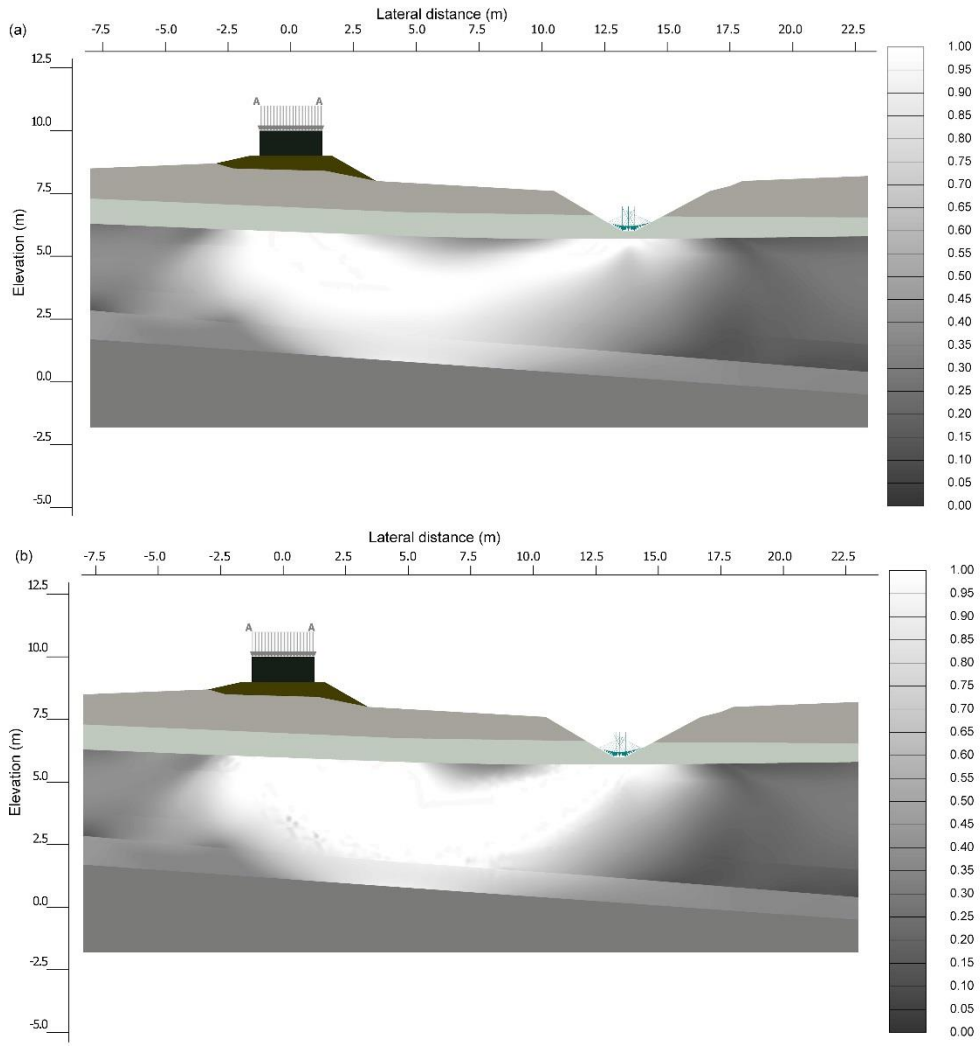

Fig. 6.33: Hardening parameter κ_1 for an embankment settlement of *a*) 0.1 m and *b*) 1 m [D'Ignazio et al. *In press*].

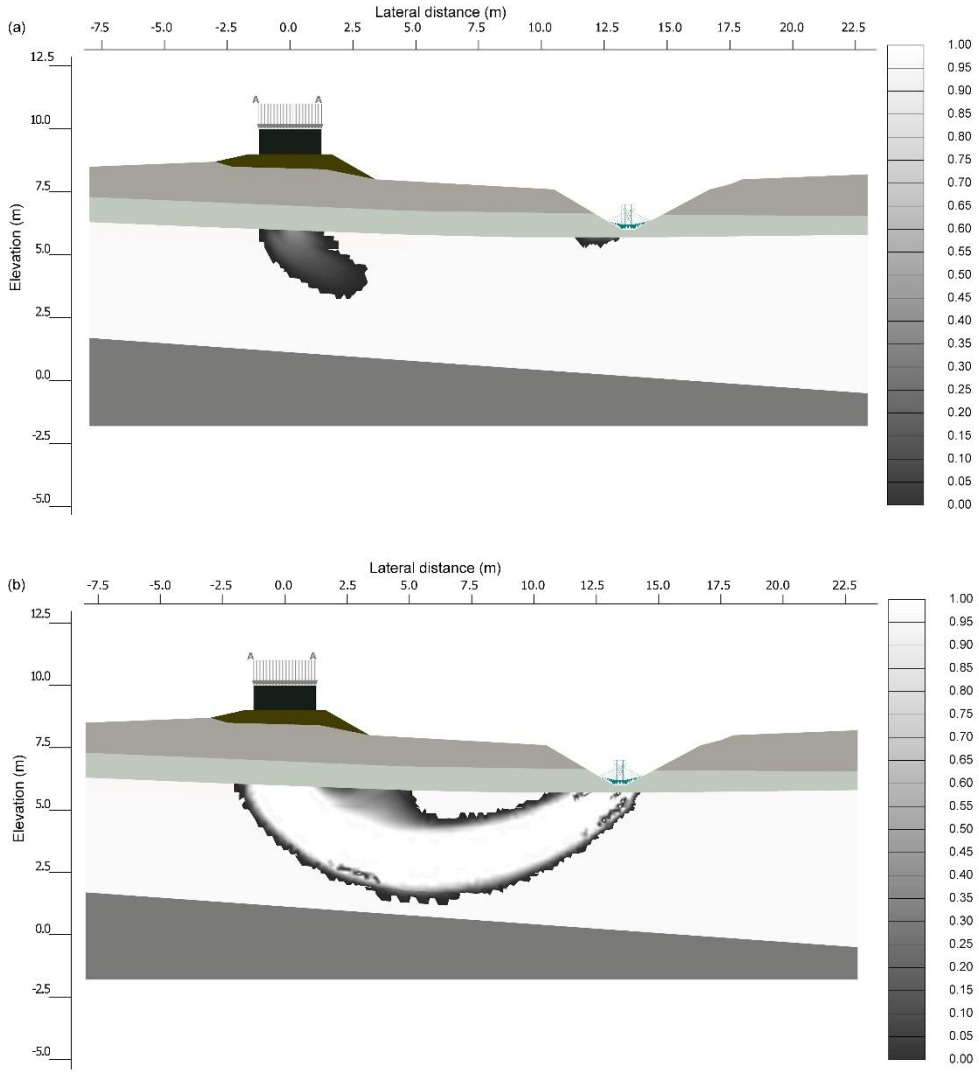

Fig. 6.34: Hardening parameter κ_2 for an embankment settlement of *a*) 0.1 m and *b*) 1 m [D'Ignazio et al. *In press*].

6.5.6 **Sensitivity analysis**

A crucial passage in this study was the derivation of the undrained shear strength for direct simple shear using field vane test results, as DSS tests are not in use in Finland. For s_u^{DSS}/s_u^A equal to 0.7, the resulting failure load is 5% higher than for s_u^{DSS}/s_u^A = 0.65 (default value). When the same ratio is equal to 0.75, the embankment fails under a load of 88.1 kPa (9% higher). This result seems to be a quite high estimate, considering that neither rate effect nor 3D geometry are accounted for.

On the contrary, uncertainties in the determination of the passive strength do not seem to influence the global behavior of the Perniö embankment, since the computed failure load is reduced only by 4% by reducing s_u^P/s_u^A from 0.5 to 0.4.

The anisotropy ratio s_u^P/s_u^A might however be affected by sample disturbance. A study carried out by Karlsrud and Hernandez-Martinez (2013) on high quality samples of Norwegian clays, suggested that disturbance in compression can affect peak strengths of 10-50%, while in extension tests only of 0-10%. As a direct consequence, peak strengths for active loading may result in higher values and, therefore, lead to a higher calculated failure load.

When modelling the dry crust using the "standard" set of soil parameters (Table 6.5-6.6), the maximum computed horizontal displacements result about 30% higher than those observed in Fig. 6.32.

A FE analysis with reduced peak shear strains (by a factor of 2) in the three directions of loading, showed nearly no influence on the peak capacity (less than 2%). As expected, a more significant impact was observed on displacements, being u_x^{max} reduced by 35% (Fig. 6.35).

By reducing the internal length parameter (l_{int}) from 0.4 m to 0.1 m, the failure load becomes 5% lower. For l_{int} = 0.7 m, a higher load (about 4%) is needed to reach the failure state.

The finite element discretization seems to have a small effect on the peak capacity, thus demonstrating how mesh dependency is avoided by the non-local strain formulation implemented in NGI-ADPSoft model. The mesh element number was increased from 1203 to 1956 and 3432. Observed differences in the failure loads calculated with different meshes are less than 3%. Moreover, both horizontal and vertical displacements did not show any relevant change for all the analyzed configurations.

The computed failure mechanism seems also mesh independent. Variations of l_{int}, and consequently shear band thickness, did not cause any change in terms of maximum depth reached by the failure zone.

The failure load increases by approximately 6% when the softening parameters c_1 and c_2 ($c_1 = c_2$) are varied from 1 (from fitting to CK_0UC tests) to 2. This was likely to be expected, as "less" strain-softening is provided right beyond the peak strength, thus affecting the peak capacity.

Small variations in stiffness or friction angle of the coarse layers did not lead to any remarkable differences, neither in terms of failure load/mechanism nor displacements. It seems, therefore, that the whole process was governed by the soft clay layers.

A summary of the effect of different parameters on the calculated failure load in the Perniö failure test is shown in Table 6.8.

Tab. 6.8: Impact of parameters variation on the computed failure load (NGI-ADPSoft model).

Parameter	Standard value(s)	Modified value	Failure load (kPa)	Difference with the failure load calculated using the standard parameters
s_u^{DSS}/s_u^A	0.65	0.7	84.8	5 %
		0.75	88.1	9 %
s_u^P/s_u^A	0.5	0.4	77.6	-4 %
l_{int} (m)	0.4	0.1	76.8	-5 %
		0.7	84.0	4 %
c_1, c_2 ($c_1 = c_2$)	1	2	85.6	6 %
γ^C, γ^{DSS}, γ^E (%)	2, 4, 8	1, 2, 4	79.2	-2 %
n. elements	3432	1203	83.2	3 %
		1956	82.3	2 %

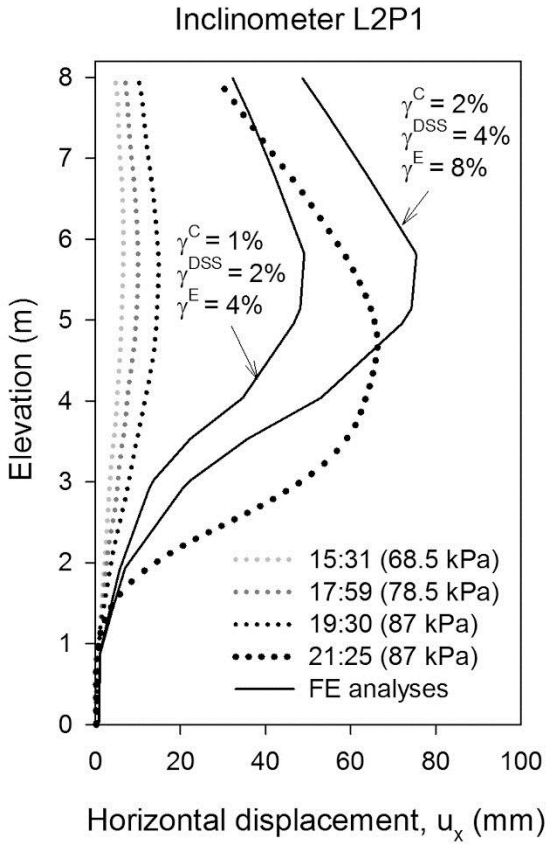

Fig. 6.35: Effect of input peak shear strains on horizontal displacements [D'Ignazio et al. *In press*].

6.6 Discussion

The computed capacity at failure from the presented analysis is 80.8 kPa, which is 7.7% lower than the experimentally observed value (87 kPa). Such a difference in the results might be related to 3D effects, which were not taken into account in the analysis. As found by Mansikkamäki (2015), the FE 3D failure load in the Perniö test can be 5 to 12% higher than the corresponding load from a 2D plane-strain analysis.

Another possible reason to explain the higher experimental value measured would be the occurrence of partial drainage of excess pore pressure in the soft clay. However, Lehtonen et al. (2015) suggested that such a phenomenon may have occurred only over a very thin zone adjacent to one of the more permeable boundaries. In addition, excess pore pressure measurements did not show any reduction during the whole loading process, thus indicating the hypothesis of pore water migration would be hard to justify. Lehtonen et al. (2015) also discussed how failure must have occurred under almost fully undrained conditions, mainly because of the short duration of the load-to-failure process, and the low permeability of the soft clay.

Strain rates in the field are normally induced by a load-controlled process, while in most of the standard laboratory tests, rates are defined through a strain-controlled procedure. Hence, it is quite challenging to compare in-situ strain rates with those from laboratory tests. In Finland, triaxial undrained tests (compression/extension) are normally run at a strain rate of about 1%/h, meaning that the tested specimen is expected to fail within a few hours. Conversely, undrained failure in the field may take several days, as discussed by e.g. La Rochelle et al. (1974). Based on the presented results, undrained shear strength values determined from triaxial compression/extension tests performed at standard rate are representative of "fast" loading conditions, as in the Perniö experiment. Therefore, triaxial test results must be carefully evaluated when used in stability analyses, as the safety level may be overestimated. For instance, in the majority of field cases, the loading is performed "slowly", at much lower strain rate (e.g. tenfold) than in a standard triaxial test. In order to model this aspect, the undrained shear strength must be reduced to take rate effect into account, so that a reasonable estimate of the failure load is provided.

The effect of strain rate on the preconsolidation pressure of soft Finnish clays, and consequently on the undrained shear strength, is described by eq. (2.4) in section 2.2. By reducing the undrained shear strength by a factor of 1.17-1.20, as suggested by the experimental observation by Länsivaara (1999, 2012), the calculated failure load in the Perniö failure test would be lower than 75 kPa (e.g. stress path A-B of Fig. 6.7). Therefore, the duration of the loading process is a crucial aspect in geotechnical design on soft clay areas, as discussed by e.g. Mansikkamäki (2015). When using a soil model as NGI-ADPSoft, which does not account for rate dependency of clays, engineering judgment becomes very important for assessing the input strength parameters.

6.7 Conclusions

Shear strain calculated from inclinometers readings showed an increase in strain rate during the experiment, even during the two hours before failure when the load was kept constant. Hence, consistency was found with the conclusions drawn by Lehtonen et al. (2015) from the pore pressure readings.

The NGI-ADPSoft soil model can appropriately model the anisotropic strain-softening response of saturated sensitive clays, provided that model parameters are carefully selected and non-local strain parameters thoughtfully chosen.

Furthermore, the anisotropic behavior of clays at failure can be accurately simulated provided that extensive soil investigation is available. Relevant tests include anisotropically consolidated triaxial compression (TXC), triaxial extension (TXE) tests and direct simple shear (DSS) tests. When there is lack of information, existing correlations for anisotropic undrained shear strength should be used with caution, while being aware of the nature of the clay.

CIUC triaxial tests on block samples of dry crust provided a realistic assessment of the undrained shear strength. Measured strength values resulted significantly lower than those measured from field vane.

While undrained strength of Perniö clay is highly anisotropic, the strength of Perniö dry crust seems to be closer to isotropic conditions, as the difference in compression strength between samples taken in vertical and horizontal direction is less than 15%. It should be pointed out that based on the observed failure geometry in the experiment, anisotropy in the dry crust would not have much influence as the failure plane crosses the dry crust mostly in the active shear zone and since the dry crust is relatively thin in the passive zone.

The predicted failure load of 80.8 kPa, based on the best estimate of soil properties, represents a very satisfactory result considering that neither rate nor 3D effects were modelled.

Undrained shear strength from triaxial tests carried out at standard strain rate appears to be representative of “fast” loading conditions, as in the failure test. Undrained shear strength should though be corrected for strain rate when loading is performed at lower rates.

The computed failure load was found to be nearly independent of FE discretization and shear band thickness. Small variations were observed when varying mesh size or internal length parameter.

The anisotropy ratio s_u^{DSS}/s_u^A was a key parameter for the correct determination of the failure load because of the shape of the failure zone. The s_u^{DSS}/s_u^A ratio evaluated using existing correlations and FV test results provided a good estimate of the failure load, even though it seems too low if compared to what suggested by e.g. Ladd et al. (1977) and Thakur et al. (2014*b*). On the other hand, results were not significantly affected by the ratio s_u^P/s_u^A. It is however recommended to perform undrained TXC, TXE and DSS on block samples of Perniö clay for a more reliable assessment of strength anisotropy.

Modelling of the pre-failure vertical displacement of the embankment was quite accurate. Computed trend of pre-failure horizontal movements was consistent with observations, even though differences were observed in terms of displacement values.

The failure mechanism in the full-scale test seems deeper than the one predicted by the plane-strain analysis. On the other hand, a better modelling of the shear mechanism is obtained when a layer with higher sensitivity than the upper clay is considered on top of the silty clay layer. The main reason is that even small differences in the post-peak properties (i.e. 20% lower residual strength) will cause more plastic strains in that layer for a given strain level, thus dragging the failure mechanism deeper down. The peak failure load will though remain the same. Furthermore, the computed shear band reached its maximum depth at a slightly different coordinate than in the failure test, based on the approximate failure surface proposed by Lehtonen et al. (2015).

7. Strength increase under old embankments on soft clays

7.1 Introduction

The main purpose of this study is to investigate the phenomenon of undrained shear strength increase which occurs underneath embankments built on soft clay deposits. Strength increase in clay layers induced by consolidation is known to improve the stability of embankments, as shown in Chapter 4. Strength increase under old embankments is an issue of high concern of the Finnish Transport Agency, as the factor of safety has to be evaluated considering undrained conditions even after consolidation has occurred. A benchmark case from Finland, the Murro test embankment, is exploited for this scope because of the large amount of available field as well as laboratory data. The embankment has been consolidating for over 20 years. CPTU tests performed in 2013 by Tampere University of Technology showed a clear increase in undrained shear strength under the embankment down to about 11 m depth.

In this chapter, after a brief description of Murro test embankment and Murro clay, the soil investigation data from 1993 and 2001 are critically compared to the more recent test results. The undrained shear strength distribution at the side and under the embankment is assessed using existing transformation models for undrained shear strength from piezocone and field vane test results. Undrained shear strength at the side of the embankment is also evaluated from measured shear wave velocities. OCR models predictions are validated through CRS test results on block samples of Murro clay and increase in preconsolidation pressure is estimated. Finally, undrained shear strength of Murro clay is studied through a theoretical effective stress based equation. Triaxial tests on block samples of Murro clay are used to derive the effective strength parameters.

7.2 Murro test embankment

In order to collect experimental data on the long term behavior of an embankment built on a soft clay deposit, a highly instrumented test embankment was constructed in Murro, Western Finland, near the city of Seinäjoki, in 1993. The project was commissioned by the Finnish Road Administration, with the purpose of exploiting the experimental observations for the design of Highway 18 between the cities of Jyväskylä and Vaasa.

Murro test embankment is 2 m high, 10 m wide (top) and 30 m long with a gradient of 1:2, as shown in Fig. 7.1. The body of the embankment was made of crushed rock (biotite gneiss) with grain size of 0-65 mm. The subsoil consisted of a 23 m thick low organic silty clay deposit with presence of Sulphur, overlain by a dry crust layer 1.6 m thick. The ground water table seems located at 0.8 m below the ground level.

The extensive instrumentation at the test site consisted of settlement plates, inclinometers, one extensometer and numerous pore pressure probes (Karstunen and Yin 2010). The embankment section, including the instruments layout is shown in Fig. 7.1.

The collected field data has been used in several studies dealing with modelling of the deformation behavior of Murro clay using advanced FE soil models including features such as anisotropy, destructuration and time-dependent behavior of clays (Koskinen et al. 2002; Karstunen et al. 2005; Koskinen and Karstunen 2006; Karstunen and Yin 2010; Koskinen 2015; Sivasithamparan et al. 2015).

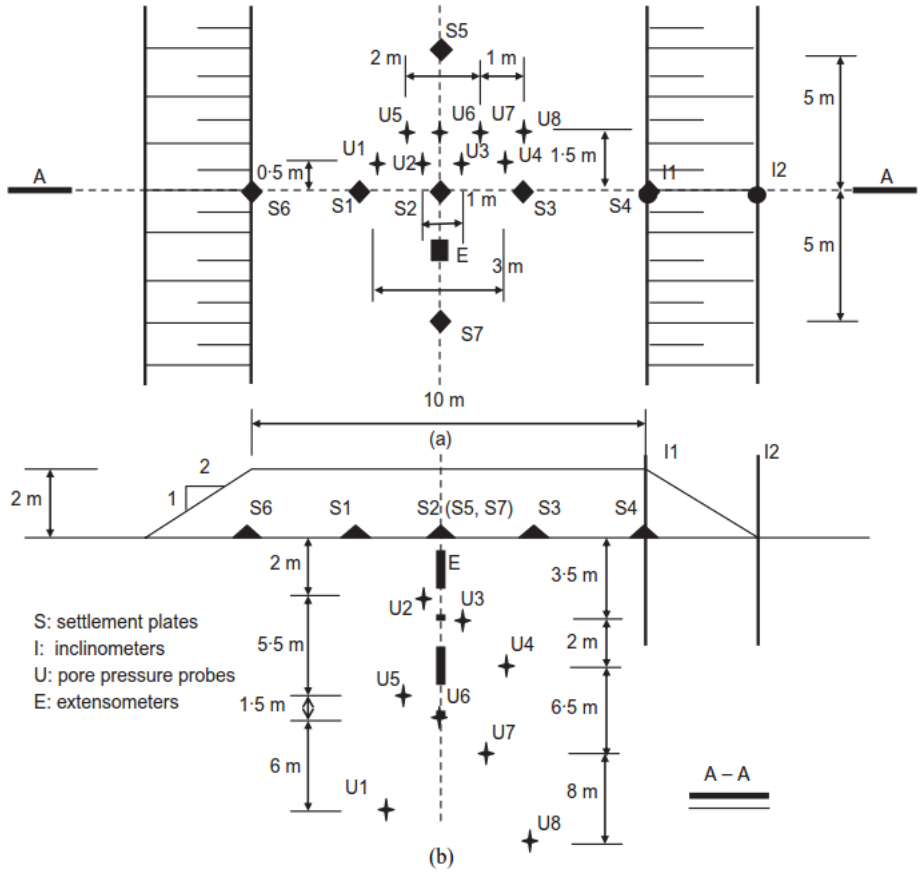

Fig. 7.1: Murro test embankment with details of instrumentation: a) plan and b) cross-section (Karstunen and Yin 2010).

7.3 Soil investigation at Murro test site

Test results from the grain size test analysis of the soil underneath Murro test embankment indicate clay content between 20-24%, accompanied by a silt content of 72-77%. Hence, the overall classification according to EN ISO 14688-2 (SFS 2005) is "clayey silt" (Fig. 7.2). However, Murro clayey silt has been always referred to as "Murro clay" and for simplicity the same nomenclature will be used in this study.

Murro clay is a sulphide clay typical of the coastal areas around the Gulf of Bothnia, with organic content ranging between 2-4%. The clay is black in color and it is characterized by a special odor because of the presence of Sulphur. (Koskinen 2014).

Soil properties of Murro clay are shown in Figure 7.2. Murro clay is a low to medium sensitive clay with sensitivity (S_t) ranging from 2 to 10. The natural water content (w) varies between 65% and 100%. The liquid limit (LL) increases from 55% near the ground surface, up to 120% at 5 m depth. After that point, LL seems to decrease with depth from 120% to about 60% below 15 m depth.

CRS (constant rate of strain) oedometer tests on 50 mm diameter piston samples suggest that Murro clay is nearly normally consolidated (Fig. 7.3). CRS tests on 132 mm block samples of Murro clay performed by Tampere University of Technology show that the clay is slightly overconsolidated (see section 7.5). One possible reason to justify the latter observation is the disturbance occurred during sampling which caused the underestimation of the preconsolidation pressure from the piston samples. Preconsolidation pressure of Murro clay is studied and discussed later in this chapter (section 7.5).

A more detailed description of the physical and mechanical characteristics of Murro clay can be found in Koskinen et al. (2002), Karstunen et al. (2005), Karstunen and Yin (2010), Koskinen (2014).

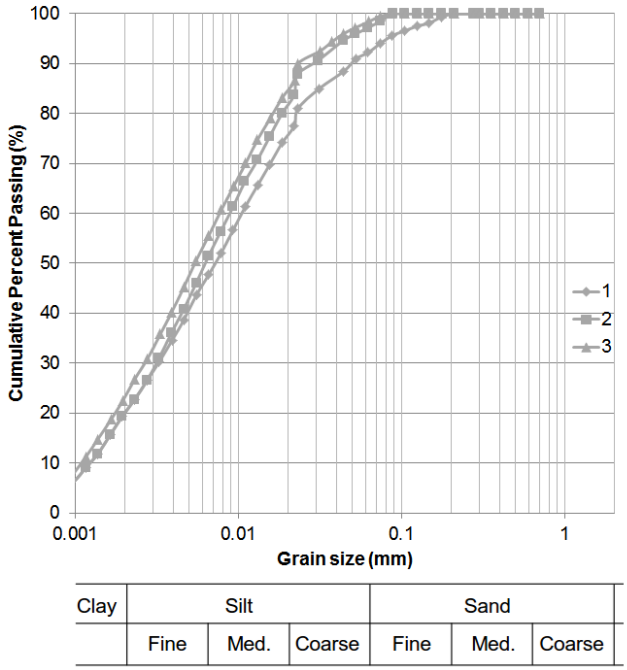

Fig. 7.2: Grain size analysis test results for Murro soil (data from Messerklinger et al. 2003).

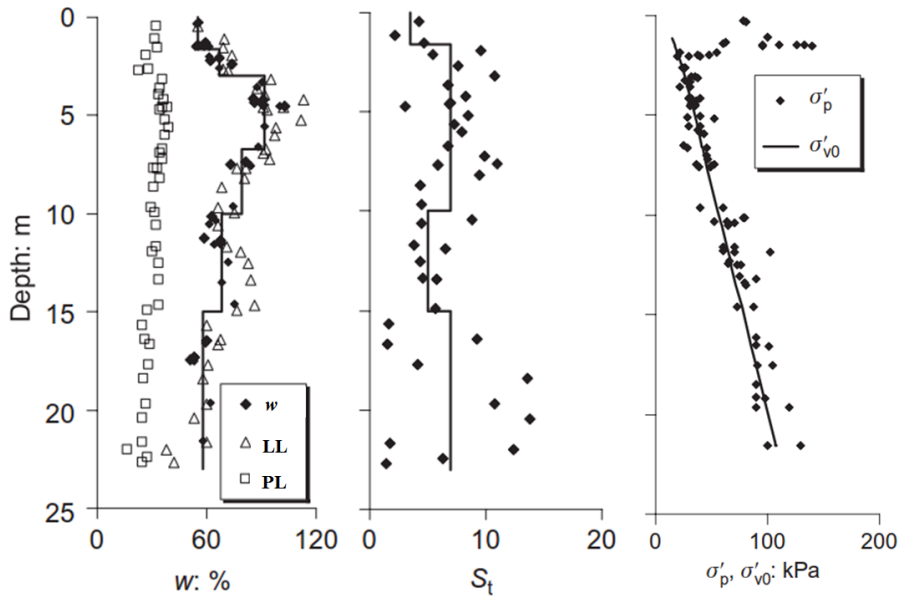

Figure 7.3: Characteristics of Murro clay (after Karstunen and Yin 2010).

Field vane, CPT, CRS oedometer and a series of triaxial tests were carried out prior to construction of the embankment. In 2001, field vane test was performed through the embankment in order to evaluate the undrained shear strength increase due to consolidation. Test results showed strength increase down to 6-7 m below the centreline of the embankment. However, below 7 m depth the undrained shear strength showed a significant reduction, compared to the initial stage (Figure 7.4). A possible explanation for such an unexpected phenomenon could be the destructuration process of the clay caused by the change in stress state (Karstunen et al. 2005; Karstunen and Yin 2010), or simply the low quality of the field vane test results.

In 2013, 20 years after construction, piezocone (CPTU) and field vane tests were carried out by Tampere University of Technology at the test site. Field vane test was repeated also in 2015, as measurements from 2013 were only available up to 10 m depth.

Tampere University of Technology has recently bought *i*) CPTU equipment with seismic and resistivity cone and, *ii*) a new field vane with casing protection which allows for rotation and torque measurements right above the vane. The aim is to spread the use of piezocone test in Finland for the determination of soft soil properties and to improve the existing correlations for strength and deformation properties of Finnish soft clays. As shown by Di Buò et al. (2016), preliminary studies have provided successful results in terms of repeatability and overall quality of both CPTU and field vane test results.

Field vane test results are only available from one side of the embankment, about 4 m off the slope. Recent test results are presented in Figure 7.4, together with the field vane test results from 1993 and 2001. Eq. (2.10) is used to convert the measured undrained shear strength into $s_{u(mob)}$. Measured $s_{u(mob)}$ agrees fairly well with $s_{u(mob)}$ measured prior to construction. However, measurements taken with the new apparatus seem moderately higher than the old measurements in the top 5 m. Such a small difference might be due to some differences in the test equipment used. Relatively good correspondence is found at greater depths, except for two points located at 12.2 m and 14.2 m, where $s_{u(mob)}$ seems lower than at the initial stage.

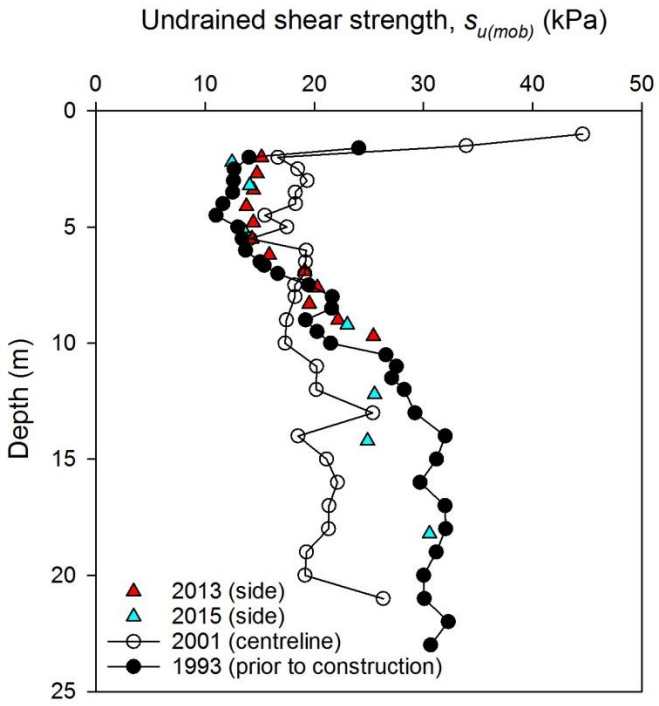

Figure 7.4: Corrected field vane test results at Murro test site prior to construction, 8 years, 20 years and 22 years after the construction of the embankment.

CPTU soundings are available from two locations: below the centreline of the embankment and at one side, at approximately the same location where the field vane test was performed. At each location, the test was repeated two times. One of the CPTU tests at the side of the embankment was stopped at 9 m depth because of technical problems.

The measured cone resistance, q_c, is corrected to account for "the unequal area effect" caused by the pore water pressure acting on the shoulder area behind the cone and on the ends of the friction sleeve (see e.g. Lunne et al. 1997*b*). The corrected total cone resistance, q_t, is given by eq. (7.1):

$$q_t = q_c + u_2 \cdot (1 - a^*) \tag{7.1}$$

Where u_2 is the pore pressure acting behind the cone and a^* is the area correction factor, equal to 0.75 for the piezocone used.

As shown in Fig. 7.5, the measured cone tip resistance under the embankment is higher than at the side, down to about 11 m depth. This would indicate that the strength has not decreased under Murro test embankment, thus contradicting the trend observed in Fig. 7.3 and strengthening the hypothesis that the field vane test results from 2001 were characterized by poor quality. Measurement errors might be possibly due to excessive rod friction.

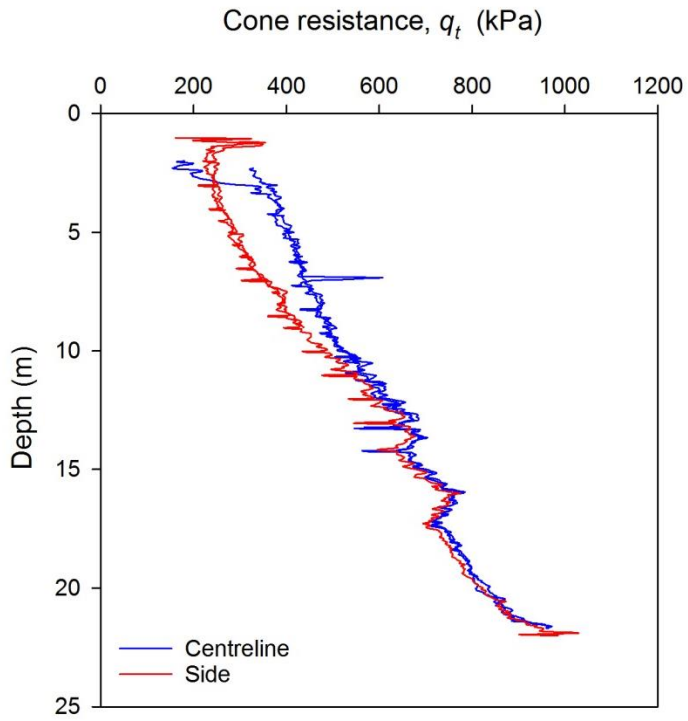

Figure 7.5: Cone tip resistance at the test site under the centreline and 4 m off the embankment slope.

7.4 Undrained shear strength of Murro clay

7.4.1 Correction of field vane measurements

Westerberg et al. (2015) compared field vane and undrained DSS test results from 5 sulphide clay sites from Sweden, located along the Eastern coast. In Sweden, DSS tests are often used as reference calibration tests for e.g. field vane and CPT (as already discussed in Chapter 5). Therefore, by assuming $s_u^{DSS} \sim s_{u(mob)}$, Westerberg et al. (2015) suggested, for Swedish sulphide clays:

$$s_{u(mob)} \approx 0.65 \cdot s_u^{FV} \tag{7.2}$$

Eq. (7.2) indicates that in sulphide soils the correction factor μ for s_u^{FV} is constant and independent of the soil plasticity. Westerberg et al. (2015) also pointed out that μ may be dependent on the stress level.

DSS tests are not in use in Finland and, hence, eq. (7.2) should be verified for Finnish clays, even though the properties of Murro clay are consistent with the soil properties of the clays studied by Westerberg et al. (2015) (clay content ranging from 6 to 35%, organic content generally lower than 6% and $S_t \sim 4$ - 14). In Finland, s_u^{FV} is corrected according to eq. (2.10) that suggests μ as a function of the liquid limit. From eq. (2.10), μ = 0.65 for LL ~ 130%, which is higher than the maximum measured LL value (see Fig. 7.3) at Murro test site.

In this study, field vane measurements are reduced based on eq. (2.10), which is commonly used in Finnish practice. Eq. (7.2) is later applied to field vane strength measurements and results are compared.

7.4.2 **Evaluation of s_u of Murro clay from piezocone test results**

In order to estimate the undrained shear strength of Murro clay, in-situ measurements obtained from piezocone and field vane test are compared. The effective cone resistance ($q_t - \sigma_{v0}$) and the excess pore pressure measured during penetration are converted into s_u from the general transformation models by Larsson and Mulabdic (1991) of eq. (7.3) and eq. (7.4), respectively.

$$s_u = \frac{q_t - \sigma_{v0}}{N_{kt}} = \frac{q_t - \sigma_{v0}}{13.4 + 6.65 \cdot LL} \tag{7.3}$$

$$s_u = \frac{\Delta u_2}{N_{\Delta u}} = \frac{u_2 - u_0}{14.1 - 2.8 \cdot LL} \tag{7.4}$$

Where q_t is the measured cone resistance corrected for pore pressure effects [see eq. (7.1)], σ_{v0} the total overburden vertical stress, u_2 the measured pore pressure acting behind the cone, u_0 hydrostatic water pressure, N_{kt} and $N_{\Delta u}$ are the cone factors for cone tip resistance and excess pore pressure, respectively. N_{kt} and $N_{\Delta u}$ are firstly evaluated according to Larsson and Mulabdic (1991) and secondly calibrated from field vane test results.

According to Larsson and Mulabdic (1991), N_{kt} increases linearly with increasing liquid limit, while $N_{\Delta u}$ decreases with increasing liquid limit. Liquid limit profile with depth is shown in Figure 7.2. LL values are assumed to be the same at the side and under the embankment after consolidation. Such a hypothesis is consistent with the observations of Larsson and Matsson (2003) (section 4.2.2). The groundwater level is also assumed not to change after consolidation.

The stress increase below the embankment is estimated using a classical elastic Boussinesq solution for trapezoidal loading. Being the groundwater table located at very shallow depth, the soil situated above the ground surface becomes partly submerged as a result of the settlement. Hence, the unit weight will reduce causing lower effective stresses in the ground because of buoyancy effects. If these buoyancy effects are not taken into account, effective stresses and, therefore, undrained shear strength may be overestimated.

The final stress distribution is modelled based on two hypotheses: *i*) all the excess pore pressure has dissipated after 20 years ($\Delta\sigma_v = \Delta\sigma'_v$, $\Delta u = 0$) and *ii*) assuming an average embankment settlement of 0.70 m, roughly corresponding to the vertical distance between the two measurement points located on top of the embankment and on the ground surface, respectively (Fig. 7.6). An average vertical settlement of 0.70 m seems consistent with field observations (e.g. Sivasithamparan et al. 2015), as measured vertical displacements vary between 0.60 and 0.80 m at different measurement points of the instrumented embankment. Hence, both σ'_{v0} and the elastic $\Delta\sigma'_v$ are calculated assuming an average settlement of 0.70 m. In this way, the vertical effective stress at the end of consolidation will be lower than if calculated from the original ground level, as shown in Fig. 7.6.

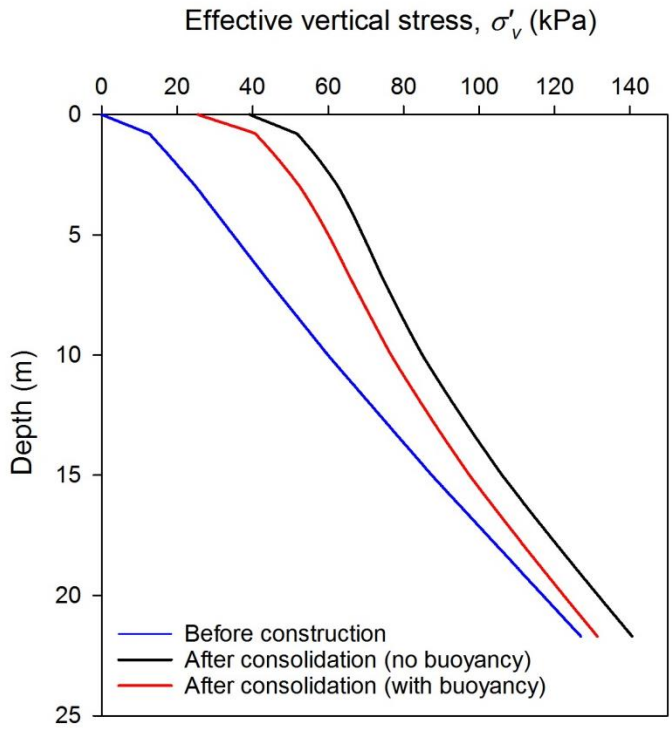

Figure 7.6: Distribution of the effective vertical stress under the embankment before and right after construction and after consolidation including buoyancy effects.

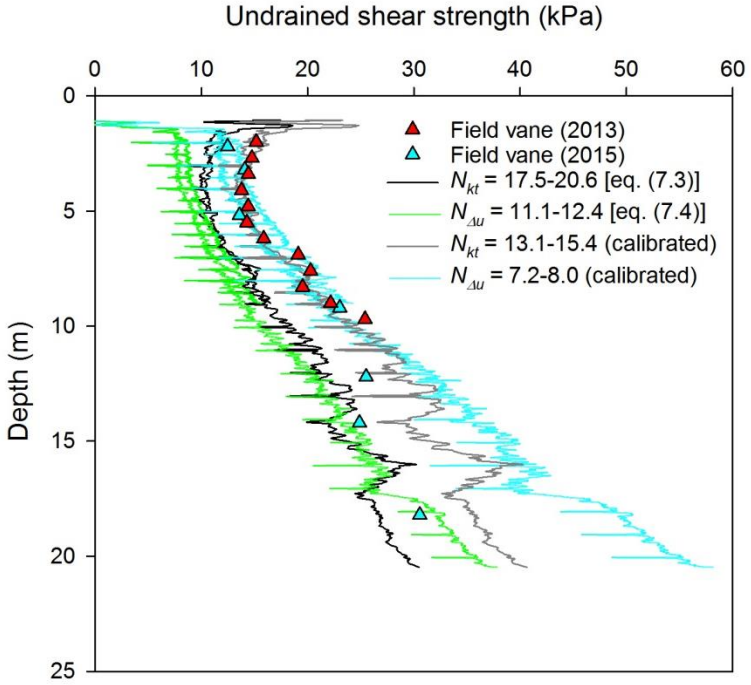

Figure 7.7: Undrained shear strength of Murro silty clay interpreted from piezocone according to Larsson and Mulabdic (1991) and calibrated from field vane test corrected using eq. (2.10).

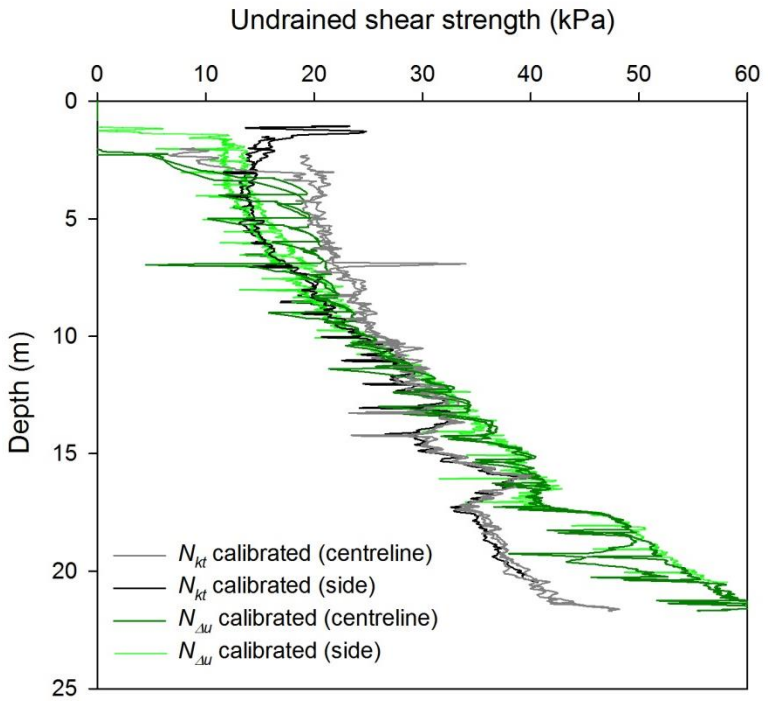

Figure 7.8: Undrained shear strength of Murro silty clay interpreted from cone tip resistance and measured excess pore pressure.

Figure 7.7 shows the undrained shear strength profile at Murro test site. Both eq. (7.3) and eq. (7.4) seem to underestimate $s_{u(mob)}$ from field vane. Calculated N_{kt} values vary in the interval 17.5-20.6, while $N_{\Delta u}$ = 11.1-12.4. Therefore, it would seem that the models for N_{kt} and $N_{\Delta u}$ suggested by Larsson and Mulabdic (1991) are not suitable for the soil conditions at Murro site.

In order to evaluate N_{kt} and $N_{\Delta u}$ which would better describe the field vane strength, eq. (7.2) is multiplied by 1.33 and eq. (7.3) by 1.54, resulting in N_{kt} = 13.1-15.4 for Murro clay, with an average value of 13.8, and $N_{\Delta u}$ = 7.2-8.0 with an average value of 7.7. Consistency is found when comparing $s_{u(mob)}$ from both models up to 13-14 m depth. At greater depths, the models show divergent results.

Lunne et al. (1976) found for five Scandinavian marine clays, cone factors varying between 15 and 19 with an average of 17, calibrated from corrected field vane test results. Based on five sulphide clay sites from Sweden, Westerberg et al. (2015) suggested an average N_{kt} = 20.2, calibrated from DSS tests. The calibrated N_{kt} values for Murro clay are generally lower than the literature values. A possible reason could be the nature of Murro clay, characterized by relatively high silt, Quartz and Feldspar content (Messerklinger et al. 2003). Larsson and Mulabdic (1991) suggest that when there is lack of information on liquid limit (LL), N_{kt} should be taken equal to 14.5 for silts and 16.3 for clays. Based on these observations, the calculated N_{kt} for Murro clay seems closer to N_{kt} = 14.5 for silts than to N_{kt} = 16.3 for clays, thus suggesting that the silty component of Murro clay may influence the global undrained response.

Using s_u values obtained from triaxial compression tests, Lunne et al (1985) found $N_{\Delta u}$ to vary between 4 and 10 for North Sea clays, while Karlsrud et al. (1996) suggested $N_{\Delta u} \approx$ 6-8. La Rochelle et al. (1988) found $N_{\Delta u} \approx$ 7-9 for three Canadian clays from uncorrected

field vane strength values. Even though the average calibrated $N_{\Delta u}$ = 7.7 for Murro clay agrees fairly well with the values reported in the literature, the reference tests used for the calibration are different (TXC vs FV).

Assuming the same calibrated N_{kt} and $N_{\Delta u}$ values for the soil underneath the embankment, undrained shear strength increase is clearly visible down to a depth of 11 m (Fig. 7.8). Interpreted undrained shear strength from excess pore pressure seem to predict slightly lower values than from cone tip resistance for the soil under the embankment. The maximum strength increase can be observed at about 3.5 m depth, where s_u under the embankment is about 7 kPa higher than in the virgin soil.

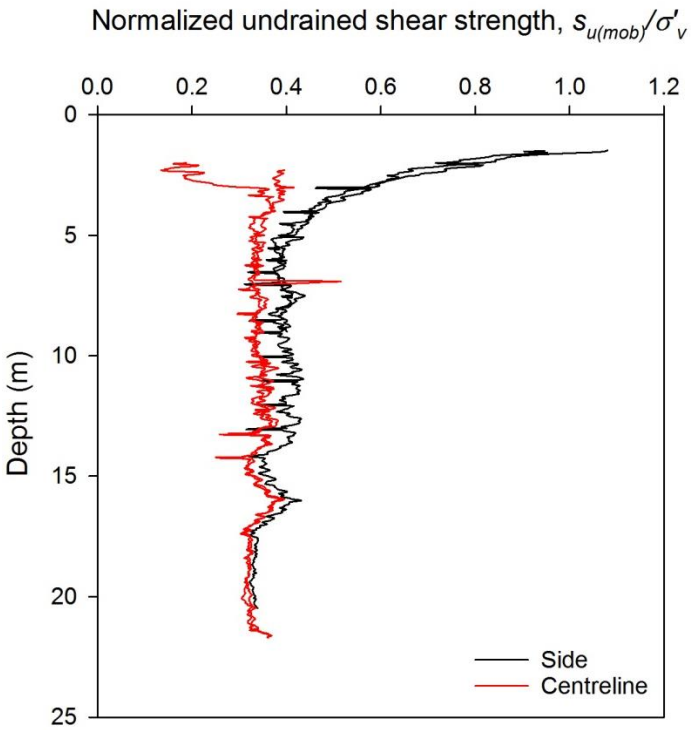

Figure 7.9: Variation and change in $s_{u(mob)}/\sigma'_v$ with depth and consolidation.

Fig. 7.9 shows the variation of the undrained strength ratio $s_{u(mob)}/\sigma'_v$ before and after consolidation. Measured $s_{u(mob)}/\sigma'_v$ values vary from 0.31 to 1.08 at the side of the embankment, with mean value of 0.42. Under the embankment, $s_{u(mob)}/\sigma'_v$ ranges from 0.13 to 0.39, with mean value equal to 0.33. The ratio $s_{u(mob)}/\sigma'_v$ after consolidation seems, hence, lower than at the initial stage. This is consistent with the experimental observations reported by Tavenas et al. (1978) from embankments built on Canadian clay deposits, as discussed in section 4.2.3, suggesting that the silty clay under the embankment changed its state from overconsolidated to normally consolidated. Therefore, $s_{u(mob)}/\sigma'_v$ = 0.33 would indicate the magnitude of the undrained shear strength ratio of Murro clay for normally consolidated state, namely the *S* parameter of eq. (2.2).

When using eq. (7.2) to reduce the measured field vane strength, N_{kt} = 15.6-18.3 with an average value of 16.5, and $N_{\Delta u}$ = 8.9-9.9 with an average value of 9.5. The calibrated N_{kt} values however differ from what suggested by Westerberg et al. (2015) for Swedish sulphide soils, namely N_{kt} = 20.2. The average $s_{u(mob)}/\sigma'_v$ is equal to 0.35 at the side of the embankment and to 0.28 under the embankment. The latter result is consistent with what Westerberg et al. (2015) suggested for sulphide soils.

The seismic piezocone module was used to estimate the magnitude of the shear wave velocities (V_s) at the test site. Information is only available from the embankment side. Mäenpää (2016) reported a detailed description of the seismic measurements using the new CPTU equipment at the test site.

As shown in section 4.1 and by eq. (4.3), the undrained shear strength s_u can be expressed as a function of shear wave velocity, liquid limit and soil density. The variation of shear wave velocity with depth, together with a comparison between the measured s_u and s_u predicted by eq. (4.3), is shown in Fig. 7.10

Eq. (4.3) seems to provide a good estimate of $s_{u(mob)}$ of Murro clay, as the trend of the calculated s_u data points appears to adapt reasonably well to the calibrated s_u from piezocone. Exception is made for three points located below 12 m depth that clearly overpredict s_u. In some cases, eq. (4.3) may be also exploited to estimate V_s from $s_{u(mob)}$.

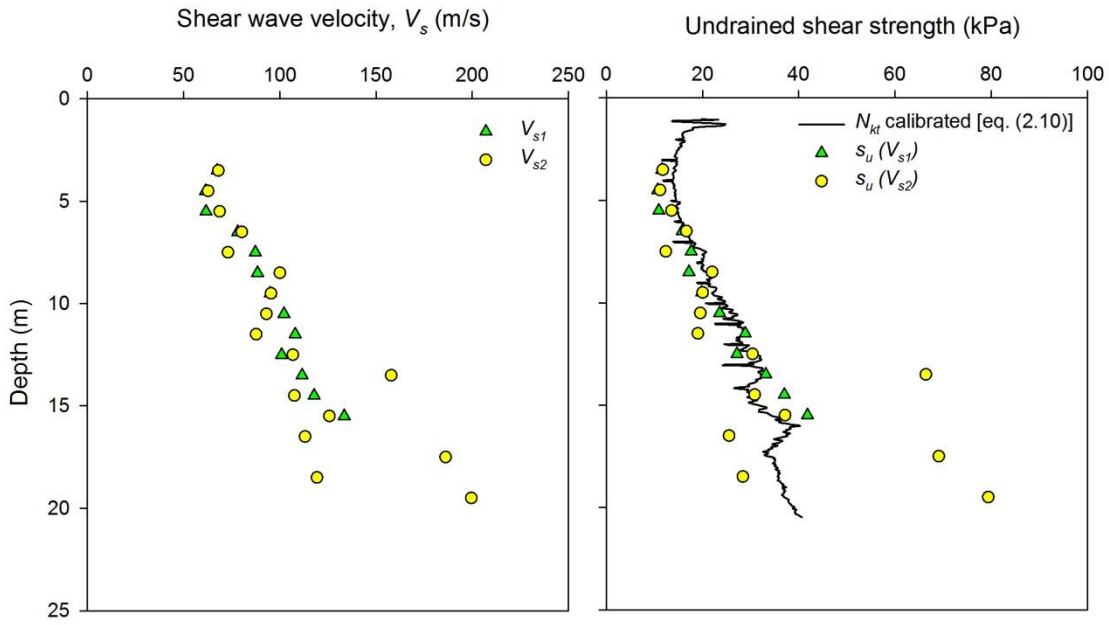

Figure 7.10: Comparison between calibrated $s_{u(mob)}$ from field vane and s_u derived from shear wave velocity measurements taken at the side of the Murro embankment.

7.5 Preconsolidation pressure of Murro clay

Murro clay has been always referred to as normally consolidated clay (Koskinen et al. 2002; Karstunen et al. 2005; Karstunen and Yin 2010; Koskinen 2014). Such a hypothesis may seem too conservative, as the aging effect would be neglected. For instance, sample disturbance may have led to such a cautious hypothesis, suggesting too conservative values of preconsolidation pressure.

Larsson and Mulabdic (1991) suggested an equation for σ'_p similar to eq. (7.3) for s_u from piezocone [eq. (7.5)]:

$$\sigma'_p = \frac{q_t - \sigma_{v0}}{N_{kt(\sigma'_p)}} = \frac{q_t - \sigma_{v0}}{1.21 + 4.4 \cdot LL} \tag{7.5}$$

Where $N_{kt}(\sigma'_p)$ is the cone factor for preconsolidation pressure.

An attempt to evaluate OCR, and hence preconsolidation pressure (σ'_p), of Murro clay from the piezocone test is done according to three different models. CRS test results on block samples of Murro clay are finally compared to the models predictions. The OCR models are derived as follows:

- *Model n.1*: OCR = σ'_p/σ'_v where σ'_p is determined from eq. (7.5) by Larsson and Mulabdic (1991).
- *Model n.2*: OCR = σ'_p/σ'_v where σ'_p is determined from eq. (7.5) by Larsson and Mulabdic (1991) and multiplied by 1.33 [calibrated for s_u from eq. (7.3)] because of the relation between s_u and σ'_p.
- *Model n.3*: OCR from eq. (7.6).

$$OCR = \left[\frac{1}{S} \cdot \frac{s_{u(mob)}}{\sigma'_v} \right]^{\frac{1}{m}} \tag{7.6}$$

Eq. (7.6) is directly derived from the basic SHANSEP eq. (2.2). The parameter S of eq. (7.6) is chosen based on the results presented in section 7.4. S corresponds to $s_{u(mob)}/\sigma'_v$ for normally consolidated state and it is taken equal to 0.33. By using S = 0.244 and m = 0.763 derived in Chapter 5 [eq. (5.2)], OCR values would be overestimated, as eq. (5.2) describes the undrained shear strength of inorganic sensitive clays.

The m parameter is derived according to the Cam Clay model, which suggests m = 1-C_s/C_c, where C_s and C_c are the swelling and compression index of the soil, respectively, determined from oedometer tests. For Murro silty clay, data reported by Sivasithamparan et al. (2015) indicates C_s/C_c = 0.06-0.11 in the top 15 m of the deposit. Hence, for an average C_s/C_c = 0.076, m = 0.92.

The variation of OCR with depth from the three models analysed is shown in Figure 7.11.

According Figure 7.11, Murro clay seems lightly overconsolidated. Based on OCR model n.2, OCR values higher than 2 are found in the top 3 m, decreasing to OCR = 1.5 at 5 m depth and then varying at between 1.3 and 1.8 at greater depths. The OCR model n.1 also suggests OCR values higher than 2 below the dry crust, decreasing until 6 m depth where OCR is about 1. Between 6 and 13 m depth, OCR seems to vary in a narrow range (OCR = 1.0-1.3). After that point, where the soil layers are probably less homogeneous, a clear trend is difficult to identify, as high fluctuations from the mean trend are observed for all the three models.

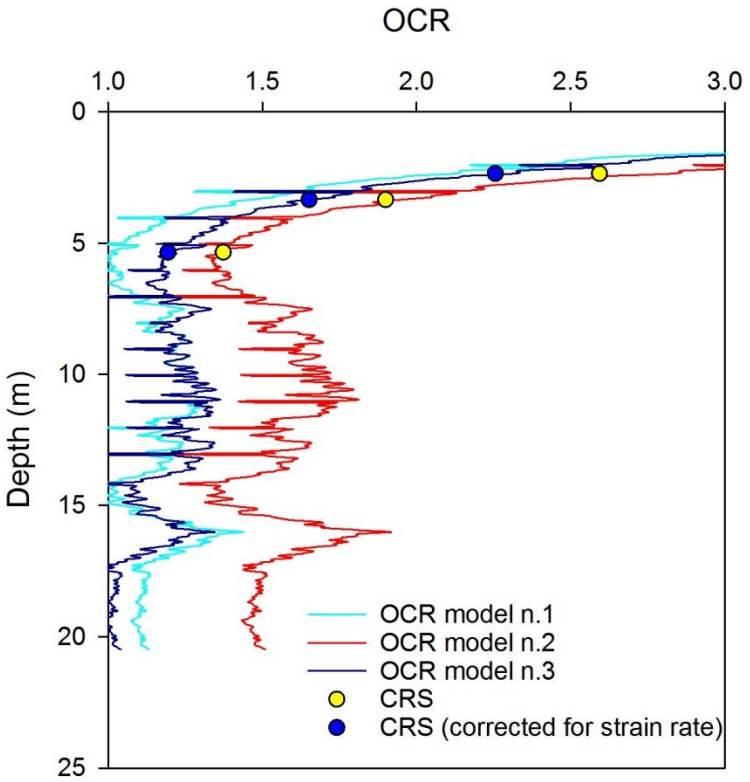

Figure 7.11: Evaluation of OCR variation with depth at Murro test site based on different transformation models and on CRS test results from block samples of Murro clay.

The OCR profile suggested by eq. (7.6) (OCR model n.3) agrees fairly well with the predictions by OCR model n.3, except from 3 to 6 m depth where OCR values appear to be slightly higher.

Predicted OCR profiles seem to find consistency with OCR values suggested by three CRS oedometer tests on block samples of Murro clay. σ'_{pCRS} values should be corrected for strain rate to be used in e.g. settlement calculations. However, the strain rate correction factor for clays equal to 1.27 suggested by Länsivaara (1999) (see section 2.2) seems too high for Murro clay. Rate effects are expected to be lower than for inorganic clays because of the high silt content of Murro clay (Mesri and Godlewski 1977). Therefore, an indicative correction factor of 1.15 is applied. Predictions by OCR model n.3 seem the most accurate, even though OCR model n.1 seems to provide a good estimate of OCR.

Fig. 7.12*a* shows a comparison between the measured strength increase [$\Delta s_{u(mob)}$] and the predicted increase in preconsolidation pressure ($\Delta\sigma'_p$) suggested by the three analysed models. The calibrated OCR model n.2 seems to give too low $\Delta\sigma'_p$ to justify the observed

strength increase. One reason might be that the combination of eq. (7.3) and (7.5) [$s_u/\sigma'_p = N_{kt}(\sigma'_p)/N_{kt}$] gives s_u/σ'_p values which are probably too low for Murro clay. Hence, a correction is needed for $s_{u(mob)}$ to obtain reliable results. On the other hand, both eq. (7.5) and eq. (7.6) can predict fairly well $\Delta\sigma'_p$. The OCR model n.1 gives the highest σ'_p increase.

Fig. 7.12*b* compares the measured $\Delta s_{u(mob)}$ with $\Delta s_{u(mob)}$ calculated as $\Delta s_{u(mob)} = S \cdot \Delta\sigma'_p$ for the different models. S is the normalized undrained strength ratio for normally consolidated state that is equal to 0.33, as shown in section 7.4. OCR models n.1 and n.3 seem to provide the best estimate of $\Delta\sigma'_p$ and, hence, $\Delta s_{u(mob)}$. All the models predict however the highest strength increase at about 6 m depth, while observations suggest that the highest $\Delta s_{u(mob)}$ occurs between 3 and 4 m depth.

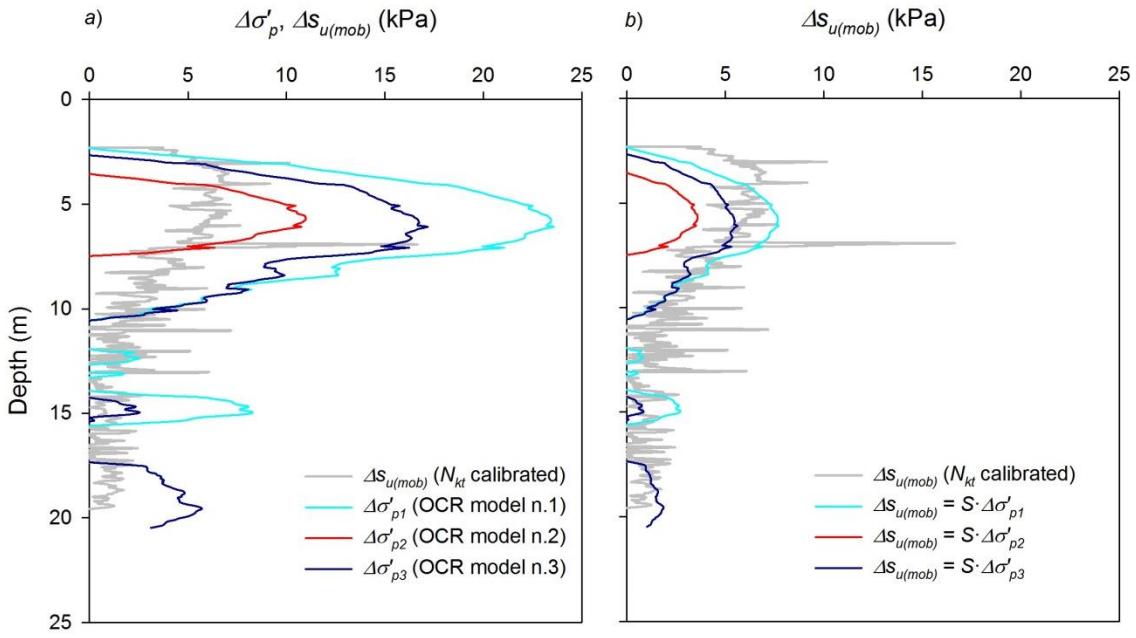

Figure 7.12: *a*) Increase of preconsolidation pressure after consolidation based on different models and *b*) predicted strength increase from the models.

7.6 Discussion

$s_{u(mob)}/\sigma'_v$ = 0.33 would seem, in the author's opinion, a considerably high value for a normally consolidated soft Finnish clay if compared to *S* values for $s_{u(mob)}$ reported in section 5.3.2. $s_{u(mob)}/\sigma'_v$ = 0.33 for NC clay is typically representative of the triaxial compression strength, as discussed in section 2.5. However, in section 7.3 Murro clay has been classified as clayey silt. The silty component, along with an organic content of 2-4%, might be the reason for such high measured normalized shear strength.

$s_{u(mob)}/\sigma'_v$ = 0.28 when $s_{u(mob)}$ is calibrated using eq. (7.2). For DSS conditions, such a value could seem more reasonable than 0.33, suggesting that eq. (2.10) might not be appropriate for sulphide soils. DSS tests on Murro clay should be performed in order to calibrate the field vane correction factor.

Several studies reported for Murro clay ϕ' = 37~39.2°, while common ϕ' values for silts are 27-30° (Rantamäki et al. 1997). The high friction angle might be explained by the high content of Quartz and Feldspar (Messerklinger et al. 2003) or possibly by the organic content, as indicated by Yu (1993), who reported ϕ' = 33~36° for Swedish silty sulphide-rich soils. One triaxial compression test done at Tampere University of Technology on a block sample of Murro clay (Fig. 7.13) from 5.20 m depth suggests ϕ' = 37.7° at large strain with an effective cohesion c' = 5 kPa, thus validating previous test results and justifying the high measured strength. Yu (1993) suggested that cohesion in sulphide soils may reflect the effect of the embedded organic fibres.

According to Janbu (1985), undrained shear strength, approximately corresponding to DSS conditions, can be theoretically derived from preconsolidation pressure (σ'_p), effective friction angle (ϕ') and attraction (a) as shown by eq. (7.7). Attraction a is linked to the effective cohesion as $a = c' \cdot \cot\phi'$.

$$s_u \approx \frac{\sin\phi'}{2} \cdot \left(\sigma'_p + a\right) \tag{7.7}$$

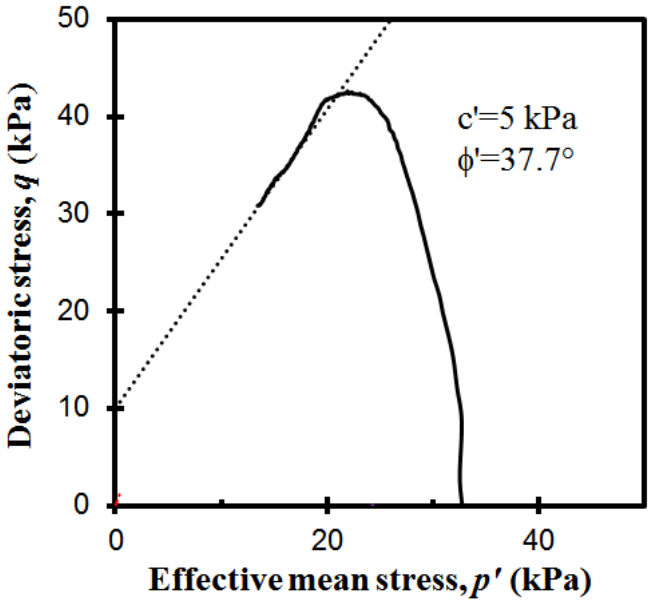

Figure 7.13: Effective stress path in the *q-p'* space from a CIUC test on block sample of Murro clay.

Typically, a is taken equal to zero for normally consolidated clays. For a = 0, eq. (7.7) reduces to the standard SHANSEP function of eq. (2.2) with $S = \sin\phi'/2$ and m = 1. For normally consolidated clays ($\sigma'_p = \sigma'_v$), eq. (7.7) for a = 0 and ϕ'=37.7° gives s_u/σ'_v equal to 0.305, against a measured value of 0.33 (or 0.28) for Murro clay. However, as shown by the triaxial test results, a is greater than zero [$a = 5 \cdot cot(37.7°) \sim 6.5$ kPa], hence supporting the higher measured s_u/σ'_v values.

Fig. 7.14 shows a comparison between the measured undrained shear strength of Murro clay and the undrained shear strength predicted by eq. (7.7). Preconsolidation pressure values are calculated according to eq. (7.5).

Predicted s_u is consistent with s_u measured at the side of the embankment, calibrated using eq. (2.10). When buoyancy is modelled, s_u under the embankment seems reasonably well approximated by eq. (7.7). Increase of preconsolidation pressure is visible up to 11 m depth, in agreement with the observed undrained shear strength increase. Nevertheless, by neglecting buoyancy effects, s_u of Murro clay might seem slightly overpredicted.

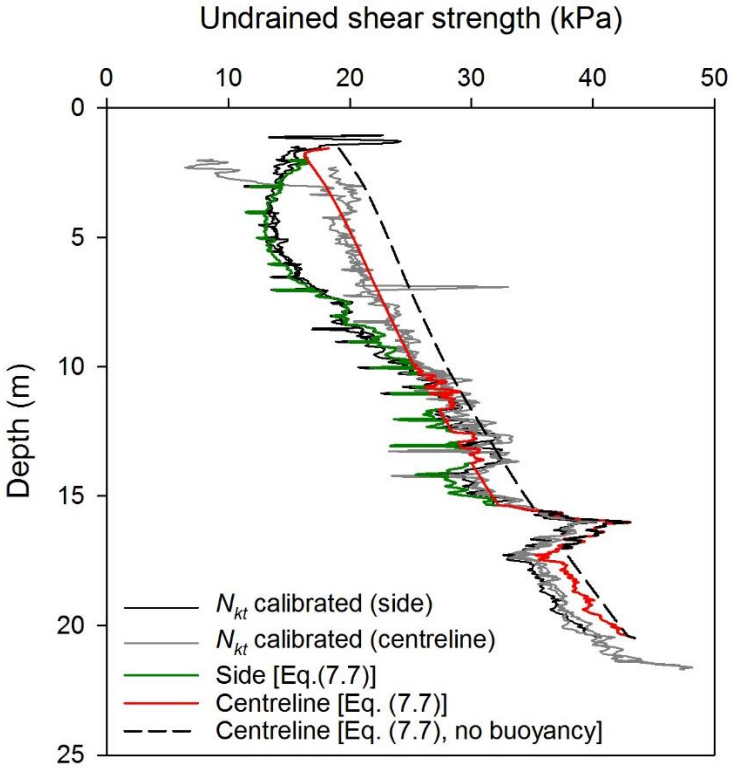

Figure 7.14: Measured and predicted undrained shear strength of Murro clay according to Janbu (1985) and influence of buoyancy on the predicted s_u.

7.7 Conclusions

CPTU test results from the centreline and the side of Murro test embankment proved that the undrained shear strength after 20 years of consolidation has increased under the embankment up to a depth of 11 m. Therefore, field vane test results from 2001 are contradicted, indicating how high quality testing is important to assess soil properties.

Murro clay became normally consolidated under the embankment after consolidation, in accordance with the findings of Tavenas et al. (1978) from embankments built on Canadian soft clays.

According to the more recent field vane test results, the transformation model proposed by Larsson and Mulabdic (1991) for Swedish clays seems to underestimate the undrained shear strength of Murro clay by 33% and 54% from cone tip resistance and excess pore pressure measurements, respectively.

The empirical correlation by Larsson and Matsson (2003) for s_u, based on shear wave velocities, seems to provide a good estimate of the undrained shear strength of Murro clay at the side of the embankment.

The average normalized undrained shear strength [$s_{u(mob)}/\sigma'_v$] for normally consolidated state of Murro clay is equal to 0.33, which is way higher than what is normally measured or assumed for normally consolidated inorganic clays. Triaxial test results on block samples of Murro clay suggested c'=5 kPa and ϕ' = 37.7°. ϕ' = 37.7° is considerably higher than ϕ' values commonly observed for Finnish soft clays. This, along with the low clay content (< 30%) and the organic content of 2-4%, may explain the high measured normalized strength.

When calibrating N_{kt} using the correction suggested by Westerberg et al. (2015) for field vane strength of sulphide clays, $s_{u(mob)}/\sigma'_v$ = 0.28 under the embankment for DSS conditions. DSS tests on Murro clay should be carried out in the future to provide a deeper knowledge of $s_{u(mob)}$.

Preconsolidation pressure from previous CRS oedometer tests would suggest that Murro clay is normally consolidated. More recent CRS tests on block samples of Murro clay performed at Tampere University of Technology show OCR values higher than 1. OCR seems greater than 2 below the dry crust and equal to 1.2-1.3 at greater depths. Based on the test results, the model by Larsson and Mulabdic (1991) for σ'_p and the "fitted" SHANSEP model presented seem to approximate reasonably well the OCR variation with depth at the test site.

Undrained shear strength of Murro clay can be approximated with relatively low error based on eq. (7.7) by Janbu, provided that σ'_p is properly modelled and cohesion (c') or attraction (a) are taken into account.

For a realistic assessment of the change in stress state underneath the embankment, buoyancy should be accounted for. Neglecting the fact that the embankment and the dry crust become partly submerged during consolidation would mean to overestimate the effective stresses and, consequently, the undrained shear strength.

8. Engineering aspects

8.1 On the use of the new transformation models for undrained shear strength

In Chapter 5, correlations for undrained shear strength specific to Finnish clays are derived for the first time. The transformation models presented are meant to serve as an engineering tool for preliminary stability analysis of embankments and/or as a framework for validation of site-specific measurements. The usability of the new correlations is quite straightforward, as only little information is required.

The new transformations models resulted almost unbiased with respect to an independent database consisting of Swedish and Norwegian clay data points. The COV of the new correlations is generally lower than 0.30, suggesting that the undrained shear strength of Finnish clays can be predicted with relatively low uncertainty provided that OCR (primary input parameter) and a secondary input parameter (e.g. index parameter) are carefully selected. For instance, simple tests such as oedometer and index tests would provide sufficient information for using the new correlations. Furthermore, the evaluation of a secondary input parameter may not always be necessary, as $s_{u(mob)}$ was found to mainly depend on OCR, as shown by eq. (5.2).

It must be though highlighted that eq. (5.2) was derived according to preconsolidation pressure (σ'_p) values from CRS oedometer test results. The reason behind such a choice is purely practical, as nowadays CRS tests are more common than IL tests in Finland and, in general, in Scandinavia. CRS tests are normally carried out at relatively high strain rates (see section 2.2) and, therefore, σ'_{pCRS} (or OCR_{CRS}) may differ from the in-situ σ'_p (or OCR) value.

However, $s_{u(mob)}$ already accounts for the high strain rates induced by "fast" shearing, being directly derived from field vane measurements (s_u^{FV}) by means of a time-to-failure correction factor. Therefore, no further correction is needed for σ'_{pCRS} to use eq. (5.2).

If all the σ'_{pCRS} values in F-CLAY/10/173 database were converted into σ'_{pIL} as $\sigma'_{pIL} = \sigma'_{pCRS}/1.27$, the regression analysis would result in [eq. (8.1)]:

$$\frac{s_{u(mob)}}{\sigma'_v} \approx 0.29 \cdot OCR_{IL}^{\ 0.70} \qquad (8.1)$$

Eq. (8.1) and eq. (5.2) give very similar results in terms of $s_{u(mob)}/\sigma'_v$, as long as the measured preconsolidation from CRS, which is given as an input parameter in eq. (5.2), is divided by 1.27. However, for OCR_{CRS} values lower than 1.27, OCR_{IL} would result in values lower than 1 (underconsolidated soil), which is quite unrealistic for Finnish clay deposits. Moreover, eq. (8.1) would overpredict $s_{u(mob)}$ for OCR_{CRS} lower than 1.27.

In particular, for normally consolidated clays eq. (8.1) would overestimate the mobilized undrained shear strength by 19% because of the higher normally consolidated strength ratio (S = 0.29) than in eq. (5.2). For OCR = 1, S = 0.244 seems more consistent with some literature values for $s_{u(mob)}/\sigma'_v$ presented in section 2.5 (S = 0.22-0.23).

8.2 On the use of NGI-ADP and NGI-ADPSoft models

8.2.1 General aspects

Special features of sensitive clays such as undrained shear strength anisotropy and strain-softening behavior are often neglected in practice, even though they can notably affect the undrained response and, consequently, the performance of an embankment, as shown in Chapter 6.

The main reason why such aspects are not always taken into account is that the testing required to obtain sufficient data for a reliable estimate of the input parameters can be quite expensive and time consuming. Furthermore, while anisotropy can be also modelled in LEM, strain-softening and strain localization demand for advanced FE analyses.

Most of the available constitutive models for anisotropic soils are based on effective stress parameters. For instance, models such as MIT-E3 (Whittle and Kavvadas 1994) or S-CLAY1S (Karstunen et al. 2005) are formulated so that they can predict the stress-path dependent variation of undrained stress-strain-strength. However, undrained shear strength in these models is indirectly determined and may depend on several parameters which are not always of simple derivation and the calibration of real undrained shear strength profile for practical applications may not be straightforward. The use and calibration of advanced effective stress models for Finnish clays has been extensively discussed by Mansikkamäki (2015).

As earlier explained in section 6.3, NGI-ADP and NGI-ADPSoft models are based on the undrained shear strength concept, where the anisotropic s_u is given as an input parameter. One advantage of using such models is that shear-induced pore pressures are implicitly taken into account by the undrained shear strength. The failure criterion is hence directly defined by the input parameters, rather than by derived parameters.

The evolution of strength reduction after peak state is also an input to the NGI-ADPSoft model. The stress-strain curves can be directly fitted from the test results through the input of residual strengths ($s_{ur}^{C,DSS,E}$), residual strains ($\gamma_r^{C,DSS,E}$) and two shape parameters c_1 and c_2 (see section 6.3). Effective stress models such as S-CLAY1S (Karstunen et al. 2005) accounts for strain-softening by including destructuration into the elasto-plastic formulation.

Provided that triaxial compression, triaxial extension and direct simple shear test results are available, the variable s_u along a shear band can be modelled and more accurate prediction of the safety level can be obtained.

8.2.2 **On the determination of the input parameters**

From a purely engineering point of view, the formulation of NGI-ADP and NGI-ADPSoft models make them easily usable for a practical approach to the aforementioned complex features of sensitive clays.

Despite the numerous input parameters required, their determination can be fairly easy when proper testing is available. On the other hand, unlike triaxial compression tests (TXC), triaxial extension tests (TXE) are very rarely performed in Finland. Even though DSS tests are not used in Finland, s_u^{DSS} can be derived from field vane measurements, which are commonly available, as shown in section 6.4.1. Proper testing is clearly encouraged, but when not possible some existing correlation could be exploited as a supporting tool.

For Perniö clay, eq. (2.15) appears to provide a good fit to the extension tests (Fig. 6.16) and, hence, a good estimate of s_u^P. Eq. (2.12), eq. (2.14) and eq. (5.2) seem to well represent the mean trend of the field vane data from Perniö (Fig. 6.17). Eq. (5.2) for $s_{u(mob)}$ of Finnish clays looks very similar to eq. (2.12) and eq. (2.14) and it may also be used to assess s_u^{DSS}.

For normally consolidated to slightly overconsolidated clays, the peak failure strain in compression (γ_p^C) is generally lower than the peak failure strain from direct simple shear (γ_p^{DSS}). The peak failure strain in extension loading (γ_p^E) is generally the lowest. Based on the available literature, γ_p^C varies in the range 0.5-4%, γ_p^{DSS} in the range 2-8% and γ_p^E in the range 3-8%, as reported by the PLAXIS user's manual (2012).

For stability calculations aimed to define a factor of safety (only for NGI-ADP) or a failure load (both models), the failure strain values become less important than the undrained shear strength. For simplicity, when extensive testing is missing, shear strain values in the three directions of loading may be set by assuming e.g. $\gamma_p^{DSS} = 2 \cdot \gamma_p^C$ and $\gamma_p^E = 4 \cdot \gamma_p^C$ as in Chapter 6.

Nevertheless, the reliability of a FE analysis is strongly dependent on the quality of the available calibration tests. Determining soil parameters from test results from disturbed samples may result in erroneous prediction of failure load as well as deformations.

When using NGI-ADP model for softening materials such as sensitive clays, it is important to remember that the capacity or factor of safety will be overestimated if peak values of undrained shear strength are used in the calculation. NGI's experience from back-calculation of failures in soft sensitive clays indicates that strain-softening typically reduces the capacity by 10-15% (Jostad et al. 2014). Therefore, peak strengths must be reduced in order to obtain the same capacity as if softening was taken into account (Fig. 8.1). As discussed in section 2.6.1, Jostad et al. (2014) suggested that peak s_u values should be reduced by 9% on average (F_{soft} = 1.09).

Results presented in Table 6.7 suggest that by using peak shear strengths in the elasto-plastic ADP analysis, the failure load in the Perniö failure experiment is overpredicted by 6.2%. Peak s_u values would need to be reduced by F_{soft} = 1.06 in order to obtain the failure load predicted by the NGI-ADPSoft model.

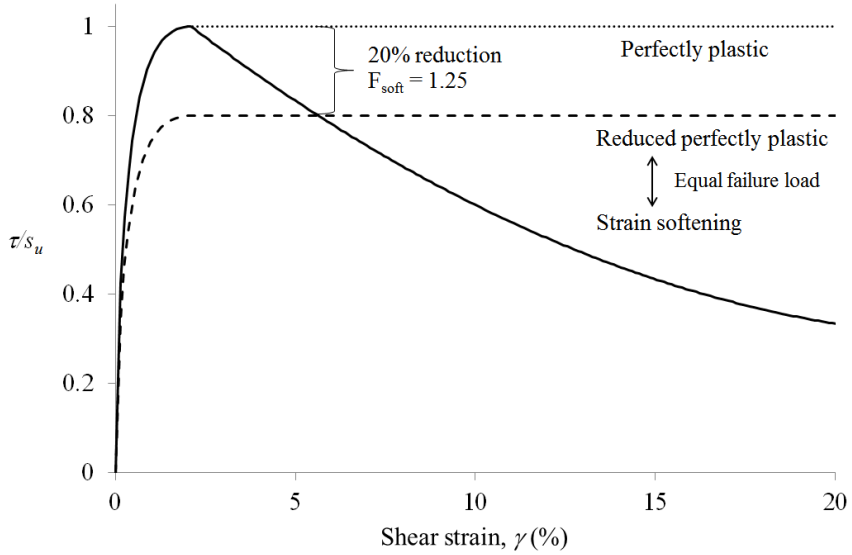

Fig. 8.1: Strain-softening behavior and perfectly plastic behavior giving the same bearing capacity (after Jostad et al. 2014)

Shear band thickness (t_{sb}) is a rate dependent parameter (see section 2.6) and it affects both rate of softening and peak capacity. NGI-ADPSoft model is however rate independent. Therefore, shear band thickness (t_{sb}) has to be given as an input parameter through the internal length scale (l_{int}). For a given input undrained shear strength, an overestimation of the internal length scale value may result in over prediction of safety.

A recommendation would be to avoid the use of too coarse FE discretization and select l_{int} larger enough than the average element size. In the back-calculation of Perniö failure experiment, the internal length scale parameter was chosen 25% larger than the average element size. The results obtained were considered very satisfactory.

8.3 On the modelling of strength increase under old embankments

8.3.1 General methodology

Undrained shear strength increase due to consolidation is known to improve the response of embankments to external loads, as discussed in Chapter 4. Test results from Murro test embankment presented in Chapter 7 have proven that the strength has increased after 20 years of consolidation. The undrained shear strength s_u increase was assessed by means of in-situ test results and simple transformation models for s_u.

Modelling of s_u increase in total stress analysis may however not be an easy task because of the non-uniform strength distribution in the subsoil beneath the embankment. In the guideline B15 released by the Finnish Transport Agency (Ratahallintokeskus 2005), a method to take into account the s_u increase is proposed. The soil underneath the embankment is divided into three zones. For each zone, the strength is determined from field vane test (Fig. 8.2). This approach may however underestimate the undrained shear strength under the embankment after a certain depth if a constant s_u is assumed.

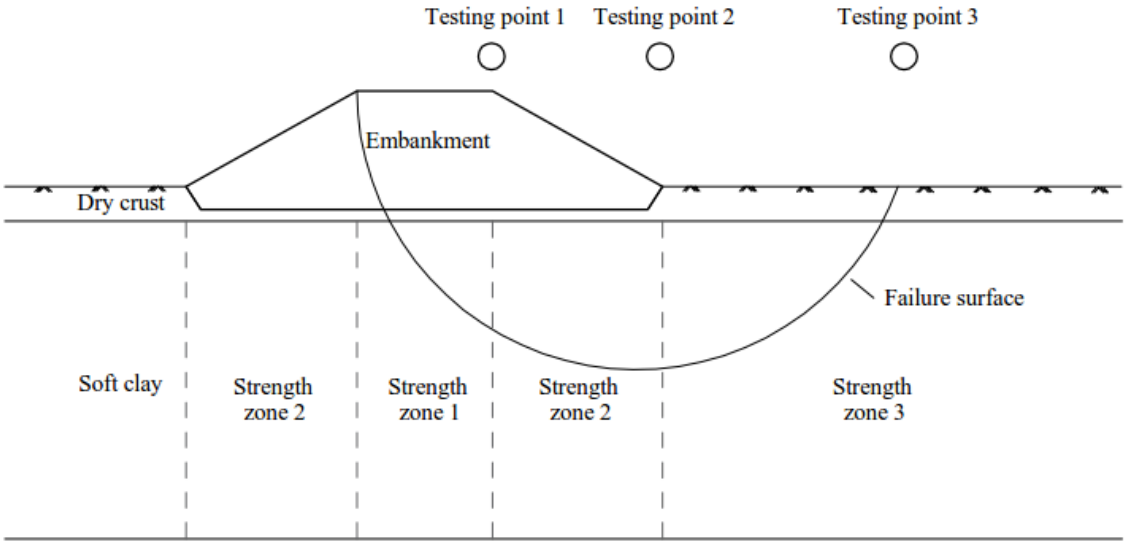

Fig. 8.2: Illustration of the method suggested by the Finnish Transport Agency to account for undrained shear strength increase under old embankments.

However, the method suggested by the FTA cannot provide a realistic modelling of the variation of s_u in the horizontal direction. A correct procedure, which would result in a more truthful description of the actual s_u distribution under an old embankment, would consist of interpolating between the s_u profiles determined at the three different testing points, as shown in Fig.8.3, and therefore using the resulting s_u distribution as input for the calculation.

The most accurate way of estimating s_u increase under embankments is from direct measurements using in-situ (CPT, field vane) or laboratory (TX, DSS) tests. In this way, input parameters for total stress analysis are unequivocally defined. However, when direct s_u measurements are not available or tests are suspected to be unreliable, transformation

models for s_u based on clay properties, such as preconsolidation pressure, can be used [e.g. eq. (2.1), eq. (5.2)].

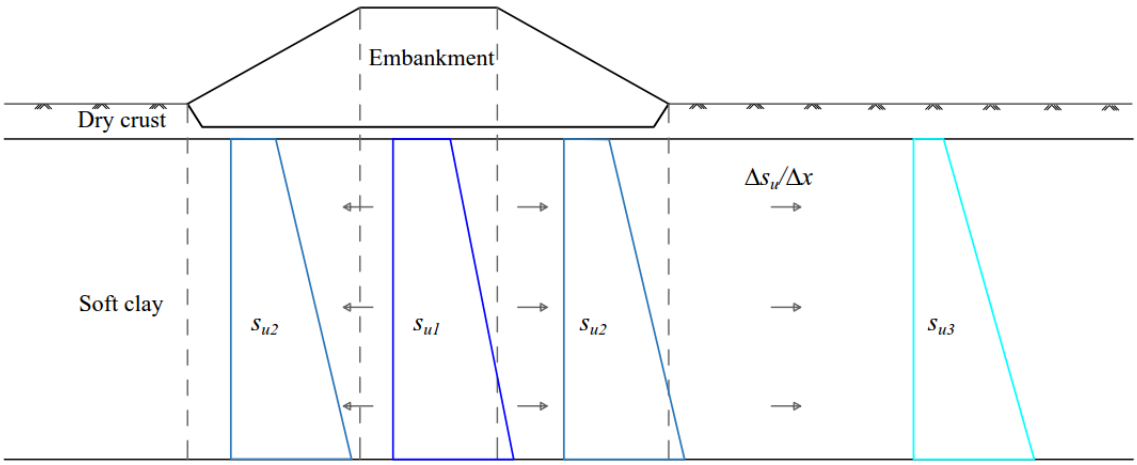

Fig. 8.3: Schematization of the undrained shear strength change in the horizontal direction under old embankments.

In general, for a given effective stress increment, there will be an increment in s_u even without any increase in preconsolidation pressure, as indicated by eq. (2.2). Such a variation is though very small in lightly overconsolidated clays and, therefore, strength increase is assumed to occur only when the vertical effective stress exceeds the preconsolidation pressure and the clay becomes normally consolidated. Under this hypothesis, the undrained shear strength increase (Δs_u) under embankments can be modelled by simply estimating the increase in preconsolidation pressure ($\Delta\sigma'_p$) resulting from the increase in effective stress due to the embankment weight, as shown by eq. (8.3).

$$\Delta s_u = S \cdot \Delta\sigma'_p \tag{8.3}$$

S is the undrained strength ratio for normally consolidated state [eq. (2.2)]. S is material as well as direction dependent (anisotropic), as discussed in Chapter 2. For field vane (or DSS) strength, S = 0.244 from eq. (5.2) for Finnish inorganic soft clays, with a coefficient of variation (COV) of 0.25. S may however significantly vary from the suggested value because of e.g. a different soil nature, as for Murro clayey silt, for which S = 0.33.

$\Delta\sigma'_p$ is a function of the change in effective stress caused by the embankment weight. In Chapter 7 it was discussed the importance of taking buoyancy effects into account, in order not to overestimate σ'_p values after consolidation. An estimate of the embankment settlement, especially for embankments built several years ago, should be made before approaching the problem of strength increase.

8.3.2 **Modelling undrained shear strength increase in LEM**

In FEM the change in preconsolidation pressure caused by consolidation can be modelled through a consolidation analysis using an effective stress model. In this way, the s_u distribution in the subsoil will be continuous also in the horizontal direction and no further division into layers, as in Fig. 8.2, will be required to account for the strength change in the horizontal direction.

Effective stress analysis appears to be more reliable for assessing the strength increase under embankments, as it generally provides less conservative *FOSs* than when s_u from field vane is used as input parameter (Tavenas et al. 1978). Furthermore, for a detailed description of the phenomenon, soil destructuration should be taken into account when modelling the transition from the overconsolidated to the normally consolidated state of sensitive clays. Nevertheless, soil parameters might be difficult to determine to calibrate such models (see e.g. Mansikkamäki 2015).

In LEM the change in preconsolidation pressure cannot be modelled. Therefore, some assumption should be made when defining the undrained shear strength distribution in the subsoil for a total stress analysis, as there is no unique methodology.

Modelling of s_u increase in LEM according to e.g. Fig. 8.3 has some disadvantages. Firstly, the undrained shear strength changes discontinuously in the horizontal direction, which is not representative of the ideal field conditions shown in Fig. 8.2. Secondly, as a result of the different modelled vertical zones, breakpoints in the geometry model will be very close one another. As a consequence, very narrow slices might cause convergence problems when using the rigorous methods. Furthermore, the optimization for non-circular slip surface may become more difficult. (Länsivaara 2015)

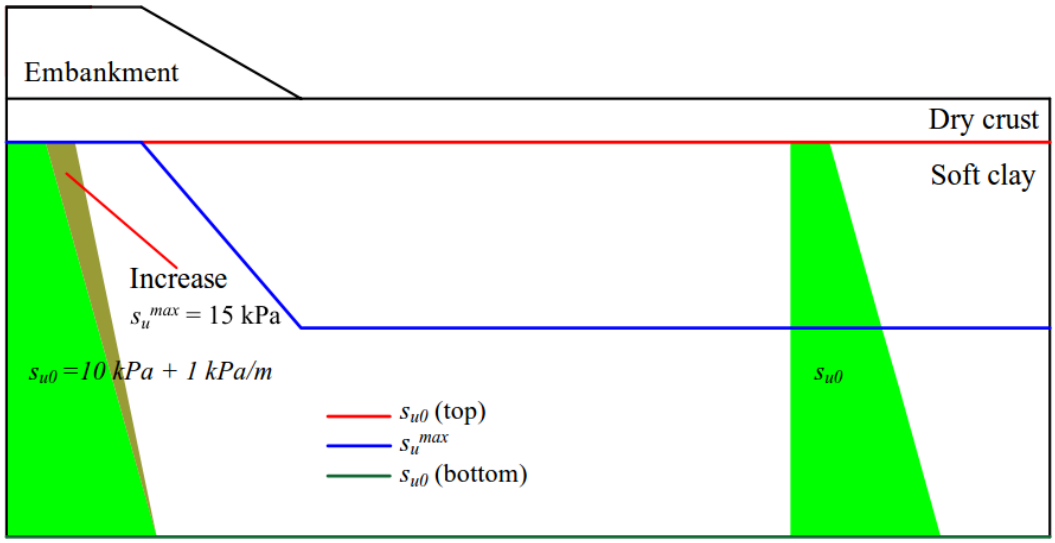

Fig. 8.4: Equal strength curve method for modelling undrained shear strength increase under old embankments (after Länsivaara 2015).

This can however be avoided by modelling the s_u increase using "equal strength curves" (Fig. 8.4). An "equal strength curve" is a curve where s_u is constant. s_u is interpolated between two or more different curves with assigned s_u value. By adopting this method, the change of strength in the horizontal direction can be more realistically modelled than in Fig. 8.2. The assumption is that the strength increases to its maximum only between the

crests of the embankment. Outside the embankment no strength increase is assumed to occur. (Länsivaara 2015)

Even though the approach shown in Fig. 8.4 may provide a reasonable description of the s_u variation in the horizontal direction, the use of only three equal strength curves may overestimate s_u after a certain depth, as shown by the s_u contour plot in Fig. 8.5. It has been experimentally demonstrated in Chapter 7 that s_u increases only down to a certain depth under Murro embankment, where s_u becomes equal to s_u prior to construction. Furthermore, no experimental information is available on the strength distribution between the centreline and the side of Murro test embankment.

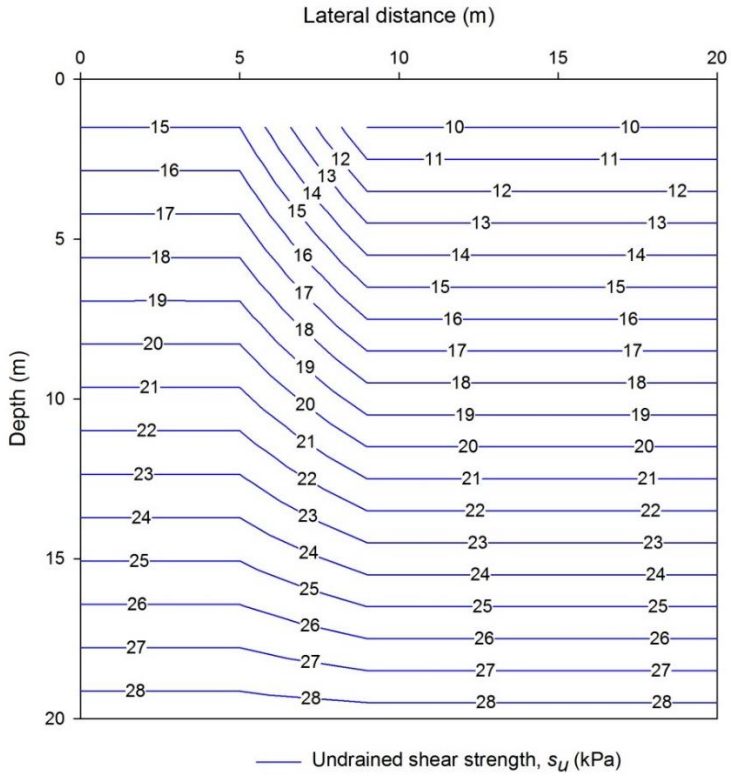

Fig. 8.5: Contour plot of the equal strength curves of Fig. 8.4 assuming a dry crust layer 1.5 m thick.

In order to validate the "equal strength curves" method, the contour plot of Fig. 8.5 is compared to the preconsolidation pressure distribution given by a FE consolidation analysis using an effective stress soil model. The analysis is performed through the finite element software PLAXIS 2D. The simple Murro test embankment geometry is assumed, since railway embankments in Finland are typically 2 m high. The embankment is modelled on top of a 1.5 m thick dry crust layer underlain by a 28.5 m thick deposit of lightly overconsolidated soft clay. The Soft Soil (SS) model (Plaxis 2012) is used to model the consolidation process in the soft clay layer. The embankment structure and the dry crust are described by the simple elasto-plastic Mohr-Coulomb model. Reasonable soil parameters are chosen for the soil layers, based on the author's experience.

The Soft Soil (SS) model is an isotropic effective stress soil model based on the Modified Cam Clay (MCC) model. The model assumes a logarithmic relationship between volumetric strain and mean effective stress. The model formulation does not include rate dependency and destructuration of soft clays. The principal input parameters are the modified compression index λ^*, the modified swelling index κ^*, the OCR, the effective

cohesion (c') and friction angle at critical state (ϕ') and the lateral earth pressure coefficient (K_0).

Input parameters for the Mohr-Coulomb and the Soft Soil model are summarized in Table 8.1 and 8.2, respectively. The parameters k_x and k_y represent the soil permeability in the horizontal and vertical direction, respectively.

Table. 8.1. Input parameters for Mohr-Coulomb model.

Layer	E' (MPa)	ν'	c' (kPa)	ϕ' (°)	γ (kN/m^3)	k_x (m/d)	k_y (m/d)	K_0
Embankment	40	0.35	1	40	20	1	1	0.36
Dry crust	10	0.30	10	30	17	2.00E-04	1.00E-04	1

Table. 8.2. Input parameters for Soft Soil model.

Layer	λ^*	κ^*	c' (kPa)	ϕ' (°)	γ (kN/m^3)	e_0	OCR	k_x (m/d)	k_y (m/d)	K_0
Soft clay	0.15	0.015	1	30	15	2	1.3	2.00E-04	1.00E-04	0.57

The FE plane-strain model used for the analysis is shown in Figure 8.6. Only one half of the embankment is considered in the analysis because of the symmetry of the problem. The lateral boundary is 30 m from the symmetry axis. The vertical boundary is at 30 m depth. The mesh used consisted of 662 15-noded triangular elements with average element size of 1.20 m (Fig. 8.6).

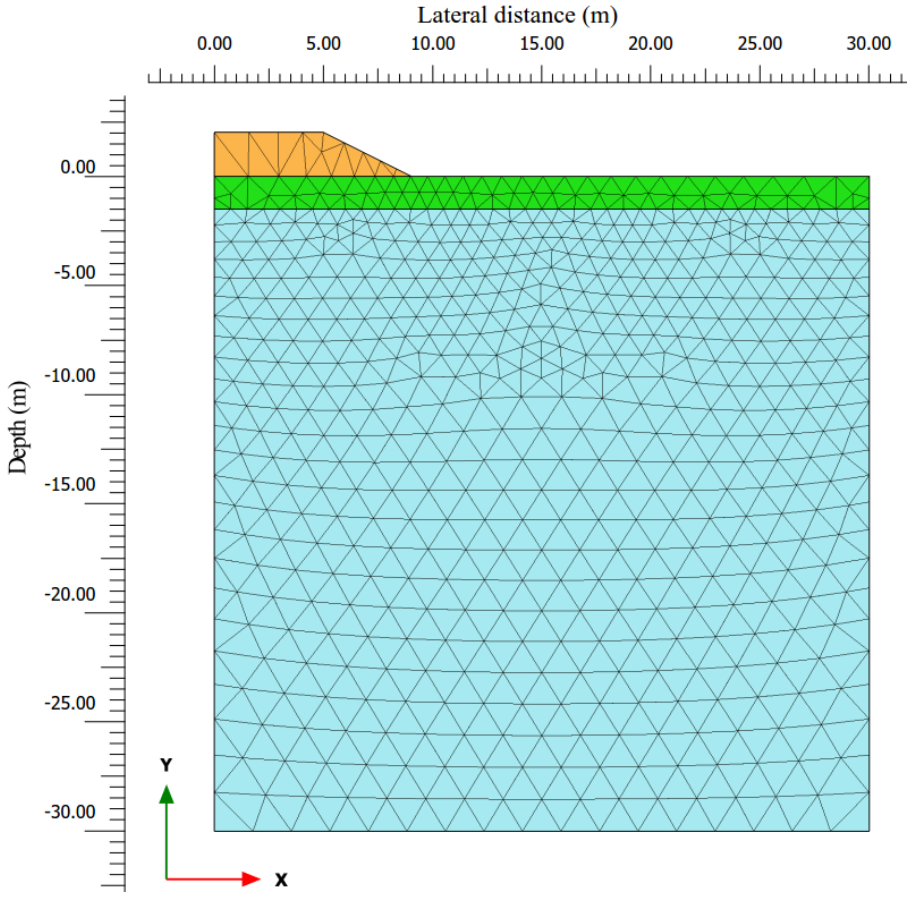

Fig. 8.6: FE mesh used for the consolidation analysis.

Full fixities are assigned to the bottom boundary, while and roller conditions are imposed at the vertical sides. The ground water table is located at 1 m depth. The initial stress state

is generated assuming K_0 conditions. K_0 is calculated according to Kulhawy and Mayne (1990). The embankment construction process is modelled through a two-day loading phase. Finally, a 40-year consolidation analysis is performed, to ensure the full dissipation of excess pore pressure and to properly simulate the stress conditions under an old embankment. The consolidation analysis is carried out using the updated pore water pressure option (large strain analysis) to account for buoyancy effects. The preconsolidation pressure distribution after consolidation is provided by the contour plot of p_p, a state parameter which describes the isotropic preconsolidation stress (Plaxis, 2012).

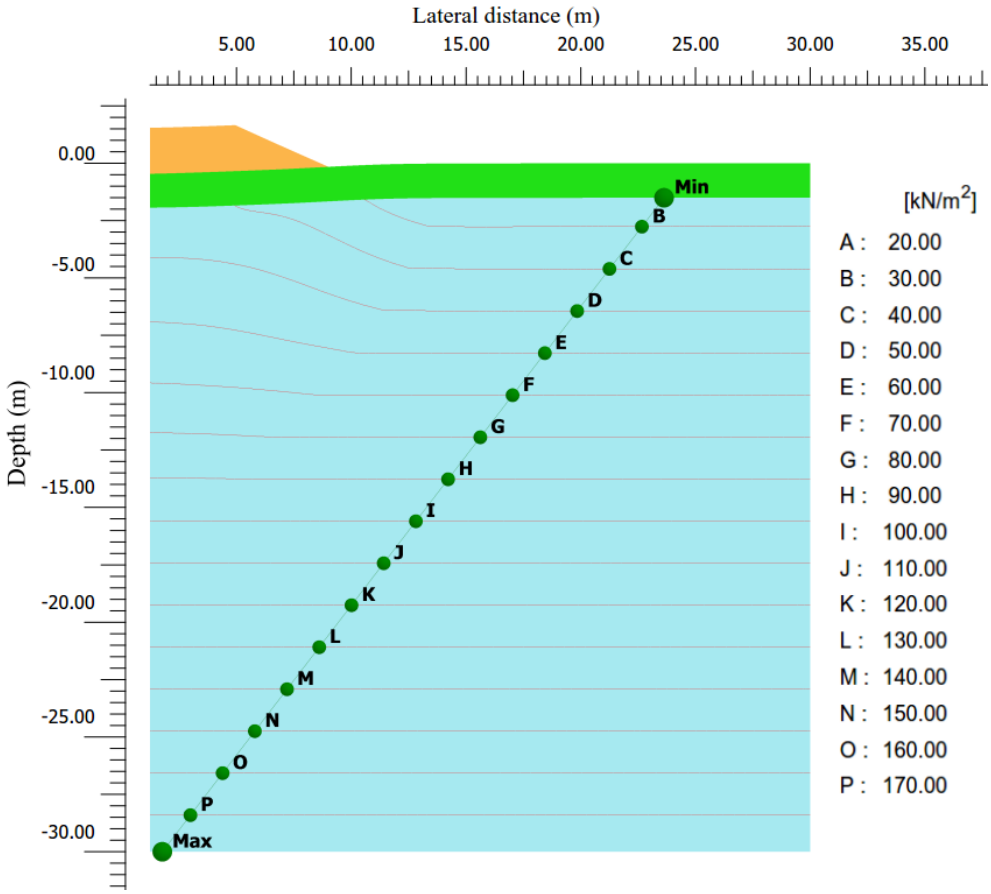

Fig. 8.7: Contour plot of isotropic preconsolidation stress p_p from the analysis using Soft Soil model.

Based on the results of the FE consolidation analysis presented in Fig. 8.7, the equal strength curve for $p_p{}^{max}$ seems to start underneath the embankment crest, in agreement with Fig. 8.4. The zone of influence in the vertical direction (hereinafter called z^*) seems to reach the depth of 13-15 m, while at Murro test embankment s_u increased down to 11 m depth, which roughly corresponds to the top width of the embankment (10 m). However, the zone of influence in the horizontal direction seems to extend farther than the embankment toe, up to 12-13 m off the centerline, where the p_p profile is roughly equivalent to p_p prior to construction. This would also suggest that the s_u profile at the Murro test embankment side shown in Chapter 7, determined from measurements taken about 4 m off the embankment slope, is representative of the soil conditions prior to construction.

In order to account for the fact that s_u only increases up to a given depth, the approach proposed in Fig. 8.4 can be improved by modelling an equal strength curve at depth equal

to z^*, where s_u is equal to s_u prior to construction and, hence, Δs_u is expected to be equal to zero.

Fig. 8.8 shows the improved approach of Fig. 8.4 based on the FE calculation results. Assuming s_{u0} = 10 kPa + 1 kPa/m and s_u^{max} = 15 kPa, under the embankment s_u = 15 kPa + 0.6 kPa until a depth equal to z^* =13 m. s_u contour plots of Fig. 8.9 show how the interpolation between equal strength curves of Fig. 8.8 is capable of modelling relatively well the s_u change in both vertical and horizontal direction.

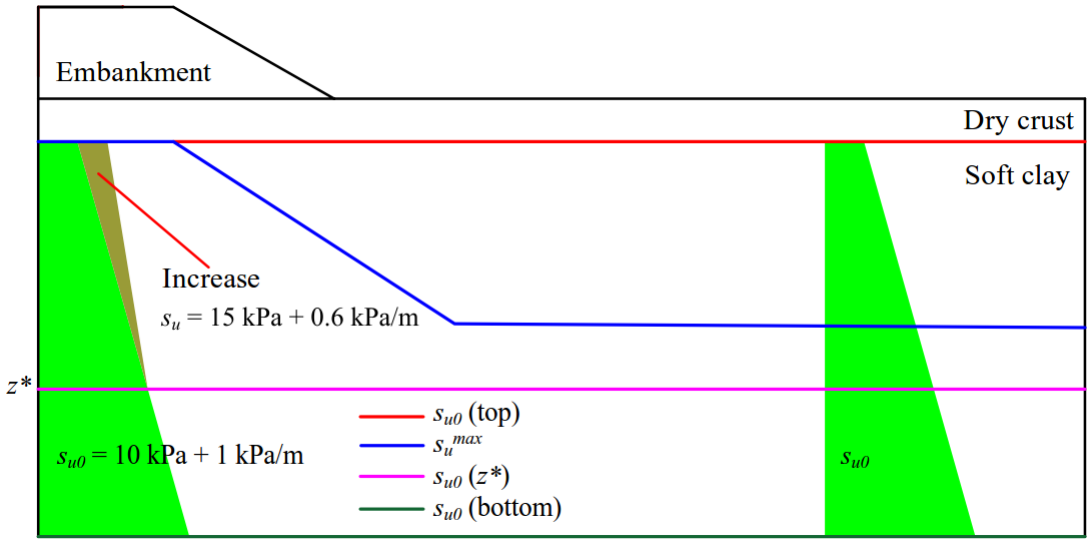

Fig. 8.8: Equal strength curve method for modelling undrained shear strength increase under old embankments based on the FE results of Fig. 8.7.

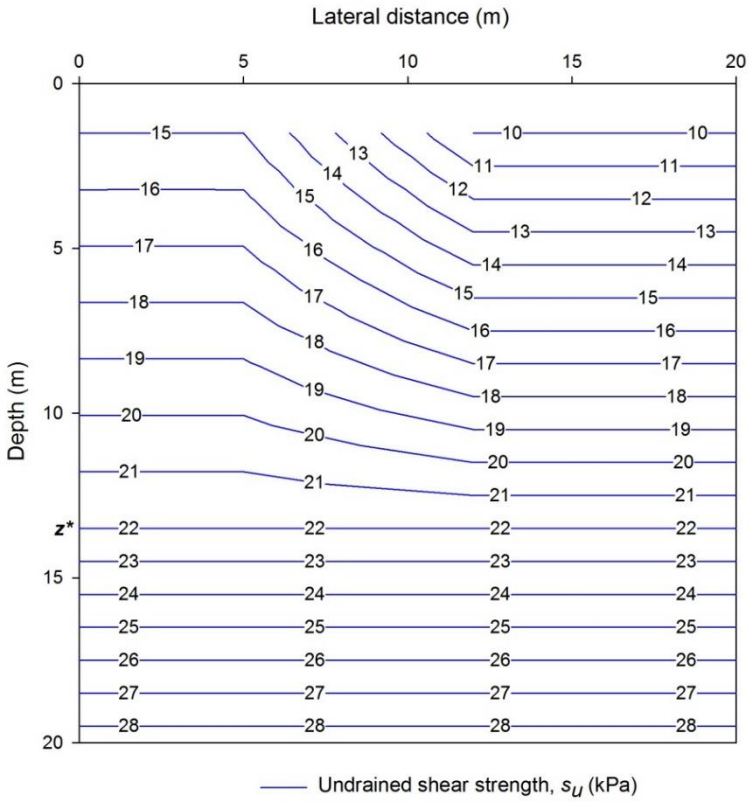

Fig. 8.9: Contour plot of the equal strength curves of Fig. 8.7 assuming a dry crust layer 1.5 m thick and z^* = 13 m.

z^* should be easily recognizable from the in-situ or laboratory test results when comparing the measured s_u or σ'_p values under the embankment with those measured prior to construction (if available) or evaluated far enough from the embankment slope. When data is lacking, z* can be evaluated from the σ'_p increase due to the embankment weight, by simply detecting the depth where $\Delta\sigma'_p = 0$.

8.3.3 **Modelling undrained shear strength increase in FEM**

One option to account for s_u increase in total stress analysis is suggested by Larsson et al. (2007), based on the ADP framework. This approach could be, for instance, applied in a FE analysis using the NGI-ADP soil model presented in Chapter 5. For the common soil profile shown in Fig. 8.10, which includes a single soft clay layer, the strength increase is directly evaluated from the increase in preconsolidation pressure, multiplied by the strength ratio for normally consolidated state for active (S^A) and direct simple shear (S^{DSS}) loading types. Outside the embankment (between points C and D), the undrained shear strength increase is assumed to be equal to zero. By increasing the input active strength ($s_u{}^A{}_{ref}$) and by appropriately changing (lowering) the anisotropy ratio for direct simple shear ($s_u{}^{DSS}/s_u{}^A$) and for passive loading ($s_u{}^P/s_u{}^A$), the anisotropic s_u along the slip surface can be modelled accounting for the improved mechanical characteristics of the clay layer. Typical S^A and S^{DSS} values are summarized in section 2.5.

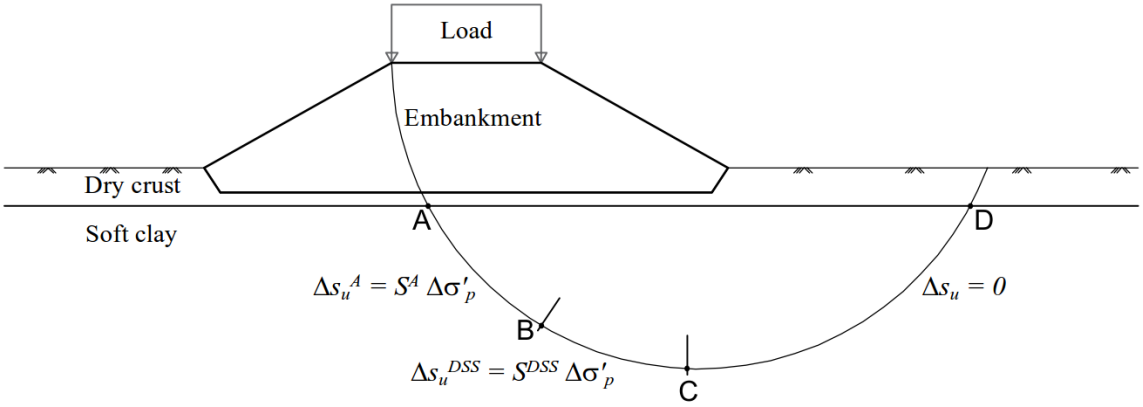

Fig. 8.10: A simple approach to s_u increase modelling under an embankment due to consolidation based on anisotropic s_u (after Larsson et al. 2007)

Fig. 8.11 shows a simple method to account for strength increase using NGI-ADP soft model. In order to satisfy the condition $\Delta s_u = 0$ at the side of the embankment by simply modelling the clay as a single layer, $s_u{}^P$ should be equal to its initial value. This can be done by modelling the increase of $s_u{}^A$ by assuming that a constant $\Delta s_u{}^A{}_{avg}$ has occurred through the whole layer (blue line in Fig. 8.11), even though the actual strength increase is not constant (red line in Fig. 8.11). In this way, the $s_u{}^A{}_{inc}$ parameter does not need to be changed and the final $s_u{}^P$ profile (red line in Fig. 8.11) can match the initial one (black dashed line in Fig. 8.11) by simply reducing the ratio $s_u{}^P/s_u{}^A$.

The increased strength for DSS conditions should be carefully modelled accounting for the fact that NGI-ADP model interpolates between $s_u{}^{DSS}$ and $s_u{}^P$ along the shear band, i.e. between points C and D, assuming that s_u at point C is representative of pure DSS conditions. Therefore, $s_u{}^{DSS}/s_u{}^A$ should be reduced from its initial value assuming that the initial $s_u{}^{DSS}$ is increased through the entire layer by e.g. $\Delta s_u{}^{DSS} = \xi \cdot \Delta s_u{}^{DSS}{}_{avg}$, where ξ is a coefficient lower than 1. In the example presented in Fig. 8.6, ξ is taken equal to 0.5. $s_u{}^{DSS}/s_u{}^A$ and $s_u{}^P/s_u{}^A$ are reduced from 0.7 and 0.4 to 0.65 and 0.35, respectively.

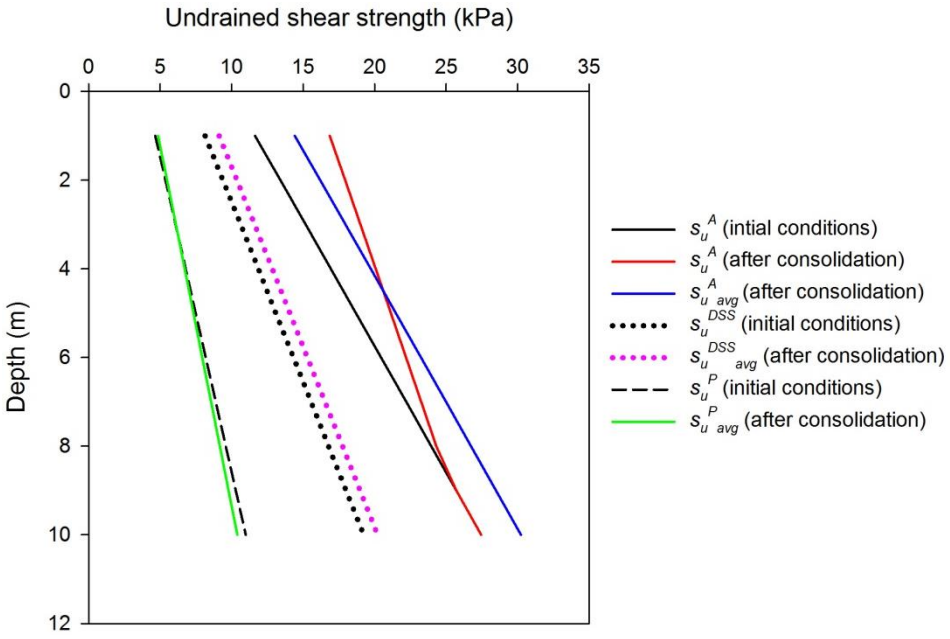

Fig. 8.11: Input s_u for the scenario of Fig. 8.10.

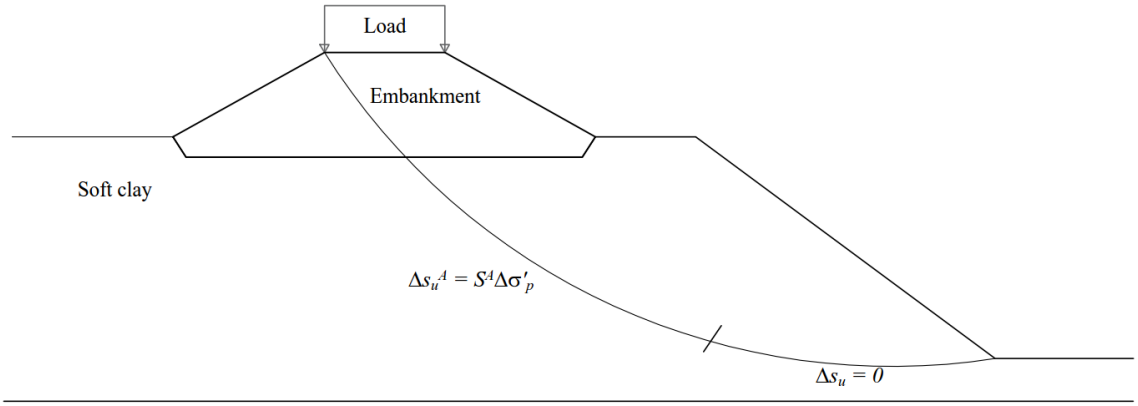

Fig. 8.12: Modelling of anisotropic s_u increase under an embankment on a slope due to consolidation based on anisotropic s_u.

For the case where the embankment is placed on a sloped terrain (e.g. on a river bank), the shape of the failure surface is often similar to the one shown in Fig. 8.12. In this case, the undrained response is mainly governed by compression. DSS conditions occur at the ending stretch of the slip surface. Hence, modelling of s_u^P is not as relevant as in the previous case. By modelling s_u^A increase after consolidation as in the case of flat terrain (Fig. 8.10 and Fig. 8.11) and assuming that s_u^{DSS} does not increase, s_u^{DSS}/s_u^A must be reduced from 0.7 to 0.61.

These proposed simplified methods should however be validated from real embankment failure cases where the strength has increased after some years of consolidation.

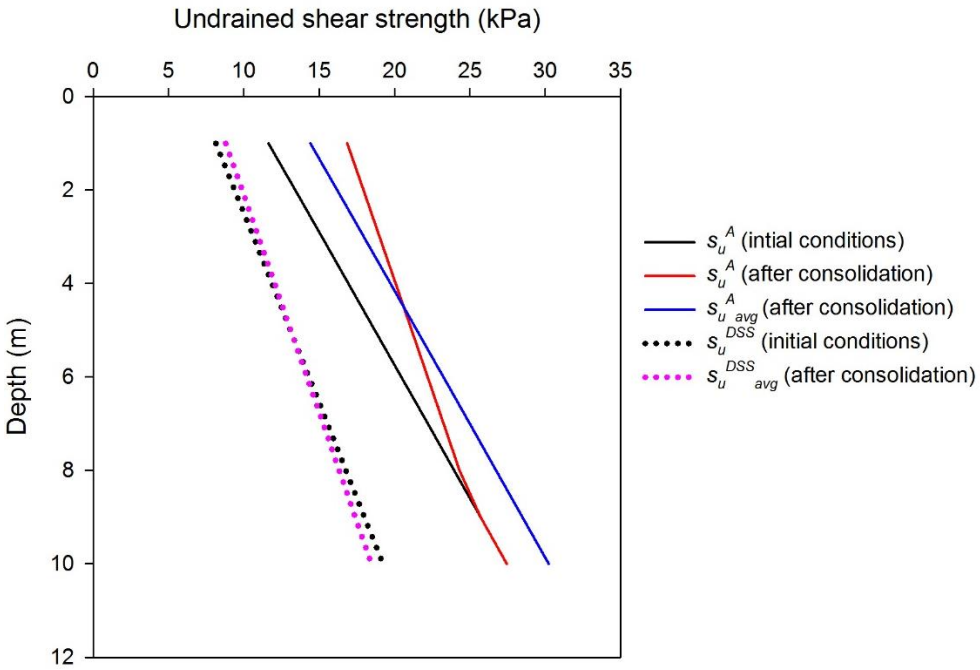

Fig. 8.11: Input s_u for the scenario of Fig. 8.12.

9. Summary, conclusions and recommendations for future research work

9.1 General

In this thesis, issues related to the undrained shear strength of Finnish clays for total stress stability analyses of embankments are studied. New correlations for s_u specific to Finnish clays are proposed. Two benchmark field cases from Finland were analyzed to study features of clays such as anisotropy of undrained shear strength and strain-softening behavior. The undrained shear strength of surficial bonded clays and the strength increase under old embankments due to consolidation are also studied.

9.2 New correlations for undrained shear strength of Finnish clays

It was shown how the mobilized undrained shear strength [$s_{u(mob)}$] of Finnish soft clays is strongly dependent on the overconsolidation ratio (OCR), increasing with increasing OCR. For normally consolidated state, $s_{u(mob)}/\sigma'_v$ = 0.244 with COV = 0.25. For OCR greater than 1, the relation $s_{u(mob)}$-OCR is non-linear, as the SHANSEP exponent m was found to be lower than 1 and equal to 0.763.

At high rates of strain, i.e. in field vane testing, s_u further correlates with some physical parameters, i.e. plasticity index, liquid limit, water content and liquidity index. The undrained shear strength s_u does not seem to be dependent on the sensitivity. The strength magnitude was observed to increase with increasing plasticity, thus suggesting that rate dependency of undrained shear strength is also a function of plasticity.

The new correlations have higher bias factors than some existing transformation models for s_u that are commonly used in practice, with COV generally lower than 0.30.

Even though a preferred approach would be to determine s_u through direct testing (e.g. CPTU, field vane, triaxial tests), the new correlations may be very helpful when data is not available or it is suspected to be unreliable.

9.3 Total stress FE analysis of the Perniö failure test

Through a 2D finite element back-calculation of the Perniö failure test using the user-defined NGI-ADPSoft model, features of sensitive clays such as undrained shear strength anisotropy and strain-softening were shown to affect the stability of the Perniö embankment. The suitability of the anisotropic NGI-ADPSoil model was positively evaluated for saturated Finnish sensitive clays. Strength anisotropy was assessed through undrained triaxial compression (TXC), triaxial extension (TXE) and field vane (FV) tests on Perniö clay. FV test results were used to verify the DSS strength predicted by existing correlations, as DSS tests are not in use in Finland. Anisotropy ratios for extension (s_u^P/s_u^A) and DSS (s_u^{DSS}/s_u^A) equal to 0.50 and 0.65, respectively, were evaluated for Perniö clay. Consistency was found between the computed (80.8 kPa) and the measured failure load (87 kPa) from the experiment, as 3D as well as rate effects were not taken into account. Mansikkamäki (2015) suggested that the 3D failure load in Perniö is 5-12% higher than in 2D analysis. Consistency was also observed between measured and calculated displacements. While the computed horizontal displacements seemed good, even though generally higher than the observations, prediction of settlement was excellent.

When peak strength values are used in the analysis without modelling strain-softening, the 2D failure load is 85.8 kPa. When the average isotropic s_u from TXC, DSS and TXE is given as input parameter, the calculated failure load is 88 kPa, which is higher than in the experiment. When isotropic s_u equal to s_u^{DSS} is used, the failure load is 80.5 kPa, while when using s_u equal to the average corrected field vane strength, the failure load is reduced to 73.9 kPa.

The advantage of modelling strain-softening was shown by the fact that the failure mechanism could be reproduced relatively well by simply modelling a deep sensitive layer with different post-peak properties, i.e. reduced residual strength.

Therefore, when accurate stability analyses are required, accounting for anisotropy and post-peak strength reduction would be a positive addition to produce more reliable results than when isotropic undrained shear strength is assumed. Extensive testing is however needed to properly define the input parameters. For the practical design cases, it is recommended to apply a correction for strain rate to the undrained shear strength values obtained from triaxial tests, as such tests are representative of rapid loading conditions as in the Perniö test.

Triaxial compression (CIUC) test results on block samples of Perniö dry crust indicated that the strength measured from field vane test is unrealistically higher than the actual in-situ undrained shear strength. When field vane strength is given as input parameter, the FE failure load is equal to 94 kPa, which is 8% higher than the 87 kPa reached in the test. In the case of Perniö, the dry crust was about 1 m thick and its strength seemed nearly isotropic (s_u^P/s_u^A = 0.88). In situations where the dry crust is thicker, extension tests should be carried out to evaluate the strength anisotropy ratio. No preconsolidation pressure could be identified from CRS oedometer tests in the top part of the dry crust, which was characterized by the presence of fissures and organic material. On the other hand, OCR values higher than 2 could be estimated in the stiff clay located right below the crust, where the soil structure seemed more homogeneous.

9.4 Undrained shear strength increase under old embankments

The phenomenon of undrained shear strength increase should be taken into account when performing undrained stability analyses of old embankments, as the global stability is expected to improve.

From CPTU test results, undrained shear strength increase was observed under Murro test embankment 20 years after construction. The maximum observed strength increase was about 54% at 3.50 m depth. The strength has increased up to 11 m depth.

Based on field vane test results from the side of Murro test embankment, a cone factor (N_{kt}) equal to 13.1-15.4 was evaluated for Murro clay, while $N_{\Delta u}$ = 7.2-8.0. For Murro clay $s_{u(mob)}/\sigma'_v$ = 0.33 under the embankment, where the soil is normally consolidated. The reasons for such a high value might be the organic content (2-4%), the silt content (>70%) and the high content of Quartz, Feldspar and Sulphur. Furthermore, a triaxial test on a block sample of Murro clay suggested a friction angle of 37.7°. However, when field vane test results are corrected by a factor of 0.65 as suggested by Westerberg et al. (2015) for Swedish sulphide clays, $s_{u(mob)}/\sigma'_v$ = 0.28 for DSS loading conditions.

A simple SHANSEP based model was found to provide a reliable estimate of the preconsolidation pressure at the test site, according to CRS oedometer test results on block samples of Murro clay. When the increase in preconsolidation pressure is known, the strength increase can be simply derived as $\Delta s_u = S \cdot \Delta\sigma'_p$, where S is $s_{u(mob)}/\sigma'_v$ for normally consolidated state (S = 0.33 for Murro clay). This methodology can be applied to real embankment cases if direct s_u measurements are not available or considered to be inaccurate.

The importance of accounting for buoyancy effects was shown. When these effects are neglected, the stress increase in the soil and, therefore, s_u are overestimated.

Undrained shear strength increase in total stress analysis in LEM can be reliably modelled by interpolation between curves with given constant s_u values. In this way, the change of s_u in the horizontal direction is taken into account, thus providing a more realistic strength distribution in the subsoil than when layers with different assigned s_u values (constant or increasing with depth) are modelled.

9.5 Recommendations for future research work

In order to continue the research on undrained shear strength of Finnish clays for total stress stability analyses, it would be of great importance to:

- Perform triaxial compression (TXC), triaxial extension (TXE) and direct simple shear (DSS) tests on Finnish clays in order to construct a multivariate database to derive correlations for active, DSS and passive strength, referring to the methodology presented in this work. The database would also serve to calibrate in-situ tests i.e. field vane and CPTU. A comparison between the Finnish and existing clay databases [e.g. from MIT (Ladd et al. 1977) and NGI (Karlsrud and Hernandez-Martinez 2013)] should be carried out to check the consistency of the new data. Testing could be extended to dry crust layers from different locations, as these layers seem to have a high impact on the safety level of embankments.

- Perform DSS tests on Murro clay and on organic sulphide clays located along the Western coast of Finland, in order to calibrate field vane and CPTU tests in these special soils.

- Collect data (e.g. CPTU, FV, DSS…) from existing old railway embankments to evaluate the strength increase due to consolidation in Finnish clays and to improve modelling and calculation methods, especially in LEM, since strength anisotropy cannot be modelled by any of the calculation programs currently in use in Finland.

10. References

Andresen, L., and Jostad, H. P. 2002. A constitutive model for anisotropic and strain-softening clay. In Proceedings of the 8th International Symposium on Numerical Models in Geomechanics, NUMOG VIII, Rome, Italy. pp. 10-12.

Andresen, L., Jostad, H.P., and Høeg, K. 2002. Numerical procedure for assessing the capacity of anisotropic and strain-softening clay. In Proceedings of the 5th World Congress on Computational Mechanics, WCM V, Wien, Austria.

Andresen, L., Saygili, G., and Grimstad, G. 2011. Finite Element analysis of the Saint-Alban embankment failure with an anisotropic undrained strength model. In Proceedings of the 15th European Conference of Soil Mechanics and Geotechnical Engineering. Athens, Greece. pp. 1111-1118.

Arulanandan, K., Shen, C., and Young, R. 1971. Undrained creep behaviour of a coastal organic silty clay. Géotechnique, 21(4): 359-375.

Bazant, Z. P. 1976. Instability, ductility, and size effect in strain-softening concrete. Journal of the Engineering Mechanics Division, 102(2): 331-344.

Bernander, S. 2000. Progressive landslides in long natural slopes. Formation, potential extension and configuration of finished slides in strain-softening soils. Licentiate thesis, Luleå University of Technology.

Berre, T. 1969. Studies of yield stress and time effect in the Drammen clay. In Bolkesji symposium on shear strength and consolidation of normally consolidated clays (papers). pp. 31-36.

Berre, T., and Bjerrum, L. 1973. Shear strength of normally consolidated clays. In Proceedings of the 8th International Conference on Soil Mechanics and Foundation Engineering, Moscow. Vol. 1.1, pp. 39–49.

Bishop, A. W. 1967. Progressive failure with special reference to the mechanism causing it. In Proceedings of Geotechnical Conference, September 1961, Oslo. Vol. 2, pp. 142-150.

Bishop, A. W. 1971. The influence of progressive failure on the choice of the method of stability analysis. Geotechnique, 21(2): 168-172.

Bjerrum, L. 1954. Geotechnical properties of Norwegian marine clays. Géotechnique, 4(2): 49–69.

Bjerrum, L. 1961. The effective shear strength parameters of sensitive clays. In Proceedings of 5th International Conference on Soil Mechanics, 17-22 July 1961, Paris, Vol. 1, pp. 23-28.

Bjerrum, L. 1967. Engineering geology of Norwegian normally consolidated marine clays as related to settlements of buildings. 7th Rankine lecture. Géotechnique, 17(2): 81–117.

Bjerrum, L. 1972. Embankments on soft ground. In Proceedings of the ASCE Specialty Conference on Performance of Earth and Earth-Supported Structures, Purdue University, Lafayette, Ind. ASCE. Vol. 2, pp. 1–54.

Bjerrum, L. 1973. Problems of Soil Mechanics and Construction on Soft Clays. State-of-the-art report. In Proceedings, 8th ICSMFE, Moscow. Vol. 3, pp. 111–159.

Bjerrum, L., and Landva, A. 1966. Direct simple-shear tests on a Norwegian quick clay. Géotechnique, 16(1): 1-20.

Brinkgreve, R. B. J. 1994. Geomaterial models and numerical analysis of softening. PhD thesis, TU Delft, Delft University of Technology.

Burland, J. B. 1990. On the compressibility and shear strength of natural clays. Geotechnique, 40(3): 329-378.

Burland, J. B., Rampello, S., Georgiannou, V. N., and Calabresi, G. 1997. A laboratory study of the strength of four stiff clays. Géotechnique, 47(2): 390-390.

Chandler, R.J. 1988. The in-situ measurement of the undrained shear strength of clays using the field vane. In Vane shear strength testing in soils: field and laboratory studies. ASTM STP 1014. ASTM, Philadelphia, Pa. pp. 13–44.

Ching J, Phoon KK. 2012. Modeling parameters of structured clays as a multivariate normal distribution. Canadian Geotechnical Journal 49(5): 522-545.

Ching, J., and Phoon, K.K. 2013. Multivariate distribution for undrained shear strengths under various test procedures. Canadian Geotechnical Journal, 50(9): 907–923. doi:10.1139/cgj-2013-0002.

Ching, J., and Phoon, K.K. 2014a. Correlations among some clay parameters - the global database. Canadian Geotechnical Journal, 51(6): 663-685.

Ching, J., and Phoon, K.K. 2014b. Correlations among some clay parameters - the multivariate distribution. Canadian Geotechnical Journal, 51(6): 686-704.

Ching J, Phoon K.K., and Chen C-H. 2014. Modeling piezocone cone penetration (CPTU) parameters of clays as a multivariate normal distribution. Canadian Geotechnical Journal 51(1): 77-91.

Dascal, O., Asce, M., Tournier, J., Tavenas, F., Asce, A. and La Rochelle, P. 1972 Failure of a test embankment on sensitive clay. In Proceedings Spec.Conf. Performance Earth Supported Struct.Am.Soc.Civ.Eng., Volume 1, pp. 1–54.

Di Buò, B., D'Ignazio, M., Selänpää, J., and Länsivaara T. 2016 Preliminary results from a study aiming to improve ground investigation data. In Proceedings of the Nordic Geotechnical Meeting (NGM) 2016, Reykjavik, Iceland. Vol. 1, pp. 187-197.

D'Ignazio, M., and Länsivaara, T. 2015. Shear bands in soft clays: strain-softening behavior in finite element Method. Rakenteiden Mekaniikka (Journal of Structural Mechanics), 48(1): 83-98.

D'Ignazio, M., Mansikkamäki, J., and Länsivaara, T. 2014. Anisotropic total and effective stress stability analysis of the Perniö failure test. In Proceedings of Conference on Numerical Methods in Geotechnical Engineering (NUMGE), Delft, Netherlands. Vol. 2, pp. 609-614.

D'Ignazio, M., Di Buò, B., and Länsivaara, T. 2015. A study on the behavior of weathered clay crust in the Perniö failure test. In Proceedings of XVI ECSMGE, 13-17 September 2015, Edinburgh, Scotland. 7: 3639-3644.

D'Ignazio, M., Phoon, K.K., Tan, S.A. and Länsivaara, T. 2016. Correlations for undrained shear strength of Finnish soft clays. Canadian Geotechnical Journal. DOI: 10.1139/cgj-2016-0037.

D'Ignazio, M., Länsivaara, T. and Jostad H.P. *In press*. Failure in anisotropic sensitive clays: a Finite Element study of the Perniö failure test. Canadian Geotechnical Journal.

Desrues, J., and Viggiani, G. 2004. Strain localization in sand: an overview of the experimental results obtained in Grenoble using stereophotogrammetry. International Journal for Numerical and Analytical Methods in Geomechanics, 28(4): 279-321.

Duncan, J. M., and Buchignani, A. L. 1976. An engineering manual for settlement studies. University of California, Department of Civil Engineering.

Eden, W. J., and Poorooshasb, H. B. 1968a. Settlement observations at Kars bridge: reply. Canadian Geotechnical Journal, 5(1): 28-45.

Eden, W. J., and Poorooshasb, H. B. 1968b. Settlement observations at Kars bridge. Canadian Geotechnical Journal, 5: 248.

Eringen, A. C. 1981. On nonlocal plasticity. International Journal of Engineering Science, 19(12): 1461-1474.

Gardemeister, R. 1973. Hienorakenteisen maalajien geologisia ja geoteknisiä tutkimustuloksia. Geotekniikan laboratorio, Report n.8. VTT Offsetpaino. Otaniemi, Helsinki, Finland. ISBN 951-38-0046-6.

Graham, J., Crooks, J., and Bell, A. 1983. Time effects on the stress-strain behaviour of natural soft clays. Géotechnique, 33(3): 327-340.

Grimstad, G., Andresen, L., and Jostad, H.P. 2012. NGI-ADP: Anisotropic shear strength model for clay. International Journal for Numerical and Analytical Methods in Geomechanics 36(4): 483-497.

Grimstad, G., Jostad, H.P., and Andresen, L. 2010. Undrained capacity analyses of sensitive clays using the nonlocal strain approach. In Proceedings of the 9th HSTAM International Congress on Mechanics, Vardoulakis mini-symposia, Limassol, Kypros, 12–14 July. pp. 153–160.

Gylland, A. S. 2012. Material and slope failure in sensitive clays. PhD thesis, Norwegian University of Science and Technology (NTNU), Trondheim.

Gylland, A. S., Nordal, S., Jostad, H. P., and Mehli, M. 2011. Pragmatic approach for estimation of slope capacity in soft sensitive clay. Electronic Journal of Geotechnical Engineering, 16: 575-590.

Gylland, A. S., Jostad, H. P., and Nordal, S. 2014. Experimental study of strain localization in sensitive clays. Acta Geotechnica, 9(2): 227-240.

Hanzawa, H. 1995. In Situ shear strength of marine clay related to aging effect. In Proceedings of the 11th European Conference IMFE, Vol. 1, 141-146.

Hansbo, S. 1957. A new approach to the determination of the shear strength of clay by the fall-cone test. Royal Swedish Geotechnical Institute.

Helenelund, K.V. 1977. Methods for reducing undrained shear strength of soft clay. In Report (3). Swedish Geotechnical Institute. pp. 1–59.

Hicher, P. Y., Wahyudi, H., and Tessier, D. 2000. Microstructural analysis of inherent and induced anisotropy in clay. Mechanics of Cohesive-frictional Materials, 5(5): 341-371.

Hoikkala, S. 1991. Continuous and incremental loading oedometer tests. M. Sc. thesis, Helsinki University of Technology, Espoo, Finland (In Finnish).

Holtz, R. D., and Broms, B. 1972. Long-term loading tests at Ska-Edeby, Sweden. In Performance of Earth and Earth-Supported Structures (pp. 435-464). ASCE.

Holzer, T.L., Höeg, K., and Arulanandan, K. 1973. Excess pore pressures during undrained clay creep. Canadian Geotechnical Journal, 10(1): 12-24.

Jaky, J. 1944. The coefficient of earth pressure at rest. Journal of the Society of Hungarian Architects and Engineers, 78(22): 355-358.

Jamiolkowski, M., Ladd, C.C., Germain, J.T., and Lancellotta, R. 1985. New devel- opments in field and laboratory testing of soils. In Proceedings of the 11th International Conference on Soil Mechanics and Foundation Engineering, San Francisco. Vol. 1, pp. 57–153.

Janbu, N. 1985. Soil models in offshore engineering. Géotechnique, 35(3): 241-281.

Jostad, H. P., and Andresen, L. 2004. Modeling of shear band propagation in clays using interface elements with finite thickness. In Proceedings of International Symposium on Numerical Models in Geomechanics, 25-27 August 2004, Ottawa, Canada. Vol. 9, pp. 121-128.

Jostad, H.P., and Grimstad, G. 2011. Comparison of distribution functions for the nonlocal strain approach. In Proceedings, 2nd International Symposium on Computational Geomechanics, Cavtat-Dubrovnik, Croatia. pp. 212–223.

Jostad, H.P., Andresen, L., and Thakur, V. 2006. Calculation of shear band thick- ness in sensitive clays. In Proceedings, 6th European Conference on Numerical Methods in Geotechnical Engineering Graz, Austria. pp. 27–32.

Jostad, H. P., Fornes, P., and Thakur, V. 2014. Effect of Strain-Softening in Design of Fills on Gently Inclined Areas with Soft Sensitive Clays. In Landslides in Sensitive Clays. Edited by Springer Netherlands. pp 305-316.

Karlsrud, K., Lunne, T., and Brattlien, K. 1996. Improved CPTU correlations based on block samples. In Proceedings, Nordic Geotechnical Conference, Reykjavik, Vol. 1, pp. 195-201.

Karlsrud, K., Lunne, T., Kort, D.A., and Strandvik, S. 2005. CPTU correlations for clays. In Proceedings of the XVIth International Conference on Soil Mechanics and Geotechnical Engineering, ICSMGE, Osaka, Japan. Vol. 2, pp. 693–702.

Karlsrud, K., and Hernandez-Martinez, F.G. 2013. Strength and deformation properties of Norwegian clays from laboratory tests on high-quality block samples 1. Canadian Geotechnical Journal, 50(12):1273-1293.

Karstunen, M., Krenn, H., Wheeler, S. J., Koskinen, M., and Zentar, R. 2005. Effect of anisotropy and destructuration on the behavior of Murro test embankment. International Journal of Geomechanics, 5(2): 87-97.

Karstunen, M., and Yin, Z. Y. 2010. Modelling time-dependent behaviour of Murro test embankment. Géotechnique, 60(10): 735-749.

Khan, M.A. 1993. Strength-deformation behavior of a weathered clay crust. PhD thesis, Department of Civil Engineering, University of Ottawa, Canada.

Kolisoja, P., Sahi, K., and Hartikainen, J. 1989. An automatic triaxial-oedometer device. In Proc.eedings of the 12th International Conference on Soil Mechanics and Foundation Engineering. 61-64.

Koskinen, M. 2014 Plastic anisotropy and destructuration of soft Finnish clays. PhD thesis, Aalto University, Helsinki.

Koskinen, M., Vepsälainen, P. and Lojander, M. 2002. Modelling of anisotropic behaviour of clays – Test embankment in Murro, seinäjoki, Finland, Finnra Report No. 16/2002. Helsinki, Finland: Finnish Road Administration.

Kulhawy, F. H., and Mayne, P. W. 1990. Manual on estimating soil properties for foundation design (No. EPRI-EL-6800). Electric Power Research Inst., Palo Alto, CA (USA); Cornell Univ., Ithaca, NY (USA). Geotechnical Engineering Group.

La Rochelle, P., Trak, B., Tavenas, F., and Roy, M. 1974. Failure of a test embankment on a sensitive Champlain clay deposit. Canadian Geotechnical Journal, 11(1): 142–164. doi:10.1139/t74-009.

La Rochelle, P., Zebdi, M., Leroueil, S., Tavenas, F., and Virely, D. 1988. Piezocone tests in sensitive clays of eastern Canada. In Proceedings of the 1st International Symposium on Penetration Testing, Orlando, Vol. 2, pp. 831-841.

Ladd, C.C. 1991. Stability evaluation during staged construction. (22nd Terzaghi Lecture.) Journal of Geotechnical Engineering, 117(4): 540–615.

Ladd, C.C., and Foott, R. 1974. New design procedure for stability of soft clays. Journal of the Geotechnical Engineering Division, ASCE, 100(7): 763–786.

Ladd, C. C., Foott, R., Ishihara, K., Schlosser, F., and Poulos, H. G. 1977. Stress-deformation and strength characteristics, state of the art report. In Proceedings of the 9th ISFMFE. Vol. 4, pp. 421-494.

Larsson, R. 1980. Undrained shear strength in stability calculation of embank- ments and foundations on soft clays. Canadian Geotechnical Journal, 17(4): 591–602.

Larsson, R., Sällfors, G., Bengtsson, P.E., Alén, C., Bergdahl, U, and Eriksson, L. 2007. Skjuvhällfasthet: utvärdering I kohesionsjord (2nd edition), Information 3. Swedish Geotechnical Institute (SGI), Linköping.

Larsson, R., and Mattsson, H. 2003. Settlements and shear strength increase below embankments-long-term observations and measurement of shear strength increase by seismic cross-hole tomography. Swedish Geotechnical Institute, SGI Report, 63, Linköping, Sweden.

Larsson, R., and Mulabdic, M. 1991. Piezocone tests in clay. Swedish Geotechnical Institute Report No.42, Linkoping, Sweden. 240.

Lefebvre, G., & Poulin, C. 1979. A new method of sampling in sensitive clay. Canadian Geotechnical Journal, 16(1): 226-233.

Lefebvre, G., and LeBoeuf, D. 1987. Rate effects and cyclic loading of sensitive clays. Journal of Geotechnical Engineering, 113(5): 476–489.

Lefebvre, G., Paré, J. J., and Dascal, O. 1987. Undrained shear strength in the surficial weathered crust. Canadian Geotechnical Journal, 24(1): 23-34.

Lehtonen, V. 2011. Instrumentation and analysis of a railway embankment failure experiment. Research report of the Finnish Transport agency, 29/2011. Finnish Transport Agency, Helsinki.

Lehtonen, V. 2015. Modelling undrained shear strength and pore pressure based on an effective stress soil model in limit equilibrium method. PhD thesis, Tampere University of Technology, Tampere.

Lehtonen, V., Meehan, C., Länsivaara, T., and Mansikkamäki, J. 2015. Full-scale embankment failure test under simulated train loading. Géotechnique, 65(12): 961-974.

Leroueil, S. 1988. Tenth Canadian Geotechnical Colloquium: Recent developments in consolidation of natural clays. Canadian Geotechnical Journal, 25(1): 85-107.

Leroueil, S. 1996. Compressibility of clays: fundamental and practical aspects. Journal of geotechnical engineering, 122(7): 534-543.

Leroueil, S., and Soares Marques, M. E. 1996. Importance of strain rate and temperature effects in geotechnical engineering. In Measuring and modeling time dependent soil behavior (eds T. C. Sheahan and V. N. Kaliakin), Geotechnical Special Publication no. 61: 1–60. New York, NY, USA: American Society of Civil Engineers (ASCE).

Leroueil, S., Samson, L., and Bozozuk, M. 1983a. Laboratory and field determination of preconsolidation pressures at Gloucester. Canadian Geotechnical Journal, 20(3): 477–490. doi:10.1139/t83-056.

Leroueil, S., Tavenas, F., & Bihan, J. P. L. 1983b. Propriétés caractéristiques des argiles de l'est du Canada. Canadian Geotechnical Journal, 20(4): 681-705.

Leroueil, S, Kabbaj, M., Tavenas, F., and Bouchard, R. 1985. Stress–strain–strain rate relation for the compressibility of sensitive natural clays. Géotechnique, 35(2): 159-180.

Leroueil, S., Magnan, J. P., and Tavenas, F. 1990. Embankments on soft clays. Ellis Horwood Limited.

Lo, K. Y. 1970. The operational strength of fissured clays. Géotechnique, 20(1): 57-74.

Locat, J., and Demers, D. 1988. Viscosity, yield stress, remolded strength, and liquidity index relationships for sensitive clays. Canadian Geotechnical Journal, 25(4): 799–806.

Lunne, T., and Andersen, K. 2007. Soft clay shear strength parameters for deep- water geotechnical design. In Proceedings, 6th International Site Investigation and Geotechnics Conference, Confronting New Challenges and Sharing Knowledge, London. pp. 151–176.

Lunne, T., Eide, O., and Ruiter, J. D. 1976. Correlations between cone resistance and vane shear strength in some Scandinavian soft to medium stiff clays. Canadian geotechnical journal, 13(4): 430-441.

Lunne, T., Christoffersen, H. P., and Tjelta, T. I. 1985. Engineering Use of Piezocone Results in North Sea Clays. In Proceedings of the Eleventh International Conference on Soil Mechanics and Foundation Engineering, Vol. 2, pp. 907-912.

Lunne, T., Berre, T., and Strandvik, S. 1997a. Sample disturbance effects in soft low plastic Norwegian clay. In Proceedings of the Conference on Recent Developments in Soil and Pavement Mechanics, Rio de Janeiro, Brazil, 25–27 June. Balkema, Rotterdam. pp. 81–102. [Also published in Norwegian Geotechnical Institute, Publication 204.]

Lunne, T., Robertson, P. K., and Powell, J. J. M. 1997b. Cone Penetration Testing in Geotechnical Practice, Blackie Academic and Professional, London.

Lunne, T., Berre, T., Andersen, K. H., Strandvik, S., and Sjursen, M. 2006. Effects of sample disturbance and consolidation procedures on measured shear strength of soft marine Norwegian clays. Canadian Geotechnical Journal, 43(7): 726-750.

Länsivaara, T. 1995. A critical state model for anisotropic soft soils. In Proceedings of the 11th European Conference of Soil Mechanics and Foundation Engineering, Copenhagen, Denmark. Vol. 6. pp. 101-106.

Länsivaara, T. 1999. A study of the mechanical behavior of soft clay. PhD thesis, Norwegian University of Science and Technology, Trondheim.

Länsivaara, T. 2012. Some aspects on creep and primary deformation properties of soft sensitive Scandinavian clays. In Proceedings of the 16th Nordic geotechnical meeting, NGM, 9-12 May 2012, Copenhagen, Denmark. pp. 397-404.

Länsivaara, T. 2015. Computational geotechnics. Course lecture notes.

Länsivaara, T., Lehtonen, V., and Mansikkamäki, J. 2011. Failure induced pore pressure, experimental results and analysis. In Proceedings of Pan-Am CGS Geotechnical conference, Toronto.

Länsivaara, T., Mansikkamäki, J., and Lehtonen, V. 2014. Effective stress based stability analysis on normally consolidated clays. In Landslides in Sensitive Clays. Edited by Springer Netherlands. pp. 317-328.

Mansikkamäki, J. 2015 Effective stress finite element stability analysis of an old railway embankment on soft clay. PhD thesis, Tampere University of Technology, Tampere.

Mansikkamäki, J. and Länsivaara, T. 2012. 3D stability analysis of a full-scale embankment failure experiment. In Proceedings of the 16th Nordic geotechnical meeting, NGM, 9-12 May 2012, Copenhagen, Denmark. pp. 405-412.

Mansikkamäki, J. Lehtonen, V., and Länsivaara, T. 2011. Advanced stability analysis of a failure test on an old railway embankment. In Proceedings of Symposium International, GEORAIL 2011, Paris, France.

Mataić, I. 2016. On structure and rate dependence of Perniö clay. PhD Thesis, Aalto University, Helsinki.

MATLAB, user's Manual. 1995. The MathWorks. Inc., Natick, MA.

Mayne, P.W. 1983. Discussion: Undrained shear strength anisotropy of normally consolidated cohesive soils. Soils and Foundations, 23(4): 143-146.

Mayne, P. W., and Mitchell, J. K. 1988. Profiling of overconsolidation ratio in clays by field vane. Canadian Geotechnical Journal, 25(1): 150-157.

Mesri, G. 1975. Discussion on "New design procedure for stability of soft clays". Journal of the Geotechnical Engineering Division, ASCE, 101(4): 409-412.

Mesri, G. 1989. A re-evaluation of $s_{u(mob)} = 0.22\sigma_p$' using laboratory shear tests. Canadian Geotechnical Journal, 26(1): 162-164.

Mesri, G., and Godlewski, P. M. 1977. Time and stress-compressibility interrelationship. Journal of the Geotechnical Engineering Division, 103(5): 417-430.

Mesri, G., and Huvaj, N. 2007. Shear strength mobilized in undrained failure of soft clay and silt deposits. In Advances in measurement and modeling of soil behaviour (GSP 173). Edited by D.J. DeGroot et al. ASCE. pp. 1–22.

Messerklinger, S., Kahr, G., Plötze, M., Giudici Trausch, J., Springman, S. M., and Lojander, M. 2003. Mineralogical and mechanical behaviour of soft Finnish and Swiss clays. In Proceedings of the International Workshop on Geotechnics of Soft Soils - Theory and Practice, Noordwijkerhout, the Netherlands (pp. 17-19).

Mäenpää, J. 2016. Seismisen CPTU-mittauksen käyttö leikkausaallon nopeuden määrittämiseen. Master's Thesis, Tampere University of Technology. (In Finnish. Title in English: Determining shear wave velocity using Seismic CPTU)

NGI, 2011. Effekt av progressiv bruddutvikling for utbygging i områder med kvikkleire, Teknisk Notat, Document n. 20092128-00-10-TN.

Phoon, K.K., and Kulhawy, F.H. 1999. Characterization of geotechnical variability. Canadian Geotechnical Journal, 36(4): 612–624. doi:10.1139/t99-038.

Pietruszczak, S. T., and Mroz, Z.1981. Finite element analysis of deformation of strain-softening materials. International Journal for Numerical Methods in Engineering, 17(3): 327-334.

Plaxis, B. V. 2012. User's manual of PLAXIS.

Rantamäki, M., Jääskeläinen, R., and Tammirinne, M. 1997. Geotekniikka (Geotechnic). Otatieto, 301 pp (In Finnish).

Ratahallintokeskus 2005. Radan stabiliteetin laskenta, olemassa olevat penkereet. Ratahallintokeskuksen julkaisuja B15, Ratahallintokeskus, Helsinki. (In Finnish. In English: Guidelines for embankments stability calculation by the Finnish Transport Agency, publication B15).

Ringesten, B. 1988. Dry crust-its formation and geotechnical properties. PhD thesis, Chalmers University of Technology, Göteborg.

Roscoe, K. H., and Burland, J. B. 1968. On the Generalized Stress-Strain Behavior of Wet Clay. In Engineering Plasticity. Edited by Cambridge University Press. pp.535-609.

Rosenqvist, I. T. 1953. Considerations on the sensitivity of Norwegian quick-clays. Géotechnique, 3(5): 195-200.

Rosenqvist, I. T. 1966. Norwegian research into the properties of quick clay-a review. Engineering Geology, 1(6): 445-450.

Sivasithamparam, N., Karstunen, M., and Bonnier, P. 2015. Modelling creep behaviour of anisotropic soft soils. Computers and Geotechnics, 69: 46-57.

Schanz, T., Vermeer, P. A., and Bonnier, P. G. 1999. The hardening soil model: formulation and verification. In Beyond 2000 in computational geotechnics. Edited by Balkema, Rotterdam. pp. 281-296.

Schofield, A.N. and Wroth, C.P. 1968. Critical state soil mechanics. McGraw-Hill, London, UK.

Selänpää, J. 2015. Personal communication.

SFS 2005. SFS-EN ISO 14688-2: Geotechincal investigation and testing. Identification and classification of soil. Part 2: Principles for a classification

Skempton, A. W. 1954. Discussion of the structure of inorganic soil. Journal of American Society of Civil Engineers, 80(478): 19-22.

Skempton, A. W. 1964. Long-term stability of slopes. Geotechnique, 14(2): 75-102.

Slunga, E. 1983. On the increase in shear strength in soft clay under an old embankment. In Proceedings of the 8th European Conference on Soil Mechanics and Foundation Engineering, Helsinki, Finland. Vol. 1: 83-89.

Suzuki, K., and Yasuhara, K. 2007. Increase in undrained shear strength of clay with respect to rate of consolidation. Soils and foundations, 47(2): 303-318.

Tavenas, F., Blanchet, R., Garneau, R., and Leroueil, S. 1978. The stability of stage-constructed embankments on soft clays. Canadian Geotechnical Journal, 15(2): 283-305.

Terzaghi, K., and Peck, R. B. 1948. Soil mechanics in engineering practice. John Wiley & Sons.

Terzaghi, K., Peck, R. B., and Mesri, G. 1996. Soil mechanics in engineering practice, 3rd Ed., Wiley, New York.

Thakur, V. 2007. Strain localization in sensitive soft clays. PhD thesis, Norwegian University of Science and Technology (NTNU), Trondheim.

Thakur, V. 2011. Numerically observed shear bands in soft sensitive clays. Geomechanics and Geoengineering: An International Journal, 6(2): 131-146.

Thakur, V., Jostad, H. P., Kornbrekke, H. A., and Degago, S. A. 2014a. How Well Do We Understand the Undrained Strain Softening Response in Soft Sensitive Clays?. In Landslides in Sensitive Clays. Edited by Springer Netherlands. pp 291-303.

Thakur, V., Oset, F., Viklund, M., Strand, S. A., Gjeskiv, V., Christensen, S., and Fauskerud, O. A. 2014b. En omforent anbefaling for bruk av anisotropifaktorer i prosjektering i norske leirer. Report n. 1/2014. ISBN n. 978-82-410-0962-4.

Thakur, V., Nordal, S., Jostad, H. P., and Andresen, L. 2005. Study on pore water pressure dissipation during shear banding in sensitive clays. In Proceedings of the 11th international conference on computer methods and advances in Geomechanics, IACMAG, Torino, Italy. Vol. 4, pp. 289-296.

Tiehallinto 2001. Teiden pohjarakenteden suunnitteluperusteet (In Finnish). Design manual by Finnish Road Authority. Helsinki.

Ukonjärvi, P. 2016. Rautatieympäristössä siipikairauksella määritettävän suljetun leikkauslujuuden luotettavuus. Master's Thesis, Tampere University of Technology. Unfinished, reference to the draft version during the time of writing. (In Finnish. Title in English: Reliability in determining undrained shear strength using the vane shear test in railway environment)

Vaid, Y. P., Robertson, P. K., and Campanella, R. G. 1979. Strain rate behaviour of Saint-Jean-Vianney clay. Canadian Geotechnical Journal, 16(1): 34-42.

Vermeer, P. A. and Brinkgreve, R. B. J. 1994. A new effective non-local strain-measure for softening plasticity. In Proceedings of 3rd International Workshop on Localization and Bifurcation Theory for Soils and Rocks, Grenoble, September 1993. pp. 89-100.

Vermeer, P. A., Vogler, U., Septanika, E. G., and Stelzer, O. 2004. Modelling strong discontinuities in geotechnical problems. In Proceedings of the 2nd international symposium on continuous and discontinuous modelling of Cohesive Frictional Materials, CDM. pp. 381-394.

Westerberg, B., Müller, R., and Larsson, S. 2015. Evaluation of undrained shear strength of Swedish fine-grained sulphide soils. Engineering Geology, 188: 77-87.

Whittle, A. J., and Kavvadas, M. J. 1994. Formulation of MIT-E3 constitutive model for overconsolidated clays. Journal of Geotechnical Engineering, 120(1): 173-198.

Won, J. Y. 2013. Anisotropic strength ration and plasticity index of natural clays. In Proceedings of the 18th International Conference on Soil Mechanics and Geotechnical Engineering, ICSMGE, 2-6 September 2013, Paris. pp. 445-448.

Wroth, C.P., and Wood, D.M. 1978. The correlation of index properties with some basic engineering properties of soils. Canadian Geotechnical Journal, 15(2):137–145.

Yu, Y. 1993. Testing and modelling of silty and sulphide-rich soils. PhD thesis, Luleå University of Technology.

11. Appendix A: Multivariate clay databases

F-CLAY/7/216

Table A.1. Basic information of the F-CLAY/7/216 database. σ'_p data points from IL oedometer test.

Location	Depth (m)	s_u^{FV} (kPa)	σ'_v (kPa)	σ'_p (kPa)	LL (%)	PL (%)	w (%)	S_t
Espoo, Kaukalahti	3.2	13.0	30.2	43.0	70.0	25.0	85.0	11.0
	4.6	7.0	38.6	60.0	60.0	25.0	75.0	11.0
	5.2	7.5	42.2	45.0	45.0	20.0	50.0	10.0
Espoo, Martinkylä	5.5	7.0	24.5	25.0	70.0	20.0	80.0	4.0
	6.0	7.0	27.0	30.0	30.0	15.0	75.0	2.0
	7.0	12.0	32.0	40.0	80.0	20.0	100.0	6.0
	8.0	12.0	37.0	40.0	90.0	15.0	120.0	5.0
Helsinki, Malmi	3.0	9.0	18.0	30.0	80.0	35.0	110.0	12.0
	4.0	11.0	23.0	35.0	75.0	30.0	100.0	10.0
	5.0	10.0	28.0	30.0	43.0	20.0	65.0	10.0
	6.0	11.0	33.0	40.0	55.0	20.0	80.0	11.0
	7.0	8.0	38.0	50.0	25.0	20.0	40.0	9.0
	8.0	16.0	43.0	50.0	22.0	20.0	25.0	13.0
Kouvola	1.5	42.0	24.2	150.0	45.0	20.0	40.0	6.5
	3.0	15.0	33.0	40.0	80.0	25.0	100.0	11.0
	5.0	21.0	43.0	50.0	110.0	25.0	130.0	8.0
	6.0	23.0	48.0	55.0	110.0	25.0	120.0	8.0
	7.0	25.0	53.0	60.0	80.0	25.0	110.0	7.0
Kurkela*	2.2	19.1	35.4	105.4	69.0	32.3	75.0	40.0
	2.7	20.0	37.8	107.8	66.3	31.6	79.0	39.5
	3.2	28.2	40.3	110.3	60.8	30.2	70.0	39.0
	3.7	25.0	42.7	112.4	55.2	28.8	62.0	38.5
	4.2	22.3	45.2	115.2	49.7	27.4	56.7	37.0
	4.7	23.7	47.6	117.6	48.8	27.2	60.0	35.0
	5.2	31.3	50.1	120.1	48.5	27.1	65.3	24.1
	6.2	28.4	55.0	127.3	48.0	27.0	52.1	24.2
	7.2	27.8	59.9	140.0	51.8	28.0	53.5	24.0
	8.2	29.9	64.8	152.3	55.8	28.9	55.7	24.0
	9.2	34.9	69.7	160.0	68.8	32.2	65.0	13.5
	10.2	34.1	74.6	163.0	82.4	35.6	77.4	10.0
	11.2	35.1	79.5	170.0	94.9	38.7	82.0	10.5
	12.2	23.3	84.4	182.3	107.3	41.8	87.7	10.5
	13.2	21.1	89.3	185.0	111.8	42.9	83.9	10.0
Loimaa	3.0	20.0	24.0	48.0	55.0	25.0	65.0	11.0
	4.0	19.0	31.0	90.0	51.0	23.0	60.0	9.0
	5.0	18.0	38.0	50.0	75.0	23.0	70.0	7.0
	7.0	24.0	52.0	65.0	48.0	23.0	65.0	9.0
	8.0	24.0	59.0	85.0	47.0	23.0	70.0	13.0
	9.0	23.0	66.0	67.0	55.0	25.0	70.0	13.0
	10.0	25.0	73.0	110.0	49.0	23.0	60.0	9.0

	11.0	25.0	80.0	120.0	51.0	23.0	60.0	8.0
	12.0	27.0	87.0	110.0	55.0	23.0	57.0	7.0
	13.0	27.0	94.0	100.0	52.0	22.0	65.0	8.0
Lokalahti	5.0	9.0	16.5	22.0	60.0	20.0	100.0	17.0
	7.0	10.0	26.5	28.0	49.0	20.0	80.0	19.0
Nurmijärvi	2.4	8.0	15.6	25.0	120.0	50.0	150.0	10.0
	3.6	7.0	20.4	30.0	52.0	25.0	75.0	9.0
	6.0	16.0	30.0	35.0	80.0	30.0	120.0	7.0
	7.0	17.0	34.0	48.0	75.0	30.0	100.0	10.0
	8.0	22.0	38.0	51.0	75.0	30.0	100.0	12.0
	9.0	24.0	42.0	60.0	90.0	30.0	100.0	13.0
	10.0	25.0	46.0	75.0	75.0	30.0	90.0	13.0
	11.0	28.0	53.0	80.0	65.0	30.0	75.0	14.0
	13.0	34.0	67.0	90.0	60.0	25.0	58.0	12.0
	14.0	22.0	74.0	130.0	65.0	25.0	60.0	8.0
	16.0	28.0	88.0	100.0	40.0	25.0	35.0	6.0
	17.0	30.0	95.0	100.0	52.0	25.0	60.0	7.0
	18.0	35.0	102.0	140.0	70.0	25.0	55.0	8.0
Otaniemi	2.7	5.0	10.1	20.0	105.0	25.0	120.0	9.0
	5.5	12.0	19.5	28.0	70.0	30.0	75.0	5.0
	6.5	11.0	24.5	35.0	70.0	25.0	65.0	4.0
	7.5	14.0	29.5	50.0	80.0	30.0	85.0	5.0
	8.5	19.0	34.5	80.0	65.0	30.0	80.0	7.0
	9.5	12.0	39.5	60.0	43.0	25.0	50.0	6.0
	10.5	15.0	44.5	80.0	47.0	25.0	55.0	8.0
Perniö (Location 1)*	2.2	9.30	28.9	74.3	79.0	32.0	75.0	14.0
	2.7	10.20	31.4	62.6	74.0	32.0	78.5	18.6
	2.6	12.20	31.0	64.7	75.0	32.0	80.8	19.1
	2.7	13.60	31.6	61.5	82.0	32.0	97.6	22.9
	2.1	19.10	28.5	73.8	76.0	32.0	88.0	25.2
	5.1	12.80	43.5	61.5	65.0	32.0	80.1	30.7
	3.1	9.30	33.5	51.5	65.0	32.0	83.0	32.0
	2.2	18.60	29.1	73.9	46.0	32.0	61.7	32.7
	5.7	11.60	46.4	64.4	58.0	32.0	80.9	33.7
	3.6	9.90	36.0	54.0	63.0	32.0	86.0	35.0
	4.2	12.80	39.1	57.1	64.0	32.0	90.0	35.5
	5.2	15.40	44.1	62.1	64.0	32.0	70.9	35.6
	6.1	13.30	48.5	66.5	38.0	32.0	47.9	36.7
	4.7	14.80	41.6	59.6	55.0	32.0	88.2	37.4
	3.2	11.30	33.9	51.9	60.0	32.0	82.3	39.1
	3.7	6.40	36.4	54.4	51.0	32.0	77.5	39.4
	4.6	10.70	41.0	59.0	76.0	32.0	96.6	41.3
	4.7	11.60	41.4	59.4	51.0	32.0	72.6	45.7
	4.1	10.40	38.5	56.5	50.0	32.0	69.6	45.7
	3.7	16.00	36.6	54.6	50.0	32.0	74.4	46.3
	5.2	9.90	43.9	61.9	59.0	32.0	84.1	46.5
	3.2	12.50	34.1	52.1	45.0	32.0	70.6	49.4
	5.7	16.80	46.6	64.6	54.0	32.0	80.1	51.1
	4.2	11.30	38.9	56.9	51.0	32.0	72.0	51.3
	5.6	11.30	46.0	64.0	50.0	32.0	75.9	57.7

Perniö (Location 2)*	1.5	38.0	19.0	64.0	89.9	36.0	58.9	64.0
	2.5	10.0	24.2	44.2	89.9	36.0	110.0	58.0
	3.0	8.7	26.4	41.4	86.3	36.0	104.0	55.5
	3.5	7.5	28.6	38.6	71.1	36.0	94.0	53.5
	4.0	8.7	30.8	40.8	60.2	36.0	84.0	52.3
	4.5	10.0	33.0	43.0	58.2	36.0	75.0	51.4
	5.0	11.0	35.2	45.2	54.1	36.0	80.0	50.4
	5.5	15.0	37.4	47.4	50.4	36.0	75.0	47.5
	6.0	17.0	39.6	49.6	52.0	36.0	80.0	43.8
	6.5	14.0	41.8	51.8	66.9	36.0	92.0	39.2
	7.0	16.0	44.0	54.0	75.5	36.0	84.0	39.5
	7.5	17.0	46.2	56.2	75.9	36.0	88.0	40.0
	8.0	15.0	48.4	58.4	76.3	36.0	87.0	40.0
	8.5	16.5	50.6	60.6	76.7	36.0	86.0	45.0
	9.0	15.0	52.8	62.8	77.2	36.0	88.0	45.0
	9.5	21.0	55.0	65.0	77.2	36.0	85.0	40.0
	2.0	13.0	21.5	45.0	75.0	25.0	75.0	11.0
	3.0	10.0	27.0	30.0	75.0	30.0	75.0	20.0
	5.0	16.0	38.0	60.0	51.0	25.0	75.0	21.0
	6.0	18.0	43.5	65.0	49.0	30.0	65.0	20.0
Raisio, Autolava	0.8	49.0	19.8	125.0	50.0	20.0	40.0	3.0
	1.5	13.0	18.5	39.0	70.0	20.0	70.0	10.0
	2.5	10.0	24.5	50.0	70.0	23.0	90.0	9.0
	3.0	12.0	27.0	38.0	75.0	25.0	90.0	8.0
	4.0	14.0	32.0	40.0	100.0	27.0	130.0	10.0
Raisio, Krookila	2.5	13.0	26.3	60.0	85.0	25.0	87.0	11.0
	3.5	11.0	30.8	40.0	80.0	25.0	90.0	12.0
	4.5	12.0	35.3	48.0	85.0	25.0	80.0	9.0
	5.5	17.0	39.8	47.0	125.0	30.0	130.0	10.0
	6.5	25.0	44.3	50.0	120.0	25.0	120.0	10.0
	7.5	23.0	48.8	50.0	110.0	25.0	110.0	9.0
	8.5	22.0	53.3	60.0	100.0	25.0	95.0	10.0
	9.5	22.0	57.8	90.0	100.0	25.0	95.0	8.0
	10.5	23.0	62.3	80.0	85.0	25.0	80.0	8.0
Raisio, Ristimaki	0.5	10.0	7.5	30.0	70.0	30.0	70.0	12.0
	1.5	10.0	12.5	35.0	75.0	40.0	85.0	9.0
	2.5	10.0	17.5	35.0	80.0	45.0	95.0	12.0
	3.5	17.0	22.5	50.0	65.0	25.0	100.0	10.0
	5.5	15.0	32.5	43.0	70.0	35.0	80.0	11.0
	8.0	18.0	45.0	50.0	55.0	30.0	75.0	9.0
Raisio, Siirinpelto	3.5	7.0	29.5	50.0	48.0	20.0	85.0	10.0
	4.5	8.0	34.5	52.0	49.0	20.0	80.0	10.0
	6.0	9.5	42.0	90.0	35.0	20.0	37.0	10.0
	7.5	10.0	49.5	90.0	30.0	20.0	52.0	11.0
Saimaan kanava	3.0	30.0	31.0	120.0	80.0	27.0	60.0	8.0
	4.0	30.0	37.0	80.0	100.0	30.0	110.0	7.5
	5.0	20.0	43.0	80.0	55.0	25.0	65.0	7.0
	6.0	20.0	49.0	85.0	32.0	22.0	70.0	10.0

	7.0	18.0	55.0	90.0	35.0	25.0	50.0	9.0
	8.0	25.0	61.0	80.0	55.0	25.0	65.0	7.0
	9.0	30.0	67.0	110.0	60.0	25.0	75.0	6.0
Salo, Salonkyla	10.0	18.0	50.0	50.0	105.0	25.0	100.0	10.0
	16.0	28.0	80.0	100.0	90.0	25.0	85.0	16.0
	20.0	28.0	100.0	160.0	90.0	25.0	75.0	10.0
Sipoo	1.0	47.0	16.0	120.0	60.0	35.0	50.0	10.0
	1.5	20.0	20.5	80.0	85.0	25.0	80.0	9.0
	3.5	24.0	32.5	80.0	80.0	25.0	85.0	12.5
	4.5	21.0	37.5	78.0	75.0	25.0	75.0	11.5
	5.5	20.0	42.5	90.0	70.0	25.0	80.0	10.5
	6.5	20.0	47.5	80.0	49.9	25.0	65.0	10.0
	7.5	21.0	52.5	125.0	44.0	25.0	60.0	9.0
	10.0	16.0	42.0	42.0	85.0	25.0	85.0	8.0
	12.0	17.0	52.0	67.0	75.0	25.0	80.0	10.0
	14.6	24.0	65.0	70.0	100.0	25.0	85.0	11.0
Somero, Joenssu	1.0	45.0	17.0	100.0	85.0	30.0	60.0	7.0
	2.0	23.0	25.0	60.0	100.0	25.0	90.0	15.0
	4.0	20.0	35.0	55.0	100.0	25.0	110.0	13.0
	6.0	28.0	45.0	75.0	80.0	25.0	110.0	14.0
	8.0	23.0	55.0	85.0	80.0	30.0	110.0	15.0
	10.0	27.0	65.0	95.0	70.0	25.0	80.0	13.0
	12.0	28.0	79.0	98.0	60.0	23.0	75.0	16.0
	14.0	33.0	93.0	100.0	52.0	23.0	70.0	10.0
	18.0	40.0	121.0	180.0	60.0	23.0	60.0	13.0
	20.0	43.0	135.0	175.0	50.0	23.0	60.0	8.0
	24.0	51.0	163.0	220.0	60.0	25.0	50.0	7.0
Somero, Kirkonkyla	4.0	35.0	39.0	130.0	75.0	27.0	70.0	14.0
	5.0	33.0	45.0	115.0	80.0	25.0	75.0	17.0
	6.0	31.0	51.0	75.0	70.0	25.0	70.0	16.0
	7.0	31.0	57.0	110.0	75.0	24.0	75.0	13.0
	8.0	33.0	64.0	110.0	55.0	23.0	65.0	12.0
	11.0	42.0	85.0	150.0	60.0	24.0	55.0	8.0
	12.0	45.0	92.0	230.0	46.0	23.0	55.0	7.0
Somero, Pajulanjoki	4.0	19.0	21.0	70.0	80.0	27.0	110.0	12.0
	5.0	17.0	25.0	79.0	75.0	27.0	100.0	13.0
	6.0	23.0	29.0	80.0	75.0	27.0	100.0	22.0
	7.0	23.0	33.0	90.0	75.0	27.0	100.0	18.0
	8.0	25.0	37.0	62.0	80.0	25.0	85.0	18.0
	9.0	27.0	42.0	105.0	75.0	25.0	80.0	12.0
	10.0	28.0	47.0	110.0	75.0	27.0	85.0	17.0
	11.0	30.0	52.0	120.0	70.0	25.0	80.0	20.0
	12.0	31.0	57.0	135.0	70.0	25.0	80.0	10.0
	13.0	32.0	62.0	100.0	65.0	25.0	75.0	21.0
Tampere	1.5	75.0	33.0	180.0	70.0	27.0	70.0	9.0
	2.5	37.0	40.0	190.0	52.0	27.0	40.0	6.0
	3.0	24.0	43.5	80.0	55.0	27.0	40.0	9.0
	3.5	18.0	47.0	60.0	60.0	25.0	70.0	17.0

	4.0	16.0	50.5	55.0	47.0	27.0	62.0	14.0
	4.5	17.0	54.0	70.0	40.0	25.0	60.0	20.0
	5.0	13.0	57.5	75.0	35.0	28.0	45.0	11.0
	5.5	14.0	61.0	77.0	32.0	25.0	42.0	10.0
	6.0	22.0	64.5	80.0	35.0	27.0	50.0	8.0
	6.5	21.0	68.0	68.0	51.0	25.0	55.0	16.0
	7.0	35.0	71.5	130.0	35.0	25.0	60.0	14.0
	7.5	42.0	75.0	115.0	31.0	26.0	50.0	9.0
	8.0	37.0	78.5	220.0	37.0	32.0	40.0	11.0
Vihti	3.0	20.0	23.0	55.0	35.0	15.0	35.0	10.0
	4.0	23.0	30.0	85.0	75.0	50.0	80.0	16.0
	6.0	21.0	44.0	85.0	60.0	30.0	65.0	7.0
	9.0	18.0	65.0	70.0	25.0	10.0	30.0	11.0
	10.0	26.0	72.0	95.0	40.0	20.0	45.0	7.0
	11.0	29.0	79.0	97.0	55.0	30.0	57.0	6.0
	12.0	32.0	86.0	120.0	48.0	25.0	52.0	9.0
	13.0	34.0	93.0	100.0	52.0	25.0	55.0	10.0
	14.0	37.0	100.0	115.0	51.0	25.0	55.0	10.0
Viiala	3.0	22.0	23.8	45.0	65.0	25.0	75.0	8.5
	4.0	22.0	29.3	40.0	48.0	25.0	60.0	9.0
	4.5	20.0	32.0	75.0	75.0	25.0	80.0	8.0
	6.0	25.0	40.3	90.0	52.0	25.0	70.0	8.5
	6.5	22.0	43.0	100.0	85.0	30.0	95.0	11.0
	7.0	35.0	45.8	95.0	100.0	35.0	100.0	14.0
	8.0	32.0	51.3	120.0	85.0	35.0	90.0	14.0
	8.5	42.0	54.0	110.0	80.0	30.0	90.0	11.0
	9.0	43.0	56.8	125.0	77.0	35.0	80.0	16.6
	9.5	55.0	59.5	130.0	95.0	25.0	80.0	15.0
	15.0	43.0	90.5	95.0	80.0	30.0	65.0	6.0
	14.0	32.0	83.5	83.5	75.0	30.0	60.0	6.0

*σ'_p data points from CRS oedometer test.

S-CLAY/7/168 database

Table A.1. Basic information of the S-CLAY/7/168 database. σ'_p data points from CRS oedometer test.

Location	Depth (m)	s_u^{FV} (kPa)	σ'_v (kPa)	σ'_p (kPa)	LL (%)	PL (%)	w (%)	S_t
Drammen (Norway)	4.0	8.3	41.2	57.4	39.3	9.7	30.7	3.0
	5.2	11.8	50.4	78.7	58.7	10.3	65.5	3.0
	6.2	11.7	57.8	89.6	65.6	18.8	65.6	3.0
	7.1	12.3	64.7	98.5	75.2	20.6	56.2	3.0
	7.5	13.0	67.1	100.0	88.5	18.7	65.3	3.0
	7.5	22.8	68.0	95.2	88.0	18.0	65.0	6.0
	7.8	25.2	70.0	105.0	60.0	29.0	52.0	8.0
	8.5	20.6	74.5	114.4	75.8	15.4	61.7	3.0
	8.5	12.3	74.5	114.4	75.8	15.4	61.7	3.0
	9.0	13.7	78.7	124.3	78.2	19.1	58.2	3.0
	9.3	11.2	80.0	104.0	33.0	23.0	32.0	8.0
	9.4	20.9	81.5	113.4	92.2	20.4	64.1	3.0
	11.9	10.0	102.6	108.0	40.2	8.8	27.6	7.0
	13.0	20.8	112.5	135.0	25.0	3.0	26.0	6.0
	13.0	14.0	112.5	129.3	25.0	3.0	25.7	7.0
	17.4	19.0	152.6	182.3	23.3	2.7	17.3	7.0
Ellingsrud (Norway)	10.5	7.8	60.0	60.0	24.0	20.0	36.0	42.5
Fredrikstad (Norway)	6.5	10.8	43.0	47.3	34.0	21.0	40.5	20.0
Haga (Norway)	2.8	41.6	52.0	315.6	41.1	26.3	37.9	
	2.8	40.4	53.0	282.5	40.6	27.5	38.8	
	3.9	40.3	72.0	274.3	40.8	26.1	36.9	
	4.9	45.0	92.0	296.2	62.5	28.2	54.2	
	5.2	48.7	97.0	257.1	68.0	29.6	60.7	
	6.2	39.3	115.0	310.5	40.4	25.4	36.5	
	6.5	39.3	121.0	150.0	39.0	25.4	34.4	
Onsøy (Norway)	1.9	10.8	12.2	61.1	50.2	32.1	65.1	3.0
	2.1	12.7	13.9	58.4	65.2	32.1	67.1	3.0
	3.5	11.8	22.4	48.2	59.9	29.4	57.6	3.0
	5.2	12.1	32.6	45.1	56.8	33.9	58.5	3.0
	5.5	12.0	34.3	46.1	56.4	34.0	58.9	3.0
	7.6	12.9	47.5	54.3	66.3	34.8	62.3	3.0
	7.9	13.5	48.9	56.3	66.2	34.9	65.8	3.0
	10.8	17.6	66.2	85.2	74.4	38.3	67.5	7.0
	11.0	19.5	67.5	86.9	72.9	36.8	69.4	7.0
	13.4	22.2	82.2	106.3	71.4	35.6	66.7	7.0
	13.6	22.0	83.5	107.0	71.5	35.6	68.9	7.0
	16.3	27.4	99.8	100.2	72.7	37.9	64.5	7.0
Studenterlunden (Norway)	15.0	16.5	87.0	108.8	37.0	20.0	33.0	5.0
	15.0	17.0	87.0	87.0	44.0	25.0	37.4	4.0
Sundland (Norway)	6.5	15.1	43.0	55.9	58.0	30.0	59.0	11.0

Location	Depth (m)	s_u^{FV} (kPa)	σ'_v (kPa)	σ'_p (kPa)	LL (%)	PL (%)	w (%)	S_t
Unknown location 1 (Norway)	3.1	14.8	21.4	49.1	56.1	29.2	59.2	
	5.0	14.6	31.3	56.2	58.8	30.2	61.2	
	7.0	13.1	43.4	64.8	63.6	31.6	68.3	
	9.2	17.6	54.8	96.8	71.3	27.9	68.7	
	10.0	17.9	61.2	83.3	68.6	27.9	68.9	
Unknown location 2 (Norway)	4.5	16.6	34.6	142.5	22.8	18.9	40.3	
	6.0	17.9	42.7	119.0	29.0	17.2	44.3	
	7.5	14.6	52.3	123.5	25.8	19.8	41.1	
	8.0	11.4	54.6	130.1	24.8	20.7	41.3	
Vaterland (Norway)	7.5	24.4	52.0	52.0	47.0	27.0	40.0	5.0
Bäckebol (Sweden)	9.1	18.2	55.4	81.8	87.1	32.1	74.7	15.0
	11.1	26.6	66.6	75.1	85.6	37.3	94.9	24.0
	13.1	32.1	78.7	84.1	86.1	39.9	89.2	
	14.1	33.2	84.7	226.6	89.7	38.4	93.3	
	15.1	34.3	91.6	177.0	89.2	38.4	92.8	
	4.0	17.7	26.7	36.1	85.8	25.3	78.4	11.0
	6.0	16.3	36.4	44.5	84.7	31.1	103.1	32.0
	7.0	16.5	41.5	51.6	83.0	35.1	88.1	28.0
Göta Älv (Sweden)	2.6	12.7	20.5	45.6	76.5	33.2	85.3	
	3.0	13.4	23.1	42.7	75.8	33.9	84.4	
	3.5	13.1	26.1	41.8	75.2	34.2	83.4	
	3.9	13.1	28.2	53.0	72.7	34.6	82.4	
	4.5	12.8	32.0	47.1	70.3	35.2	83.0	
	5.0	12.7	34.4	53.6	78.8	35.9	92.2	
	5.5	12.5	37.3	60.1	82.1	35.9	98.1	
	5.9	12.5	39.4	69.0	75.8	33.2	93.8	
	6.9	12.6	46.2	63.4	69.6	32.6	83.4	
	7.9	13.3	51.8	65.4	65.7	31.3	79.4	
	8.9	14.7	56.9	63.4	78.1	35.5	83.0	
Järva Krog (Sweden)	5.0	18.6	48.8	72.0	88.1	37.7	93.2	26.0
	7.0	21.1	61.7	69.5	51.4	24.4	57.5	20.0
	9.0	25.8	74.4	79.5	50.4	23.9	62.6	23.0
Kalix (Sweden)	2.0	13.5	15.0	40.1	201.8	73.9	180.1	17.0
	3.0	14.8	16.5	31.8	191.3	70.4	176.0	15.0
	5.0	15.8	23.2	37.8	157.8	61.0	136.1	10.0
Lilla Mellösa (Sweden)	2.1	8.7	14.9	20.9	129.7	47.5	130.8	
	2.8	8.4	18.4	21.1	129.7	47.0	122.6	
	3.6	8.6	21.8	25.3	124.2	43.7	114.9	
	4.2	9.4	24.7	28.5	119.3	41.0	111.1	
	5.0	10.3	28.3	32.6	110.0	38.2	108.3	
	5.7	10.8	31.9	35.9	105.1	36.0	100.7	
	6.4	11.2	35.2	40.2	100.7	31.7	97.4	
	7.1	12.1	39.2	45.1	93.0	30.0	95.2	
	7.9	13.2	43.4	49.9	84.8	27.3	83.1	

Location	Depth (m)	s_u^{FV} (kPa)	σ'_v (kPa)	σ'_p (kPa)	LL (%)	PL (%)	w (%)	S_t
	8.5	14.2	47.0	54.3	82.1	26.2	82.6	
	9.0	17.0	50.0	65.0	76.0	25.0	69.9	17.5
	9.1	15.3	50.5	58.4	78.8	25.1	78.2	
	9.9	17.4	55.3	64.4	73.8	22.3	72.2	
	10.7	18.4	61.2	71.5	71.1	23.4	71.1	
	11.5	18.6	67.5	79.1	73.3	22.3	74.4	
	12.4	18.6	74.8	86.7	73.3	22.9	83.1	
Munkedal (Sweden)	3.2	25.0	37.7	126.6	65.1	31.3	98.9	
	4.1	22.7	45.4	105.0	64.0	31.0	97.0	
	6.1	31.6	63.5	102.9	61.6	30.4	92.7	
	7.2	22.1	73.3	122.8	60.3	30.1	90.4	
	8.1	22.7	82.2	135.5	59.2	29.8	88.5	
	9.2	29.2	91.9	132.9	57.9	29.5	86.3	
	10.1	30.9	100.3	143.5	56.7	29.2	84.2	
	12.2	28.7	120.7	149.8	54.1	28.5	79.7	
	16.2	33.5	160.4	184.5	49.3	27.3	71.2	
	17.1	34.4	169.7	215.4	48.1	27.0	69.2	
	21.2	31.5	212.9	240.8	43.1	25.8	60.4	
Nörrkaping (Sweden)	2.1	10.9	27.5	42.8	82.0	35.5	85.0	
	2.9	10.0	31.2	42.8	83.0	35.8	120.0	
	3.4	10.3	33.9	43.8	79.0	34.8	115.0	
	4.1	10.6	37.5	45.8	75.0	33.8	110.0	
	4.7	11.2	40.2	48.5	60.0	30.0	85.0	
	5.3	12.0	43.1	50.8	65.0	31.3	77.0	
	5.9	13.1	45.8	54.4	70.0	32.5	70.0	
	6.6	14.3	49.5	59.1	71.0	32.8	82.0	
	7.3	15.6	52.4	64.7	72.0	33.0	95.0	
	7.8	16.1	55.1	69.4	71.0	32.8	90.0	
	8.6	16.5	59.1	78.3	70.0	32.5	85.0	
	9.4	16.7	64.1	89.6	60.0	30.0	65.0	
	10.3	16.9	69.0	101.6	70.0	32.5	72.0	
	11.1	16.9	74.7	113.5	35.0	23.8	40.0	
	12.0	17.0	80.3	125.8	40.0	25.0	40.0	
	12.9	17.5	86.0	136.1	40.0	25.0	40.0	
Skå-Edeby (Sweden)	10.0	15.6	60.0	84.0	51.0	23.0	63.0	20.0
	2.0	11.1	12.5	24.1	126.1	58.5	122.5	8.0
	4.0	6.9	21.0	24.9	66.4	30.2	95.9	18.0
	6.0	10.5	31.5	38.1	51.3	24.1	71.8	14.0
	8.0	13.8	44.7	40.1	55.5	26.6	73.0	23.0
	9.9	15.0	59.1	59.5	50.7	24.1	64.6	21.0
Stora an (Sweden)	1.5	10.2	10.4	43.8	113.8	40.0	107.8	
	2.0	8.9	11.3	26.0	115.3	40.7	109.3	
	2.3	8.2	11.9	24.0	125.0	54.2	122.8	
	3.1	7.2	14.0	18.7	118.3	42.2	117.5	
	3.8	7.1	16.4	20.2	123.5	37.7	113.8	
	4.6	9.0	19.6	28.9	104.1	46.0	107.1	
	5.3	11.3	22.8	31.7	104.9	41.5	103.4	

Location	Depth (m)	s_u^{FV} (kPa)	σ'_v (kPa)	σ'_p (kPa)	LL (%)	PL (%)	w (%)	S_t
Svartiolandet	2.0	8.8	14.0	36.0	92.5	32.4	91.3	
(Sweden)	2.5	8.5	16.2	33.1	81.2	27.6	87.7	
	3.0	8.4	18.4	31.6	76.4	24.6	80.6	
	3.7	8.3	22.1	31.6	70.5	26.4	78.8	
	4.3	8.2	25.0	32.4	68.7	26.4	78.8	
	4.9	8.5	28.3	34.9	67.5	27.0	78.8	
	5.5	9.3	32.0	37.9	58.0	24.0	74.6	
	6.0	9.7	36.0	41.2	53.2	20.5	65.7	
	6.4	10.3	37.9	43.4	51.4	20.5	65.1	
	6.8	11.0	40.1	46.3	49.6	19.3	63.9	
	7.3	11.9	43.4	51.1	49.6	19.3	63.9	
	7.9	13.0	46.3	55.5	49.6	21.0	62.1	
	8.5	13.7	50.4	60.7	49.6	21.0	60.9	
	9.0	14.6	54.4	65.4	49.0	19.3	59.7	
	9.6	15.5	58.1	71.3	49.0	19.9	58.0	
	10.3	16.8	62.5	76.8	51.4	19.3	57.4	
Tuve (Sweden)	2.1	5.9	6.9	16.7	110.0	40.0	121.0	
	3.1	6.7	9.2	15.2	105.0	40.0	115.5	
	4.0	7.7	12.0	22.1	100.0	40.0	110.0	
	5.0	8.7	14.7	25.5	100.0	40.0	110.0	
	6.0	9.5	17.4	27.5	95.0	40.0	104.5	
	7.0	10.4	20.5	47.1	75.0	30.0	82.5	
	7.9	13.2	23.5	45.1	83.0	30.0	91.3	
	8.9	15.8	26.9	55.9	95.0	30.0	104.5	
	10.0	19.2	30.4	54.9	87.0	30.0	95.7	
	11.0	19.9	33.8	61.3	86.0	30.0	94.6	
	11.5	20.4	35.5	63.2	85.0	30.0	93.5	
	12.1	21.0	38.2	66.2	85.0	30.0	93.5	
	12.6	21.4	39.5	68.1	84.0	30.0	92.4	
	13.2	22.2	41.6	70.6	83.0	30.0	91.3	
Ursvik (Sweden)	2.0	5.6	11.3	29.6	47.9	18.5	57.5	14.0
	4.0	6.9	20.2	49.4	49.2	21.7	97.8	18.0
	5.0	7.2	25.7	50.2	40.3	14.7	60.1	22.0
	6.0	9.0	31.9	62.3	49.9	21.7	59.5	27.0
	6.9	11.7	38.1	55.6	47.3	21.1	55.0	26.0
	8.0	11.2	44.7	91.8	47.3	21.7	51.8	26.0
	10.0	16.1	58.4	100.8	44.7	19.2	53.1	17.0

Tampereen teknillinen yliopisto
PL 527
33101 Tampere

Tampere University of Technology
P.O.B. 527
FI-33101 Tampere, Finland

ISBN 978-952-15-3804-9
ISSN 1459-2045